



**Universitatea
„Politehnica” București**



**Facultatea de Energetică
Școala doctorală
Energetică**



**Université de
Strasbourg**



**École doctorale
MSII**



**Institut National des Sciences
Appliquées Strasbourg**



**Laboratoire I Cube
Département Mécanique (D-M)**

Thèse présentée pour obtenir le grade de
Docteur de l'université de Strasbourg

Discipline/Specialite : ÉNERGÉTIQUE

**Analyse théorique et expérimentale d'un système de micro-cogénération
biomasse à moteur Stirling**

**Analiza teoretică și experimentală a unui sistem de micro-cogenerare cu
engine Stirling utilizând biomasa**

Author: Eng. Ștefan - Dominic VORONCA, M.Sc., M.Sc.

Directeurs de THÈSE	
George DARIE	Professeur, Universitatea Politehnica din Bucuresti,
Monica SIROUX	Professeur, INSA STRASBOURG ICUBE
Raporteurs :	
Céline MORIN	Professeur Université Polytechnique Hauts-de-France
Daniela POPESCU	Professeur, Universitatea Tehnica Gheorghe Asachi din Iasi
Examineurs :	
Sanda Carmen GEORGESCU	Professeur, Universitatea Politehnica din Bucuresti,
George DARIE	Directeur de thèse, Professeur, Universitatea Politehnica din Bucuresti,
Monica SIROUX	Directeur de thèse, Professeur, INSA STRASBOURG ICUBE

22 September 2021

Original Document No. 1



Universitatea
„Politehnica” București



Facultatea de Energetică
Școala doctorală
Energetică



Université de
Strasbourg



École doctorale
MSII



Institut National des Sciences
Appliquées Strasbourg



Laboratoire I Cube
Département Mécanique (D-M)

Nr. Decizie Senat ... din2021

TEZĂ DE DOCTORAT

**ANALYSE THEORIQUE ET EXPERIMENTALE
D'UN SYSTEME DE MICRO-COGENERATION
BIOMASSE A MOTEUR STIRLING**

**ANALIZA TEORETICĂ ȘI EXPERIMENTALĂ A
UNUI SISTEM DE MICRO-COGENERARE CU
MOTOR STIRLING UTILIZÂND BIOMASA**

Autor: Ing. Ștefan - Dominic VORONCA, M.Sc., M.Sc.

Conducători de doctorat: Prof. dr. ing. George DARIE
Prof. dr. ing. Monica SIROUX

COMISIA DE DOCTORAT

Președinte	Prof. dr. ing. Sanda Carmen GEORGESCU	de la	Universitatea „Politehnica” din București
Conducători de doctorat	Prof. dr. ing. George DARIE	de la	Universitatea „Politehnica” din București
	Prof. dr. ing. Monica SIROUX	de la	Institut National des Sciences Appliquées Strasbourg
Referent	Prof. dr. ing. Céline MORIN	de la	Université Polytechnique Hauts-de-France
Referent	Prof. dr. ing. Daniela POPESCU	de la	Universitatea Tehnică „Gheorghe Asachi” din Iași

BUCURESTI
22 septembrie 2021

Document original nr. 1

ANALYSE THEORIQUE ET EXPERIMENTALE D'UN SYSTEME DE MICRO- COGENERATION BIOMASSE A MOTEUR STIRLING

Résumé de la Thèse

La micro-cogénération est une technologie par laquelle on produit simultanément de l'électricité et de la chaleur pour le chauffage et l'eau chaude sanitaire des logements, d'une manière décentralisée. La puissance électrique produite est inférieure à 50 kW_{el}.

Cette technologie récupère les pertes de "chaleur fatale" considérées comme des "déchets thermiques" produits dans les cycles thermodynamiques pour la production d'énergie mécanique.

La technologie de la micro-cogénération offre des avantages importants.

A grande échelle, les enjeux portent sur la réduction des consommations d'énergie primaire, réduction des émissions de CO₂, évitement de la construction de centrales et de réseaux.

Au niveau de l'individu, les enjeux sont liés à la nouvelle stratégie de la Commission Européenne pour stimuler la rénovation intitulée "Une vague de rénovation pour l'Europe - Verdir nos bâtiments, créer des emplois, améliorer la vie". La mise en œuvre de cette stratégie est ciblée sur la décarbonation et l'intégration des énergies renouvelables qui doit faire essentiellement référence à l'énergie issue de sources renouvelables produites sur place ou à proximité. La rénovation des bâtiments doit accélérer l'intégration des énergies renouvelables, notamment locales, et favoriser une utilisation plus extensive de la chaleur résiduelle.

Dans ce contexte, l'utilisation plus élargie de la biomasse en tant que combustible, représente une réponse à cette nouvelle orientation et offre plusieurs avantages : on utilise de l'énergie renouvelable, la neutralité carbone, la disponibilité et le bas-prix.

Dans ce contexte, l'utilisation plus élargie de la biomasse en tant que combustible, représente une réponse à cette nouvelle orientation et offre plusieurs avantages : on utilise de l'énergie renouvelable, la neutralité carbone, la disponibilité et le bas-prix.

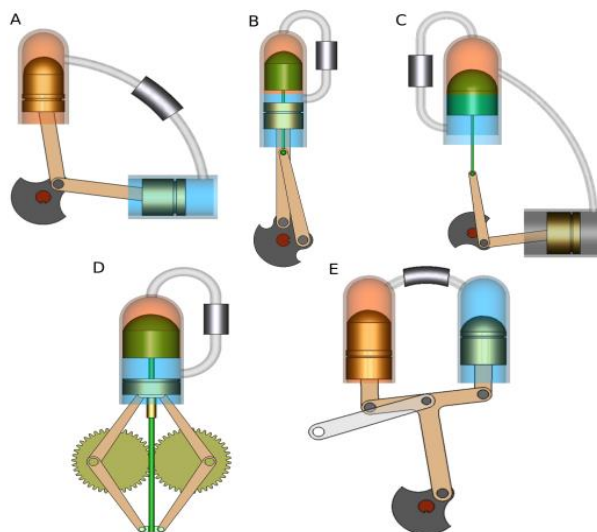


Figure 1 - Différentes configurations des moteurs Stirling

Le travail de cette thèse a pour objectif de réaliser une analyse théorique et expérimentale d'un système de micro-cogénération biomasse à moteur Stirling (Figure 1).

Le premier chapitre de la thèse présente une étude bibliographique qui apporte des réponses sur le choix du sujet de thèse. Dans cette partie est présenté le contexte énergétique européen. La réduction des émissions de 55% d'ici 2030, considérée comme une première étape nécessaire vers la neutralité carbone de l'UE fixée pour 2050, demande la promotion de la décarbonisation du chauffage et du refroidissement, qui sont responsables de 80% de l'énergie consommée dans les bâtiments résidentiels. Deux tiers de cette énergie proviennent de combustibles fossiles, respectivement 76,5%.

Étant donné que les systèmes autonomes représentent 88 % du marché global de l'approvisionnement en chaleur de l'Union européenne, l'une des priorités est de s'attaquer à la décarbonisation du chauffage par la promotion de systèmes autonomes modernes et efficaces utilisant des sources d'énergie renouvelables. Par conséquent, la production de chaleur à partir de biomasse solide et, en outre, la production simultanée d'électricité dans le même système autonome sont prises en considération.

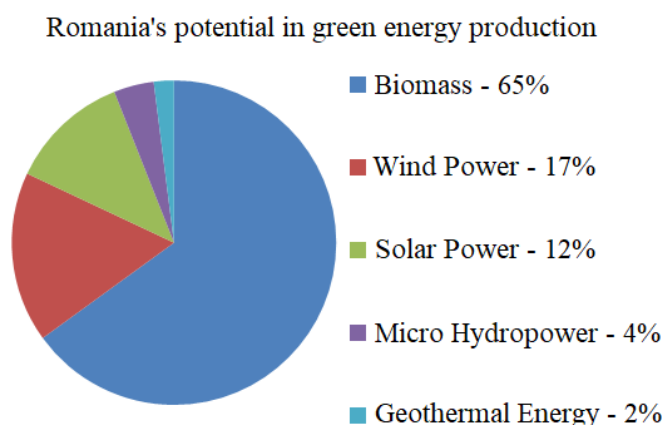


Figure 2 - Potentiel des énergies renouvelables en Roumanie
(source : <https://www.interregeurope.eu/>)

Les systèmes de micro-cogénération à base de biomasse sont de plus en plus populaires car ils peuvent aider les clients à passer du statut de consommateurs à celui de producteurs, en produisant de l'électricité pour l'autoconsommation ou même en la revendant au réseau. En conséquence, un système de micro-cogénération à combustion de biomasse solide équipé d'un moteur Stirling est étudié expérimentalement et théoriquement.

Pour encadrer ce travail, le premier chapitre présente les notions sur la biomasse (Figure 2 et Figure 3), les systèmes de microcogénération biomasse, le transfert de chaleur, le cycle de Carnot et de Stirling, les types de moteurs Stirling les paramètres spécifiques, les aspects théoriques, les calculs simplifiés, tous liés au moteur Stirling.

Le chapitre 2 fait référence aux caractéristiques de la biomasse solide et à son impact favorable sur les émissions de gaz à effet de serre. Le pouvoir calorifique supérieur et le pouvoir calorifique inférieur ainsi que les relations qui les relient ont été déterminés pour plusieurs types de biomasse : déchets forestiers, granulés de sapin, briquettes de chêne, sciure de hêtre, granulés de hêtre, briquettes de hêtre.

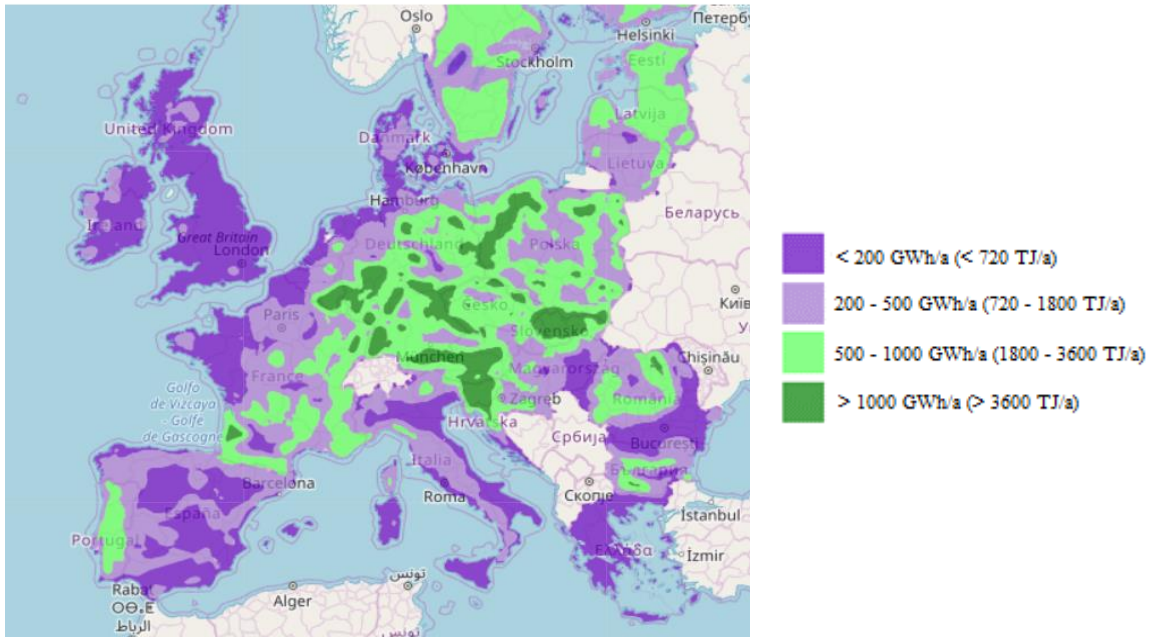


Figure 3 - Le potentiel énergétique de biomasse type bois en Europe
(source : <https://heatroadmap.eu/>)

Les considérations sur la teneur en eau de la biomasse se sont concentrées sur l'importance de son évaluation initiale et de son contrôle ultérieur, conformément à la méthode d'essai et aux procédures connexes recommandées par les normes spécifiques.

Sur la base de divers échantillons de biomasse, les niveaux d'humidité humide et sèche ont été déterminés. Le séchage a eu lieu dans une atmosphère d'azote pour éviter l'oxydation.

Le pouvoir calorifique supérieur a été déterminé à l'aide d'un calorimètre (Figure 4). Des détails sur ce processus de mesure sont fournis dans le chapitre deux.

Sur la base des relations trouvées dans la littérature scientifique, le pouvoir calorifique inférieur de tous les échantillons de biomasse a été calculé et le prix de l'énergie équivalente reposant exclusivement sur le coût du carburant a été obtenu. Les relations (1) - (4) provenant de la littérature scientifique ont été utilisées pour calculer la puissance calorifique inférieure des combustibles biomasse analysée.

$$\text{LHV} = \text{HHV} - 2.12 \cdot \text{H} - 2.45 \cdot \text{W}_t - 0.8 \cdot \text{O} \quad (1)$$

$$\text{LHV} = \text{HHV} - 5.83 \cdot (\text{W}_t + 9 \cdot \text{H}) \quad (2)$$

$$\text{LHV} = \text{HHV} - 2257 \cdot \text{w}_t \quad (3)$$

$$\text{w}_t = \text{W}_t / 100 \quad (4)$$

Tableau 1 - Formules utilisées pour le calcul de la puissance calorifique inférieure des combustibles analysés

Conformément à l'importance accordée aux questions de cendres dans le cadre de l'extension requise de l'utilisation de la biomasse, la teneur en cendres de la biomasse solide a été mesurée en utilisant un four à moufle (Figure 5). Des détails sur les procédures de mesure utilisées pour cette détermination sont fournis dans le chapitre 2.

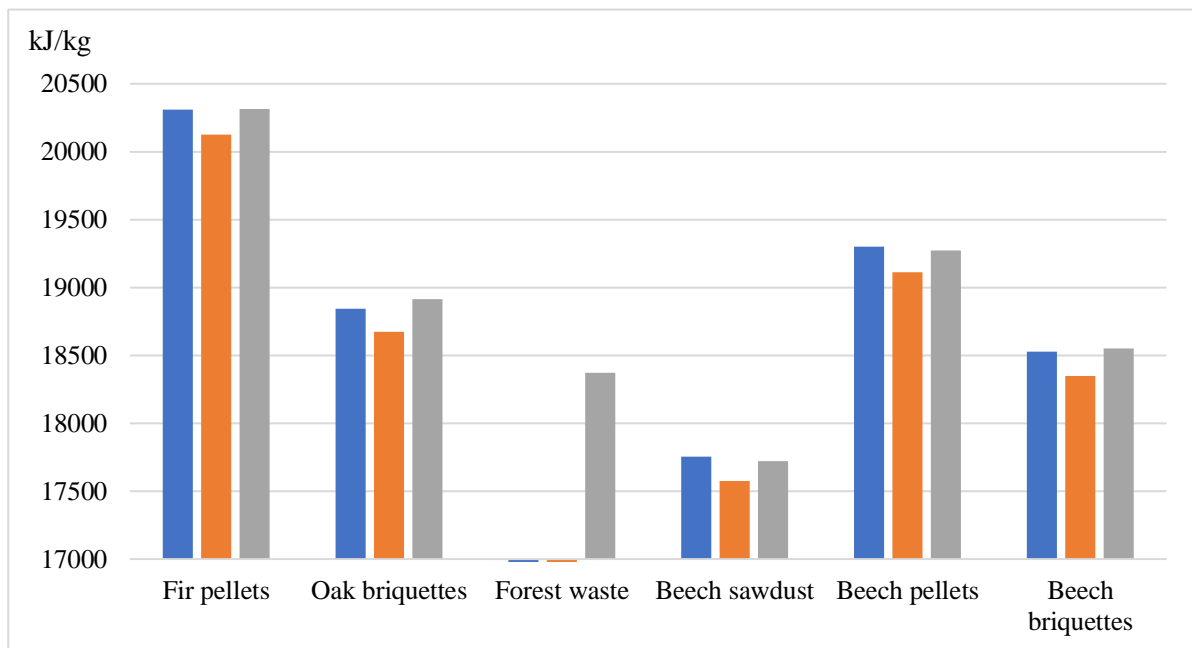


Figure 4 - Puissance calorifique supérieure des combustibles analysés

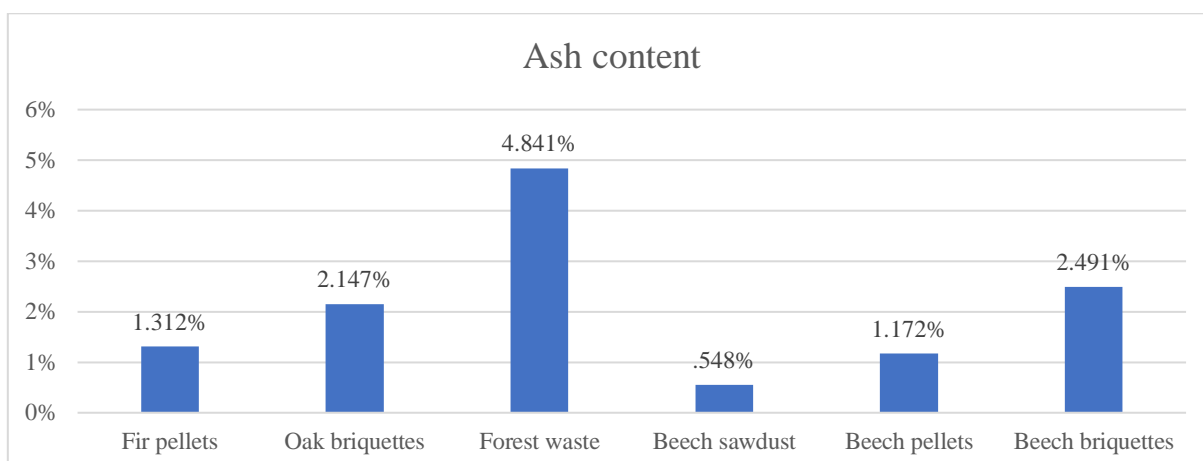


Figure 5 - Analyse des cendres des combustibles considérés.

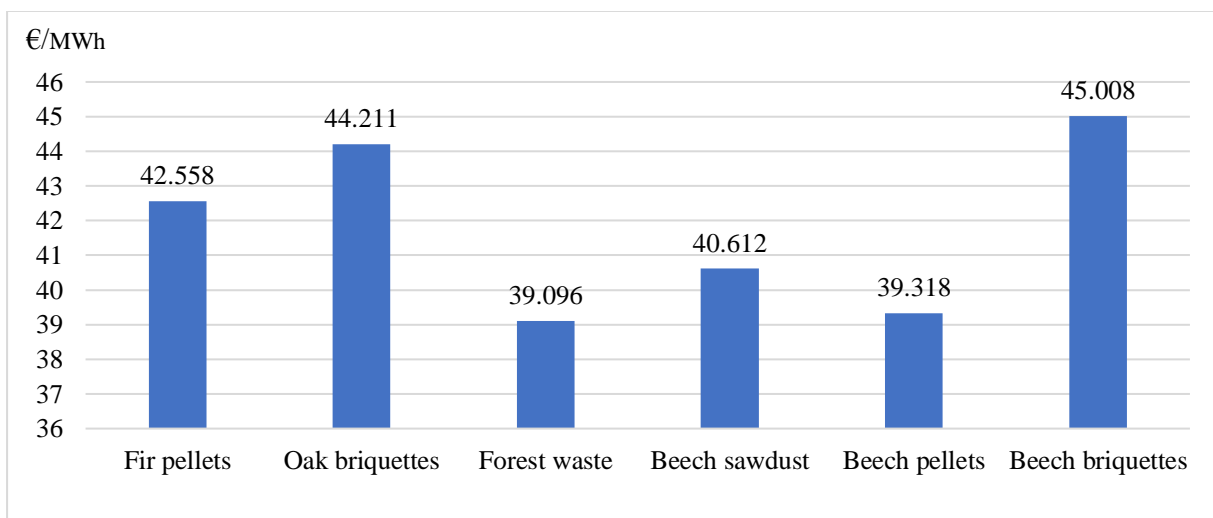


Figure 6 - Rapport entre le prix et l'énergie produite par les combustibles analysés

Enfin, des calculs économiques décrivant la rentabilité d'un investissement dans une nouvelle centrale de chauffage utilisant les échantillons de biomasse solide ont été développés (Figure 6). La durée de vie de la centrale thermique a été fixée à 20 ans. Dans ces conditions, compte tenu du fait que les investissements dans la production de chaleur doivent se refléter dans le prix de vente (€/MW_{th}), une augmentation par rapport au prix du combustible de 35% a été adoptée.

Pour chaque essence de bois, la projection du cash-flow a été réalisée (Figure 7). Pour les données d'entrée considérées, les délais de récupération varient du plus petit, à savoir les briquettes de hêtre, au plus grand, les déchets de forêt.

Pour une durée de vie de 20 ans, le retour sur investissement est raisonnablement court, sachant que la fourniture de chaleur au sein des systèmes de chauffage urbain locaux a un fort impact social et que les prix de vente (variant de 53 à 61 €/MW_{th} dans cet exemple) devraient être abordables.

Dans des pays comme la France où la parité d'achat du pouvoir d'achat est adéquate, dans d'autres pays comme la Roumanie, la nécessité de subventionner localement la fourniture de chaleur est toujours présente.

Des performances financières attrayantes soutiennent l'idée que tous les investissements sont économiquement valables.

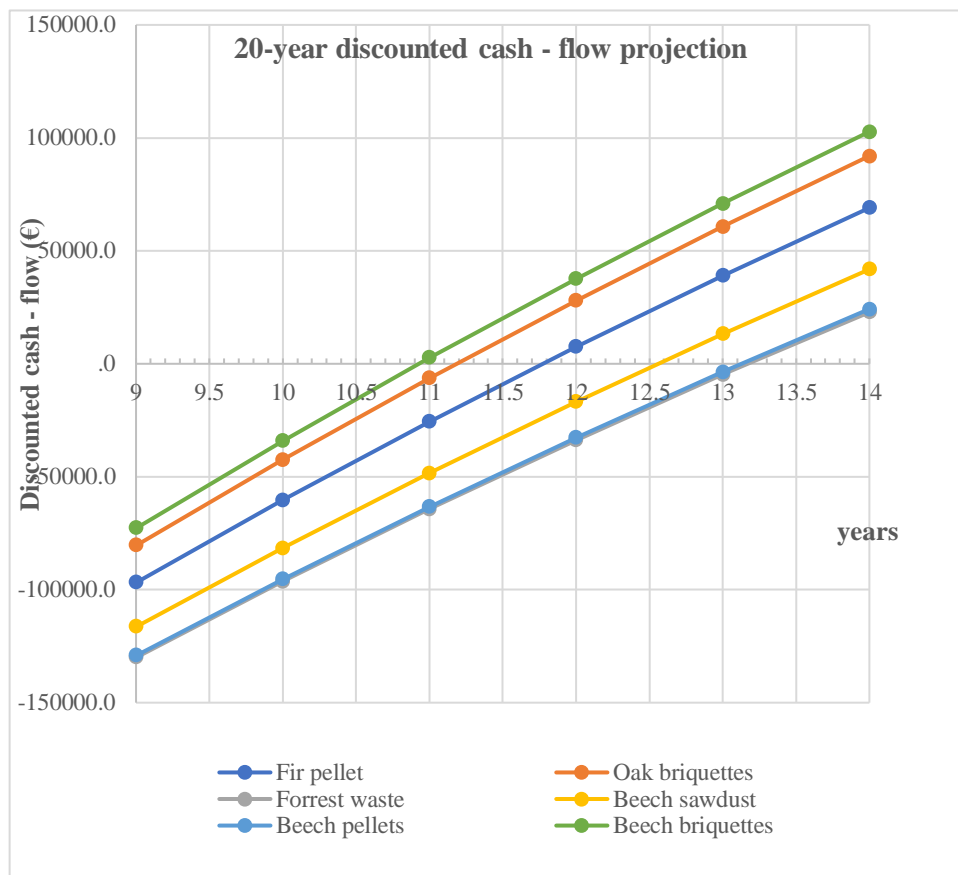


Figure 7 - Projection du discounted cash - flow pour les combustibles analysés

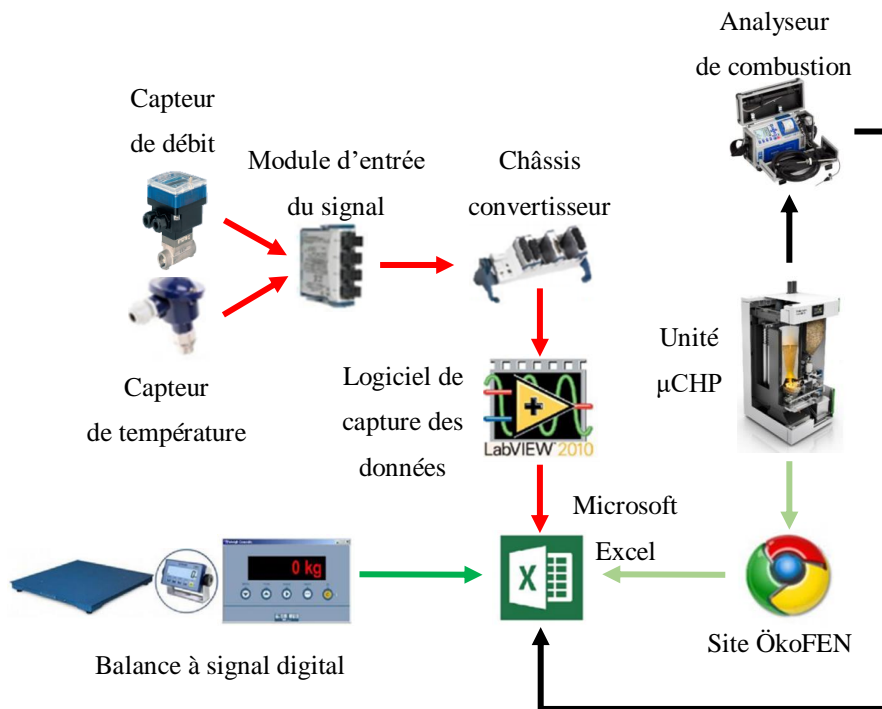
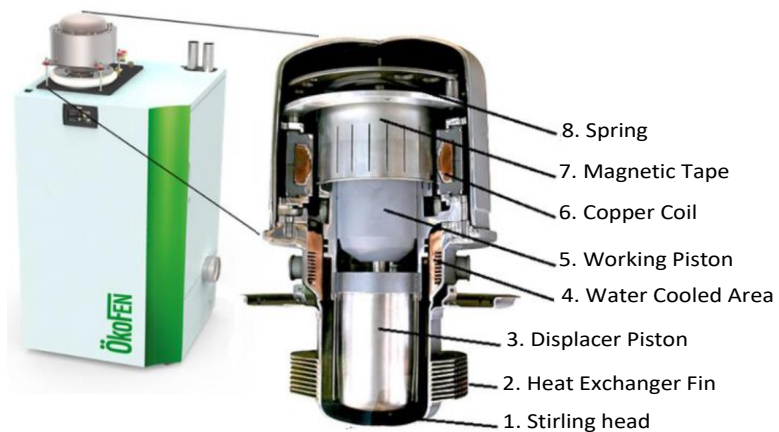


Figure 8 - Banc d'essai du système de micro-cogénération

La troisième partie de la thèse est consacrée au dispositif expérimental mis en place au cours de la thèse (Figure 8). Une description détaillée du banc d'essai du système de micro-cogénération est présentée.



Légende :

1. Carcasse du Stirling
2. Echangeur de chaleur (source chaude)
3. Piston déplaceur
4. Zone refroidie par de l'eau (source froide)
5. Piston moteur
6. Bobine de cuivre
7. Bande magnétique
8. Ressort

Figure 9 - Le système de micro-cogénération biomasse à moteur Stirling

Il s'agit d'une installation de micro-cogénération biomasse à moteur Stirling (Figure 9). Le moteur Stirling est un moteur à piston libre de type dynamique. En plus du moteur Stirling,

L'objectif de l'étude expérimentale a été d'observer l'influence du débit de l'agent thermique et de la puissance de sortie thermique sur le comportement de l'installation de micro-cogénération. Dans la deuxième partie de ce chapitre les résultats expérimentaux sont présentés.

Tableau 2 : Les configurations testées

Configurations	10kW _{th}	12kW _{th}	14kW _{th}
Debit F1	10F1	12F1	14F1
Debit F2	10F2	12F2	14F2
Debit F3	10F3	12F3	14F3

Les températures et les débits ont été mesurés à l'aide des capteurs de température et de débitmètres. Le rendement global et les rendements thermique et électrique ont été déterminés pour chaque configuration.

Les résultats obtenus ont montré que, si le débit n'est pas suffisant pour évacuer la puissance thermique produite par l'unité de micro-cogénération, la température de l'agent thermique va augmenter, réduisant ainsi les performances thermiques du système.

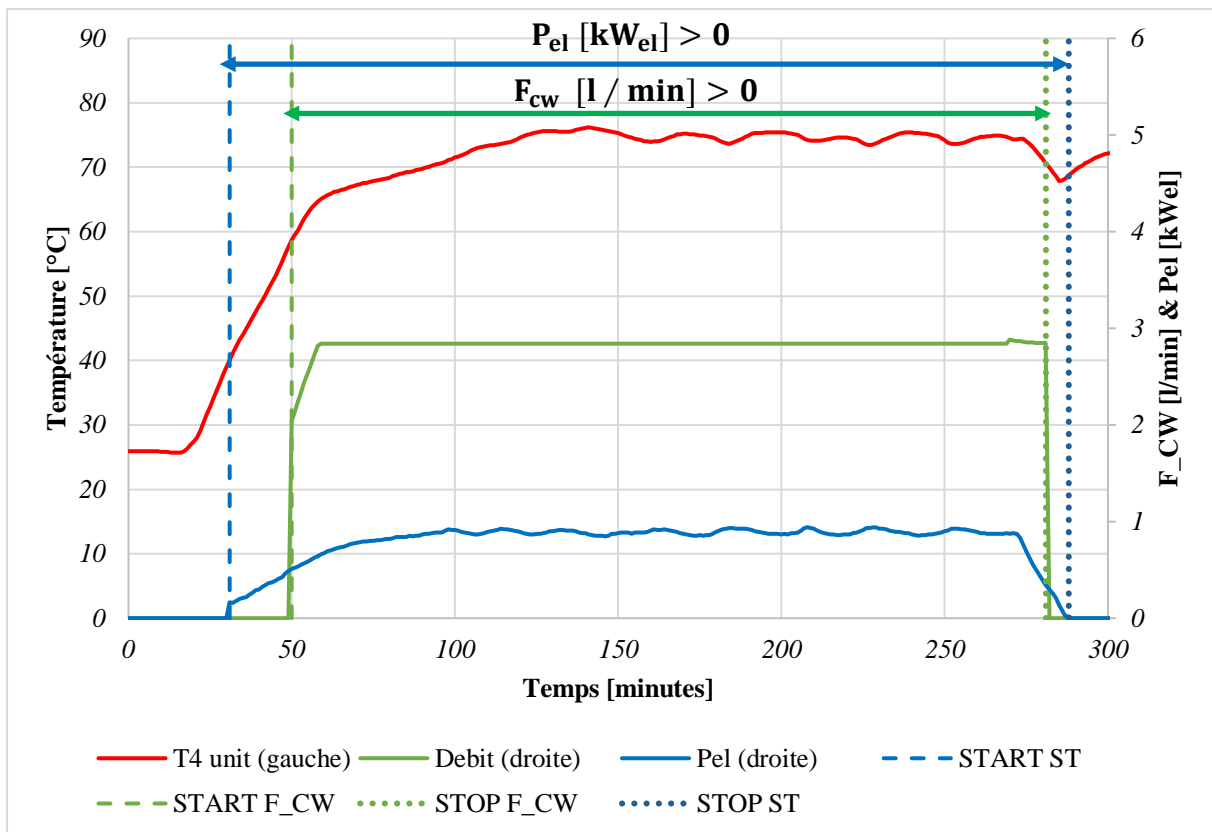


Figure 11 - Effets d'un débit d'agent caloporteur faible sur les performances du système

Dans le chapitre quatre un modèle mathématique décrivant le système de micro-cogénération biomasse a été développé (Figure 13). Le modèle mathématique est basé sur le processus de combustion de 4 différents combustibles. Les 3 premières sont le chêne, le hêtre et le sapin de Douglas. Les teneurs en carbone, hydrogène, azote, soufre et oxygène présentes dans les

sources de combustible ainsi que le pouvoir calorifique inférieur sont tirés de la base de données Phyllis (base de données TNO).

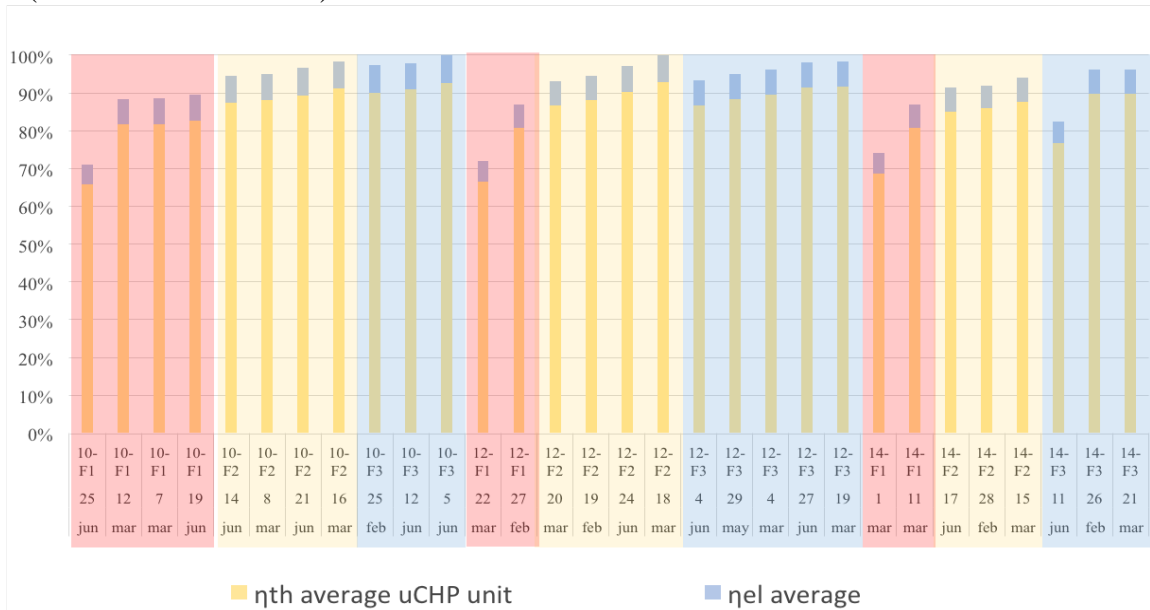


Figure 12 - Rendements thermiques et électriques obtenus pour les différentes configurations testées

Les combustibles sont secs et la teneur en humidité est donc nulle. La base de données Phyllis ne contient pas la densité de masse du combustible ; ce paramètre est donc tiré d'une autre base de données (Köppen). Comme la densité massique est donnée sous forme de fourchette, elle a été considérée comme la moyenne des deux intervalles donnés. La 4ème espèce de combustible est celle utilisée pour les expériences à l'INSA Strasbourg, France.

Le volume de la chambre de combustion est imposé, dans un ordre de grandeur comparable à celui du modèle d'unité de cogénération ÖkofEN Pellematic Condens_e, présent à l'INSA Strasbourg.

Le modèle permet d'obtenir la température adiabatique de combustion, les puissances thermique et électrique, le rendement thermique de l'installation et le rendement électrique de l'installation.

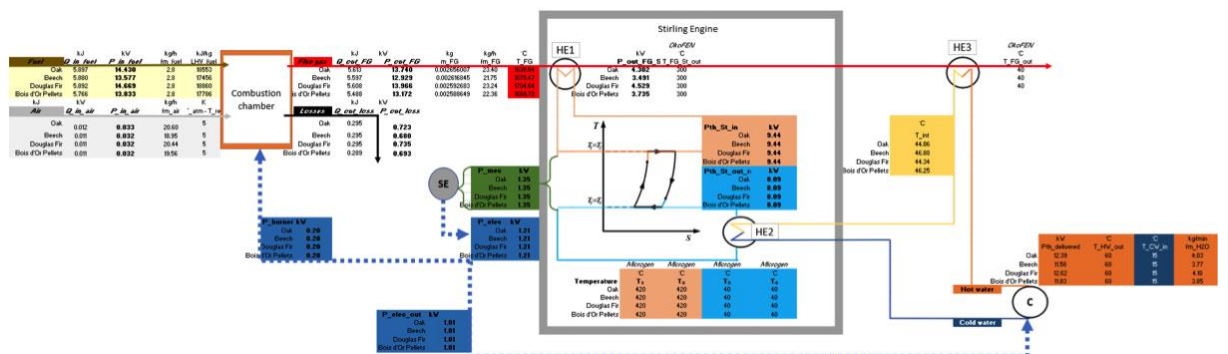


Figure 13 - Modèle mathématique décrivant le système de micro-cogénération biomasse

L'impact des différents combustibles à différentes humidités et des différents excès d'air sur la production de puissance thermique et de puissance électrique a été ainsi mis en évidence (Figure 14 et Figure 15).

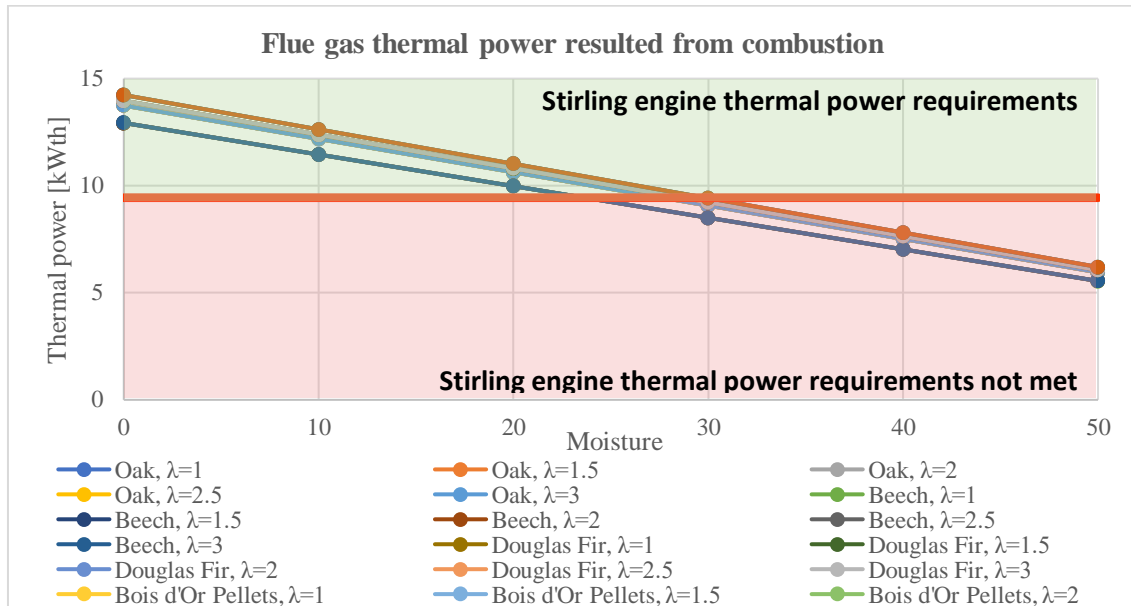


Figure 14 - Impact des différents combustibles a différentes humidités et des différents excès d'air sur la production de puissance thermique du moteur Stirling

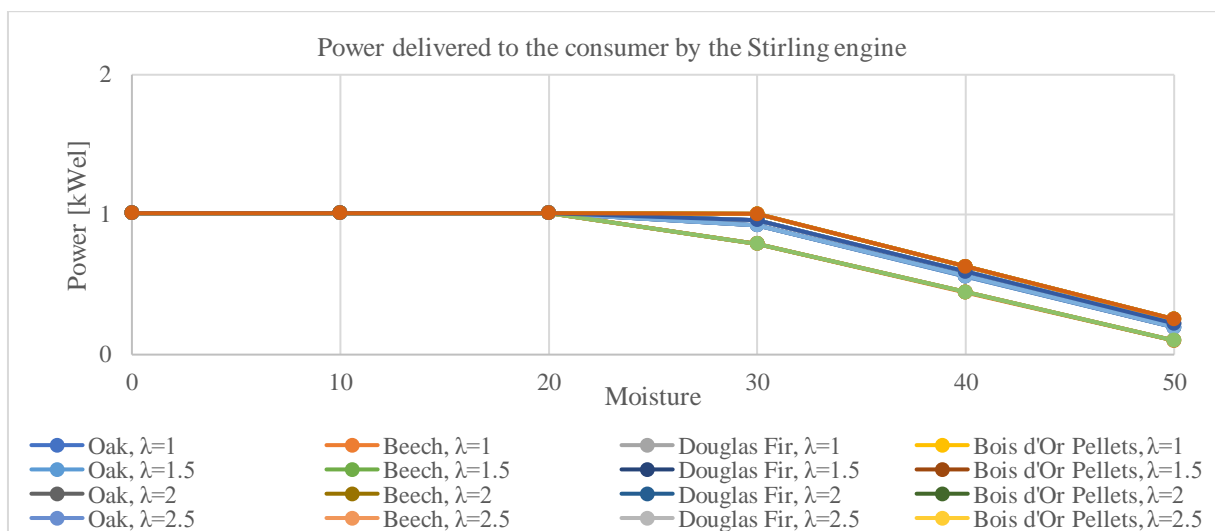


Figure 15 - Impact des différents combustibles a différentes humidités et des différents excès d'air sur la production de puissance électrique du moteur Stirling

Les rendements décrivant les performances globales de l'unité de micro-cogénération à biomasse solide avec moteur Stirling visent à montrer que l'utilisation d'un combustible sec est recommandée pour obtenir les meilleures puissances utiles. Si la puissance thermique n'est pas entièrement nécessaire, le combustible peut avoir une humidité allant jusqu'à 20% pour que le moteur Stirling fonctionne à la charge nominale.

Le cas mentionné ci-dessus est intuitivement celui de la saison d'été, où le besoin en énergie thermique est plus faible que celui de la saison d'hiver. Il est donc crucial d'utiliser du combustible sec pendant les saisons froides, pour obtenir la puissance thermique maximale disponible, à condition que le système n'ait pas été surdimensionné pour la maison du consommateur. Si c'est le cas, des combustibles de moindre qualité en termes d'humidité peuvent être utilisés, car leur rendement thermique ne créera pas de surplus de puissance thermique.

Le présent chapitre conclut qu'une étude des besoins du consommateur est nécessaire, afin de mieux déterminer l'adéquation de la qualité du combustible au système de cogénération en fonction des besoins du consommateur, travail qui sera effectué dans le chapitre suivant.

Et sur un marché avec une taille assez significative, une optimisation du type logiciel du fonctionnement des systèmes autonomes à micro-cogénération, à partir de la décomposition de la consommation de combustible proposée dans cette thèse, puisse aider à obtenir une meilleure corrélation entre les coûts de la production séparée ou simultanée avec le prix de combustibles et le prix de l'énergie électrique dans le réseau local de la distribution d'électricité.

Conclusions

Le travail de cette thèse a permis de réaliser une analyse théorique et expérimentale d'un système de micro-cogénération biomasse à moteur Stirling.

Le premier chapitre a présenté le contexte énergétique et une étude bibliographique sur la biomasse, les systèmes de micro cogénération biomasse et les moteurs thermiques. La dernière partie de ce chapitre a présenté une synthèse sur le moteur Stirling.

Le deuxième chapitre a présenté une analyse sur plusieurs types de biomasse : déchets forestiers, granulés de sapin, briquettes de chêne, sciure de hêtre, granulés de hêtre, briquettes de hêtre. Ces combustibles ont été d'abord analysés en termes de pouvoir calorifique supérieur. Plusieurs caractéristiques ont été étudiées ensuite : l'influence de l'humidité, le coût, la complexité de l'équipement nécessaire pour transporter et brûler le combustible, la disponibilité du combustible, le stockage du combustible, les émissions causées par la combustion, les technologies des chaudières utilisant la biomasse. Une analyse économique d'une chaudière à condensation biomasse d'une centrale thermique de chauffage urbain a été également menée. Les résultats obtenus ont montré une rentabilité modérée pour l'ensemble des combustibles analysés. L'intérêt de la micro cogénération biomasse (production d'énergie renouvelable décentralisée) a été finalement mis en évidence dans le contexte énergétique et environnemental actuel.

Le troisième chapitre a porté sur la présentation du banc d'essai de l'unité de micro-cogénération biomasse à moteur Stirling mis en place au cours de la thèse et la présentation des résultats expérimentaux. L'objectif de cette étude expérimentale a été d'observer l'influence du débit de l'agent thermique et de la puissance de sortie thermique sur le comportement de l'installation de micro-cogénération. Les essais ont été effectués pour neuf configurations différentes (correspondant à trois débits de l'agent thermique différents et à trois puissances de sortie thermique différentes : 10 kW, 12 kW et 14 kW). Les températures et les débits ont été obtenus à l'aide des capteurs de température et de débitmètres. Les rendements thermique et électrique et le rendement global ont été déterminés pour chaque configuration. Les résultats expérimentaux ont montré que, si le débit n'est pas suffisant pour évacuer la puissance thermique produite par l'unité de micro-cogénération, la température de l'agent thermique va augmenter, réduisant ainsi les performances thermiques du système.

Le quatrième chapitre a porté sur le développement d'un modèle mathématique décrivant le système de micro-cogénération biomasse. La température adiabatique de combustion, les puissances thermique et électrique, le rendement thermique de l'installation et le rendement électrique de l'installation ont été obtenus. Une analyse paramétrique a permis de mettre en évidence l'impact des différents combustibles à différentes humidités et différents excès d'air

sur la puissance thermique et de puissance électrique du système de micro-cogénération biomasse.

Les rendements décrivant les performances globales de l'unité de micro-cogénération à biomasse solide avec moteur Stirling visent à montrer que l'utilisation d'un combustible sec est recommandée pour obtenir les meilleures puissances utiles. Si la puissance thermique n'est pas entièrement nécessaire, le combustible peut avoir une humidité allant jusqu'à 20% pour que le moteur Stirling fonctionne à la charge nominale.

Le cas mentionné ci-dessus est intuitivement celui de la saison d'été, où le besoin en énergie thermique est plus faible que celui de la saison d'hiver. Il est donc crucial d'utiliser du combustible sec pendant les saisons froides, pour obtenir la puissance thermique maximale disponible, à condition que le système n'ait pas été surdimensionné pour la maison du consommateur. Si c'est le cas, des combustibles de moindre qualité en termes d'humidité peuvent être utilisés, car leur rendement thermique ne créera pas de surplus de puissance thermique.

Mots-clés : micro-cogénération, biomasse, moteur Stirling, bâtiment, production d'énergie

CONTENT

INTRODUCTION.....	27
CHAPTER 1	
BIBLIOGRAPHIC STUDY.....	31
1.1. A RENOVATION WAVE FOR EUROPE - GREENING OUR BUILDINGS, CREATING JOBS, IMPROVING LIVES	31
1.2. CHALLENGES FOR THE ENERGY DEMAND IN THE RESIDENTIAL SECTOR.....	32
1.3. THE SOLID BIOMASS COMBUSTION MICRO-COGENERATION REPRESENTS AN OPPORTUNITY.....	32
1.4. THE THERMOCHEMICAL CONVERSION OF BIOMASS THROUGH A DIRECT GRID COMBUSTION TECHNOLOGY	34
1.5. THE BIOMASS-BASED MICRO-COGENERATION SYSTEMS ARE BECOMING INCREASINGLY POPULAR.....	34
1.6. THE MICRO-COGENERATION SYSTEMS EQUIPPED WITH STIRLING ENGINES.....	35
1.7. ENGINES GENERALITIES	37
1.7.1. Heat transfer	37
1.7.2. Engines thermodynamic cycles	38
1.7.2.1. Carnot cycle	38
1.7.2.2. Stirling cycle	42
1.7.3. Types of Stirling engines	45
1.7.4. Parameters of Stirling engines.....	45
1.7.5. Stirling engine ideal cycle	47
1.7.5.1. Isothermal transformation $1 \rightarrow 2$	49
1.7.5.2. Isochore transformation $2 \rightarrow 3$	49
1.7.5.3. Isothermal transformation $3 \rightarrow 4$	49
1.7.5.4. Isochore transformation $4 \rightarrow 1$	49
1.7.6. Stirling engine irreversible cycle.....	50
1.7.6.1. Geometric analysis	51
1.7.6.2. The regenerator.....	51
1.7.6.3. Isothermal compression $3 \rightarrow 4$	52
1.7.6.4. Isochoric heating process $4 \rightarrow 1$	52
1.7.6.5. Isothermal heating process $1 \rightarrow 2$	53
1.7.6.6. Isochoric cooling process $2 \rightarrow 3$	53
1.7.6.7. Total heat added	53
1.7.6.8. Total heat rejected	54
1.7.6.9. Net amount of work realized.....	54
1.7.6.10. Mean effective pressure	54
1.7.6.11. Thermal efficiency.....	55
1.8. CONCLUSIONS	55

CHAPTER 2	
BIOMASS EXPERIMENTAL STUDY.....	57
2.1. INTRODUCTION	57
2.2. BIOMASS	57
2.3. LOWER HEATING VALUE AND HIGHER HEATING VALUE.....	58
2.4. FUEL MOISTURE DETERMINATION	59
2.4.1. Biomass moisture content.....	59
2.4.2. ASTM E871 - 82 Standard Test Method for Moisture Analysis of Particulate Wood Fuels.....	59
2.4.3. Samples Drying	60
2.5. HIGHER HEATING VALUE DETERMINATION.....	62
2.6. LOWER HEATING VALUE DETERMINATION.....	63
2.7. COST PER UNIT OF THERMAL ENERGY PRODUCED	64
2.8. SIMPLE ECONOMICS	66
2.9. CONCLUSIONS	69
CHAPTER 3	
EXPERIMENTAL STUDY ON THE BIOMASS MICRO - COGENERATION UNIT WITH A STIRLING ENGINE	71
3.1. INTRODUCTION	71
3.2. MATERIALS AND METHODS.....	73
3.3. RESULTS.....	88
3.3.1. Flow rate results	88
3.3.2. Thermal agent temperature in correlation with the thermal agent flow	90
3.3.3. Generated power and Stirling engine work fluid temperature	93
3.3.4. Fuel mass flow consumption and efficiencies.....	94
3.4. CONCLUSIONS AND PERSPECTIVES.....	97
CHAPTER 4	
MATHEMATICAL MODEL.....	101
4.1. FUEL DESCRIPTION	101
4.2. DETERMINATION OF LOWER HEATING VALUE (LVH) AND COMPARISON WITH LITERATURE.....	102
4.3. ENERGY BALANCE IN THE COMBUSTION CHAMBER	104
4.3.1. Determination of the flue gas real specific wet volume $v_{real,wetFG}$ and the heat amount produced by the fuel entering the combustion chamber $Q_{in,fuel}$	105
4.3.2. Determination of the mass of air which enters the combustion chamber m_{air} and of heat inlet of air $Q_{in,air}$	107
4.3.3. Determination of the adiabatic combustion temperature by using volumes and enthalpies	108
4.3.4. Determination of the adiabatic combustion temperature by using masses and enthalpies	112
4.3.4.1. Air and Flue Gas masses calculation at wet ash free state	114
4.3.4.2. Gaskell Equation for enthalpy calculation	117

4.3.4.3.	Howard Shomate Equation and JANAF coefficients for enthalpy calculation	122	
4.3.4.4.	Combustion adiabatic temperature, comparison of results	127	
4.4.	COMBUSTION POWER CALCULUS	127	
4.5.	STIRLING ENGINE KEY POINTS, POWER AND ENERGY CALCULUS	128	
4.6.	USEFUL THERMAL POWER DELIVERED TO THE END USER.....	132	
4.7.	COMPARISON BETWEEN DIFFERENT FUEL MOISTUERS AND AIR EXCESSES	135	
4.8.	COMPARISON OF EFFICIENCIES IN DIFFERENT CONFIGURATIONS ($\Lambda=I$, $W=J$)	142	
4.9.	CONCLUSIONS	146	
CHAPTER 5			
MATHEMATICAL MODEL FOR THE SIMULATION OF TRANSIENT REGIMES.149			
5.1.	TESTS FOR TRANSIENT REGIMES.....	149	
5.2.	MATHEMATICAL MODEL FOR TRANSIENT REGIMES	149	
5.2.1.	Introduction	149	
5.2.2.	The power generation simulation.....	151	
5.2.2.1.	Stirling cycle calculus	151	
5.2.2.2.	Thermal power delivered to the Stirling hot source and Equivalent Inlet Enthalpy calculation	153	
5.2.2.3.	Outlet thermal power and internal thermal power of the Stirling engine calculation.....	153	
5.2.2.4.	Distribution in time of the mass flow consumption of fuel.....	154	
5.2.3.	The thermal power generation simulation	154	
5.2.3.1.	Calculus of the thermal power sent to end - user.....	154	
5.2.3.2.	Calculus of the thermal power recovered from flue gases	155	
5.2.3.3.	Calculus of the thermal power recovered from water vapor condensation ..	155	
5.2.4.	Time - distribution for the fuel mass consumption	155	
5.2.5.	Simulation results	156	
5.3.	INVESTMENT PROJECT PROFITABILITY INDICES.....	161	
5.3.1.	Profitability indices, calculation and aplicability	161	
5.3.2.	Input data for the economic simulation of the transient tests	164	
5.3.3.	Economic simulation of the Test code VN MASTER 10-1 mar 07	164	
5.3.4.	Economic simulation of the Test code VN MASTER 14-3 jun 11.....	166	
5.3.5.	Economic simulation of the Test code VN MASTER 10-1 jun 25.....	167	
5.3.6.	Economic simulation of the Test code VN MASTER 10-1 jun 18.....	169	
5.4.	CONCLUSIONS.....	171	
CONCLUSIONS.....			173
ABREVIATIONS.....			179
BIBLIOGRAPHY.....			181
DISSEMINATION OF RESEARCH RESULTS.....			191
ANNEXES.....			193

FIGURE LIST

Number	Title	Page
CHAPTER 1		
1.1.	Renewable energy potential in Romania	32
1.2.	The energy potential of wooden biomasse in Europe	33
1.3.	Cylinder through which heat passes	37
1.4.	The principle of the Carnot cycle	39
1.5.	The Carnot Cycle: pressure-Volume and Temperature - entropy diagrams	40
1.6.	Comparison between real engines cycle (left) and Carnot cycle (right)	40
1.7.	Carnot Engine Stage 1: Isothermal expansion	41
1.8.	Carnot Engine Stage 2: Adiabatic expansion	41
1.9.	The Carnot Engine Stage 3: Isothermal compression	42
1.10.	The Carnot Engine Stage 4: Adiabatic compression	42
1.11.	Dependence of the pressure difference and pressure ratio with the mean pressure	43
1.12.	The Stirling Cycle: pressure - Volume and Temperature - entropy diagrams	44
1.13.	Configurations of Stirling Engines	45
1.14.	"Slider-crank" mechanism	46
1.15.	"2 piston" configuration	46
1.16.	Stirling engine ideal cycle	48
1.17.	Stirling engine integrated to a micro-cogeneration system (van Loo, 2008)	48
1.18.	Stirling engine irreversible cycle	50
CHAPTER 2		
2.1.	Drying Oven SLW 53	59
2.2.	The wet moisture levels of different types of wood biomass	60
2.3.	Calorimeter IKA C 200-System	61
2.4.	The higher heating value and lower heating value for different types of wood biomass (Formula 2.1 - blue, Formula 2.2 - brown, Formula 2.3 - grey)	62
2.5.	The energy price for different type of wood biomass	63
2.6.	Nabertherm Muffle furnace L 9/11/SKM	64
2.7.	The ash content for all considered wood species	65
2.8.	The cash - flow projection for all considered wood species	66
2.9.	The discounted cash - flow projection for all considered wood species	67
CHAPTER 3		
3.1.	A biomass cogeneration unit with Stirling engine	72
3.2.	The principal schema of the ÖkoFEN Condens_e cogeneration unit	73
3.3.	ÖkoFEN Pellematic Condens_e Stirling Engine	75
3.4.	Data acquisition schema	75
3.5.	Compiling Excel data from the 3 sources in accordance with the experiment timespan	76
3.6.	Calculation algorithm of the combustion temperature T_1^{FG}	79
3.7.	The measurement points on the ÖkoFEN Condens_e cogeneration unit	80
3.8.	The algorithm used in Excel for determining the experiment phase	82
3.9.	An example of a flow during the start phase	82
3.10.	An example of a flow during the constant phase	83
3.11.	An example of a flow during the ending phase	83
3.12.	An example of a flow function in its entirety	84
3.13.	An example of a flow function in its entirety	84
3.14.	Calculating the DBCNIV just before a new mass value	86
3.15.	Calculating the DBCNIV for a fuel mass equalling the next	86

3.16.	The overview of the μ CHP to user circuit and the points of temperature measurement	87
3.17.	Flow rate results for the F1 setting, for thermal output powers of 10 kW _{th} , 12 kW _{th} and 14kW _{th}	88
3.18.	Flow rate results for the F2 setting, for thermal output powers of 10 kW _{th} , 12 kW _{th} and 14 kW _{th}	88
3.19.	Flow rate results for the F3 setting, for thermal output powers of 10 kW _{th} , 12 kW _{th} and 14 kW _{th}	89
3.20.	Thermal agent and flow rate result correlation for the F1 setting, for thermal power outputs of 10 kW _{th} , 12 kW _{th} and 14 kW _{th}	89
3.21.	Thermal agent and flow rate result correlation for the F2 setting, for thermal power outputs of 10 kW _{th} , 12 kW _{th} and 14 kW _{th}	90
3.22.	Thermal agent and flow rate result correlation for the F3 setting, for thermal power outputs of 10 kW _{th} , 12 kW _{th} and 14 kW _{th}	90
3.23.	Heat exchanger temperatures for a thermal power output of 10 kW _{th} with the 3 flow settings	91
3.24.	Heat exchanger temperatures for a thermal power output of 12 kW _{th} with the 3 flow settings	91
3.25.	Heat exchanger temperatures for a thermal power output of 14 kW _{th} with the 3 flow settings	91
3.26.	Generated power output and Stirling work fluid temperature for the F1 flow setting	92
3.27.	Generated power output and Stirling work fluid temperature for the F2 flow setting	92
3.28.	Generated power output and Stirling work fluid temperature for the F3 flow setting	93
3.29.	The fuel mass flow consumption of the studied configurations	94
3.30.	Power and thermal efficiencies, and the thermal losses in all the studied configurations	95
3.31.	Proposed algorithm for the μ CHP functioning	98
 CHAPTER 4		
4.1.	Lower heating value as function of moisture content (van Loo, 2008)	101
4.2.	Obtained lower heating values through the 3 formulas	102
4.3.	Superposition of Figure 1 (van Loo, 2008) and obtained results	102
4.4.	Differences between LHV values obtained through literature and the relation (4.1)	103
4.5.	Combustion chamber energy balance	103
4.6.	The iteration algorithm used to determine the flue gas temperature	110
4.7.	Obtained flue gas temperatures and errors between iterations for Oak specie	110
4.8.	Obtained flue gas temperatures and errors between iterations for Beech specie	111
4.9.	Obtained flue gas temperatures and errors between iterations for Douglas Fir specie	111
4.10.	Obtained flue gas temperatures and errors between iterations for Bois d'Or Pellets	111
4.11.	Energy balance of combustion	112
4.12.	Flue gas temperature function with a step of 10 K	119
4.13.	Flue gas temperature function with a step of 1 K	120
4.14.	Flue gas temperature results	125
4.15.	Flue gas temperature refined results	125
4.16.	Stirling Cycle pressure - Volume diagram	128
4.17.	Operational performances of the Stirling cycle related to the Combustion process	130
4.18.	The Stirling cycle outgoing heat recovery through the consumer's hot water delivery system	131
4.19.	Overview of the μ CHP system	134
4.20.	Adiabatic temperature of combustion found in literature (van Loo, 2008)	135
4.21.	Adiabatic combustion temperatures for the 4 species	135
4.22.	Thermal power entered in combustion for different configurations and fuels	137

4.23.	Flue gas thermal power resulted from combustion of different fuels	137
4.24.	The overview of the Stirling engine with the partial load functioning parameters	139
4.25.	The power delivered to the consumer by the Stirling engine	139
4.26.	The domestic hot water mass flow delivered to the consumer	140
4.27.	Thermal power delivered to the consumer	140
4.28.	Thermal efficiency of the μ CHP system, reported to the wet fuel thermal power of the same configuration	141
4.29.	Power efficiency reported to the fuel thermal power of the same configuration	142
4.30.	Added μ CHP efficiencies reported to the fuel power of the same configuration	142
4.31.	The thermal efficiencies of the configurations reported to the fuel power with “zero” fuel moisture	143
4.32.	The power efficiencies of the configurations reported to the fuel power with “zero” fuel moisture	144
4.33.	The μ CHP efficiencies of the configurations reported to the fuel power with “zero” fuel moisture	145

CHAPTER 5

5.1.	Raw and refined mass flow recorded during an experiment	149
5.2.	Stirling engine and Stirling cycle temperature - entropy diagram	152
5.3.	An example of measured and calculated power and heat delivered to end - user	154
5.4.	The test - dependent efficiency for the power generation, the heat generation and overall	158
5.5.	Comparison between the test - dependent fuel mass calculated and measured values	159
5.6.	The test - dependent relative errors for fuel mass calculated values and measured values (considered as reference)	159
5.7.	Graphic method for the determination of the Internal Rate of Return	161
5.8.	A test (code VN MASTER 10-1 mar 07) whose power generation lasts longer that the heat generation	164
5.9.	Gross and Discounted Payback Time (code VN MASTER 10-1 mar 07)	165
5.10.	A test (code VN MASTER 14-3 jun 11) whose power generation starts earlier that the heat generation but stops quicker, so that in the end, the micro - cogeneration unit produces heat exclusively	166
5.11.	Gross and Discounted Payback Time (code VN MASTER 14-3 jun 11)	167
5.12.	A test (code VN MASTER 10-1 jun 25) whose heat generation lasts longer that the heat generation	168
5.13.	Gross and Discounted Payback Time (code VN MASTER 10-1 jun 25)	169
5.14.	A test (code VN MASTER 10-1 jun 18) whose heat generation starts earlier than the power generation but stops earlier, so that the micro - cogeneration unit produces power exclusively	170
5.15.	Gross and Discounted Payback Time (code VN MASTER 10-1 jun 18)	171

TABLE LIST

Number	Title	Page
CHAPTER 1		
1.1.	The parameters from the relation (1.1)	37
1.2.	The parameters from the relations (1.2) - (1.3)	38
1.3.	The parameters from the relations (1.7) - (1.9)	39
1.4.	Generic notations for piston configuration	46
1.5.	Input data for calculation	48
1.6.	Generic notations for the geometric analysis	51

CHAPTER 2

2.1.	Wet and dry moisture levels for different types of wood biomass	61
2.2.	The higher heating value and lower heating value for different types of wood biomass	63
2.3.	The fuel price and the energy price for different type of wood biomass	63
2.4.	The ash content for all considered wood species	65
2.5.	The investment performances for all wood species	67

CHAPTER 3

3.1.	Stirling engine fitted μ CHP/CHP units	72
3.2.	Measured parameters and equipment used in measurement	77
3.3.	Constants used in calculus	78
3.4.	Calculated parameters shown in results	78
3.5.	Functions used to determine the polynomial coefficients	79
3.6.	The 9 tested configurations of the 3 thermal outputs paired to the 3 thermal agent flow rates	81
3.7.	The 5 stages of the experimental study	81
3.8.	Functions used for determining the 3 rd degree equation of the flow in the starting phase	83
3.9.	Functions used for determining the 1 st degree equation of the flow in the constant phase	83
3.10.	Functions used for determining the 2 nd degree equation of the flow in the ending phase	83
3.11.	Initial fuel mass and the accurate, refined fuel mass	85
3.12.	Configuration thermal power and agent flow	93
3.13.	Ranking of configuration in function of total efficiency	94
3.14.	Thermal agent properties and partial load functioning for the configurations	96
3.15.	Time required to reach the configured temperature of the thermal agent for each configuration	97

CHAPTER 4

4.1.	Input parameters and their notations	100
4.2.	Properties of the air entering combustion	102
4.3.	Parameters necessary to calculate the fuel volume	104
4.4.	Calculated properties of air	106
4.5.	Calculated specific volumes	107
4.6.	Excel functions used to determine the coefficients of the 5 th degree regressions for the specific volume heat coefficients	108
4.7.	Obtained results for output heat and losses after combustion	112
4.8.	Balance equation results	113
4.9.	Specific masses of air and flue gas components	113
4.10.	Balance results for verifying the wet ash free masses	114
4.11.	The combustion adiabatic temperature equation's components	117
4.12.	The equation (4.88) function	120
4.13.	Refining the result of the equation (4.88) function	120
4.14.	The equation function (4.95) and (4.103) right member and (4.104) left member	124
4.15.	Refining the result of the equation function (4.95) and (4.103) right member and (4.104) left member	125
4.16.	Comparison of results obtained for three different methods of calculation	126
4.17.	Parameters used for power calculus in combustion	126
4.18.	Results of mass flows and powers entering and exiting the combustion process	127
4.19.	Input parameters and their values for the Stirling engine	128
4.20.	Thermodynamic values of pressure and volume within the theoretical Stirling cycle	129

4.21.	Ingoing and outgoing powers within the Stirling cycle	131
4.22.	Parameters used for the calculation of the thermal power delivered to the end user	132
4.23.	Excel functions used to determine the coefficients of the 2 nd degree regressions for heat capacity	132
4.24.	Found function for the intermediary temperature of the water fuelling the consumer with thermal power	133
4.25.	Intermediary hot water temperature values	133
4.26.	Balance test of the flue gas power exiting the Stirling cycle	133
4.27.	The configurations of the biomass species studied	134
4.28.	Partial load functioning of the Stirling engine input parameters	138
 CHAPTER 5		
5.1.	The 5 stages of the experimental study	149
5.2.	Parameters used in determining the accuracy of the fuel mass flow function	151
5.3.	Parameters used in the power generation simulation	152
5.4.	Parameters used in the thermal power generation simulation	154
5.5.	Efficiency of power generation and the related fuel mass consumption determined for all 32 transient tests	156
5.6.	Efficiency of heat generation and the related fuel mass consumption determined for all 32 transient tests	157
5.7	Comparison between the measured values and calculated values for the fuel mass consumption for all 32 transient tests	158
5.8	Transient tests in which the relative error stays under the acceptable value of $\pm 5\%$	159
5.9	Input data for the economic simulation of the transient tests	164
5.10	Performances of the μ CHP for the Test code VN MASTER 10-1 mar 07	165
5.11	Financial performances of the μ CHP for the Test code VN MASTER 10-1 mar 07	165
5.12	Investment performances of the μ CHP for the Test code VN MASTER 10-1 mar 07	165
5.13	Performances of the μ CHP for the Test code VN MASTER 14-3 jun 11	166
5.14	Financial performances of the μ CHP for the Test code VN MASTER 14-3 jun 11	167
5.15	Investment performances of the μ CHP for the Test code VN MASTER 14-3 jun 11	167
5.16	Performances of the μ CHP for the Test code VN MASTER 10-1 jun 25	168
5.17	Financial performances of the μ CHP for the Test code VN MASTER 10-1 jun 25	168
5.18	Investment performances of the μ CHP for the Test code VN MASTER 10-1 jun 25	169
5.19	Performances of the μ CHP for the Test code VN MASTER 10-1 jun 18	169
5.20	Financial performances of the μ CHP for the Test code VN MASTER 10-1 jun 18	170
5.21	Investment performances of the μ CHP for the Test code VN MASTER 10-1 jun 18	171
5.22	Fuel consumption and generated power and heat for the selected transient tests	174
5.23	Investment performances for the selected transient tests.	174

NOTATIONS

% X	component	%	LHV	lower heating value	MJ/kg
A, a	coefficient	-	ln	natural logarithm	-
AC	alternative current	-	m	mass	kg
afm	accurate fuel mass	-	m	meter	-
AND	logic operator	-	m	specific mass	kg/kg
AR	ash recipient	-	m	minute	-
B	coefficient	-	M	mega	-
C	carbon	-	M	molar mass	kg/kmol
C	Celsius, Carnot	-	n	number of rotations per second	rot/s
C	heat capacity	J/mol K	N	Newton	-
c	specific mass heat coefficient	kJ/(kg*K)	N	nitrogen	-
C, c	coefficient	-	N	normal	-
CC	combustion chamber	-	nr	number of repetitions	-
Cl	chlorine	-	O	oxygen	-
c_p	specific mass heat coefficient at constant pressure	kJ/(kg*K)	OR	logic operator	-
c_v	specific volume heat coefficient at constant pressure	kJ/(m ³ N*K)	p	per	-
D	coefficient	-	p	pressure	Pa
d	displacement	M	Pa	Pascal	N/m ²
DBCNIV	difference between consecutive non-identical values	-	PHW	partially heated water	-
E	coefficient	-	Q	heat	kJ
F	coefficient	-	R	gas constant of Helium	kJ/(kg·K)
F	flow rate	l/min	r	rotation, radius, range	-
f	frequency	Hz	RM	universal gas constant	kJ/(kmol·K)
f	function	-	S	sulphur	-
fm	mass flow	kg/h	s	entropy	kJ/K
G	coefficient, giga	-	SE	Stirling engine	-
g	gram	-	T	Temperature	K
H	coefficient	-	T	Terra	-
H	heat, enthalpy	kJ/kg	t	temperature	°C
H	hydrogen	-	t	reduced temperature	K
h	hour	hour	ton	ton	ton
HE	heat exchanger	-	v	specific volume	m ³ N/kg
HHV	higher heating value	-	V	volume	-
IFR	inner fuel reservoir	-	Vol	volume	m ³
IWC	interior water circuit	-	W	moisture, warm, water	%
J	Joule	-	W	watt	-
K	Kelvin, factor	-	WV	way valve	-
k	kilo	-	x	abscissa	-
k	thermal conductivity, ratio	-	x	humidity	g/kg
L	length	M	x	variable unknown	-

SUBSCRIPTS AND SUPERSCRIPTS

agent	air	int	intermediate
air	agent	K	Kolin
atm	atmosphere	k	compression
burner	burner	loss	loss
C	chamber	loss	loss
chamb	cold	max	maximum
cold	combustion	mec	mechanical
comb	compression	min	minimum
comp	cold space	n	number
CW	cold water	net	net
D	displacer, dry	out	out, outlet
daf	dry ash free	P, piston	piston
delivered	delivered	probe	probe
dry	dry	R	regenerator
el, elec	electrical	real	real
exp	expansion	ref	reference

Content

f	final	reg	regenerator
FG	flue gases	S	volume, swept
fuel	fuel	St	Stirling
gas	gas	Stir	Stirling
H	hot space	t	total
He	Helium	th	theoretical
hot	hot	th	thermal
HW	hot water	vapor	vapor
i	initial	w, wet	wet
i	iteration	waf	wet ash free
in	in, inlet	water	water
inc	incomplete	x	2,3

GREEK LETTERS

γ	adiabatic index	-	μ	micro	-
Δ, δ	difference	-	μ	molar mass	kg/mol
ε	compression ratio	-	ρ	density	kg/m ³
η	efficiency	%	\varnothing	diameter	mm
λ	air excess	-	φ	angle, rotation	radian

MATH CHARACTERS

%A	ash content	%	\Downarrow	decrease	%
%C	carbon content	%	Σ	sum	%
%H	hydrogen content	%	<	Smaller	-
%N	nitrogen content	%	=	equal	-
%O	oxygen content	%	>	Greater	-
%S	sulphur content	-	cos	cosinus	-
%W _t	moisture content	-	ln	natural logarithm	-
\nearrow	increase	-	$^{\circ}$	centesimal degree	-
\int	integral operator	-	sin	sinus	-
\rightarrow	to	-			

INTRODUCTION

Brief presentation of chapters

In Chapter 1 - Bibliographic study the European context very recently upgraded is emphasized. The emission reduction with 55% by 2030, seen as a first and necessary step towards the EU carbon neutrality set for 2050, ask for the promotion of the decarbonisation of heating and cooling, which is responsible for 80% of energy consumed in residential buildings. Two thirds of this energy came from fossil fuels, respectively 76,5%.

Because the stand-alone systems account for 88% from the European Union overall heat supply market, to tackle the decarbonisation of the heating through the promotion of the modern and effective stand-alone systems using renewable energy sources represents one of the priorities.

Consequently, the production of heat from solid biomass and, additionally, the simultaneous generation of electricity within the same stand-alone system is taken into consideration.

Biomass-based micro-cogeneration systems are becoming increasingly popular because could help customers to move from consumers to prosumers, by producing electricity for self-consumption or even selling it back to the grid.

In consequence, a solid biomass combustion micro-cogeneration system equipped with a Stirling engine is experimentally and theoretically investigated.

To frame this work, in this chapter, heat transfer notions are presented, the Carnot and Stirling cycle are explained, types of Stirling engines are listed, specific parameters, theoretical aspects, simplified calculations, all related to the Stirling engine are included.

Chapter 2 - Fuel moisture determination makes reference to the solid biomass characteristics and its favourable impact on the emissions of GHG.

In terms of energy content, the higher heating value and the lower heating value and the relations interconnecting them have been revealed.

Considerations on biomass moisture content have focused on the importance of its initial assessment and its further monitoring in accordance with the test method and related procedures recommended by the specific standards.

Based on various biomass samples, wet and dry moisture levels have determined. The drying in a nitrogen atmosphere to avoid oxidation has occurred.

The higher heating value using a bomb calorimeter was determined. Details about this measuring process have been provided.

Based on relations found in specific literature, the lower heating value for all biomass samples has been calculated and the equivalent energy price exclusively relying on the fuel cost has been obtained.

In line with the importance given to the ash issues within the required biomass use extension, the solid biomass ash content has been measured by using a muffle furnace.

Details about the measuring procedures used in this determination have been also provided.

Finally, simple economic calculus depicting the profitability of an investment into a new heating plant using the solid biomass samples have been developed.

Attractive financial performances are supporting the idea that all investments are economically valid.

Chapter 3 - Experimental study on the biomass micro-cogeneration unit with a Stirling engine refers in a very extensive and detailed manner to materials and methods used, and to obtained results.

Framed by an introduction focused on the most relevant issues related to the necessity and adequacy of works which have been performed, a thorough technical and operational description of experimental facility used for laboratory tests has been provided.

In total, 9 tested configurations of the 3 thermal outputs paired to the 3 thermal agent flow rates have been performed. For each configuration, all 5 stages in time have been monitored and examples have been included.

In terms of results, values for flow rates, thermal agent temperatures in correlation with the thermal agent flows, generated powers and Stirling engine work fluid temperatures, fuel mass flows consumption and efficiencies have been used to fully characterize this laboratory facility's experimental characterization.

In Chapter 4 - Mathematical model, the process of combustion of 4 different sources of fuel has been developed.

Based on information found in literature, the calculated lower heating values have been compared with the specialized references and utilized in the establishment of the energy balance in the combustion chamber.

Volumes and masses of various agents entering and exiting the combustion chamber have been estimated and the combustion calculus performed with the main purpose of determining the adiabatic combustion temperature using volumes and enthalpies, and masses and enthalpies respectively.

To validate the results, other two statistical methods using Gaskell equation and Howard Shomate Equation and JANAF coefficients for enthalpy calculation, the errors between the three sets of values being under the threshold considered acceptable in all scientific works.

Combustion power calculus have been performed and the results of mass flows and powers entering and exiting the combustion process obtained.

For the Stirling engine, pressures and volumes in all key points of the Stirling cycle with regeneration have been calculated and the operational performances of the Stirling cycle related to the combustion process have been determined.

The useful thermal power delivered to the end user has been also estimated.

The comparison between different fuel moistures and air excesses has served in validating the values found for the adiabatic temperature of combustion with those found in the literature, and an overview of the Stirling engine operating to partial loads showed.

Additionally, a comparison between operational efficiencies has been used to conclude that these efficiencies aim to show that using a dry fuel is recommended for the best useful power outputs.

It is stressed that, if thermal power is not entirely needed, the fuel may have a moisture of up to 20% for the Stirling engine to function at nominal load.

The beforementioned case is intuitively the one of summer season, where the thermal energy need is lower than that of the winter season.

The paramount conclusion of this chapter is that it is therefore crucial to use dry fuel in the cold seasons, to obtain the maximum thermal power available, provided that the system has not been over-dimensioned for the consumer home.

If it is the case, lower quality fuels in terms of moisture can be used, because their thermal output will not create a surplus of thermal power.

In Chapter 5 - Mathematical model for the simulation of transient regimes, the behaviour of the micro-cogeneration unit in various transient regimes of operation is investigated.

For the 32 laboratory tests which have been performed, a transient mathematical model of the fuel mass flow is proposed. The simulations of transient regimes are expected to show that the uncertainty related to the consumption of fuel in the form of wood pellets is significant.

The mathematical model proposed is that of an inverse algorithm. The model input data are considered the production of power, the production of thermal power, the temperatures measured by the sensors inside the micro-cogeneration unit, on the path of the flue gas, from the combustion chamber to the exhaust, as well as different points of the circuit connecting the unit to the consumer.

The model output is the corresponding consumption of fuel, under the form of wooden pellets. The nonlinearities induced by the temperature - dependent physical properties used in the enthalpies' determination is the Gauss - Seidel method.

The inventory of financial performances of investments and the related quantification indices used to economically assess the profitability of an investment are analysed.

Based on the results of the mathematical model which is used to simulate the transient regimes of the μ CHP operation, for a selection of most relevant transient tests, the overall fuel

consumptions of the μ CHP and the related generated amounts of electricity and heat delivered from the μ CHP to the end user are obtained.

For the concerned tests, the results of the mathematical model are used to determine the investment performances.

In correlation with the proposed input data for the investigated case of investment, the results of the economic simulation of the chosen transient regimes of operation will be used to analyse the factors that are influencing the most.

* * *

This doctoral thesis with 232 pages is structured in 5 chapters and conclusions. A brief description in French language is also provided. Chapter 1 has 26 pages, chapter 2 has 14 pages, chapter 3 has 30 pages, chapter 4 has 48 pages and the conclusions cover 5 pages. In addition, the abbreviations used are listed, the bibliography with 98 references and 30 internet pages is included, the dissemination of results containing 6 author's work and the 5 annexes are included, too. The thesis has 106 figures and 77 tables.

CHAPTER 1

BIBLIOGRAPHIC STUDY

1.1. A RENOVATION WAVE FOR EUROPE - GREENING OUR BUILDINGS, CREATING JOBS, IMPROVING LIVES

On 14 July 2021, the European Commission unveiled its plan called the European Green Deal to meet 55% emission reduction by 2030, first step of the carbon neutrality set for 2050.

In line with the provisions of this plan and to pursue this dual ambition of energy gains and economic growth, in 2020 the Commission published a new strategy to boost renovation called ‘A Renovation Wave for Europe - Greening our buildings, creating jobs, improving lives’. This strategy aims to double annual energy renovation rates in the next 10 years. As well as reducing emissions, these renovations will enhance quality of life for people living in and using the buildings, and should create many additional green jobs in the construction sector.

For this strategy’s implementation, the decarbonisation and the integration of renewables, this referring to energy from renewable sources produced on-site or nearby are vital. Building renovation should speed up the integration of renewables in particular from local sources, and promote broader use of waste heat. It should integrate energy systems at local and regional levels helping to decarbonise transport as well as heating and cooling.

Among several areas of intervention identified based on European Commission’s analysis and a public consultation, the promotion of the decarbonisation of heating and cooling, which is responsible for 80% of energy consumed in residential buildings is a key issue. In this respect, modernising the heating and cooling systems of buildings is essential to decarbonise the EU building stock, to deploy local renewable energy potential and to reduce the EU’s dependence on imported fossil fuels.

In the European Union, heating, cooling and domestic hot water account for around 80% of energy consumed in residential buildings. In 2017, two thirds of this energy came from fossil fuels, respectively 76,5%. As indicated by the European Commission, many plants, installations and equipments are old and inefficient and half are beyond their service lifetime (European Commission, Com 662 final, 2020).

Despite the consistent development of the existing district heating systems in several Member States (notably the cases of Denmark and Latvia, countries where the heat supply from district heating is up to 60%), the related share within the European Union overall heat supply market stays only at 12%, against the stand-alone systems which account for 88% of it (European Commission, Com 662 final, 2020).

1.2. CHALLENGES FOR THE ENERGY DEMAND IN THE RESIDENTIAL SECTOR

According to the impact assessment for the 2030 Climate Target Plan, the residential sector would have to undergo the highest reduction in energy demand in heating and cooling, ranging between -19% to -23%, compared to 2015. The annual rate of replacement of heating equipment would have to reach around 4% in both the residential and services sector. During the same time period, the share of renewables and waste heat would have to increase to 38-42% to reach the objective. By 2030 it is presumed that:

- the roofs and walls will increase the green surface of cities and improve the urban climate and biodiversity;
- the buildings will be equipped with smart and digitalised appliances, providing real time data on how, when and where energy is consumed;
- recharging electric vehicles, namely bikes, cars and vans, in residential and office buildings will be a common experience complementing publicly accessible charging infrastructure;
- many more Europeans will be prosumers, producing electricity for self-consumption or even selling it back to the grid and;
- fossil fuels will gradually disappear from heating and cooling.

In line with the goals settled out by the European Commission in terms of emission reduction, the present doctoral thesis is strongly related to the decarbonisation of the heating through the promotion of the modern and effective stand-alone systems using renewable energy sources and to help customers to move from consumers to prosumers (Voronca, 2019), by producing electricity for self-consumption or even selling it back to the grid.

1.3. THE SOLID BIOMASS COMBUSTION MICRO-COGENERATION REPRESENTS AN OPPORTUNITY

The gradual elimination of fossil fuel use within residential stand-alone systems for heating purposes is possible by an increased use of renewable energy sources. As generally known, of all renewable energy resources, biomass is abundant and important (Bernotat, 2004, Motta, 2018).

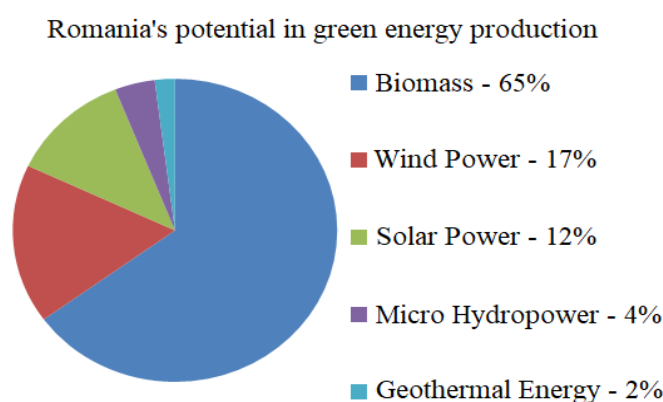


Figure 1.1 - Renewable energy potential in Romania
(source : <https://www.interregeurope.eu/>)

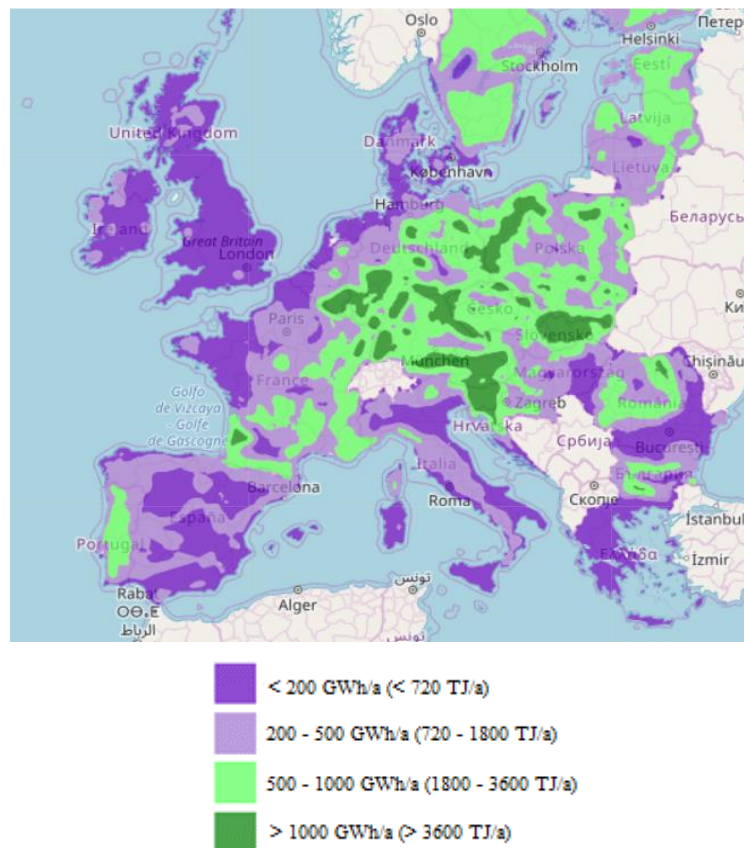


Figure 1.2 – The energy potential of wooden biomasse in Europe
(source : <https://heatroadmap.eu/>)

The previous remark makes reference also to the Romanian (Figure 1.1) and the European (Figure 1.2) energy potential of biomass (Eurobserv'er, 2020). The biomass is the leading source of renewable energy consumed in France (La Tribune, 2019). The available types of biomass, its use at industrial and local level, the applicable standards for biomass are very similar.

The biomass is increasingly used as an alternative fuel for space heating, electricity generation and combined heat and power (Saidur, 2011, Tuțică, 2017).

The biomass is suitable for replacing the fossil fuels that feed the traditional cogeneration system but, because of its intrinsic properties, is considerably more suitable for small- and micro-scale stand-alone cogeneration systems (Damien, 2008).

Biomass encompasses a wide variety of materials: wood from various sources, agricultural residues, and animal and human waste. It consists mainly of complex polymers of carbon, hydrogen, oxygen, nitrogen, suffers in small quantities and inorganic elements (van Loo, 2008, Damien, 2008).

Fuels from solid biomass that can be used by micro-cogeneration systems can be, for example, in the form of wood pellets, logs, wood logs, wafers (van Loo, 2008). The wood heating remains one of the major energy sources used within district heating networks, individual dwellings, collective boiler rooms and public buildings (Sartor, 2014).

The production of heat from solid biomass and, additionally, the simultaneous generation of electricity within the same stand-alone system is considered one of the main contributions to sustainable development.

1.4. THE THERMOCHEMICAL CONVERSION OF BIOMASS THROUGH A DIRECT GRID COMBUSTION TECHNOLOGY

For thermochemical conversion of biomass into energy, the direct combustion process is considered relevant for this work. This is the most technologically simple, less expensive and commonly used process for transforming biomass into primary energy. This combustion is carried out in the presence of oxygen at a temperature above 900 °C generating an energy of the order of 14 to 18 MJ/kg with an efficiency of about 75% (Deglise, 1982).

During the combustion reaction, the fuel first passes through endothermic evaporation to remove moisture from the biomass at a temperature of about 100°C. After evaporation, begins the combustion stage where the decomposition of macromolecules occurs at a temperature of the order of 200 °C forming gases (van Loo, 2008, Evans, 2010). These gases consist mainly of carbon monoxide (CO) and hydrogen (H₂). The latter is at the origin of the flame by oxidizing in contact with the air. For this step, the temperature can rise up to 800 - 1000 °C (Evans, 2010).

The main products of biomass combustion are carbon dioxide (CO₂), water vapor (H₂O), carbon monoxide (CO), and nitrogen oxides (NO_x). Other products can be mentioned, such as dust, volatile organic compounds (VOCs). The solid residue of combustion is the ash. A high ash content gives rise to fouling problems (Mameri, 2018).

When considering the direct combustion, three different combustion techniques for biomass are considered (Wolf, 2013):

- the grid combustion which technologically relies on a process by which solid biomass is placed on a grid and materials are moved slowly through the boiler; the mixture is then burned with air supplied through holes in the grid;
- fluidized bed combustion, where biomass is usually mixed with sand and kept suspended in a mixture with incoming air;
- fuel pulverisation for which the biomass is crushed into powder and burned.

1.5. THE BIOMASS-BASED MICRO-COGENERATION SYSTEMS ARE BECOMING INCREASINGLY POPULAR

Biomass-based micro-cogeneration systems are becoming increasingly popular and various research has been carried out in this area (Mameri, 2018). Studies related to the feasibility of a μ -CHP Rankine system powered by a biomass boiler and a solar collector have been performed (Aoun, 2008, Brou, 2015).

An experimental study and modelling in the TRNSYS environment of two prototype micro-cogeneration reactors, a gas Stirling engine and a wood pellet steam engine (Bouvenot, 2015). The objective of the study was to evaluate the energy and environmental performance of the two cogeneration plants in the configuration where coupling with a building is carried out.

Another work whose objective was to determine the best integration of a heat storage system with a biomass cogeneration plant supplying a district heating network in Liège (Belgium) has been published (Sartor, 2018).

The aim was to minimize the cost of heat from a heating installation by reducing its environmental impacts while respecting the policies put in place by the Belgian government for this type of installation.

When looking to the power generation within micro-cogeneration systems devoted to the residential applications, in the literature is indicated that, in terms of power range, installations of the order of kW_{el} are much more suitable (Bianchi, 2013).

An investigation on the possibilities of using biomass-based cogeneration in Sweden and the Baltic States for group dwellings, led to the conclusion that small-scale cogeneration (annual demand of $500 \text{ MW}_{\text{th}}$) offers great prospects if the total heat demand in a region is sufficiently high (Bernotat, 2004).

Moreover, it was highlighted that such cogeneration system may serve as a backup in case of high demand for electricity, namely delivery of balancing services within the regional or local power systems.

In the case of using solid biomass as a fuel, there are several types of cogenerations which could be suitable for biomass micro-cogeneration units (Mameri, 2018). Among these cogeneration reactors that can be coupled to biomass boilers, the use of Stirling external combustion engines has been indicated as one possible (Arashnia, 2015, Damirchi, 2016).

In France, the micro-cogeneration is considered for unit with a rated power capacity of less than $36 \text{ kW}_{\text{el}}$. The fuels used in cogeneration units, can be of fossil origin or renewable origin such as geothermal energy, solar energy, biogas or biomass.

Among renewable energies, biomass is the only one that allows energy storage in the form of stable hydrocarbon molecules, available to supply heat production facilities (Mameri, 2018).

Currently in France, biomass energy is the most important source of renewable energy. It represents more than half of final energy production and contributes to reducing the consumption of fossil fuels.

The total installed power capacities on solid biomass reached $1,495 \text{ MW}_{\text{el}}$ at the end of 2016 (source: <https://www.ecologie.gouv.fr/biomasse-energie>).

1.6. THE MICRO-COGENERATION SYSTEMS EQUIPPED WITH STIRLING ENGINES

Compared to the internal combustion engines which represent an advanced technology with a relatively good electrical efficiency with an electrical power ranging from 1 to $33 \text{ kW}_{\text{el}}$, the Stirling type with external combustion offer the possibility of using different fuels including wood, and despite a low efficiency compared to their theoretical performance, and a fairly high cost, the micro-cogeneration units using these engines reduce greenhouse gas emissions (Mameri, 2018).

It is shown that a reduction in CO₂ emissions between 500 kg and 1.000 kg per year per household can be achieved for 1 kW_{el} micro-cogeneration units using a Stirling engine (Peacock, 2005).

According to the literature, the Stirling engine appears to be the most mature technology for the use of biomass in the case of micro-cogeneration for small-scale decentralised electricity generation.

Despite their low electrical efficiency, Stirling engines are still used for low-power cogeneration applications thanks to their high thermal efficiency.

In particular, micro-cogeneration units with a Stirling engine have an electrical efficiency between 12 and 35% while the overall efficiency is between 85 and 90% (Kimming, 2011, Maraver, 2013).

An experimental study on a 20 kW_{th} wood pellet burner coupled to a Stirling engine has been conducted (Cardozo, 2014).

The influence of several parameters on the energy performance of the Stirling engine has been investigated: the type of pellets used, the fouling of the engine head due to the unburned, the impact of the distance between the burner and the head of the Stirling engine and the cyclic operation of the engine.

As expected, the conclusion was that the heat exchange at the head gradually deteriorates with fouling and that the thermal efficiency depends strongly on the position of the engine relative to the burner.

The overall efficiency of the system has been estimated at 72%.

A similar study on a biomass micro-cogeneration unit with a gamma-type Stirling engine with the rated power of the unit is of the order of 100 W was performed (Arashnia, 2015).

The results show that a maximum efficiency of 16% is achieved for a moderate speed of the Stirling engine of about 500 - 600 rpm. Moreover, the tests have confirmed the fact that the Stirling engines are capable of achieving a very high-power output.

The thermal efficiency of the Stirling engine has been increased by 20%. The authors concluded that the results are encouraging to initiate the design of a one kW micro-cogeneration system for rural electrification.

Finally, another dedicated study has revealed that, unlike the internal combustion engine, Stirling engines require little maintenance and are quiet (Monteiro, 2009).

In consequence, a solid biomass combustion micro-cogeneration system equipped with a Stirling engine is experimentally and theoretically investigated.

1.7. ENGINES GENERALITIES

1.7.1. Heat transfer

The 2nd law of thermodynamics expressed by German physicist and mathematician Rudolph Clausius through the “Clausius statement” states that heat can only be transmitted from a higher temperature source to a lower temperature source (Kirilin, 1976). The amount of heat flow is proportional to the slope of the temperature decrease at the point of flow and with the substances’ thermal conductivity (Rohsenow, 1973, Voronca, 1997):

$$\delta Q = -k \cdot S \cdot \left(\frac{\delta T(x; t)}{\delta x} \right) \cdot \delta t \quad (1.1)$$

Table 1.1 - The parameters from the relation (1.1)

Symbol	Parameter	Measuring unit
δQ	quantity of heat	Joule (J)
S	cylinder surface	Square meters (m ²)
δx	distance traversed by the quantity of heat δQ	Meters (m)
δt	time necessary for the quantity of heat δQ to traverse the distance δx	Seconds (s)

The notation $\frac{\delta T(x,t)}{\delta x}$ represents the partial derivative of the temperature T (at an arbitrary point x , to which the t moment in time corresponds) by the total distance δx travelled by the heat flux δQ . It can be referred to as the slope of temperature. The coefficient of proportionality in relation (1.1) is k , which is the thermal conductivity of the substance, expressing its ability to conduct heat. It is measured in Watt (which is Joules divided by second) divided by the product of Kelvin and meter ($\frac{W}{(m \cdot K)}$). The relation (1.1) expresses that the quantity of heat δQ (Joule) traversing the surface S (m²) for a set amount of time δt (seconds), is proportional to the temperature drop δT (Kelvin) found at point x and time t , over a short distance δx (meters) considering the direction of the flow. The minus sign indicates that the flow is in the direction of the temperature drop.

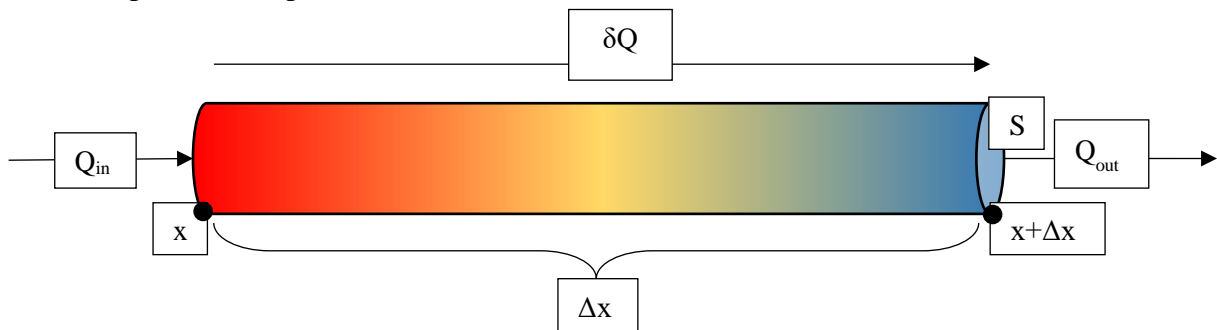


Figure 1.3 - Cylinder through which heat passes

In a cylinder like in Figure 1.3., with a section (S) and thickness (Δx), the net quantity of heat which enters the cylinder (δQ) is that which enters at point x and leaves at $(x + \Delta x)$ in the amount of time (δt), as shown in the relations (1.2) - (1.3).

$$\delta Q = k \cdot S \cdot \left(\frac{\delta T(x + \Delta x; t)}{\delta x} - \frac{\delta T(x; t)}{\delta x} \right) \cdot \delta t \quad (1.2)$$

$$\delta Q = \rho \cdot c \cdot \delta T \cdot (S \cdot \Delta x) \quad (1.3)$$

Table 1.2 - The parameters from the relations (1.2) - (1.3)

Symbol	Parameter	Measuring unit
δQ	quantity of heat	J
ρ	substance density	kg/m ³
c	heat transfer coefficient or specific heat	W/(m ² · K)
δT	temperature increase	K
S	cylinder surface	m ²
Δx	distance traversed by the quantity of heat δQ	m
$S \cdot \Delta x$	volume traversed by the quantity of heat δQ	m ³

The relation (1.3) shows that when a quantity of heat (δQ) enters a volume containing a substance ($S \cdot \Delta x$), there is a temperature increase (δT). This increase is proportional to the quantity of heat received and inversely proportional to the volume ($S \cdot \Delta x$), substance density (ρ) and substance specific heat (c_p).

The heat transfer coefficient or specific heat (c_p) expresses the amount of heat necessary in order to raise the temperature of 1 kilogram of the substance by 1 degree (Celsius or Kelvin). For compressible gasses, the quantity differs depending on whether the operation is done at constant volume (c_v) or constant pressure (c_p).

By combining relation (1.2) and relation (1.3), the relation (1.4) is obtained:

$$\rho \cdot c \cdot \delta T \cdot (S \cdot \Delta x) = k \cdot S \cdot \left(\frac{\delta T(x + \Delta x; t)}{\delta x} - \frac{\delta T(x; t)}{\delta x} \right) \cdot \delta t \quad (1.4)$$

and the relation (1.5):

$$\frac{\delta T}{\delta t} = \frac{k}{\rho \cdot c} \cdot \frac{\left(\frac{\delta T(x + \Delta x; t)}{\delta x} - \frac{\delta T(x; t)}{\delta x} \right)}{\Delta x} \quad (1.5)$$

The relation (1.5) shows that the temperature increase (δT) during the amount of time (δt), varies according to the variation of the temperature slope ($\delta T/\delta x$), over the distance (Δx). The coefficient of proportionality of this equation is $k/(\rho \cdot c)$ which is the thermal conductivity of the substance (k) divided by the substance density (ρ) and by the heat transfer coefficient or specific heat (c). By setting the distance Δx to 0, Equation (1.5) becomes the partial differential equation of heat, which is relation (1.6).

$$\frac{\delta T}{\delta t} = \frac{k}{\rho \cdot c} \cdot \frac{\delta^2 T}{\delta x^2} \quad (1.6)$$

1.7.2. Engines thermodynamic cycles

1.7.2.1. Carnot cycle

It was proposed by the French physicist Said Carnot in 1824 and it is a theoretical construct which expresses the utmost limit of efficiency that a thermodynamic engine can provide

(Kirillin, 1976). It describes a state in which a thermodynamic system exists, by cyclically performing processes which delivers work or heat to its surroundings.

Whether a piston is moved by transforming the heat into mechanical work, or heat is extracted or delivered into a system. The “Carnot heat engine” by which a system respecting the Carnot cycle is called, is a purely theoretical construct and cannot be built, due to its’ “perfection” (Giordano, 2009).

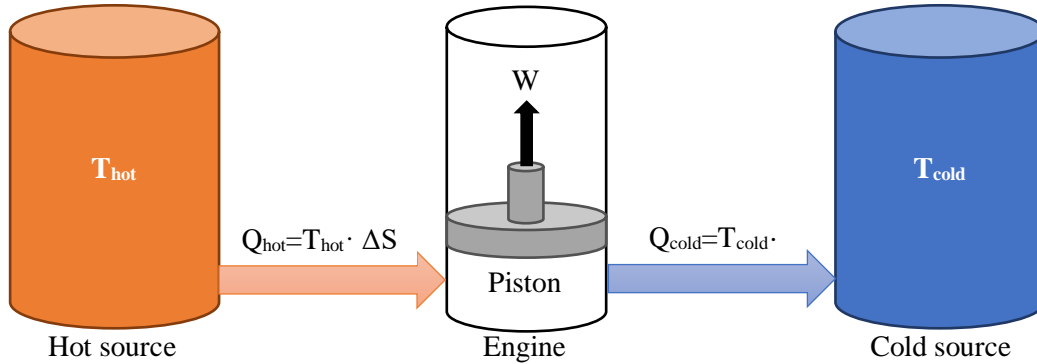


Figure 1.4 - The principle of the Carnot cycle

The construct is defined in Figure 1.4 by 2 reservoirs of heat with different temperatures, defined as T_{hot} and T_{cold} . The thermal capacity is so large, that the temperatures are unchanged by a single cycle. The reversibility of the cycle (whose direction can be reversed with infinitesimal changes to the systems’ properties) results in no generation of entropy, which is conserved. An amount of entropy (ΔS) is transferred from the hot source, to the cold source.

There is no work being done, since the volume is constant and an amount of energy ($T_{hot} \cdot \Delta S$) leaves the hot reservoir, while a smaller amount of energy ($T_{cold} \cdot \Delta S$) is received by the cold reservoir. The work performed by the engine is the one resulted from this process ($T_{hot} \cdot \Delta S - T_{cold} \cdot \Delta S$).

$$Q_{hot} = T_{hot} \cdot \Delta S \tag{1.7}$$

$$Q_{cold} = T_{cold} \cdot \Delta S \tag{1.8}$$

$$W = Q_{hot} - Q_{cold} = T_{hot} \cdot \Delta S - T_{cold} \cdot \Delta S = \Delta S \cdot (T_{hot} - T_{cold}) \tag{1.9}$$

Table 1.3 - The parameters from the relations (1.7) - (1.9)

Symbol	Parameter	Measuring unit
Q_{hot}	hot source heat	J
Q_{cold}	cold source heat	J
T_{hot}	heat transfer coefficient or specific heat	K
T_{cold}	temperature increase	K
ΔS	entropy	J/K

In Figure 1.5, the pressure - volume (p -V) and temperature - entropy (T - s) diagrams of the Carnot cycle are shown. The cycle is formed by 2 isothermal stages and 2 adiabatic stages. The theoretical process is ideal and reversible. Temperature remains constant from point 1 to point

2 ($T_1=T_2$) and from point 3 to point 4 ($T_3=T_4$) and there is no heat transfer from point 2 to point 3 ($Q_{23}=0$) or from point 4 to point 1 ($Q_{41}=0$).

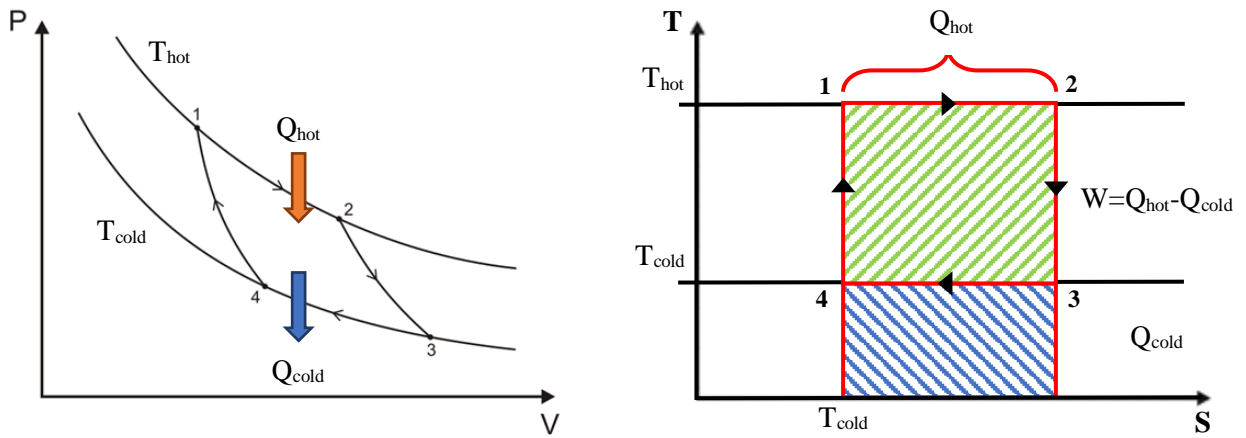


Figure 1.5 - The Carnot Cycle: pressure - Volume and Temperature - entropy diagrams

The theoretical thermodynamic efficiency of the Carnot Cycle is defined in the relation (1.10). Since there is no loss of entropy when transferring energy from the hot source to the engine (ΔS_1) or when transferring it from the engine to the cold source (ΔS_2), the two are equal and defined as the same differential of entropy ($\Delta S_1 = \Delta S_2 = \Delta S$).

$$\eta_{th,Carnot} = \frac{W}{Q_{hot}} = \frac{Q_{hot} - Q_{cold}}{Q_{hot}} = \frac{\Delta S_1 \cdot T_{hot} - \Delta S_2 \cdot T_{cold}}{\Delta S_1 \cdot T_{hot}} = 1 - \frac{T_{cold}}{T_{hot}} \quad (1.10)$$

When applying heat to a real material, its entropy changes with temperature. Carnot's theorem states that there can be no engine that operates between 2 heat sources more efficiently than a Carnot cycle operating between the same sources.

Figure 1.6 shows the difference in cycle between a real engine cycle and the Carnot cycle in Temperature - entropy coordinates. Upon fluid expansion, the entropy is increased and upon compression it is decreased. The fluid changes state from liquid to liquid and vapour (and even vapour if in superheated mode). The engine is not frictionless, therefore additional losses appear.

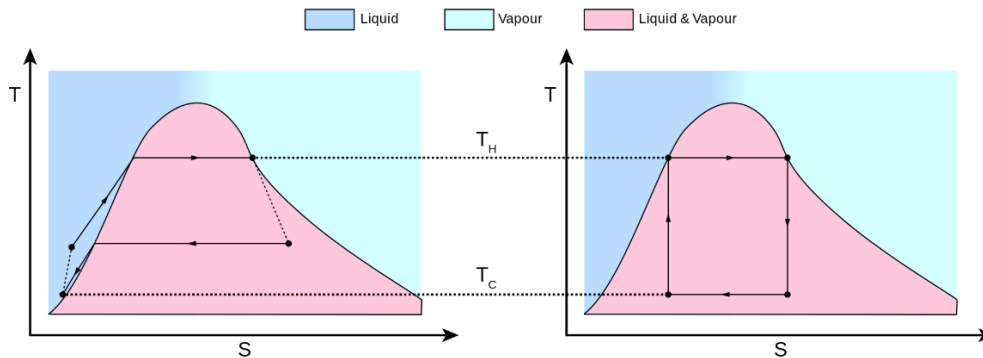


Figure 1.6 - Comparison between real engines cycle (left) and Carnot cycle (right) (Source: Giordano, 2009)

The Carnot cycle, as a heat engine has 4 stages.

The first one is isothermal expansion, through which the system receives heat from the hot source, the second one is reversible adiabatic expansion, through which the engine delivers work by raising the piston, the third one is the adiabatic expansion, through which heat is transferred to the cold source and the fourth one, through which the internal energy of the gas is increased and the cycle is repeated.

Stage 1: Isothermal expansion ($1 \rightarrow 2$).

From the hot source of the cycle, heat (Q_{hot}) is reversibly transferred at a constant temperature (T_{hot}) through isothermal heat addition or absorption, as shown in Figure 1.7.

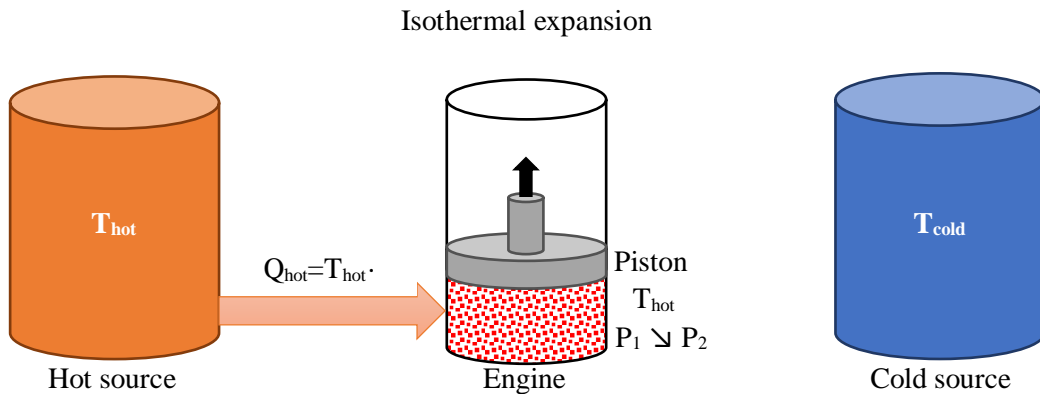


Figure 1.7 - Carnot Engine Stage 1: Isothermal expansion

The gas inside the piston expands and work is done through pushing the piston upwards. In this stage, the pressure drops, but the temperature (T_{hot}) remains constant due to its thermal contact with the hot source, therefore the expansion is isothermal. The heat absorbed by the piston (Q_{hot}) results in an increase of entropy (ΔS_1).

Stage 2: Reversible adiabatic expansion ($2 \rightarrow 3$)

Inside the engine, its gas is thermally insulated from both sources, its heat remains constant through an adiabatic process, as shown in Figure 1.8.

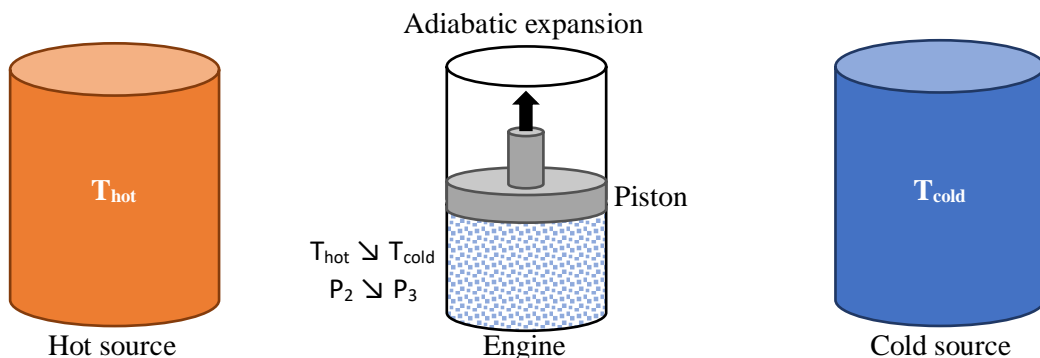


Figure 1.8 - Carnot Engine Stage 2: Adiabatic expansion

The expansion of gas results in a pressure reduction and work is done on the surrounding by raising the piston. The amount of work is equal to the amount of internal energy lost during this process. Without heat input, gas temperature drops (T_{cold}), while the entropy remains unchanged.

Stage 3: Isothermal compression ($3 \rightarrow 4$)

At a constant lower temperature (T_{cold}), heat is transferred to the cold source through the process of isothermal heat rejection, as shown in Figure 1.9.

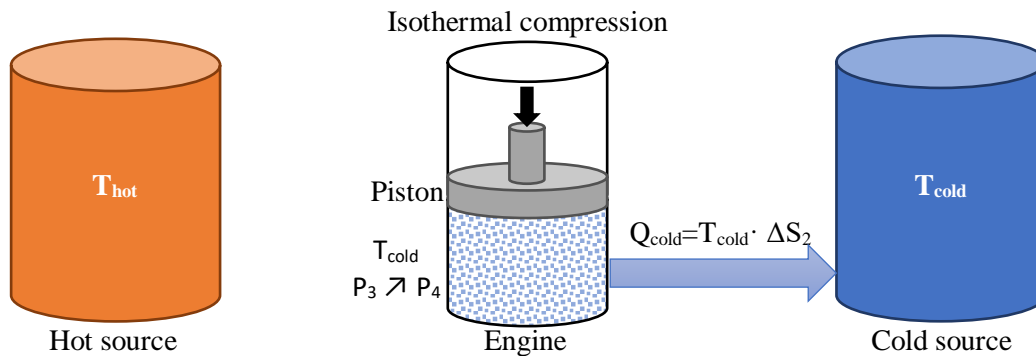


Figure 1.9 - The Carnot Engine Stage 3: Isothermal compression

Inside the engine, the cold source is now in thermal contact with the gas. Work is being done on the gas by its surroundings, pushing the piston down, resulting in an amount of energy (Q_{cold}) to leave the engine towards the cold source, leading to a decrease in entropy (ΔS_2). The amount of entropy remains conserved ($\Delta S_1 = \Delta S_2$) due to the Clausius equality (Kirillin, 1976).

Stage 4: Reversible adiabatic compression ($4 \rightarrow 1$)

Inside the engine the gas is thermally insulated from both the hot source and the cold source, as shown in Figure 1.10.

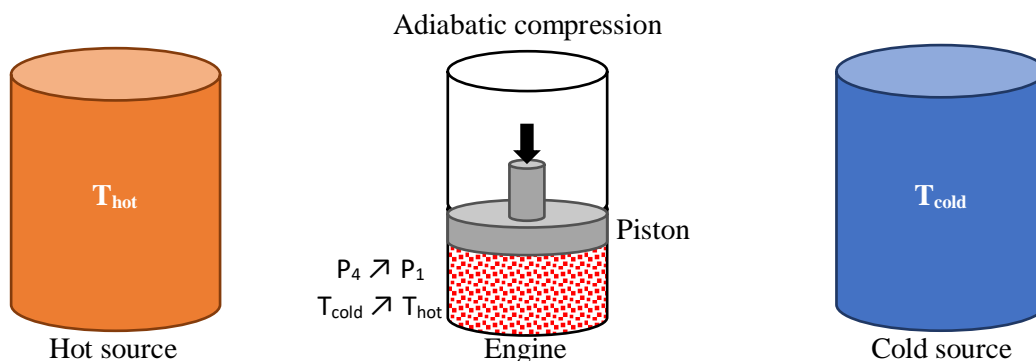


Figure 1.10 - The Carnot Engine Stage 4: Adiabatic compression

The engine is considered frictionless; therefore, the process is reversible. Work is being done on the gas by its surroundings by continuing to push the piston downwards, leading to an increase into its internal energy and to an increase in temperature (T_{hot}).

1.7.2.2. Stirling cycle

The Stirling engine was invented by Robert Stirling in 1816 (Gras, 2015, Kolin, 1991). He introduced the concept of fuel economy through a regenerator used in its closed-cycle design. The engine was built as an alternative to steam engines used at the time, but proved challenging to use on long-term, due to material limitations at the time. Its use has been reimplemented by

the Dutch company “Philips” in the 20th century (Hargreaves, 1991), due to its malleability to a multitude of heat sources and its silent operation (both audibly and radio interference).

In 2003 the first combined-heat and power units were commercialized in domestic applications. Stirling engines can also be used in solar applications, by pairing with a solar concentrator.

In the literature (Sarkat, 2015) is indicated that the working medium of the Stirling Engine is gaseous matter (i.e., air, hydrogen, helium, nitrogen etc.). It operates through cyclic expansion and compression of gas at different temperatures, in order to produce a net conversion of energy in the form of heat to that of mechanical work.

In the literature (Invernizzi, 2010), is indicated that in modern Stirling engines, the working fluids are usually helium or hydrogen for engines of high performances. Both, helium and hydrogen, present good thermo-physical characteristics, and allow the design of engines with high heat fluxes and moderate pressure losses (Invernizzi, 2010).

The literature (Dong, 2019) provides a detailed comparison between the helium, nitrogen and argon utilized as the working fluids which led to the conclusion that it is appropriate to select helium as the working fluid in the current operational conditions. To support this recommendation, in this study, the following particularities have been observed (Dong, 2019).

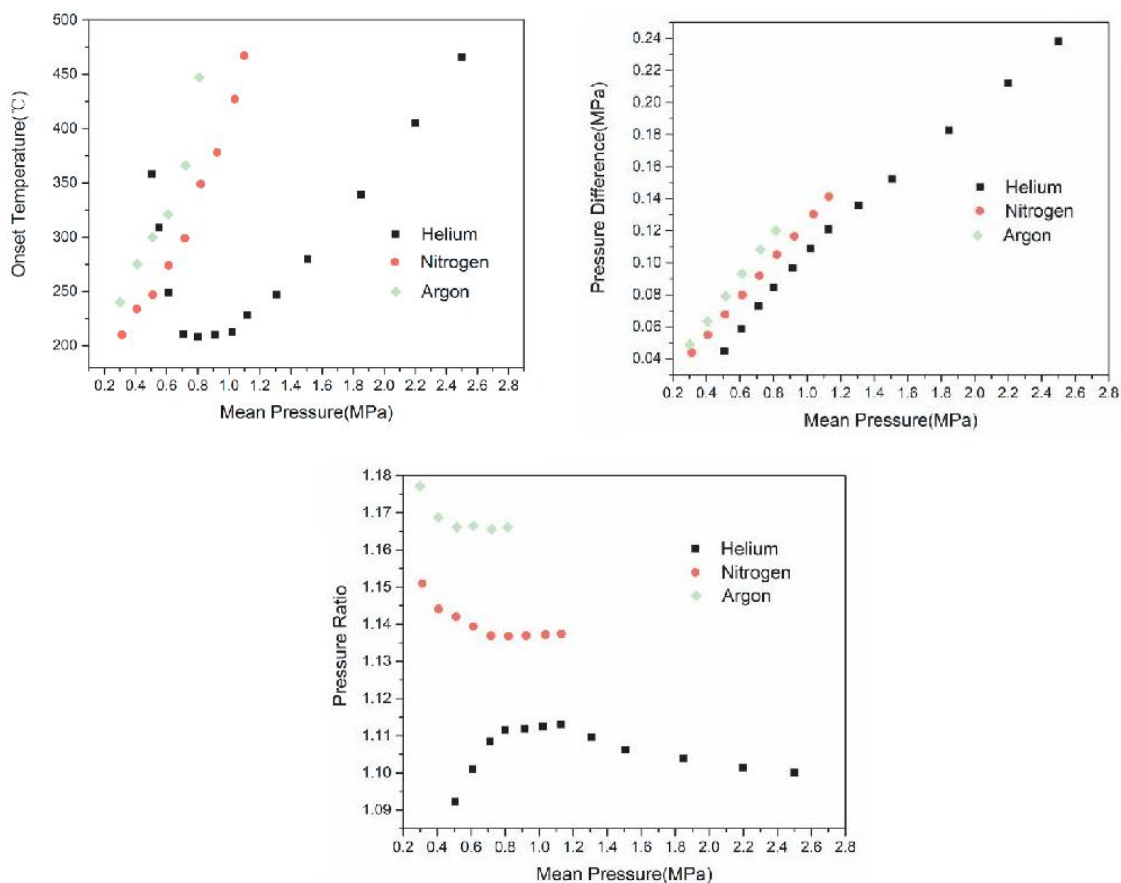


Figure 1.11 - Dependence of the pressure difference and pressure ratio with the mean pressure
 (Source: Dong, Sh., Shen, G. Xu, M. Zhang, Sh., An, L., *The effect of working fluid on the performance of a large-scale thermoacoustic Stirling engine*, Energy, Volume 181, Elsevier, 2019, pp. 378-386.)

For helium, to obtain the lowest onset temperature of 205 °C, the relatively optimum mean pressure is 0.7 - 1.0 MPa, against the nitrogen and argon which can only operate in low-pressure area (below 1.2 MPa) when utilizing low-temperature waste heat (Figure 1.9). Working frequency of helium is nearly three times that of nitrogen and argon regardless of operating conditions; the mean pressure and heating temperature barely influence the working frequency. The pressure ratio of helium has the optimum value with the variation of mean pressure (1.1 MPa), while the maximum pressure ratio of nitrogen and argon can only be obtained in the low-pressure area (Figure 1.11).

The ideal Stirling cycle is reversible, because the engine produces power or work when the gas is heated and vice-versa, when power or work is introduced in the cycle, it functions like a heat pump or refrigerator (Figure 1.12).

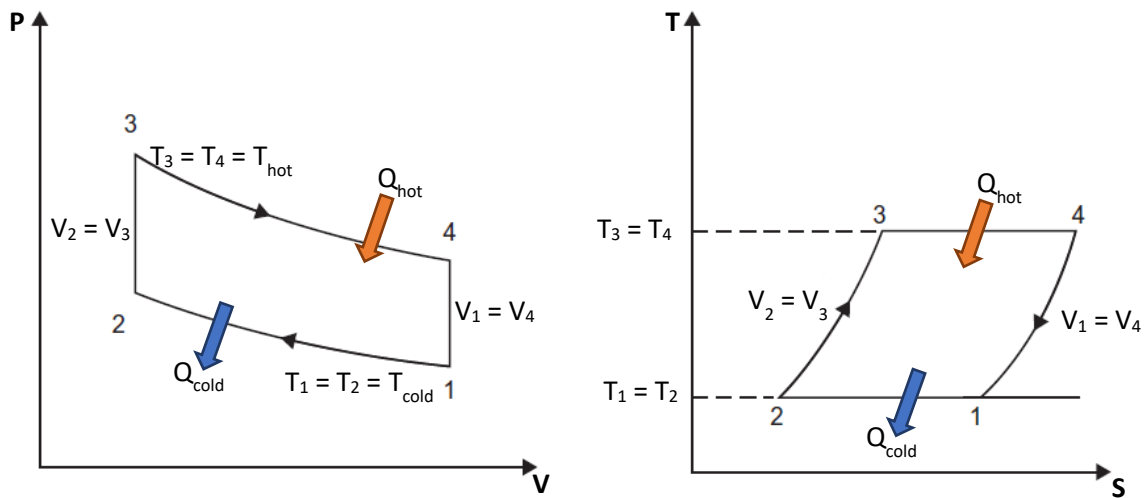


Figure 1.12 - The Stirling Cycle: pressure - Volume and Temperature - entropy diagrams

The reversed Stirling cycle is used in the field of cryogenics to attain low temperatures to liquify helium (-269 °C) or hydrogen (-252.87 °C).

The Stirling Engine is comprised of two pistons inside a cylinder, separated by a regenerator. It does not exchange working gas in each cycle, the gas is permanent, unlike internal combustion engines. The heat of the hot source is supplied from outside the working environment, allowing any heat source to be used (biomass, solar, gas, etc.). The Stirling Engine has higher thermal efficiencies in comparison Otto and Diesel Engines, because the heat transfer occurs at constant temperatures, therefore having a thermal efficiency identical to the Carnot Cycle as shown in Formula 1.11.

$$\eta_{th,Stirling} = 1 - \frac{T_{cold}}{T_{hot}} \quad (1.11)$$

The Stirling cycle has few maintenance points and is quiet, because of its uniform torque, smooth pressure changes and lack of valves and exhaust pipes. One downside is that it needs high pressures in order to work at competitive efficiency, which may cause important sealing problems. Another is that the temperature difference between the hot source (T_{hot}) and the cold source (T_{cold}) should be maintained high for a good thermal efficiency, which causes cylinder stress at both hot and cold ends, requiring the use of high strength materials, which are expensive.

The gasses commercially used (Helium or Hydrogen) are ideal, because of their faster heat transfer due to low molecular mass and high heat conductivity. The Stirling cycle is only suitable for domestic applications, because it cannot sustain fast changes in power output, therefore excluding automotive applications.

1.7.3. Types of Stirling engines

An exhaustive analysis was performed on the different configurations and their domains of usage (Egas, 2018). There are 3 main configurations, distinguishable between the manner in which the air is moved between the hot source and the cold source:

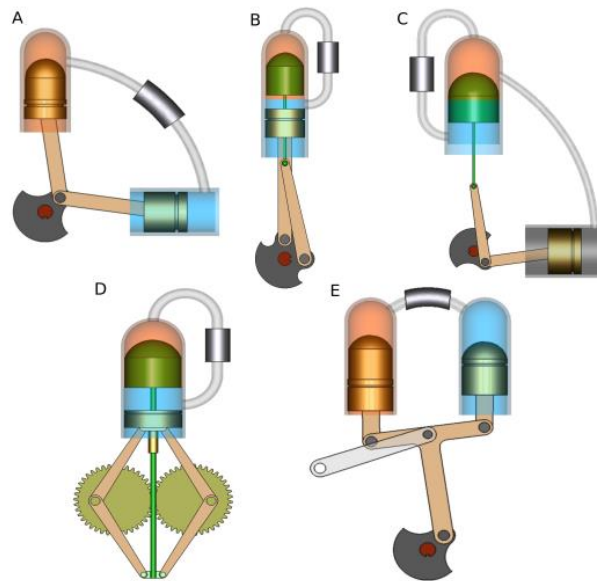


Figure 1.13 - Configurations of Stirling Engines (Egas, 2018)

The Alpha configuration shown in Figure 1.13 A, in which there is one piston in the hot source cylinder and one piston in the cold source cylinder, while the gas is driven between the two cylinders by the pistons, which are joined on a crankshaft at the same point. The Alpha configuration can also have a Ross yoke instead of a crank drive, as shown in Figure 1.13 E.

The Beta configuration shown in Figure 1.13 B, in which a single cylinder being in contact with both the hot source and the cold source, contains a piston and a displacer that pushes the gas between the hot and cold parts. The Beta configuration can also have a rhombic drive that replaces the crank, as shown in Figure 1.13 D.

In the Gamma configuration shown in Figure 1.13 C, one cylinder contains a displacer, connected to a hot source and a cold source and the other cylinder contains a power piston. The two pistons are joined and placed in parallel to form a single space, to distribute pressure evenly on the cylinders. A crankshaft joins the two pistons at a 90° phase-out.

1.7.4. Parameters of Stirling engines

For the Stirling engines, the essential parameters to determine the performances of the ideal cycle are the volume of compression (V_{comp}), which is a variable parameter, the volume of

expansion (V_{exp}), which is variable, too, the volume of cooling (V_{comp}), which is constant and the volume of regeneration of heat, which is constant. Finally, the angle of compression (φ) is variable and relevant for all parameters.

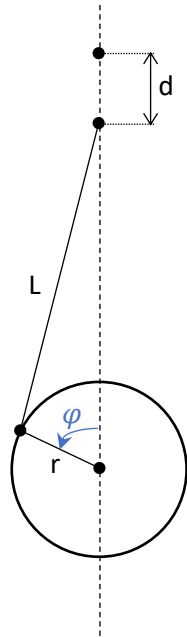


Figure 1.14 - "Slider-crank" mechanism

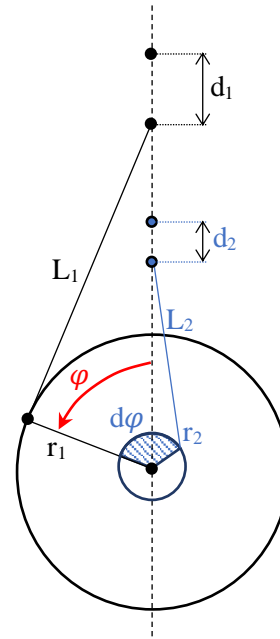


Figure 1.15 - "2 piston" configuration

Table 1.4 - Generic notations for piston configuration

d	displacement	m
φ	crank rotation	°
r	crank range	m
L	crank length	m
$d\varphi$	phase shift (piston - piston or piston - displacer)	°

In the case of the slider - crank mechanism (typically for 1 piston configuration), the movement of the mobile engine parts is due to a uniform rotation ω of a motor shaft cyclically from 0° to 360° . In Figure 1.14, the principle of a slider-crank mechanism is presented. The displacement is calculated with the relation (1.12):

$$d = r \cdot (1 - \cos \varphi) + \frac{1}{2} \cdot \lambda \cdot r \cdot \sin^2 \varphi, \quad (1.12)$$

where λ is the ratio between the range and the length (relation 1.13):

$$\lambda = \frac{r}{L}. \quad (1.13)$$

If the section of the piston (S_{piston}) is known, the volume of gas (V_{gas}) which is found above the piston could be calculated for any given angle (φ):

$$V_{gas} = d \cdot S_{piston}. \quad (1.14)$$

In the case of the Alpha configuration, where there are 2 pistons (Figure 1.15), or in the case of the Beta and Gamma configurations, where there is a piston and a displacer, the phase shift between the pistons or piston and displacer ($d\varphi$) should be considered (Grass, 2015):

$$d_2 = r_2 \cdot [1 - \cos(\varphi - d\varphi)] + \frac{1}{2} \cdot \lambda_2 \cdot r_2 \cdot \sin^2(\varphi - d\varphi), \quad (1.15)$$

where is the ration between the range and the length (relation 1.16):

$$\lambda_2 = \frac{r_2}{L_2}. \quad (1.16)$$

The relations (1.12) and (1.13) are similarly used to determine the displacement d_1 , like in the case of determination of the displacement d for the "1 piston" configuration.

Depending on the gas that has been chosen inside the Stirling Engine, its mass should be determined using the relation (1.17) which is the equation Clapeyron - Mendeleev (Kirillin, 1976):

$$m = \mu \cdot \frac{p \cdot V}{R \cdot T}. \quad (1.17)$$

For all three types of Stirling Engines, the expansion volume V_{exp} , is calculated through the relation (1.18):

$$V_{exp} = S_{exp} \cdot r_{exp} \cdot (1 - \cos \varphi) + \frac{1}{2} \cdot S_{exp} \cdot \lambda_{exp} \cdot r_{exp} \cdot \sin^2 \varphi \quad (1.18)$$

The volume of compression V_{comp} , however, is calculated differently for each of the 3 configurations (i.e., Alpha, Beta and Gamma).

For the Alpha configuration, the relation (1.19) is applied:

$$V_{comp} = S_{comp} \cdot r_{comp} \cdot (1 - \cos(\varphi - \delta \cdot \varphi)) + \frac{1}{2} \cdot S_{comp} \cdot \lambda_{comp} \cdot r_{comp} \cdot \sin^2 \varphi. \quad (1.19)$$

For the Beta configuration, the relation (1.20) is applied:

$$V_{comp} = S_{comp} \cdot r_{comp} \cdot (1 - \cos(\varphi - \delta \cdot \varphi)) + \frac{1}{2} \cdot S_{comp} \cdot \lambda_{comp} \cdot r_{comp} \cdot \sin^2 \varphi - V_{exp}. \quad (1.20)$$

For the Gamma configuration, the relation (1.21) is applied:

$$V_{comp} = S_{comp} \cdot r_{comp} \cdot (1 - \cos(\varphi - \delta \cdot \varphi)) + \frac{1}{2} \cdot S_{comp} \cdot \lambda_{comp} \cdot r_{comp} \cdot \sin^2 \varphi + V - V_{exp}. \quad (1.21)$$

The compression ratio which is normally the ration between the expansion volume and the compression volume can be determined, in the case of applications with large dead volume with the empirical relation (1.22) found in literature (Egas, 2018, Kolin, 1991):

$$CR_K(T_{hot}; T_{cold}) = 1 + \frac{T_{hot} - T_{cold}}{1100}. \quad (1.22)$$

The relation (1.22) has been developed by Ivo Kolin from the Inter University Center Dubrovnik, Croatia.

1.7.5. Stirling engine ideal cycle

For a Stirling engine ideal cycle (Figure 1.16), the following hypotheses are considered. The $1 \rightarrow 2$ and $3 \rightarrow 4$ transformations are isothermal, therefore the temperature of the hot side (T_H) stays constant throughout the $1 \rightarrow 2$ transformations, the relation (1.23) and the temperature of the cold side (T_C) stays constant throughout the $3 \rightarrow 4$ transformations, the relation (1.24), so that the following are established:

$$T_H = T_1 = T_2 \quad (1.23)$$

$$T_C = T_3 = T_4 \quad (1.24)$$

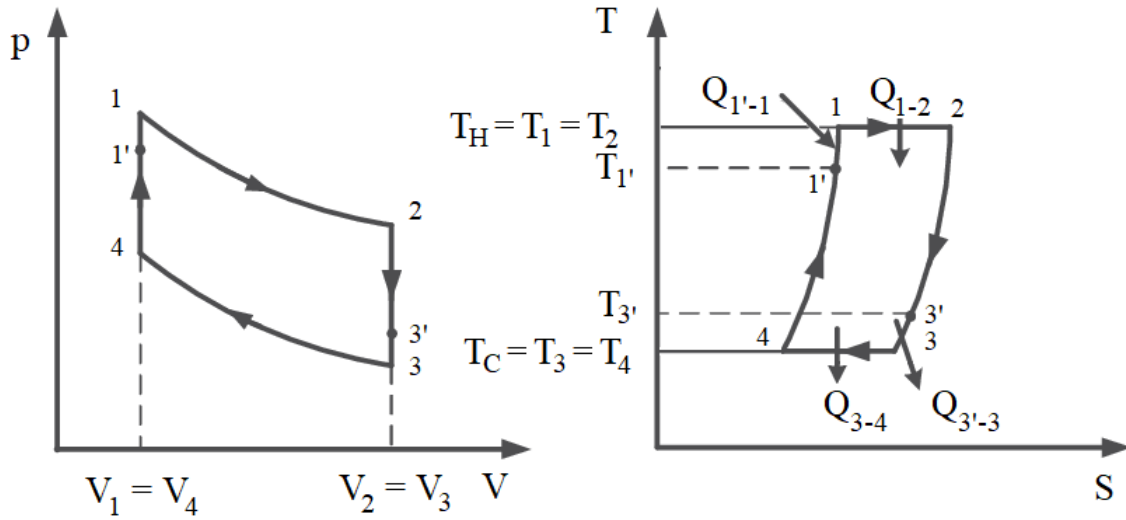


Figure 1.16 - Stirling engine ideal cycle (Dobre, 2012)

The Stirling engine integrate to a micro-cogeneration system is presented in the Figure 1.17.

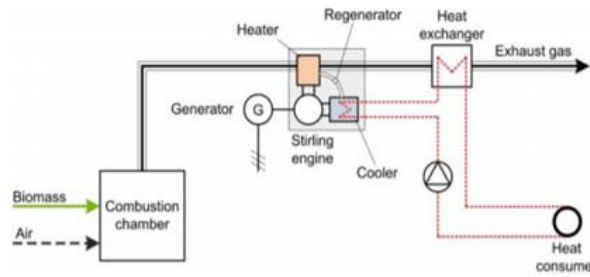


Figure 1.17 - Stirling engine integrated to a micro-cogeneration system (van Loo, 2008)

The $2 \rightarrow 3$ and $4 \rightarrow 1$ transformation are isochore, therefore the volume remains maximum (V_{\max}) throughout the $2 \rightarrow 3$ transformations, the relation (1.25) and it remains minimum (V_{\min}) throughout the $1 \rightarrow 4$ transformations, the relation (1.26). The compression ratio between the maximum and minimum volume is ε (1.27) and its value is known.

$$V_{\max} = V_2 = V_3, \quad (1.25)$$

$$V_{\min} = V_1 = V_4, \quad (1.26)$$

$$\varepsilon = \frac{V_{\max}}{V_{\min}}. \quad (1.27)$$

The only pressure known is the maximum one, in point 1 (1.28):

$$p_{\max} = p_1. \quad (1.28)$$

The data has been centralized in Table 1.5.

Table 1.5 - Input data for calculation

Point	Pressure	Volume	Temperature
1	$p_1 = p_{\max}$	$V_1 = V_{\min}$	$T_1 = T_H$
2	p_2	$V_2 = V_{\max}$	$T_2 = T_H$
3	p_3	$V_3 = V_{\max}$	$T_3 = T_C$
4	p_4	$V_4 = V_{\min}$	$T_4 = T_C$

1.7.5.1. Isothermal transformation 1 → 2

The pressure of the 2nd point is determined in Equation (1.29). The temperature of the hot source remains constant, in accordance to the relation (1.23) which defines the isothermal transformation and the pressure is determined as a product of known parameters through the relation (1.26), since the ratio of volumes is known.

$$\frac{p_1 \cdot V_1}{T_1} = \frac{p_2 \cdot V_2}{T_2} \xrightarrow{(1.23)} p_2 = p_1 \cdot \frac{V_1}{V_2} \xrightarrow{(1.27)} p_2 = p_{\max} \cdot \frac{1}{\varepsilon} \quad (1.29)$$

1.7.5.2. Isochore transformation 2 → 3

The pressure of the 3rd point is determined in the relation (1.30). The volume remains constant, in accordance to the relation (1.25) - which defines the isochore transformation, and the pressure is determined using the values for the pressure in the 2nd point as defined in the relation (1.29).

$$\frac{p_2 \cdot V_2}{T_2} = \frac{p_3 \cdot V_3}{T_3} \xrightarrow{\text{Eq.(1.25)}} p_3 = \frac{p_2 \cdot T_3}{T_2} \xrightarrow{\text{Eq.(1.29)}} p_3 = \frac{p_1 \cdot V_1}{V_2} \cdot \frac{T_3}{T_2} \xrightarrow{\text{Eq.(1.27)}} p_3 = \frac{p_{\max}}{\varepsilon} \cdot \frac{T_C}{T_H} \quad (1.30)$$

1.7.5.3. Isothermal transformation 3 → 4

The pressure of the 4th point is determined in the relation (1.31). The temperature of the cold source remains constant in accordance to the relation (1.24) - which defines the isothermal transformation, and the pressure is determined as a product of known parameters as defined in the relation (1.30).

$$\begin{aligned} \frac{p_3 \cdot V_3}{T_3} &= \frac{p_4 \cdot V_4}{T_4} \xrightarrow{\text{Eq.(1.24)}} p_4 = p_3 \cdot \frac{V_3}{V_4} \xrightarrow{\text{Eq.(1.24)}} p_4 = \left(\frac{p_{\max}}{\varepsilon} \cdot \frac{T_C}{T_H} \right) \cdot \frac{V_{\max}}{V_{\min}} \xrightarrow{\text{Eq.(1.27)}} p_4 \\ &= p_{\max} \cdot \frac{T_C}{T_H} \end{aligned} \quad (1.31)$$

1.7.5.4. Isochore transformation 4 → 1

To verify the relation (1.29), the relation (1.30) and the relation (1.31), the pressure in the 1st point must be the maximum one, as shown in the relation (1.32). The volume remains constant - which defines the isochore reaction, and the pressure is determined as a product of known parameters as defined in the relation (1.31).

$$\frac{p_4 \cdot V_4}{T_4} = \frac{p_1 \cdot V_1}{T_1} \xrightarrow{\text{Eq.(1.26)}} p_1 = \frac{p_4 \cdot T_1}{T_4} \xrightarrow{\text{Eq.(1.27)}} p_1 = p_{\max} \cdot \frac{T_C}{T_H} \cdot \frac{T_H}{T_C} \rightarrow p_1 = p_{\max} \quad (1.32)$$

The isothermal transformation of 1 → 2 is described by the relation (1.33).

$$p_1 \cdot V_1 = p_2 \cdot V_2 = p \cdot V = ct \quad (1.33)$$

The heat received by the hot side in the isothermal reaction 1 → 2 is described in the relation (1.34), since the product of pressure and volume is constant as shown in the relation (1.33).

$$Q_{1 \rightarrow 2} = \int_{V_1}^{V_2} p \, dV \stackrel{\text{Eq.(1.33)}}{=} Q_{1 \rightarrow 2} = \int_{V_1}^{V_2} \frac{ct}{V} \, dV = ct \int_{V_1}^{V_2} \frac{dV}{V} = p_1 \cdot V_1 \cdot \ln \frac{V_2}{V_1} = p_1 \cdot V_1 \cdot \ln \varepsilon. \quad (1.34)$$

The ideal gas law of the state 1 is stated in the relation (1.35).

$$m \cdot R \cdot T_1 = p_1 \cdot V_1. \quad (1.35)$$

The heat received by the hot side in the isothermal reaction $1 \rightarrow 2$ can therefore be described through the relation (1.36).

$$Q_{1 \rightarrow 2} = m \cdot R \cdot T_1 \cdot \ln \varepsilon. \quad (1.36)$$

Similarly, the heat released by the cold side in the isothermal reaction $3 \rightarrow 4$ can be described in the relation (1.37).

$$Q_{3 \rightarrow 4} = p_3 \cdot V_3 \cdot \ln \frac{1}{\varepsilon} = m \cdot R \cdot T_3 \cdot \ln \frac{1}{\varepsilon}. \quad (1.37)$$

The amount of work produced is the difference between the 2 heat exchanges and is described in the relation (1.38).

$$W = Q_{1 \rightarrow 2} - |Q_{3 \rightarrow 4}| = m \cdot R \cdot (T_1 \cdot \ln \varepsilon - T_4 \cdot \ln \varepsilon). \quad (1.38)$$

The thermal efficiency of the ideal cycle is expressed by the relation (1.39):

$$\eta_{\text{Stirling}} = \frac{W}{Q_{1 \rightarrow 2}} = \frac{m \cdot R \cdot (T_1 \cdot \ln \varepsilon - T_4 \cdot \ln \varepsilon)}{m \cdot R \cdot T_1 \cdot \ln \varepsilon} = 1 - \frac{T_4}{T_1} = \eta_{\text{Carnot}}, \quad (1.39)$$

which lead to the conclusion that, for the Stirling engine ideal cycle, the thermal efficiency is identical with the thermal efficiency of Carnot cycle between the same temperatures T_1 and T_4 .

1.7.6. Stirling engine irreversible cycle

The overall hypothesis is that the pressure drops in the exchangers are ignored. Therefore, the instantaneous pressure is constant throughout the Stirling engine at any given time.

In Figure 1.18, the initial data are p_1 , t_1 , t_3 , $c_{p \text{ agent}}$, γ where p_1 is the initial pressure of the agent (ideal gas), T_1 is the initial temperature of the agent (ideal gas), T_3 is the temperature entering the Stirling engine $c_{p \text{ agent}}$ is the heat capacity of the agent at constant pressure, $c_{v \text{ agent}}$ is the heat capacity of the agent at constant volume, γ is the adiabatic index, ε_k is the compression ratio of the compressor and η_{reg} is the regenerator efficiency.

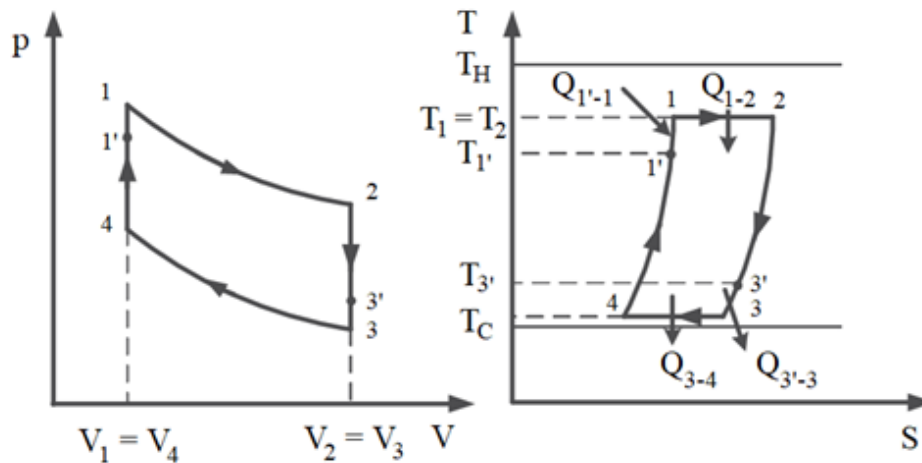


Figure 1.18 - Stirling engine irreversible cycle (Dobre, 2012)

1.7.6.1. Geometric analysis

For the geometric analysis purpose, the generic notation is presented in Table 1.6.

Table 1.6 - Generic notations for the geometric analysis

V_{Stotal}	Total dead volume	m^3
V_{SH}	Dead volume for the hot space	m^3
V_{SR}	Dead volume for the regenerator	m^3
V_{SC}	Dead volume for the cold space	m^3
k_{SH}	Ratio for hot space dead volume	-
k_{SR}	Ratio for regenerator dead volume	-
k_{SC}	Ratio for cold space dead volume	-
V_{D}	Displacer volume	m^3
V_{P}	Piston volume	m^3
k_{Stotal}	Total dead volume ratio	m^3
V_{S}	Total swept volume	m^3

The total dead volume V_{Stotal} is determined with the relation (1.40):

$$V_{\text{Stotal}} = V_{\text{SH}} + V_{\text{SR}} + V_{\text{SC}} = (k_{\text{SH}} + k_{\text{SR}} + k_{\text{SC}}) \cdot V_{\text{S}}, \quad (1.40)$$

where:

$$k_{\text{SH}} = V_{\text{SH}}/V_{\text{S}}, k_{\text{SR}} = V_{\text{SR}}/V_{\text{S}}, k_{\text{SC}} = V_{\text{SC}}/V_{\text{S}}. \quad (1.41)$$

$$V_{\text{Stotal}} = k_{\text{ST}} \cdot V_{\text{4}} = (V_{\text{Stotal}} + V_{\text{D}} + V_{\text{P}}) \cdot k_{\text{ST}}, \quad (1.42)$$

$$V_{\text{S}} = k_{\text{SDP}} \cdot (V_{\text{D}} + V_{\text{P}}), \quad (1.43)$$

$$k_{\text{Stotal}} = \frac{k_{\text{SDP}}}{V_{\text{S}}} = \frac{k_{\text{SDP}}}{1 + k_{\text{SDP}}} \quad (1.44)$$

1.7.6.2. The regenerator

The regenerator efficiency is determined with the relation (1.45):

$$\eta_{\text{reg}} = \frac{T_{1'} - T_4}{T_1 - T_4}, \quad (1.45)$$

the temperature $T_{1'}$ can be calculated with the relation (1.46):

$$T_{1'} = T_4 + \eta_{\text{reg}} \cdot (T_1 - T_4). \quad (1.46)$$

If the regenerator has equal efficiency in heating and cooling ($Q_{1-1'} = Q_{3-3'}$), the working fluid temperature is obtained with the relation (1.47):

$$T_{3'} = T_1 - \eta_{\text{reg}} \cdot (T_1 - T_4) = T_4 + \eta_{\text{reg}} \cdot (T_1 - T_4). \quad (1.47)$$

If there are large dead volumes, the regenerator must have a suitable working fluid temperature (T_{R}), which can be determined by using the arithmetic mean (1.48).

$$T_R = \frac{T_{1'} + T_{3'}}{2} = \frac{T_1 + T_4}{2}. \quad (1.48)$$

Through the relation (1.31) it can be seen that the temperature of the regenerator is not dependent on the regenerator effectiveness.

1.7.6.3. Isothermal compression 3 → 4

In the literature (Torres García, 2018, Deetlefs, 2014), the equation of state for the isothermal compression process 3 → 4 with dead volumes of the hot space (V_{SH}), of the regenerator (V_{SR}) and of the cold space (V_{SC}) and with the temperatures in the hot space (T_1), regenerator (T_R) and cold space (T_4) and m total mass of working fluid mass contained in the Stirling engine is:

$$p = \frac{m \cdot R}{\frac{V_H}{T_1} + \frac{V_{SH}}{T_1} + \frac{V_{SR}}{T_R} + \frac{V_C}{T_4} + \frac{V_{SC}}{T_4}} = \frac{m \cdot R}{\frac{V_H}{T_1} + K + \frac{V_C}{T_4}}. \quad (1.49)$$

The cold fluid is compressed from $V_{C3}=V_D+V_P$ to $V_{C4}=V_D$. The hot fluid volume (V_H) throughout this process is 0. The compression work can be calculated with the relation (1.50):

$$\begin{aligned} Q_{4-3} = W_{4-3} &= \int_{V_{C3}}^{V_{C4}} p \, dV_C = m \cdot R \cdot T_4 \int_{V_{C3}}^{V_{C4}} \frac{dV_C}{V_C + K \cdot T_4} = \\ &= m \cdot R \cdot T_4 \cdot \ln \frac{V_{C4} + K \cdot T_4}{V_{C3} + K \cdot T_4} = m \cdot R \cdot T_4 \cdot \ln \frac{V_D + K \cdot T_4}{V_D + V_P + K \cdot T_4}. \end{aligned} \quad (1.50)$$

The compression work therefore depends only on the factor K , which englobes the dead volumes of the Stirling engine.

1.7.6.4. Isochoric heating process 4 → 1

The amount of heat transferred during the isochoric heating process is calculated with the relation (1.51):

$$Q_{4-1} = m \cdot c_v \cdot (T_1 - T_4), \quad (1.51)$$

where c_v is specific heat at constant volume $J/(kg \cdot K)$. Without regeneration, the above-mentioned amount of heat added by the external source and for ideal regeneration, this amount is released by the ideal regenerator.

The regenerator heat released from an imperfect one during the process is:

$$Q_{4-1'} = m \cdot c_v \cdot (T_{1'} - T_4) = \eta_{reg} \cdot m \cdot c_v \cdot (T_1 - T_4). \quad (1.52)$$

The heat added from an external source during process 1' → 1 is:

$$Q_{1'-1} = m \cdot c_v \cdot (T_1 - T_{1'}) = (1 - \eta_{reg}) \cdot m \cdot c_v \cdot (T_1 - T_4). \quad (1.53)$$

The equation above shows that heat input depends only on the regenerator effectiveness.

1.7.6.5. Isothermal heating process 1 → 2

The hot source working fluid changes from $V_{H1}=V_D$ to $V_{H2}=V_D+V_P$. The working fluid swept volume of the cold source (V_C) is null. The heat added to the cycle is:

$$\begin{aligned} Q_{1-2} &= W_{1-2} = m \int_{V_{H1}}^{V_{H2}} p \, dV_H = m \cdot R \cdot T_1 \int_{V_{H1}}^{V_{H2}} \frac{dV_H}{V_H + K \cdot T_1} = \\ &= m \cdot R \cdot T_1 \cdot \ln \frac{V_{H2} + K \cdot T_1}{V_{H1} + K \cdot T_1} = m \cdot R \cdot T_1 \cdot \ln \frac{V_D + V_P + K \cdot T_1}{V_D + K \cdot T_1}. \end{aligned} \quad (1.54)$$

1.7.6.6. Isochoric cooling process 2 → 3

During the isochoric cooling process, the heat rejected is:

$$Q_{2-3} = m \cdot c_v \cdot (T_4 - T_1) = -m \cdot c_v \cdot (T_1 - T_4) \quad (1.55)$$

Without a regenerator, the above-mentioned amount is rejected to an external cold source. In the case of an ideal regenerator, this amount of heat is absorbed.

In the case of an imperfect regenerator, the heat absorbed by it through the process 2 → 3' is:

$$Q_{2-3'} = m \cdot c_v \cdot (T_{3'} - T_1) = -\eta_{\text{reg}} \cdot m \cdot c_v \cdot (T_1 - T_4) \quad (1.56)$$

The heat rejected to an external cold source through the process 3' → 3 is:

$$Q_{3'-3} = m \cdot c_v \cdot (T_4 - T_{3'}) = -(1 - \eta_{\text{reg}}) \cdot m \cdot c_v \cdot (T_1 - T_4) \quad (1.57)$$

$$W_{2-3} = Q_3 - Q_2 \quad (1.58)$$

1.7.6.7. Total heat added

For an imperfect regenerator, the cycle must have heat added to it from an external source.

$$Q_{\text{in}} = Q_{1'-1} + Q_{1-2} \quad (1.59)$$

$$\begin{aligned} Q_{\text{in}} &= m \cdot c_v \cdot \left[(T_1 - T_{1'}) + (\gamma - 1) \cdot T_1 \cdot \ln \frac{V_{H2} + K \cdot T_1}{V_{H1} + K \cdot T_1} \right] = \\ &= m \cdot c_v \cdot \left[(1 - \eta_{\text{reg}}) \cdot (T_1 - T_4) + (\gamma - 1) \cdot T_1 \cdot \ln \frac{V_D + V_P + K \cdot T_1}{V_D + K \cdot T_1} \right], \end{aligned} \quad (1.60)$$

where the adiabatic index is:

$$\gamma = \frac{c_p}{c_v}. \quad (1.61)$$

The amount of heat added from external source depends on the regenerator efficiency and on the dead volumes. The total heat added from the external source, without regeneration, is:

$$Q_{\text{in}} = Q_{4-1} + Q_{1-2}. \quad (1.62)$$

In the case of an ideal regeneration, the amount would be:

$$Q_{in} = Q_{1-2}. \quad (1.63)$$

1.7.6.8. Total heat rejected

The total heat rejected from the Stirling cycle to the external source, in the case of imperfect regeneration is:

$$Q_{out} = Q_{3'-3} + Q_{3-4} \quad (1.64)$$

$$\begin{aligned} Q_{out} &= m \cdot c_v \cdot \left((T_4 - T_{3'}) + (\gamma - 1) \cdot T_4 \cdot \ln \frac{V_{C4} + K \cdot T_4}{V_{C3} + K \cdot T_4} \right) \\ &= -m \cdot c_v \cdot \left((1 - \eta_{reg})(T_1 - T_4) + (\gamma - 1) \cdot T_4 \cdot \ln \frac{V_D + V_P + K \cdot T_4}{V_D + K \cdot T_4} \right) \end{aligned} \quad (1.65)$$

The amount of heat rejected from the engine depends on the regenerator efficiency and on the dead volumes. The total heat rejected to the external source, without regeneration, is:

$$Q_{out} = Q_{2-3} + Q_{3-4} \quad (1.66)$$

1.7.6.9. Net amount of work realized

The energetic surplus of the two isothermal processes $1 \rightarrow 2$ and $3 \rightarrow 4$ is converted into useful mechanical work. For an engine with an imperfect regenerator and with dead volumes, the net amount of work is:

$$\begin{aligned} W_{net} &= Q_{in} - Q_{out} = Q_{1'-1} + Q_{1-2} + Q_{3'-3} + Q_{3-4} = Q_{3-4} + Q_{3-4} = \\ &= m \cdot R \cdot \left(T_1 \cdot \ln \frac{V_{H2} + K \cdot T_1}{V_{H1} + K \cdot T_1} - T_4 \cdot \ln \frac{V_{C3} + K \cdot T_4}{V_{C4} + K \cdot T_4} \right). \end{aligned} \quad (1.67)$$

With the notations:

$$\begin{cases} V_{H2} = V_{C3} = V_D + V_P = V_3 \\ V_{H1} = V_{C4} = V_D = V_1 \end{cases} \quad (1.68)$$

The net amount of work becomes:

$$W_{net} = m \cdot R \cdot \left(T_1 \cdot \ln \frac{V_D + V_P + K \cdot T_1}{V_D + K \cdot T_1} - T_4 \cdot \ln \frac{V_D + V_P + K \cdot T_4}{V_D + K \cdot T_4} \right) \quad (1.69)$$

The net cycle work depends on the dead volumes.

1.7.6.10. Mean effective pressure

The cycle mean pressure p_m and the total volume of the piston translation movement (V_P) can be used to determine the net amount of work of the engine:

$$V_{H2} - V_{H1} = V_{C2} - V_{C1} = V_2 - V_1 = V_P \quad (1.70)$$

$$W_{net} = p_m \cdot V_P \quad (1.71)$$

$$(1.72)$$

$$p_m = \frac{m \cdot R}{V_P} \left(T_1 \ln \frac{V_D + V_P + K \cdot T_1}{V_D + K \cdot T_1} - T_4 \ln \frac{V_D + V_P + K \cdot T_4}{V_D + K \cdot T_4} \right)$$

For a null dead volume, using the perfect gas law and taking into account the isothermal ($T_1=T_2$) and isochoric ($V_2=V_3$) transformations, the mean pressure is:

$$p_m = V_1 \cdot \frac{p_1 - p_4}{V_2 - V_1} \cdot \ln \frac{V_2}{V_1}. \quad (1.73)$$

1.7.6.11. Thermal efficiency

Thermal efficiency is obtained by using the relations (1.57) - (1.58):

$$\eta_{\text{Stirling}} = \frac{W_{\text{net}}}{Q_{\text{in}}} \quad (1.74)$$

$$\eta_{\text{Stirling}} = \frac{T_1 \cdot \ln \frac{V_D + V_P + K \cdot T_1}{V_D + K \cdot T_1} - T_4 \cdot \ln \frac{V_D + V_P + K \cdot T_4}{V_D + K \cdot T_4}}{T_1 \cdot \ln \frac{V_D + V_P + K \cdot T_1}{V_D + K \cdot T_1} + (T_1 - T_4) \cdot \frac{1 - \eta_{\text{reg}}}{\gamma - 1}} \quad (1.75)$$

The Stirling engine efficiency depends on the dead volume and the regenerator effectiveness. For a null dead volume, the efficiency will be:

$$\eta_{\text{Stirling}} = \frac{T_1 - T_4}{T_1 + \frac{1 - \eta_{\text{reg}}}{(\gamma - 1)} \cdot \frac{T_1 - T_4}{\ln \frac{V_2}{V_1}}} \quad (1.76)$$

In the case of an ideal regeneration ($\eta_{\text{reg}}=1$), which yields the highest Stirling efficiency, the thermal efficiency is:

$$\eta_{\text{Stirling}} = \frac{T_1 - T_4}{T_1}, \quad (1.77)$$

relation which is identical with the relation (1.39) for a Stirling engine ideal cycle.

1.8. CONCLUSIONS

The emission reduction with 55% by 2030, ask for the promotion of the decarbonisation of heating and cooling, which is responsible for 80% of energy consumed in residential buildings. Two thirds of this energy came from fossil fuels, respectively 76,5%.

Because the stand-alone systems account for 88% from the European Union overall heat supply market, the production of heat from solid biomass and, additionally, the simultaneous generation of electricity within such system is taken into consideration.

Various bibliographic references related to theoretical and applicative works recently carried out have revealed that biomass, the micro-cogeneration and the Stirling engine represent altogether an opportunity to be capitalised.

Because an extended use of a technical approach relying on the solid biomass combustion micro-cogeneration system equipped with a Stirling engine towards the fulfilment of European Commission requirements, such technology is experimentally and theoretically investigated.

To frame this work, in this chapter, heat transfer notions are presented, the ideal Carnot and Stirling cycles are overviewed, the types of Stirling engines are listed, several specific parameters and properties are mentioned, the Stirling engine irreversible cycle is calculated.

CHAPTER 2

BIOMASS EXPERIMENTAL STUDY

2.1. INTRODUCTION

An interesting option to consider was the biomass residue, resulted from industrial activities, such as lumberyards and furniture factories. This is a double opportunity, since it decreases the amount of biomass waste, which could otherwise lead to pollution and it provides a fuel source at an advantageous price. There are other options in wood biomass, besides firewood, while considering the hypothesis of it being used as a fuel for cogeneration purposes.

Wood waste may arise in many industrial and commercial conditions and is rarely traded but used on site (Voronca, 2017, Voronca, 2019). The reporting enterprise may be able to state or estimate the quantity used or to state the heat obtained from it. A special case of wood waste is the production and use of black liquor. Wastes from the residues of crops are also important sources of fuel and may be used in special plants designed to accept them, such as straw-burning boiler (Garnier, 2004)

In comparing industrial fuels, the literature (Saidura, 2011) recommends 6 characteristics to be considered:

1. the cost per unit of thermal energy gained;
2. the complexity of the equipment needed on-site to transport and burn the fuel;
3. the availability of the fuel;
4. the problems associated with the storage of the fuel;
5. the emissions caused by combustion;
6. historical success of the technology for boilers using the respective fuel.

2.2. BIOMASS

Solid biomass (mainly fuelwood used for cooking in developing countries) is by far the largest renewable energy source, representing more than 10% of world total primary energy supply (TPES), or three-quarters of global renewables supply (Garnier, 2004).

Biomass is a carbon neutral source of energy. When combusted, the biomass carbon reacts only with the oxygen in the air to form carbon dioxide, which is released into the atmosphere, the quantity of CO₂ produced being equal to that which was taken-in during the growing stage (Saidura, 2011). However, the same plants use CO₂ during their lifetime to provide nutrients for self-sustaining.

An ongoing field study of the effects of elevated atmospheric CO₂ on a brackish wetland on Chesapeake Bay, was undertaken by Bert G. Drake (Drake, 2014). It started in 1987 and remains unique as the longest continually running investigation of the effects of elevated CO₂ on an ecosystem. This study suggests that rising CO₂ can add substantial amounts of carbon to ecosystems through stimulation of carbon assimilation, increased root exudates to supply nitrogen fixation, reduced dark respiration, and improved water and nitrogen use efficiency (Drake, 2014).

In 1987, it was observed the absorption and respiration of CO₂ by the swamp rose mallow (*hibiscus mocheutos*), in highly concentrated CO₂ filled closed spaces and their respective impacts on their surroundings. The results found that as CO₂ levels rose, plants released 10% less CO₂ back into the atmosphere.

Since the beginning of the study, atmospheric CO₂ increased 18%, sea level rose 20 cm, and growing season temperature varied with approximately the same range as predicted for global warming in the 21st century (2013). The study emphasized that the plants' absorption ratio remained the same. This was linked to a lack of nitrogen required by the plants to maintain proteins and to a shrinkage in the plants' shoot and leaf holes. With a lower amount of nitrogen, comes a lower amount of protein, therefore a lower plant respiration and less CO₂ released into the atmosphere (Drake, 2014).

2.3. LOWER HEATING VALUE AND HIGHER HEATING VALUE

In literature it is generally admitted that the higher heating value (HHV) is defined as the heat released during combustion per mass unit fuel under the constraints that the water formed during combustion is in liquid phase and that the water and the flue gas have the same temperatures as the temperature of the fuel prior to combustion (van Loo, 2008).

In relation with the higher heating value, the lower heat value (LHV) is defined as the heat released during combustion per mass unit of fuel under the constraints that the water formed during combustion is in a gaseous phase and that the water and the flue gas have the same temperature as the fuel prior to combustion (van Loo, 2008) calculate the cost.

In total, 6 fuels available from suppliers were analysed in term of higher heating value to calculate the cost. Obtaining the lower heating value was done using the following formulas:

$$\text{LHV} = \text{HHV} - 2.12 \cdot H - 2.45 \cdot W_t - 0.8 \cdot O \quad (2.1)$$

$$\text{LHV} = \text{HHV} - 5.83 \cdot (W_t + 9 \cdot H) \quad (2.2)$$

$$\text{LHV} = \text{HHV} - 2257 \cdot w_t \quad (2.3)$$

$$w_t = W_t/100 \quad (2.4)$$

In the relations (2.1) - (2.4), LHV is the lower heating value in kJ/kg, HHV is the higher heating value, in kJ/kg, H is the percent hydrogen (%), W_t is the percent moisture (%), O is the percent oxygen (%) and w_t is the whole of amount of water in kg/kg of fuel.

In the relations (2.1) - (2.4), LHV is the lower heating value in kJ/kg, HHV is the higher heating value, in kJ/kg, H is the percent hydrogen (%), W_t is the percent moisture (%), O is the percent oxygen (%) and m is the whole of amount of water, produced by the combustion of 1kg of fuel, in kg.

Formula (1) considers humidity itself and water cotenants of the fuel as separate elements (Lee, 2016). Formula (2) considers humidity and the amount of hydrogen that would take part in forming moisture (Badea, 2014). Formula (3) considers the heat necessary for water vaporization, which is 2,257 kJ/kg at 0°C (Wright, 2009). As all 3 formulas link biomass lower heating value to the moisture content, the latter must be first determined.

2.4. FUEL MOISTURE DETERMINATION

2.4.1. Biomass moisture content

It is well known that the moisture will evaporate at low temperatures (< 100°C). Since vaporization uses energy released from the combustion process, it lowers the temperature in the combustion chamber, which slows down the combustion process (van Loo, 2008). In wood-fired boilers, for example, it has been found that the combustion process cannot be maintained if the wood moisture content exceeds 60 per cent on a wet basis (w.b.).

The wet wood requires so much energy to evaporate contained moisture, and subsequently to heat the water vapour, that temperatures are reduced below the minimum temperature required to sustain combustion (van Loo, 2008).

The moisture content of biomass fuels varies considerably, depending on the type of biomass and biomass storage. In some cases, it will be necessary to dry the biomass fuel prior to combustion to be able to sustain combustion (van Loo, 2008).

Increasing moisture content will reduce the maximum possible combustion temperature (the adiabatic combustion temperature) and increase the necessary residence time in the combustion chamber, thereby giving less room for preventing emissions as a result of incomplete combustion (van Loo, 2008). Consequently, moisture content is a very important fuel variable and this is the reason for which this variable has to be initially assessed and further monitored.

2.4.2. ASTM E871 - 82 Standard Test Method for Moisture Analysis of Particulate Wood Fuels

The moisture content was determined in accordance with the test method and related procedures described in the ASTM E871 - 82 Standard (ASTM, 2019).

As presented, within the recommendations in using this standard (ASTM, 2019), the test procedures described in this test method can be used to determine the total weight basis moisture of any particulate wood fuel meeting the requirements specified in this test method.

This test method covers the determination of total weight basis moisture in the analysis sample of particulate wood fuel. The particulate wood fuel may be sanderdust, sawdust, pellets, green tree chips, hogged fuel, or other type particulate wood fuel having a maximum particle volume of 16.39 cm³ (1 in.³). It is used for calculating other analytical results to a dry basis. Moisture, when determined as herein described, may be used to indicate yields on processes, to provide the basis for purchasing and selling, or to establish burning characteristics (ASTM, 2019).

The values stated in SI units are to be regarded as the standard. The values given in parentheses are for information only.

This standard does not purport to address all of the safety concerns, if any, associated with its use. It is the responsibility of the user of this standard to establish appropriate safety, health, and environmental practices and determine the applicability of regulatory limitations prior to use.

As indicated (ASTM, 2019), this international standard was developed in accordance with internationally recognized principles on standardization established in the Decision on Principles for the Development of International Standards, Guides and Recommendations issued by the World Trade Organization Technical Barriers to Trade (TBT) Committee.

2.4.3. Samples Drying

The European norm ISO 589:2008 Hard Coal - Determination of Total Moisture describes two methods for determination of the total moisture content of hard coals, a two-stage method and a single-stage method. For either method there is a choice between drying in air and drying in a nitrogen atmosphere.

Depending on the coal rank, there may be systematic differences between the results obtained by drying in the different atmospheres on subsamples of a sample.

Drying in a nitrogen atmosphere is suitable for all hard coals, while drying in air is only suitable for hard coals not susceptible to oxidation.

To determine the fuel moisture, a drying oven of a SLW 53 SIMPLE model with forced convection and a maximum temperature attainable of 300 °C was used (Figure 2.1).



Figure 2.1 - Drying Oven SLW 53

(Source: <https://www.pol-eko.com.pl/drying-ovens-with-nitrogen-blow/>)

The drying oven SLW 53 ensures samples are dried between 105 °C - 110 °C in a drying oven featuring nitrogen blow possibility with flow equal to about 15 times the capacity of the oven per hour. The technical specifications are showed in Annex 2.

This laboratory oven is equipped with a dry nitrogen blow system of the chamber and the chamber capacity is 56 litres.

The calibration in nitrogen is performed in 9 points (corners + geometrical centre) of the chamber at one initially selected temperature in accredited laboratory. Calibration is further confirmed by calibration certificate.

The samples have a moisture content inferior to 50% and they are to be dried for 24 hours at 105°C, to not devolatilize. The probes were weighted before and after being dried. In the case of a moisture content superior to 50%, the drying time increases to 48 hours at the same temperature.

In terms of humidity, that of industrial wood wastes is inferior to 10% and that of forest residues inferior to 50% (Badea, 2013).

Formula (5) defines wet moisture (M_W) percentage is the weight of moisture ($m_{i, probe}$) per initial probe mass, that which contains moisture.

Formula (6) defines dry moisture is the mass of moisture per final probe mass, with the moisture mass subtracted.

M_W is the wet moisture, M_D is the dry moisture $m_{i, probe}$ is the initial probe mass (before drying), $m_{f, probe}$ is the final probe mass (after drying) and M is the moisture mass.

$$M_W = \frac{M}{m_{i, probe}} \quad (2.5)$$

$$M_D = \frac{M}{m_{f, probe}} \quad (2.6)$$

Results show forest waste contains the most humidity, since it is gathered on-site and untreated.

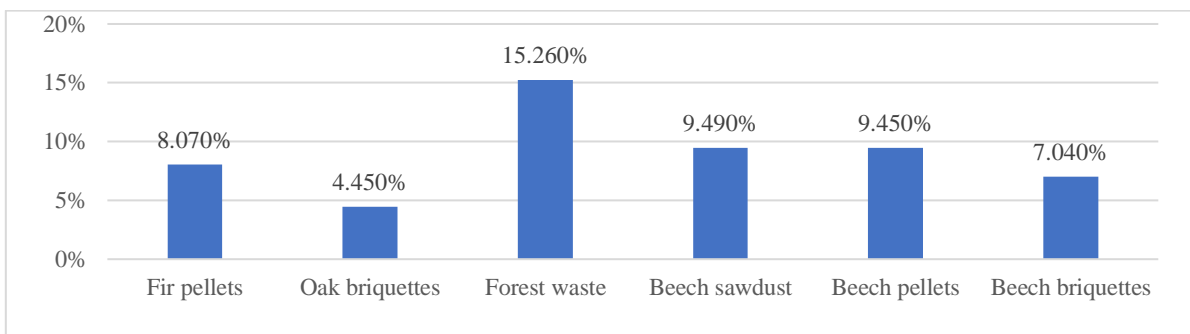


Figure 2.2 - The wet moisture levels of different types of wood biomass

Apart from the sawdust which was kept in a dry storage room, the rest of the biomass has a moisture percentage inferior to 10%, which is understandable since moisture is part of the briquette and pellet standard.

While France has a national standard of maximum 10% moisture (Garcia-Marayer, 2015), most providers in Romania meet the ENPlus standard which offers the same 10% moisture level for its 3 standard classes: ENplus-A1, ENplus-A2 and EN-B.

Table 2.1 - Wet and dry moisture levels for different types of wood biomass

Wood specie	Initial Mass [g]	Final Weight [g]	Moisture [g]	Wet Moisture	Dry Moisture
Forest waste	672.42	569.78	102.64	15.26%	18.01%
Fir pellet	305.88	281.21	24.67	8.07%	8.77%
Oak briquettes	229.89	219.65	10.24	4.45%	4.66%
Beech sawdust	816.3	738.82	77.48	9.49%	10.49%
Beech pellets	333.39	301.88	31.51	9.45%	10.44%
Beech briquettes	178.05	165.52	12.53	7.04%	7.57%

2.5. HIGHER HEATING VALUE DETERMINATION

The higher heating value (HHV) was determined using an IKA C200 bomb calorimeter (Figure 2.3).



Figure 2.3 - Calorimeter IKA C 200-System

(Source: <https://www.ika.com/en/Products-Lab-Eq/Calorimeters-Oxygen-Bomb-calorimeter-csp-330/C-200-cpdt-8802500/>)

The higher heating value (HHV) was determined using an IKA C200 bomb calorimeter. The Calorimeter C 200 is a compact semi-automated calorimeter to determine calorific values of liquid and solid samples. Suitable for educational purposes (e.g., technical schools, universities) and for commercial, industrial laboratories with a low number of samples. The system can be adapted to individual laboratory tasks by adding further accessories.

The C 200 includes the following components: the basic device (measuring cell) C 200 including power pack and ignition adaptor, the decomposition vessel C 5010, the Oxygen station C 248 and additional consumables for installation and calibration. The technical specifications are showed in Annex 2.

The sample was weighed beforehand, an inflammable string inserted into the probe to connect it to the coil which would heat and cause ignition. The bomb was sealed and pressured to 30 bar. Distillate water was introduced into the calorimeter tank, to favour heat transfer.

2.6. LOWER HEATING VALUE DETERMINATION

To calculate the lower heating value (LHV) using Formula (2.1) and Formula (2.2), the hydrogen and oxygen percentages taken into consideration were those proposed by the Technische Universität Wien BIOBIB Database (Reisinger, 1996).

Also, without an ultimate analysis, the hydrogen and oxygen composition of forest waste could not be determined. Even if the species of the forest waste composition were known, the ratio in which they participated would have been hard to determine exactly. A repeated HHV test would have needed to be undertaken, to statistically determine the participation of the 2 elements in the composition.

The comparison between the LHV values obtained by using the relations (2.1) - (2.3) are suggested in Figure 2.4.

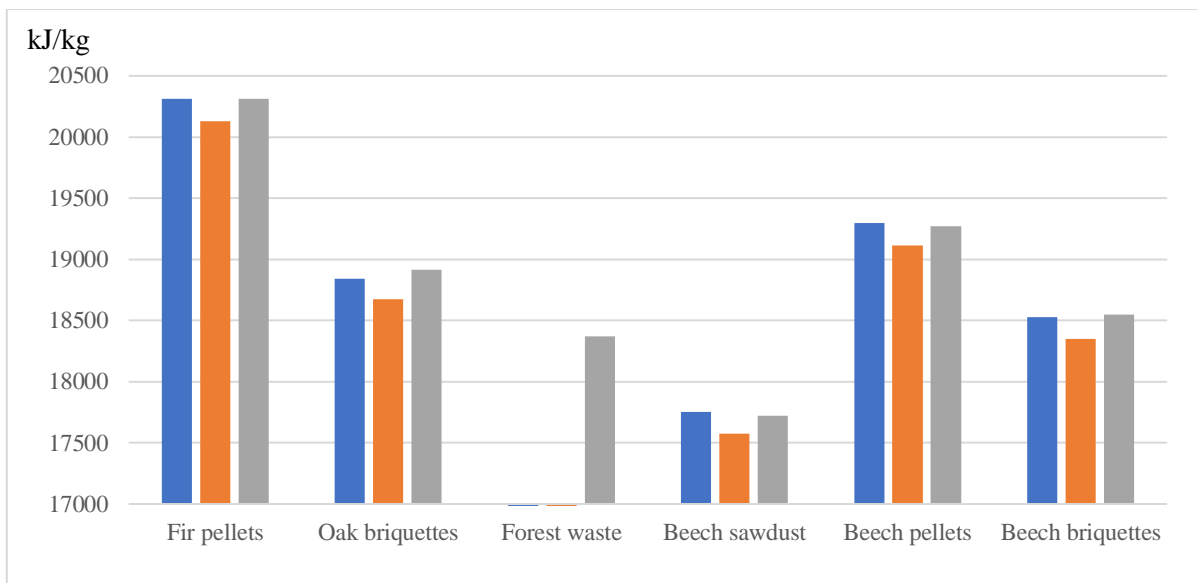


Figure 2.4 - The higher heating value and lower heating value for different types of wood biomass (Formula 2.1 - blue, Formula 2.2 - brown, Formula 2.3 - grey)

The results of this LHV calculation are indicated in the Table 2.2.

Table 2.2 - The higher heating value and lower heating value for different types of wood biomass

Wood specie	HHV [kJ/kg]	W _t [%]	H [%]	O [%]	LHV [kJ/kg]		
					Formula 1	Formula 2	Formula 3
Fir pellet	20496	8.07	6.14	43.46	20311	20127	20314
Oak briquettes	19014	4.45	5.98	44.00	18841	18674	18914
Forrest waste	18714	15.26	N/A	N/A	N/A	N/A	18370
Beech sawdust	17937	9.49	5.82	45.67	17754	17576	17723
Beech pellets	19486	9.45	6.07	43.81	19299	19112	19273
Beech briquettes	18710	7.04	6.07	43.81	18529	18350	18551

2.7. COST PER UNIT OF THERMAL ENERGY PRODUCED

Having determined the LHV, the cost of fuel per unit of thermal energy gained is determined by using the relation (2.7):

$$\text{Energy Price } [\text{€}/\text{MWh}] = \frac{\text{Fuel price } [\text{€}/\text{ton}]}{\text{Average}(\text{LHV}_{F1}, \text{LHV}_{F2}, \text{LHV}_{F3}) \text{ [kJ/kg]}} \cdot \frac{1}{0.000277778 \text{ [kWh/kJ]}} \quad (2.7)$$

The comparison of the values for the heat unit in function of the wood species is shown in the Figure 2.5.

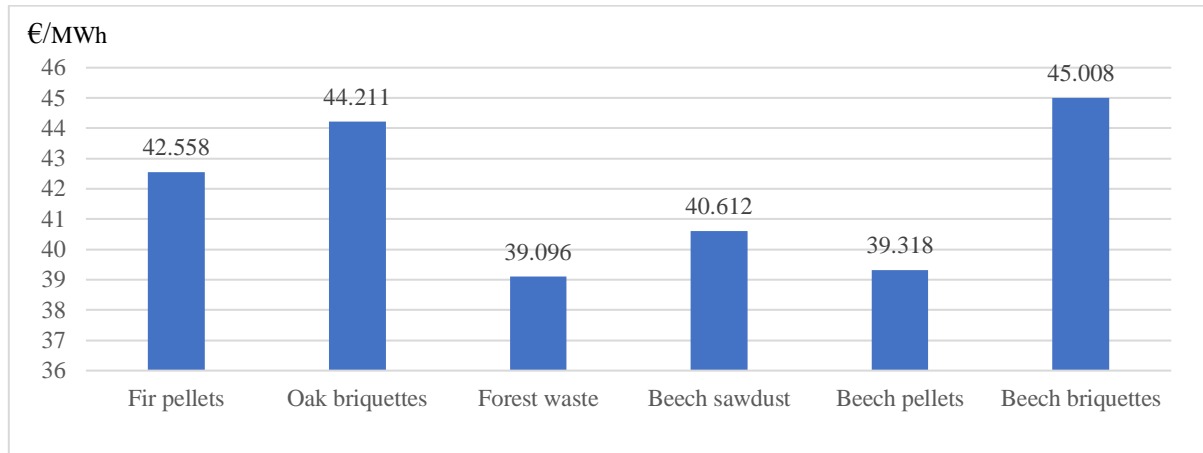


Figure 2.5 - The energy price for different type of wood biomass

The results of this heat unit price calculation are indicated in the Table 2.3.

Table 2.3 - The fuel price and the energy price for different type of wood biomass

Wood specie	Fuel price [€/ton]	Energy price [€/MWh]
Fir pellet	239.4	42.43
Oak briquettes	231	44.08
Forrest waste	199.5	39.10
Beech sawdust	199.5	40.47
Beech pellets	210	39.19
Beech briquettes	231	44.86

In respect to the quantity of energy gained, beech pellets and forest waste are the most profitable. However, in the calculated cost one of the immediate components, other factors need to be considered such as ash deposition in the boiler, which may shorten device life and fuel density, in domestic applications space is a key issue.

An ash content analysis was done by heating the samples at 800°C with a Nabertherm Muffle furnace L 9/11/SKM with flap door.



Figure 2.6 - Nabertherm Muffle furnace L 9/11/SKM

(Source <https://www.nabertherm.com/en/products/laboratory/muffle-furnaces/>)

Each of the probes stayed inside for a period of 40 minutes. It is to be noted that the pellets needed over 2 hours until the coke transformed to ash.

These test results have a 10% margin of error, because the crucibles containing the probes lost mass upon manipulation.

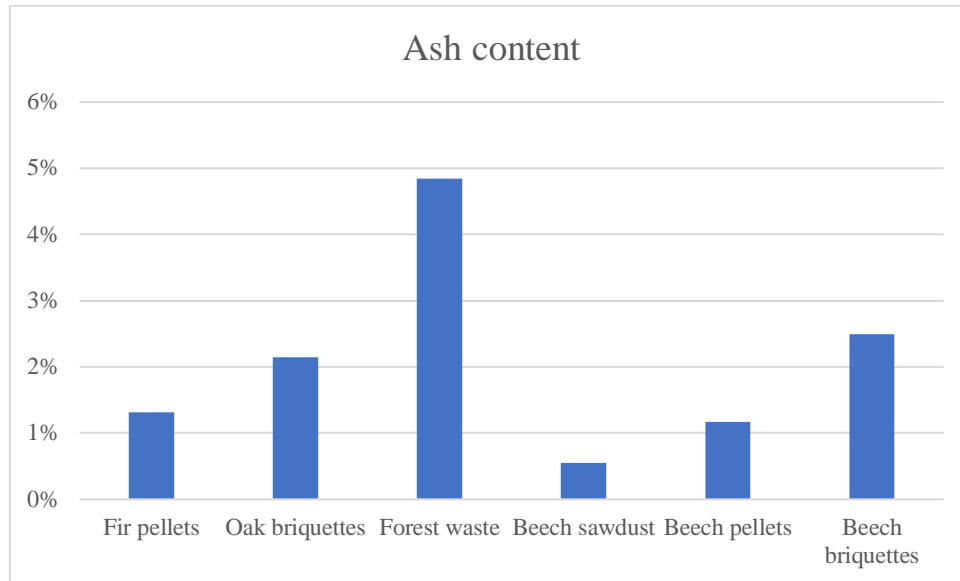


Figure 2.7 - The ash content for all considered wood species

The results show in the Table 2.4 that forest waste has the highest content of ash, since leaves and branches have a higher cellulose amount than the wood used in fabricating briquettes and pellets.

Table 2.4 - The ash content for all considered wood species

Wood specie	Ash content
Fir pellets	1.31%
Oak briquettes	2.15%
Forest residue	4.84%
Beech sawdust	0.55%
Beech pellets	1.17%
Beech briquettes	2.49%

2.8. SIMPLE ECONOMICS

With the results from the Table 2.2 and the Table 2.3, simple economics related to the heat generation are presented.

It is considered a wood fired boiler in condensation, with the rated capacity of 1 MW_{th}, operated within a heating plant, to generate the thermal energy supplied through a local district heating system to end users during the cold season. The similar geographic locations of both, France and Romania, with the same continental climate allow to adopt for the heating season an amount of 4.000 hours/year of this local public service delivery. This means an annual heat production of 4.000 MW_{th}/year.

The wood fired boiler rated efficiency is 100% due to the recovery of the condensation latent heat of the water vapours within the exhausted flue gases. This value is a bit lower than the efficiencies currently reported by the boilers' manufacturers in their technical and commercial offers presented to their customers. This chosen value is appropriate because of its credible influence on the fuel consumption.

In the literature (Otepka, 2013) is indicated that the specific investment costs for heating plants include the overall investment costs of the heating plant (boiler house and storage with all installations without land and development costs) referred to as the sum of nominal power [kW] of all heat generators.

The related specific investment cost of the heat plan is the ratio between the investment costs and all nominal power. As one of the most advanced countries in the use of biomass for energy purposes is Austria, an average value for the specific investment costs of new plant installations in this country of 519 €/kW_{th} (Otepka, 2013), has been adopted.

For the heat plant equipped with a wood fired boiler with the rated capacity of 1 MW_{th}, a total investment cost of 519.000 € is required.

The heat plant lifespan has been taken 20 years. Under such premises, taken into consideration that the investments in heat generation should be reflected in the selling price (€/MW_{th}h), an increase compared to fuel price of 35% has been adopted.

For each wood specie, the cash-flow projection has been performed. The adopted discount rate is 5%. Mainly related to the cost of capital, this discount rate value is often used to perform financial analyses for the investments financed from European Structural Instruments.

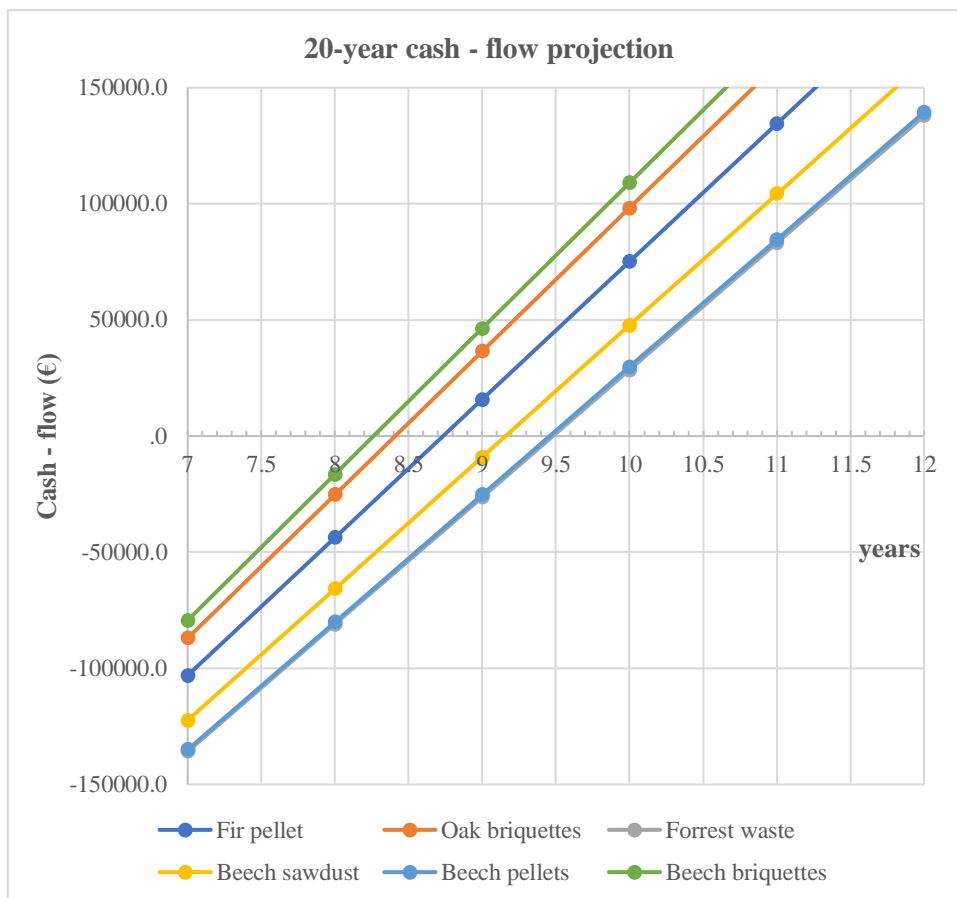


Figure 2.8 - The cash - flow projection for all considered wood species

The cash - flow projection for all wood species is showed in the Figure 2.8. For the considered input data, the simple payback periods vary from the smallest, namely the beech briquettes to the greatest, the Forrest waste.

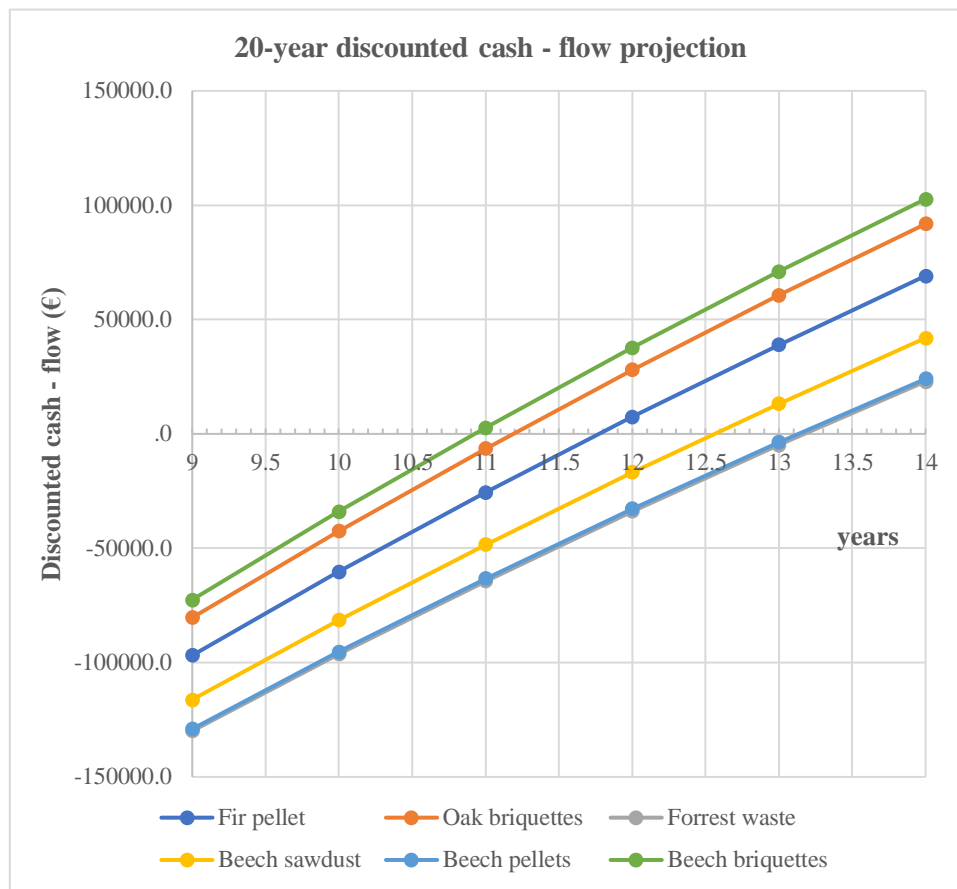


Figure 2.9 - The discounted cash - flow projection for all considered wood species

The discounted cash - flow projection for all wood species is showed in the Figure 2.9. Similarly, for the considered input data, the discounted payback periods vary from the smallest, namely the beech briquettes to the greatest, the Forrest waste.

The investment performances in term of Internal Rate of Return and the Net Present Value are indicated in the Table 2.5.

Table 2.5 - The investment performances for all wood species

Discount rate 5%	Simple Payback years	Discounted Payback years	Internal Rate of Return %	Net Present Value €
Beech briquettes	8,27	10,95	10,44%	263.677
Oak briquettes	8,4	11,2	10,18%	250.068
Fir pellet	8,75	11,8	9,62%	221.280
Beech sawdust	9,2	12,1	8,95%	187.084
Beech pellets	9,5	13,2	8,51%	164.752
Forrest waste	9,5	13,2	8,47%	163.181

For a lifespan of 20 years, the payback is reasonably short knowing that delivering heat within local district heating systems has a strong social impact and the selling prices (varying from 53 to 61 €/MW_{th}h in this example) should be affordable.

For countries like France where the power purchasing parity is adequate, in other countries like Romania, the need to locally subsidize the heat supply is still persistent.

In terms of investment performances, as long as the associated values of the Internal Rate of Return (%) are exceeding the discount rate (5%) and the Net Present Value (€) gets positive values and reasonably well fitted to the initial investment amount (519.000 €), all investments are economically valid.

In this simple example, the operational expenditures haven't been taken into account.

Factors like the local availability of the biomass within a geographical circle with a radius smaller than 30 km (to limit the transport cost influence on the total fuel cost), the long-term commitment for the biomass supply at an affordable price, the fouling issues (mainly related to the moisture content and the tar, the ash removal and disposal, are normally inventoried when deciding to invest in heat generation for district heating purposes.

2.9. CONCLUSIONS

Solid biomass is a viable replacement for coal, even if the lower heating values are superior to lignite (14,654 - 19,305 kJ/kg or less) and somewhat comparable to the sub-bituminous B (22,097 - 24,423 kJ/kg) and comparable to the sub-bituminous C (19,306 - 22,097 kJ/kg), for example (Radovič, 2007).

It was taken into account the situation where the biomass fuel was to be purchased from a supplier. If the resource is available on-site, the transportation costs are avoided, increasing the profit (Cruceru, 2012, Voronca, 2012).

This is in line with the provisions of the new strategy to boost renovation called 'A Renovation Wave for Europe - Greening our buildings, creating jobs, improving lives' (European Commission, Com 662 final, 2020), which are strongly considering the decarbonisation and the integration of renewables, this referring to energy from renewable sources produced on-site or nearby are vital (Cruceru, 2013).

In the case of purchasing biomass, fuel availability could be solved by coupling a biomass fired cogeneration unit to an electric vehicle.

A furniture company used an O.R.C. to transform its wood biomass from waste to heat and power (Voronca, 2014, Voronca, 2017). A perspective to be investigated is the addition of an electric truck which would serve a cheap means of transport and an energy buffer to be charged by the O.R.C. facility.

Simple economics demonstrate that investing in the promotion of biomass towards the decarbonisation of district and individual heating is feasible. In certain situations, when taking into consideration the European common biomass market, particularities among the EU citizens

in terms of annual income, could require additional public support in order to preserve this heat supply available, accessible, affordable and profitable.

When looking deeper into the domain of stand-alone heating systems which account for 88% of it (European Commission, Com 662 final, 2020), the promotion of cogeneration on biomass at individual level makes a lot of sense due to the favourable effect of transforming the power and heat consumers into prosumers.

CHAPTER 3

EXPERIMENTAL STUDY ON THE BIOMAAS MICRO-COGENERATION UNIT WITH A STIRLING ENGINE

3.1. INTRODUCTION

To facilitate the energy transition, it is necessary to develop sustainable energy technologies. In the literature (Bouvenot, 2014) it is indicated that the micro combined heat and power (μ CHP) is such technology, which produces simultaneously decentralized heat and electricity energy at low power (electrical power lower than 50 kW_{el}).

This technology recovers the “fatal heat” losses considered as “heat waste” produced in thermodynamics cycles for mechanic energy generation (Bianchi, 2013). Micro-CHP technology offers significant benefits: reduced primary energy consumptions, reduced CO₂ emissions, avoidance of central plant and network construction (Mameri, 2018).

Micro-CHP technology can contribute to the transition of the traditionally centralized energy supply system towards a more sustainable system (Martinez, 2018).

A biomass engine has been tested in INSA Strasbourg to characterize its performances. The unit used to co-generate heat and power is the model PELLEMATIC Condens_e and it was manufactured by the Austrian company “ÖkoFEN” (ÖkoFEN, 2017).

The unit has been tested for peak shaving purposes in local grids and yielded profitable in transition heating periods (spring and autumn) and winter, while in the summer the heat produced was greater than the demand (Gliński, 2019).

It has been paired with an open-source Building Energy Management System (oBEMS) aimed in reducing the building energy demand (Jones, 2018).

The ÖkoFEN micro cogeneration unit is fitted with a free-piston type Stirling engine which has a broad use in biomass, biogas and natural gas cogeneration.

Several studies of μ CHP applications equipped with a Stirling engine were reviewed. In terms of fuel comparison, it was found that sugarcane pellets and commercial biomass pellets have similar temperature outputs (Cardoso, 2019).

The Stirling engine efficiency was slightly lower when using sugarcane pellets. The ash level accumulations are higher for sugarcane pellets; therefore, the heat exchanger surface must be cleaned more frequently for this type of fuel or the efficiency of the Stirling engine decreases.

A Stirling engine was used placed between a gasification unit and an internal combustion engine (Bartela, 2018). The high temperature of the hot raw gas stream was found to be an economically attractive hot source for a Stirling engine.

In this finance-oriented study, it was found that profitability depends on the required investment costs and the investment becomes more profitable as the cost of biomass rises.

The thermal efficiency for different domestic hot water temperatures was studied (Valenti, 2014). The analyzed temperatures were of 30 °C, 50 °C and 70 °C and it was found that the thermal efficiency was between 90 % for 30 °C and 84 % for 70 °C.

It was also found that pressure does not affect the Stirling engine temperature ratio and that higher pressures and temperatures on the hot side increase the Stirling engine's thermal power absorption.

The integration of a Stirling engine in a biomass integrated gasification combined heat and power (BIGCHP) was studied (Bartela, 2017). It was found that the functioning is best oriented towards producing power, because it is more costly than thermal power.

The functioning with pellets of different diameters (Ø6 mm and Ø8 mm) was analyzed (Cardozo, 2014). For the Ø8 mm diameter of pellets, the temperature ratio of the Stirling engine lowers, and the regenerator effectiveness is higher. Also, a higher thermal efficiency was recorded using Ø8 mm diameter pellets.

Agricultural biomass and wood waste were used as fuel to power a μ CHP fitted with a free-piston Stirling engine (Damirchi, 2016). The power obtained was 10.71 W_{el} from the pruning of trees and 25.79 W_{el} from sawdust.

A conceptual design and performance analysis of a free-piston Stirling engine was conducted (Qiu, 2019). The components of a free-piston type Stirling engine were simulated and optimized using different thermodynamic parameters and dimensional sizes.

A free-piston Stirling engine was also used for a μ CHP application, running on natural gas (Park, 2018). The study found that the developed Stirling engine had a good power efficiency even when functioning in a partial-load mode.

A pairing of a Gamma-type Stirling engine with a fluidized bed combustor was realized and it was found that the fluidized bed enabled the heat recovery produced in the gas phase (Urciuolo, 2018). Also, it was found that higher temperatures can be achieved by placing the heater of the Stirling engine in the fluidized bed, instead of the conventional flue gas stream.

A CHP application using a Stirling engine was studied in order to cover a 1.23 MW_{th} heat demand from a village (Katona, 2018). It was concluded that CHP units fitted with Stirling engines totaling 1 MW_{th} could cover 70% of the heat demand, the rest being covered by a biomass furnace.

Before being implemented as μ CHP, the Stirling engine was tested for CHP plants (Biedermann, 2004). With a thermal power of 475 kW_{th} and power of 75k W_{th} , it obtained similar efficiencies to the μ CHP applications.

A transient model of a μ CHP unit running on Diesel fuel was realized in the TRNSYS software, describing the functioning process as a 5-stage process (Ulloa, 2013).

The dynamic model proposed found that during the start-up and steady states, the produced power is proportional to the temperature difference between the Stirling engine block and the burner.

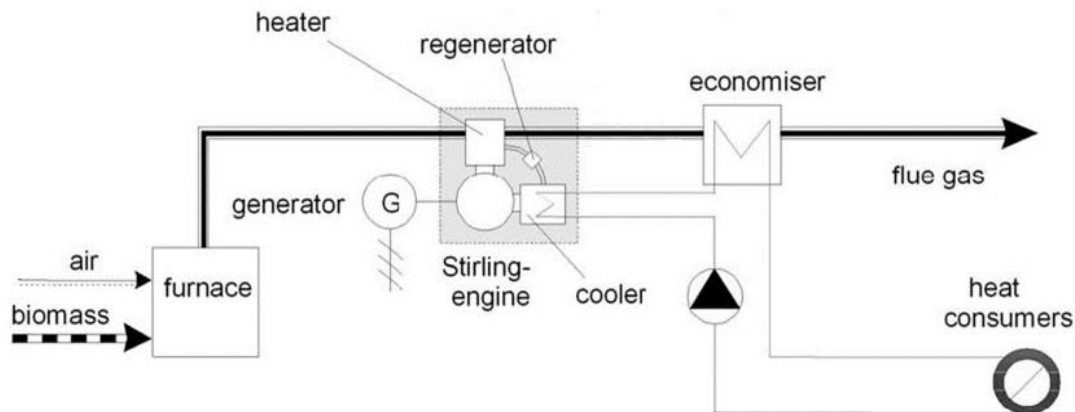
The characteristics of the units presented in the studies are synthesized in Table 3.1. In some studies, certain categories of information were not available.

Table 3.1 - Stirling engine fitted μ CHP/CHP units

Source	Stirling type	Working fluid	Thermal power [kW _{th}]	Power [kW _{el}]	T ^{Stirling} [°C]	Fuel use	Fuel type	η_{th}	η_{el}
Cardozo 2019	N/A	Nitrogen	20	1	549	Combustion	Pellets	81%	9%
Bartela 2018	N/A	N/A	N/A	N/A	N/A	Gasification	Biomass	46%	23%
Valenti 2014	N/A	Nitrogen	8	1	823	Combustion	Natural gas	90%	9%
Bartela 2017	Alpha	N/A	N/A	N/A	600	N/A	N/A	N/A	N/A
Cardozo 2014	Gamma	Nitrogen	20	1	500-660	N/A	Biomass	N/A	N/A
Damirchi 2016	Gamma	Helium	N/A	1	370-410	Combustion	Land waste	N/A	N/A
Qiu 2019	Free piston	N/A	1.1	1	N/A	N/A	Biomass	38%	42%
Park 2018	Free piston	N/A	N/A	1	525	Combustion	Natural gas	N/A	23%
Urciuolo 2018	Gamma	N/A	15-40	0.3	625	N/A	Pellets	N/A	N/A
Katona 2018	N/A	N/A	N/A	N/A	N/A	N/A	Wood residue	N/A	N/A
Biedermann 2004	N/A	Helium	475	75	N/A	N/A	Chopped wood	74%	12%
Ulloa 2013	Alpha	Nitrogen	6	0.92	460-480	Combustion	Diesel	N/A	N/A

3.2. MATERIALS AND METHODS

The ÖkoFEN PELLEMATIC Condens_e is an improved version of the Pellematic Condens, which has been fitted with a Stirling engine. Its output is described by a nominal thermal power of 12 kW_{th} and a nominal power of 1 kW_{el}. Its partial thermal power can descend up to 18 kW_{th}. According to the manufacturer, the machines' thermal efficiency at nominal load is 97.7 %. It weighs 294 kg and contains 69 l of working fluid (water). It runs on wooden pellets, being fitted with an internal 30 kg fuel reservoir, and connected to an additional 120 kg fuel silo. A principal schema of a generic Stirling engine biomass cogeneration unit is shown in Figure 3.1.


Figure 3.1. A biomass cogeneration unit with Stirling engine

(Source: Sjaak van Loo and Jaap Koppejean, *The Handbook of Biomass Combustion and Co-firing*, Earthscan London 2008, <https://boilersinfo.com/>, pp. 195)

The machine detects when its fuel resources are low and initiates an aspiration process from its fuel silo. This automation is useful because it minimizes the user input. Its energetic class is that of A+. Its energy efficiency index is that of 125 and its seasonal thermal energy efficiency is that of 88 %. Its boiler temperature ranges from 25 °C to 85 °C. Its maximum operating pressure is 3 bar. It has been tested by manufacturers to withstand pressures up to 4.6 bar.

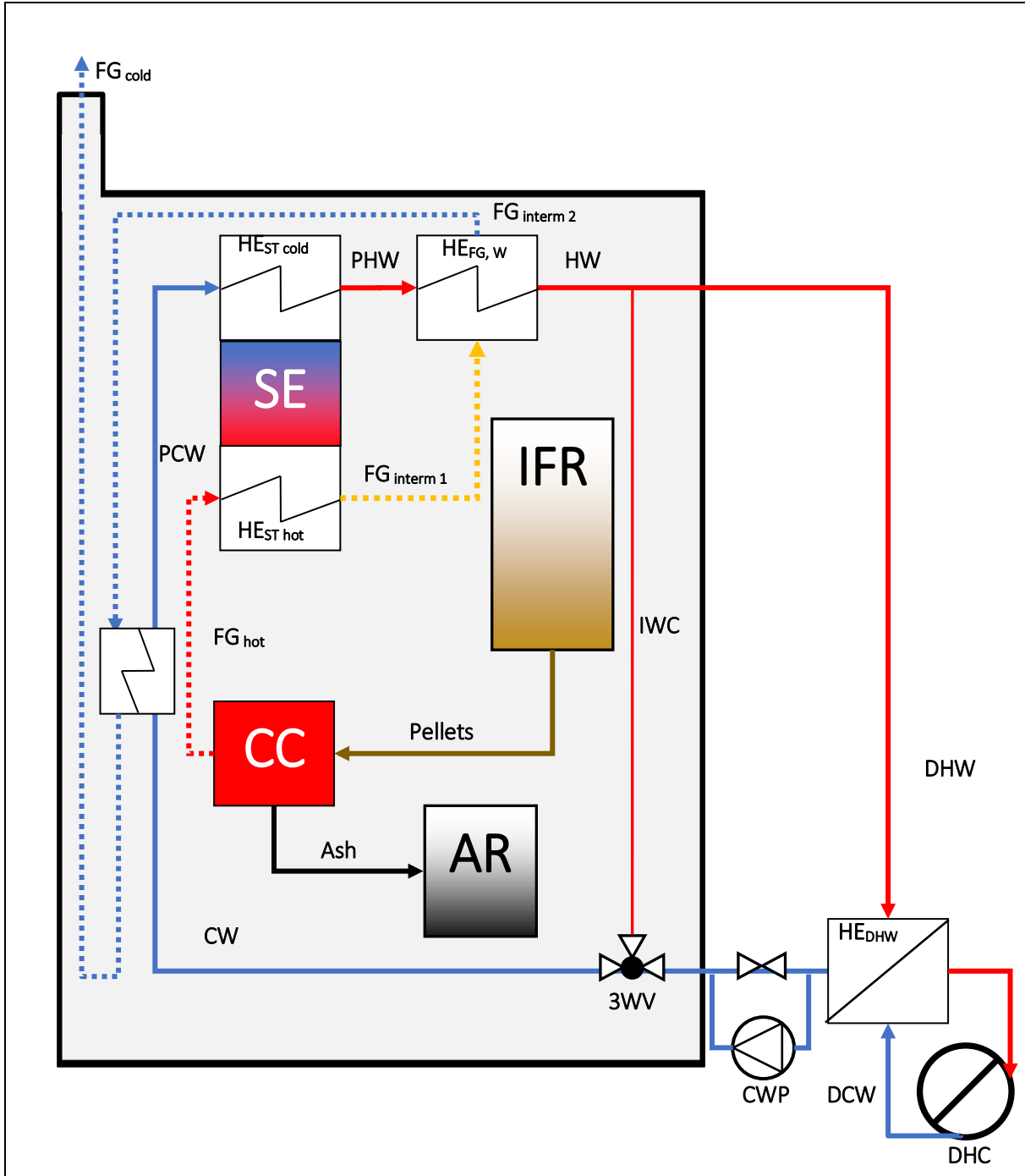


Figure 3.2 - The principal schema of the ÖkoFEN Condens_e cogeneration unit

The ÖkoFEN PELLEMATIC Condens_e is an improved version of the Pellematic Condens, which has been fitted with a Stirling engine. Its output is described by a nominal thermal power of 12 kW_{th} and a nominal power of 1 kW_{el}. The burner is electrical, and it consumes 0.2 kW_{el}. Its partial thermal power can descend up to 18 kW_{th}. According to the manufacturer, the machines' thermal efficiency at nominal load is 97.7 %. It weighs 294 kg and contains 69 l of work fluid (water). It runs on wooden pellets, being fitted with an internal 30kg fuel reservoir,

and connected to an additional 120 kg exterior fuel silo. The machine detects when its fuel resources are low and initiates an aspiration process from its fuel silo. This automation is useful because it minimizes the user input.

Its energetic class is that of A+. Its energy efficiency index is that of 125 and its seasonal thermal energy efficiency is that of 88 %. Its boiler temperature ranges from 25 to 85 °C. Its maximum operating pressure is 3 bar. It has been tested by manufacturers to withstand pressures up to 4.6 bar.

Figure 3.2 shows the principal schema of the ÖkoFEN Condens_e cogeneration unit. When starting, the machine first cleans the exhaust pipe mechanically of the previously deposited ash and combustion residue, evacuating them in the ash recipient (AR). Afterwards, the inner fuel reservoir (IFR) storage is verified and biomass aspiration from the exterior fuel silo is started if the inner reservoir fuel level is deemed insufficient.

The electrical burner starts heating electrically until combustion can be realized. The air and biomass then enter the combustion chamber (CC), producing heat through combustion, which is transferred to the heater of the Stirling engine ($HE\ ST_{hot}$).

The Stirling engine (SE) transforms the thermal power into mechanical power and through the generator into power. The cooler of the Stirling engine ($HE\ ST_{cold}$) transfers the rejected heat from the Stirling engine to the cold water (CW). This partially heated water (PHW) is then heated in a 2nd step by the first intermediate temperature flue gasses ($FG_{interm\ 1}$).

The water entering the cogeneration system is initially heated by the second intermediate temperature flue gasses ($FG_{interm\ 2}$), resulting in a preheated cold water (CW) entering the cold side of the Stirling engine, with the role to cool it down. The cold flue gasses (FG_{cold}) are then evacuated.

In a 1st phase, the machine does not send the hot water (HW) towards the domestic hot water heat exchanger (HE_{DHW}). The hot water produced (HW) is recirculated through the interior water circuit (IWC) until an acceptable temperature is reached. After this temperature is at an acceptable level, the cold-water pump (CWP) starts working and the hot water produced (HW) is passed through the domestic hot water heat exchanger (HE_{DHW}), where domestic cold water (DCW) receives heat from the hot water (HW) produced by the machine and increases its temperature, becoming domestic hot water (DHW).

The hot water (HW), after exchanging temperature with the domestic cold water (DCW), lowers its temperature and becomes cold water (CW), to serve again in cooling the cold source of the Stirling engine ($HE\ ST_{cold}$) and the cycle is restarted.

As shown in Figure 3.3, the displacement piston (3) pushes helium through the regenerator (2) from the Stirling head (1) to the cooler (4). The spring (8) on the opposite casing at the bottom pushes the piston back upwards. The helium is alternatively heated and cooled, and as a result it expands and contracts again. The working piston (5) is moved up and down by these pressure waves. The magnetic working piston (5) is surrounded by a fixed magnetic coil (6) with copper windings (7). The cycle is repeated 50 times per second, generating AC power at 50 Hz.

The maximum electrical output is 1050 W_{el}. Its characteristics of electrical output are 230 V, ranging from 186 to 264 V. The dimensions without burner are 450 mm in height and 300 mm in diameter. The engine efficiency is at 26 % and its designed life is 50,000 hours. It is hermetically sealed and not requiring maintenance.

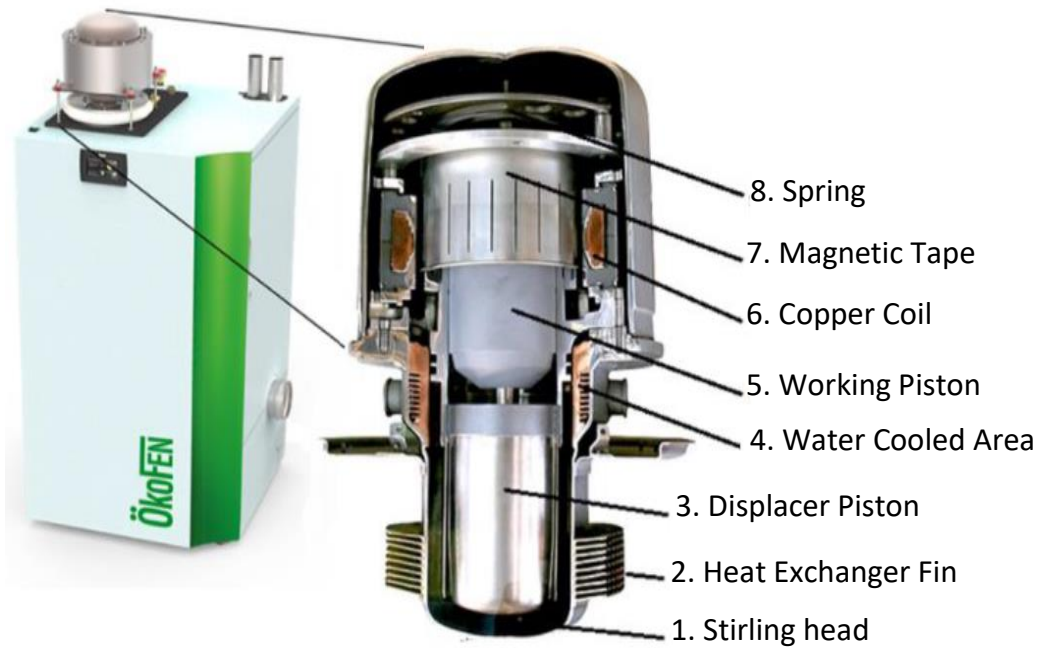


Figure 3.3 - ÖkoFEN Pellematic Condens_E Stirling Engine
 (Source: http://www.okofen-e.com/en/pellematic_condens_e/)

The ÖkoFEN Pellematic Condens_e machine has its own internal sensors that can be accessed locally, as well as through an internet connection. It can also be remotely controlled, so that the end-user can command it to start heating the home before arriving. It also has an automatic module which enables the machine when it detects a certain temperature difference between ambient temperature and outside temperature. The machine was tested in an ON-OFF regime.

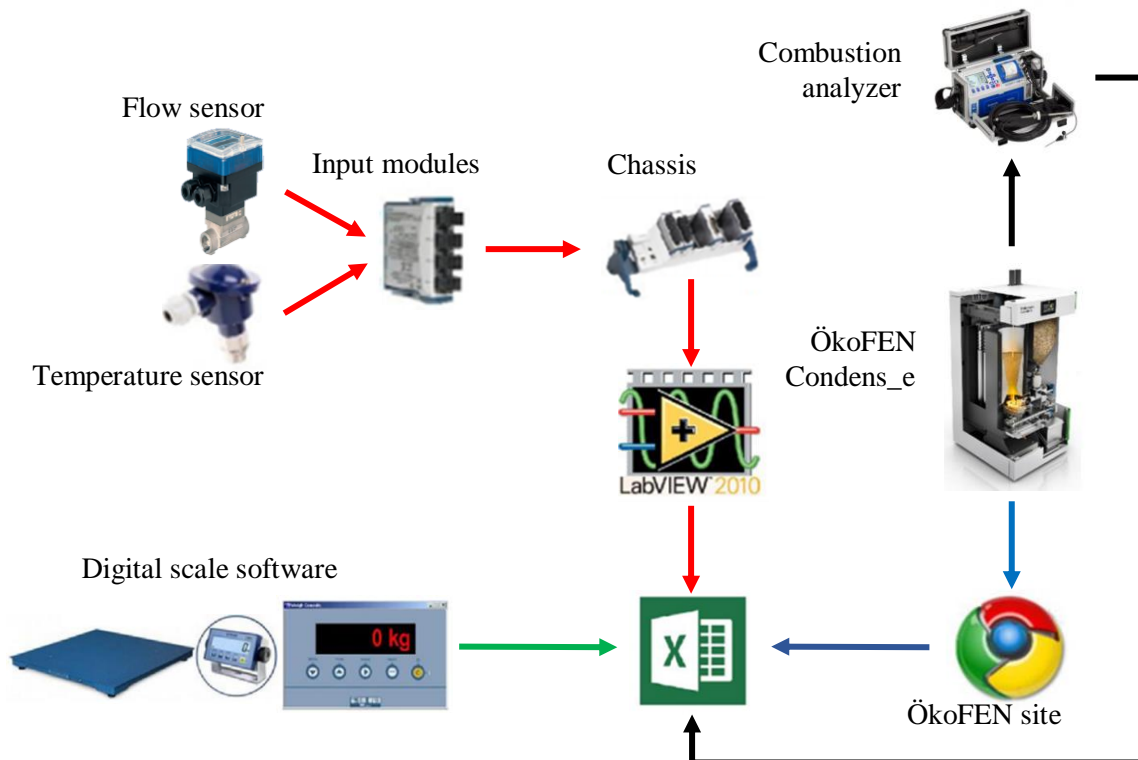


Figure 3.4 - Data acquisition schema

Data was registered from the moment that the machine was turned on and one hour after it was turned off, to observe parameters during cooling. The first tests were done on a total period of 270 minutes (4.5 hours), including the cooling period.

The data acquisition system is presented in Figure 3.4. The red arrow set represents the process of measuring the thermal power output of the machine, the blue arrows that of electrical power output, combustion temperature, Stirling head temperature, average flue gas temperature output and the green arrows that of mass flow. The thermal power output was measured by thermal agent flow and thermal agent temperature. The thermal agent flow (water) was recorded by a Type SE35 Inline flowmeter made by Burkert, connected to a 100 S/s/channel, 4-Channel C Series Universal Analog Input Module, model NI 9219 made by National Instruments, connected to a National Instruments CompactDAQ Chassis, connected to a LabVIEW algorithm that registered the data once every minute in Excel. The thermal agent temperature was recorded with a JUMO PT100 model, connected to a C Series Temperature Input Module made by National instruments, connected to the National Instruments CompactDAQ Chassis, connected to the LabVIEW algorithm writing in Excel.

The blue arrow set represents the process of measuring the electrical power output, combustion temperature, Stirling head temperature, average flue gas temperature, which were recorded internally by the ÖkoFEN PELLEMATIC Condens_e and the data were recorded once per minute. The data was accessed through the Internet, by logging in to the machine's account on the producer's website.

The green arrow set represents the process of measuring the fuel mass which was recorded on a DINI ARGEO WALL-E Floor Series floor scale and connected to the PC with an RS232 to USB cable, then exported to Excel via the DINI-TOOLS program. At the end of each experiment, the relevant data would be selected and all 3 sources of data (thermal, power and mass) would be compiled, as shown in Figure 3.5. The timespan which was used to compile the data was considered to start from the moment that the machine started functioning towards producing thermal power. The stages of the experiment will be explained later in this chapter.

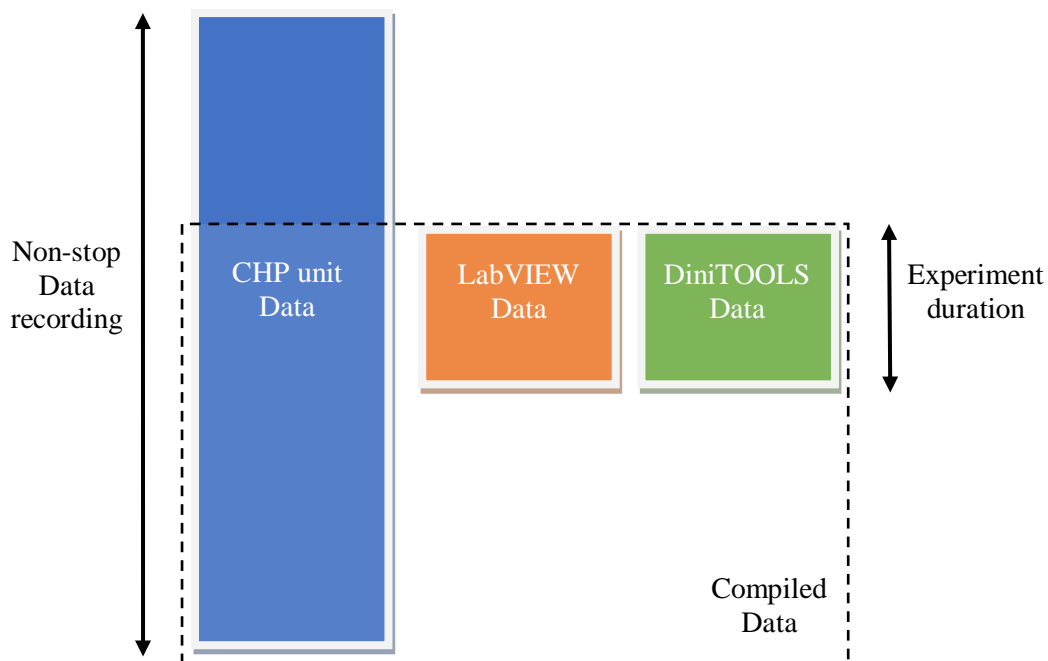


Figure 3.5 - Compiling Excel data from the 3 sources in accordance with the experiment timespan

The measured parameters are centralized in Table 3.2. They are mostly related to the parameters of the thermal agent (water) in different points of measurement, but also to the flue gas exit composition and to the flue gas temperature in the vicinity of the Stirling engine. The power output of the Stirling engine was measured directly through the sensors of the micro-cogeneration unit.

The fuel mass had a high degree of uncertainty since the scale had a 0.2 kg sensitivity and the machine itself was weighed during the experiments.

Table 3.2 - Measured parameters and equipment used in measurement

Measured parameter	Equipment used	Equipment model	Symbol	Unit
Cold water flow	Flow sensor	SE35	F_{CW}	$\frac{l}{min}$
μ CHP unit inner water temperature 1	Condens_E temperature sensor	N/A	T_1^{unit}	$^{\circ}C$
μ CHP unit inner water temperature 2	Condens_E temperature sensor	N/A	T_2^{unit}	$^{\circ}C$
μ CHP unit inner water temperature 3	Condens_E temperature sensor	N/A	T_3^{unit}	$^{\circ}C$
μ CHP unit inner water temperature 4	Condens_E temperature sensor	N/A	T_4^{unit}	$^{\circ}C$
cold water exiting the DHW HE temperature 5	Temperature sensor	JUMO PT100	T_5^{pipe}	$^{\circ}C$
hot water entering the DHW HE temperature 6	Temperature sensor	JUMO PT100	T_6^{pipe}	$^{\circ}C$
hot water exiting the μ CHP unit temperature 7	Temperature sensor	JUMO PT100	T_7^{pipe}	$^{\circ}C$
cold water exiting the μ CHP unit temperature 8	Temperature sensor	JUMO PT100	T_8^{pipe}	$^{\circ}C$
Flue gas final temperature	Combustion analyzer	ECOM EN2	T_4^{FG}	$^{\circ}C$
Stirling hot head outer temperature 1	Condens_E temperature sensor	N/A	$T_{hot 1}^{ST}$	$^{\circ}C$
Stirling hot head inner temperature 2	Condens_E temperature sensor	N/A	$T_{hot 2}^{ST}$	$^{\circ}C$
Stirling cold head temperature	Condens_E temperature sensor	N/A	T_{cold}^{ST}	$^{\circ}C$
Power output	Condens_E power sensor	N/A	P	kW_{el}
Fuel mass	Weight scale	DINI ARGEO WALL-E Floor Scale	m_{fuel}	kg
Room air temperature	Combustion analyzer	ECOM EN2	$T_{air room}$	$^{\circ}C$
Exiting flue gas O ₂ content	Combustion analyzer	ECOM EN2	$\%O_2^{FG}$	%
Exiting flue gas CO content	Combustion analyzer	ECOM EN2	$\%CO^{FG}$	ppm
Exiting flue gas NO content	Combustion analyzer	ECOM EN2	$\%NO^{FG}$	ppm
Exiting flue gas NO _x content	Combustion analyzer	ECOM EN2	$\%NO_x^{FG}$	ppm
Exiting flue gas SO ₂ content	Combustion analyzer	ECOM EN2	$\%SO_2^{FG}$	ppm
Exiting flue gas CO ₂ content	Combustion analyzer	ECOM EN2	$\%CO_2^{FG}$	%
Exiting flue gas air excess	Combustion analyzer	ECOM EN2	λ	—

To determine the thermal power transferred through the thermal agent from the micro-cogeneration unit to the consumer, the properties of water present in Table 3.3 were considered and the parameters in Table 3.4 were determined.

Table 3.3 - Constants used in calculus

Constant	Symbol	Value	Unit
Water density	ρ_{water}	997	kg/m ³
Water specific heat at constant pressure	$c_{\text{p}}^{\text{water}}$	4.18	kJ/kg · K
Flue gas – water heat exchanger efficiency	$\eta_{\text{HE}}^{\text{FG-W}}$	0.98	-

Table 3.4 - Calculated parameters shown in results

Calculated parameter	Symbol	Means of calculation	Unit
Thermal power output of the μ CHP unit	$P_{\text{th}}^{\text{unit}}$	Formula X	kW _{th}
Thermal power of water passing through HE _{cold} ^{FG}	$P_{\text{th} \ 1}^{\text{unit}}$	Formula X	kW _{th}
Thermal power of water passing through HE _{cold} ST	$P_{\text{th} \ 2}^{\text{unit}}$	Formula X	kW _{th}
Thermal power of water passing through HE _{med} ^{FG}	$P_{\text{th} \ 3}^{\text{unit}}$	Formula X	kW _{th}
Thermal power of water passing through HE _{DHW}	$P_{\text{th}}^{\text{pipe}}$	Formula X	kW _{th}
Flue gas temperature exiting the combustion chamber CC	T_1^{FG}	Combustion calculus	°C
Flue gas temperature exiting HE _{hot} ST	T_2^{FG}	Formula Y	°C
Flue gas temperature exiting HE _{med} ^{FG}	T_3^{FG}	Formula Y	°C
Carnot efficiency	η_{c}	Formula	-

The formula used to calculate the thermal power of the thermal agent (water) is presented below as the relation (3.1):

$$P_{\text{th} \ i}^{\text{unit}} = \frac{F_{\text{cw}}}{60} \cdot \rho_{\text{water}} \cdot c_{\text{p}}^{\text{water}} (T_{i+1}^{\text{unit}} - T_i^{\text{pipe}}) \quad (3.1)$$

To calculate the flue gas temperatures, an iterative calculus was made. The relation (3.2) is used to calculate the thermal power of the flue gas and through the relation (3.3), the flue gas temperature T_i^{FG} is calculated.

$$P_{\text{th} \ i}^{\text{unit}} = \eta_{\text{HE}}^{\text{FG-W}} \cdot P_{\text{th} \ i}^{\text{unit FG}} \quad (3.2)$$

$$P_{\text{th} \ i}^{\text{unit FG}} = v_{\text{thCO}_2\text{FG}} \cdot \left(\rho_{\text{CO}_2}^{\text{FG}} \cdot c_{\text{pCO}_2}^{\text{FG}} \cdot T_{i+1}^{\text{FG}} - \rho_{\text{CO}_2}^{\text{FG}} \cdot c_{\text{pCO}_2}^{\text{FG}} \cdot T_i^{\text{FG}} \right) + v_{\text{thSO}_2\text{FG}} \cdot \left(\rho_{\text{SO}_2}^{\text{FG}} \cdot c_{\text{pSO}_2}^{\text{FG}} \cdot T_{i+1}^{\text{FG}} - \rho_{\text{SO}_2}^{\text{FG}} \cdot c_{\text{pSO}_2}^{\text{FG}} \cdot T_i^{\text{FG}} \right) + v_{\text{thN}_2\text{FG}} \cdot \left(\rho_{\text{N}_2}^{\text{FG}} \cdot c_{\text{pN}_2}^{\text{FG}} \cdot T_{i+1}^{\text{FG}} - \rho_{\text{N}_2}^{\text{FG}} \cdot c_{\text{pN}_2}^{\text{FG}} \cdot T_i^{\text{FG}} \right) + v_{\text{thH}_2\text{Oair}} \cdot \left(\rho_{\text{H}_2\text{O}}^{\text{FG}} \cdot c_{\text{pH}_2\text{O}}^{\text{FG}} \cdot T_{i+1}^{\text{FG}} - \rho_{\text{H}_2\text{O}}^{\text{FG}} \cdot c_{\text{pH}_2\text{O}}^{\text{FG}} \cdot T_i^{\text{FG}} \right) + (\lambda - 1) \cdot v_{\text{thdryair}} \cdot \left(\rho_{\text{wet air}}^{\text{FG}} \cdot c_{\text{pwet air}}^{\text{FG}} \cdot T_{i+1}^{\text{FG}} - \rho_{\text{wet air}}^{\text{FG}} \cdot c_{\text{pwet air}}^{\text{FG}} \cdot T_i^{\text{FG}} \right) + (\lambda - 1) \cdot v_{\text{thH}_2\text{OFG}} \cdot \left(\rho_{\text{H}_2\text{O}}^{\text{FG}} \cdot c_{\text{pH}_2\text{O}}^{\text{FG}} \cdot T_{i+1}^{\text{FG}} - \rho_{\text{H}_2\text{O}}^{\text{FG}} \cdot c_{\text{pH}_2\text{O}}^{\text{FG}} \cdot T_i^{\text{FG}} \right) \quad (3.3)$$

For this calculation to be possible, the heat transfer coefficient and the density are presumed to be equal for both T_{i+1} and T_i .

For the Stirling engine, the thermal power absorbed was determined through the relation (3.6).

$$\eta_c = 1 - \frac{T_{hot\ 2}^{ST}}{T_{cold}^{ST}} \quad (3.4)$$

$$\beta = \frac{T_{hot\ 2}^{ST} - T_{cold}^{ST}}{T_{hot\ 1}^{ST} - T_{cold}^{ST}} \quad (3.5)$$

$$P_{th}^{unit\ FG\ i} = \frac{P_{th\ i}^{unit}}{\eta_{HE}^{FG-W} \cdot \beta} \quad (3.6)$$

The principle of the calculation algorithm is shown in Figure 3.6.

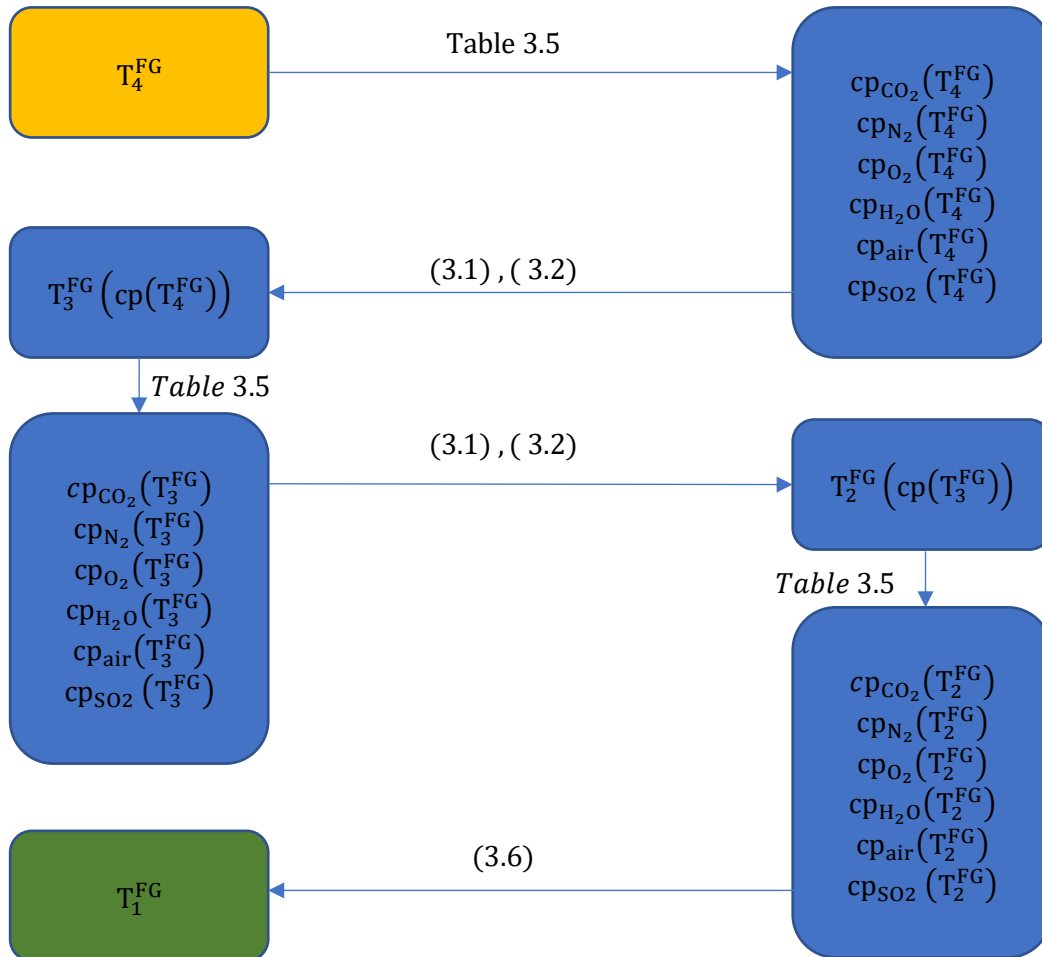


Figure 3.6 - Calculation algorithm of the combustion temperature T_1^{FG}

To calculate the heat transfer coefficient for the flue gas, polynomial functions were calculated using the Microsoft Excel functions shown in **Table 3.5**, based on property tables [<https://www.engineeringtoolbox.com/>] of heat coefficients $\left[\frac{\text{kJ}}{\text{kg}\cdot\text{m}^3}\right]$ and densities $\left[\frac{\text{kg}}{\text{m}^3}\right]$ of all composing elements of the flue gas.

Table 3.5 - Functions used to determine the polynomial coefficients

Coefficient	Excel Function
x^5	= @INDEX(LINEST(known Y's, known X's^{1,2,3,4,5}),1)
x^4	= INDEX(LINEST(known Y's, known X's^{1,2,3,4,5}),1,2)
x^3	= INDEX(LINEST(known Y's, known X's^{1,2,3,4,5}),1,3)
x^2	= INDEX(LINEST(known Y's, known X's^{1,2,3,4,5}), 1,4)
x^1	= INDEX(LINEST(known Y's, known X's^{1,2,3,4,5}),1,5)
x^0	= INDEX(LINEST(known Y's, known X's^{1,2,3,4,5}),1,6)

Figure 3.7 shows the measured and calculated parameters of the thermal agent and flue gas on the micro-cogeneration unit.

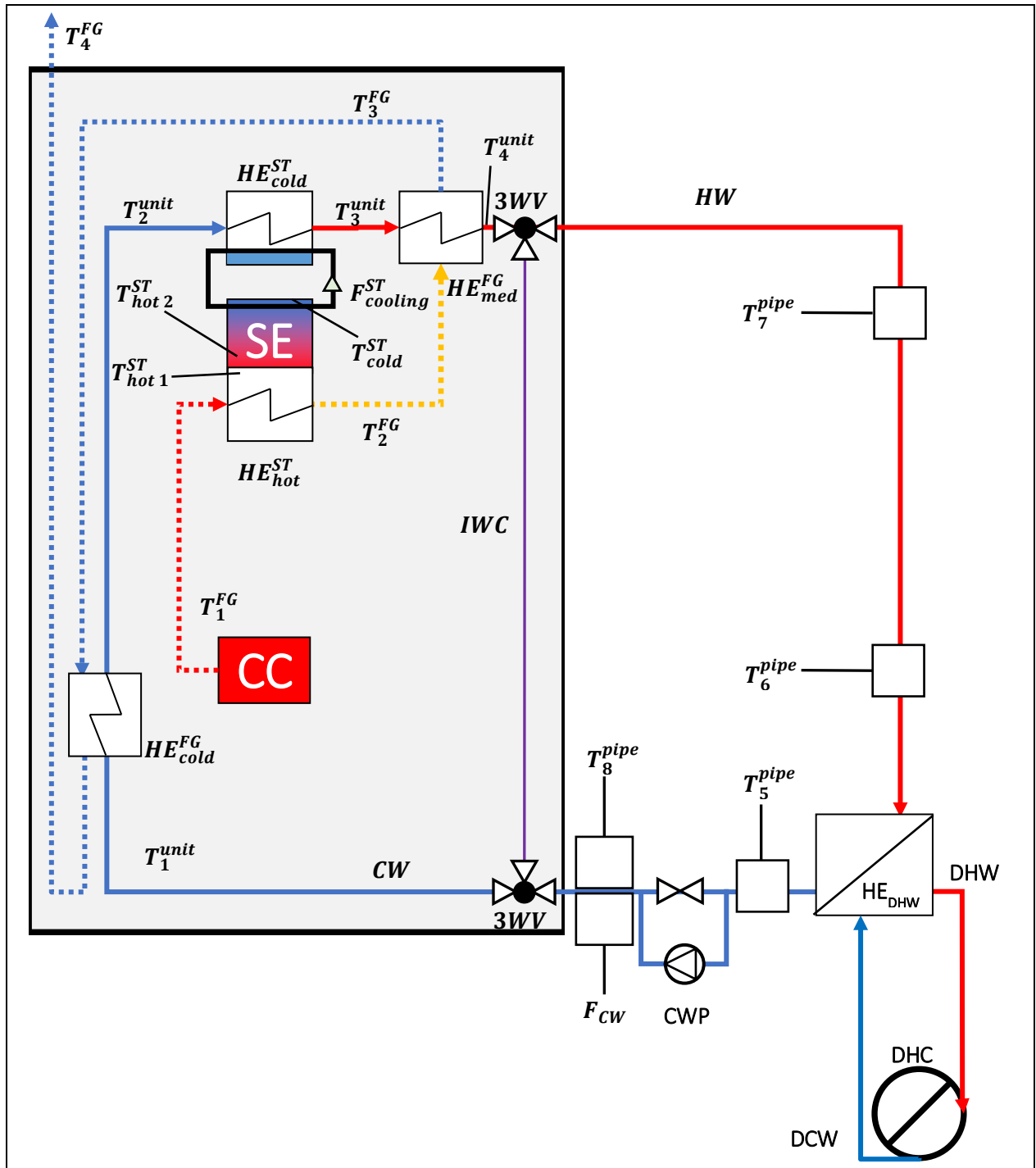


Figure 3.7 - The measurement points on the ÖkoFEN Condens_e cogeneration unit

The measurement points of parameters are shown in figure 3.7. Measurements were done by varying the thermal agent (water) flow rate and the thermal output configuration of the machine. The flow rate variation was done by manipulating a pump in the thermal agent's circuit.

The polynomial function coefficients for the composing gases densities are shown in Annex 3, in the Table A3.1 and the polynomial function coefficients for the composing gases heat transfer coefficients are shown in Annex 3, in the Table A3.2.

The pump has 3 settings of flow rate, which will be referred to as Flow 1, Flow 2 and Flow 3, since the value is not an absolute one from the beginning, but it starts from a certain value and raises until it is stabilized.

The thermal output variation was done by regulating the machines' settings. The thermal output configuration powers were 10 kW_{th}, 12 kW_{th}, 14 kW_{th}. It should be noted that the advised setting by the manufacturer for maximizing the lifetime expectancy of the machine was 12 kW_{th} with Flow 3.

The purpose of varying the thermal agent flow rate and the thermal output power configuration was to determine how the capacity to evacuate the produced heat was impacted.

In terms of efficiency, the question was “is it more efficient to send heat from the machine to the end-user with a slower speed, consuming less fuel or is it more efficient to send more heat, consuming more fuel?”.

This would determine how the machine fits an end-user household, in order to obtain the best use of fuel. Each 3 flows were paired with each 3 thermal power outputs and resulted 9 configurations in total, as shown in Table 3.6.

Table 3.6 - The 9 tested configurations of the 3 thermal outputs paired to the 3 thermal agent flow rates

Thermal power	Flow 1	Flow 2	Flow 3
10kW _{th}	10kW _{th} , F1	10kW _{th} , F2	10kW _{th} , F3
12kW _{th}	12kW _{th} , F1	12kW _{th} , F2	12kW _{th} , F3
14kW _{th}	14kW _{th} , F1	14kW _{th} , F2	14kW _{th} , F3

The flow rate was measured once per minute during start and end of functioning and arbitrarily in short intervals of 1 to 10 minutes after stabilization. Once the flow stabilized, the variation was between -1.12 % and 0.42 %.

Table 3.7 - The 5 stages of the experimental study

Stage	Description
Boot	combustion process has started
Start	thermal power evacuation process has started
Constant	thermal power production is constant
Stop	thermal power production is stopping
End	thermal power production ended

For each configuration, the flow was divided into 5 stages: boot phase, start phase, constant phase, end phase and stop phase, as explained in Table 3.7. A flow was considered “constant” if the thermal power produced varied with less than 5% in comparison to the highest value recorded for the experimental cycle. The stop time was noted manually in the moment when the machine was to stop producing thermal power, and any flow recorded after that time was considered as part of the “stop phase”. If the thermal agent temperature had not been recorded in Excel by the LabVIEW algorithm, it meant that the experiment was over, therefore, the stage was that of “end”.

$$\begin{aligned}
 &= \text{if}(\text{noted_stage} = \text{"stop"}, \text{"stop"} \\
 &\quad \text{if}(\text{recorded_temperature} = \text{"null"}, \text{"end"} \\
 &\quad \text{if}(\text{thermal_power_generated} = 0, \text{"boot"}, \\
 &\text{if}(\text{thermal_power_generated} \\
 &\quad > 0.95 \cdot \text{maximum_thermal_power_generated}, \text{"constant"}, \text{"start"}))))
 \end{aligned} \tag{3.7}$$

If neither of the two met the conditions, the flow was considered as part of the starting phase. This was done by using 4 IF clauses in Excel, shown in the relation 3.7 and explained in Figure 3.8.

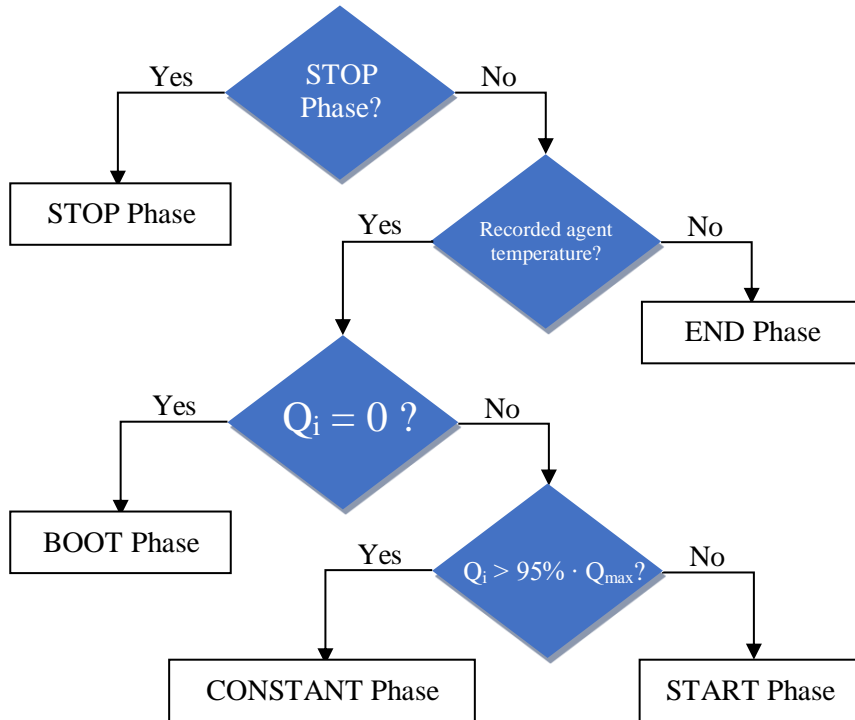


Figure 3.8. - The algorithm used in Excel for determining the experiment phase

Out of the 5 phases of the experiment, the ones considered for the flow were the start, constant and end phase. The thermal output of the machine depended on whether it was sending thermal agent to the heat exchanger with the end-user, therefore the flow had a big impact on which stage the experiment was in.

Figures 3.9 to 3.11 show the three phases of the flow. By using the INDEX and the LINEST functions in Microsoft Excel, the coefficients of the 3rd degree equation (start phase), 1st degree equation (constant phase) and 2nd degree equation (ending phase) were automatically calculated, for a more precise calculation of the functions.

The functions are shown in Tables 3.8 to 3.10. It is important to note that every time a new phase started, the minute by which the flow varied was reset to 0.

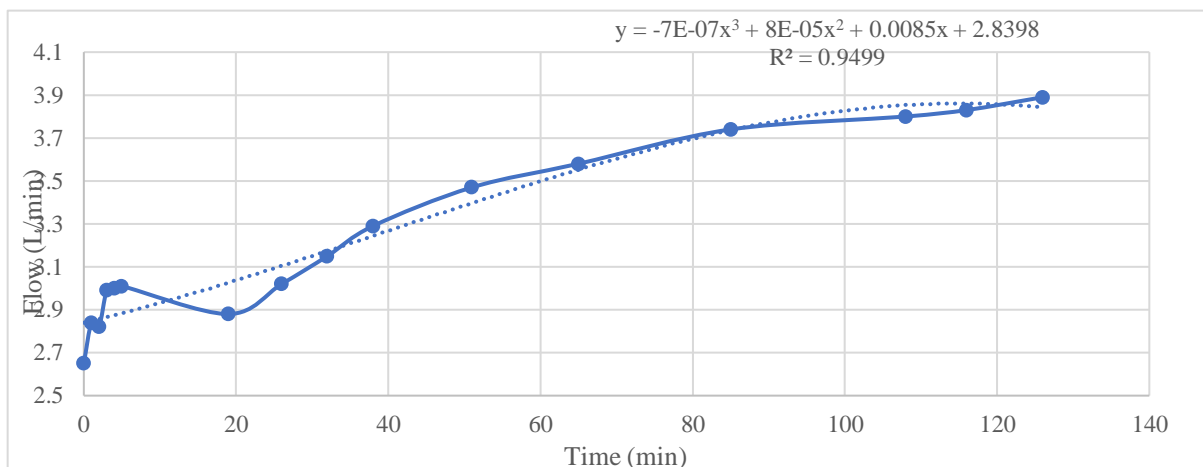


Figure 3.9 - An example of a flow during the start phase

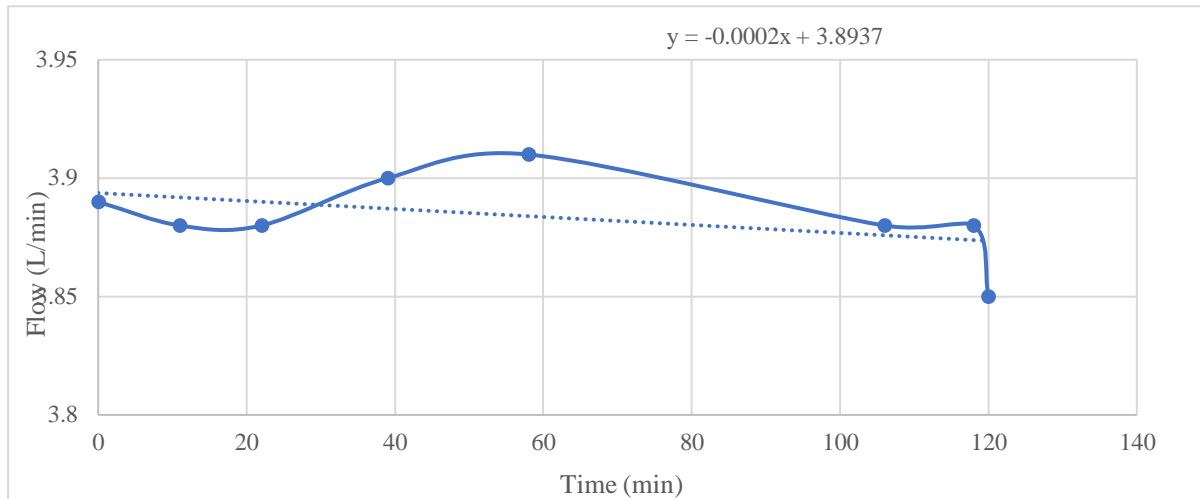


Figure 3.10 - An example of a flow during the constant phase

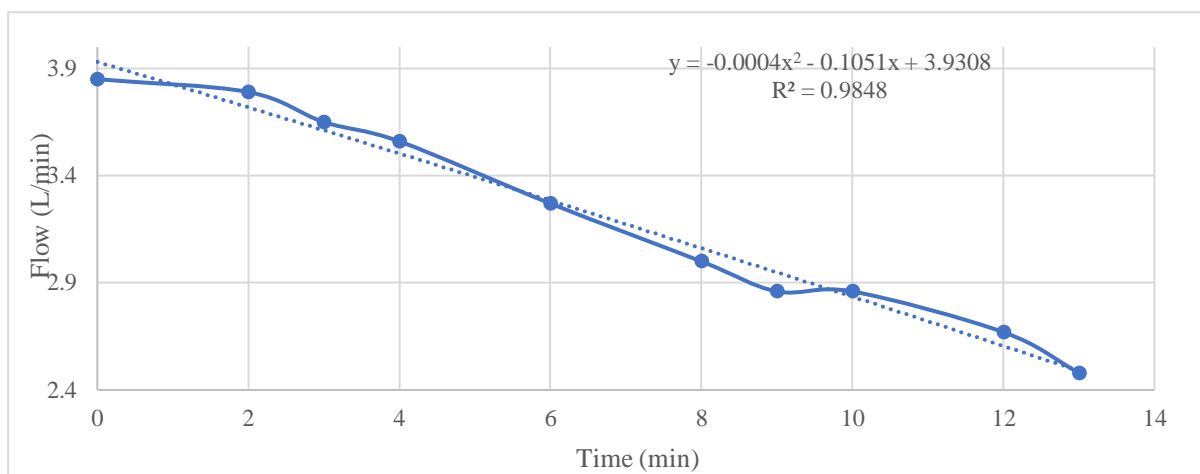


Figure 3.11 - An example of a flow during the ending phase

Table 3.8 - Functions used for determining the 3rd degree equation of the flow in the starting phase

Coefficient	Microsoft Excel function
x^3	=@INDEX(LINEST(known Y's, known X's^{1,2,3}),1)
x^2	=INDEX(LINEST(known Y's, known X's^{1,2,3}),1,2)
x^1	=INDEX(LINEST(known Y's, known X's^{1,2,3}),1,3)
x^0	=INDEX(LINEST(known Y's, known X's^{1,2,3}),1,4)

Table 3.9 - Functions used for determining the 1st degree equation of the flow in the constant phase

Coefficient	Microsoft Excel function
x^1	=SLOPE(known Y's, known X's)
x^0	=INTERCEPT(known Y's, known X's)

Table 3.10 - Functions used for determining the 2nd degree equation of the flow in the ending phase

Coefficient	Excel function
x^2	=@INDEX(LINEST(known Y's, known X's^{1,2}),1)
x^1	=INDEX(LINEST(known Y's, known X's^{1,2}),1,2)
x^0	=INDEX(LINEST(known Y's, known X's^{1,2}),1,3)

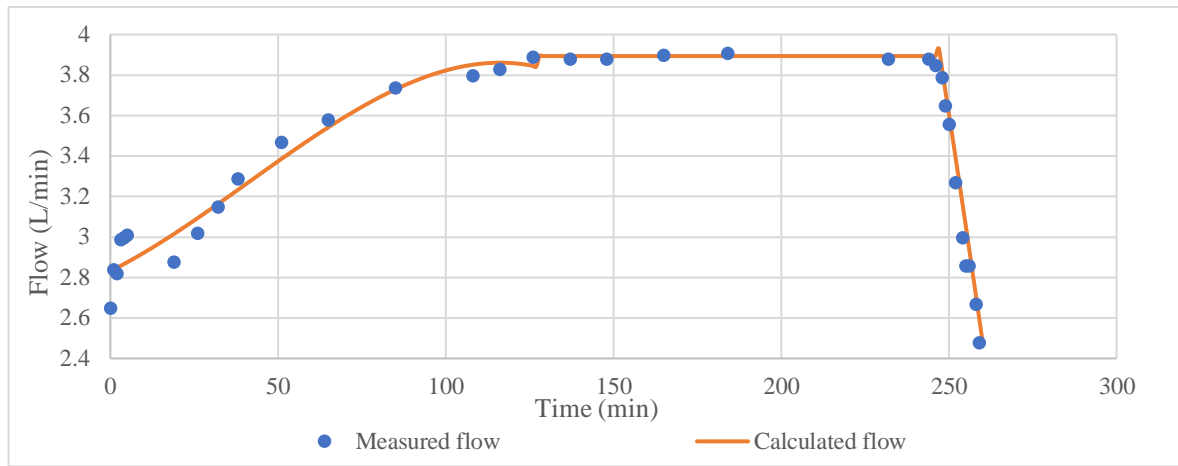


Figure 3.12 - An example of a flow function in its entirety

Figure 3.12 shows the calculated flow in comparison to the measured one. The constant phase was considered equal to the coefficient of the 1st degree function.

The starting phase and the ending phase were calculated using the obtained relations. By tread lining the flow, values are obtained for each minute of functioning, enabling the correlation with the other data that was obtained in a 1-minute interval.

An advantage of this process is that using the obtained equation, the flow can be simulated over a larger period or in ON-OFF scenarios, by modifying the constant phase duration, without any impact to the other 2 phases. The fuel mass flow was determined by recording the weight of the whole machine loaded with pellets every minute.

In the STOP phase of the experiment, when the machine was no longer consuming pellets, therefore its weight remained the same, the weight would be recorded, and it would be subtracted from all the weights measured until that point. This showed the effective mass of biomass that was consumed in the experiment.

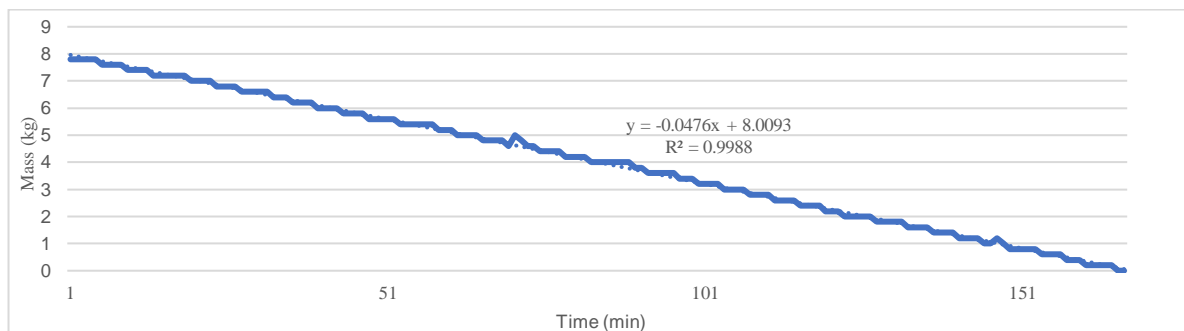


Figure 3.13 - An example of a flow function in its entirety

As Figure 3.13 shows, these weights were recorded and the “SLOPE” function was used in Excel to determine the consumption of biomass during the experiment, in order to calculate the fuel power consumed. The Excel function is shown in relation 3.8.

$$F_{\text{fuel}} = \text{ABS}(\text{SLOPE}(\text{known Y's, known X's}) \cdot 60) \quad (3.8)$$

The “ABS” function was used in the formula because the slope shows the decrease of fuel mass in the inner reservoir of the machine, therefore its value is negative. The aim was to obtain the hourly mass consumption of the machine therefore, since values are recorded every minute, the positive slope result was multiplied by 60 to obtain it.

The weight scale used had a precision of 0.2 kg. Since the weight relation (3.8) used for determining the hourly fuel mass flow depended on 2 consecutive mass values, if the weight change in the fuel was less than the precision of 0.2 kg, it would practically be 0 as shown in Table 3.11 for minutes 0 to 6 and for minutes 7 to 10. A division of the mass values needed to be made to describe any changes of mass inferior to 0.2 kg, for the calculation of the fuel power to be possible between any given 2 minutes.

$$fm_i = 60 \cdot (m_{fuel_i} - m_{fuel_{i+1}}) \left[\frac{kg}{h} \right] \quad (3.9)$$

$$P_{fuel_i} = fm_i \cdot LHV_{fuel} \quad (3.10)$$

Table 3.11 - Initial fuel mass and the accurate, refined fuel mass

Minute	Fuel mass	Number of repetitions	Consecutive difference	Difference between consecutive non-identical values	Accurate fuel mass
0	12.6	0	0	0	12.6
1	12.6	1	0	-0.028571429	12.57142857
2	12.6	2	0	-0.057142857	12.54285714
3	12.6	3	0	-0.085714286	12.51428571
4	12.6	4	0	-0.114285714	12.48571429
5	12.6	5	0	-0.142857143	12.45714286
6	12.6	6	0	-0.171428571	12.42857143
7	12.4	0	-0.2	0	12.4
8	12.4	1	0	-0.05	12.35
9	12.4	2	0	-0.1	12.3
10	12.4	3	0	-0.15	12.25
11	12.2	0	-0.2	0	12.2

The division was done by first recording the number of repetitions of the same fuel mass in the column “number of repetitions”, using an IF clause in MS Excel as shown in the relation (3.11). For example, the fuel mass 12.6 kg in minute 0 was the first value recorded, therefore the number of repetitions nr_0 is 0. In minute 1, the fuel mass was identical to the 12.6 kg fuel mass in minute 0, therefore the number of repetitions nr_1 becomes the previous number of repetitions plus 1 ($nr_{i+1} = nr_i + 1$).

$$nr_{i+1} = IF(m_i <> m_{i+1}, 0, nr_i + 1) \quad (3.11)$$

The column “Consecutive difference” is used to determine the consecutive difference of fuel mass between 2 non-identical consecutive fuel mass values, as shown in the relation (3.12).

$$cd_i = fm_i - fm_{i-1} \quad (3.12)$$

The column “Distance between consecutive non-identical values” divides the distance between consecutive non-identical values of the fuel mass into smaller thresholds, as shown in the relation (3.13). If the next number of repetitions $nr_{i+1} = 0$ or the next fuel mass value is a new one, the current difference between consecutive non-identical values will be the difference between the initial value of the fuel mass and the next value of the fuel mass ($cd_{i+1} = fm_i - fm_{i+1}$) multiplied by the current number of repetitions divided by the total number of consecutive occurrences of that flow mass ($nr_i/(nr_i + 1)$).

Note that the consecutive occurrences number is equal to the number of repetitions to which the 1st occurrence is added. If, however, the next number of repetitions is not 0, the next

difference between consecutive non-identical values ($DBCNIV_{i+1}$) will be divided to the number of repetitions + 1 and multiplied by the current number of repetitions of that value.

$$DBCNIV_i = IF\left(nr_{i+1} = 0, cd_{i+1} \cdot \frac{nr_i}{nr_i + 1}, DBCNIV_{i+1} \cdot \frac{nr_i}{nr_i + 1}\right) \quad (3.13)$$

For example, the DBCNIV value is calculated in minute 6 just before the new mass value of minute 7, as shown in Figure 3.14, the case will be that of the next number of repetitions equal to 0 ($nr_7 = 0$), in which the value of the DBCNIV will be the next consecutive difference ($cd_7 = -0.2$) multiplied with the current number of repetitions ($nr_6 = 6$) and divided by the total number of occurrences ($nr_6 + 1 = 7$).

SUM						
=IF(C9=0,D9/(C8+1)*C8,E9/(C8+1)*C8)						
	A	B	C	D	E	F
1	Minute	Fuel mass	Number of repetitions	Consecutive difference	Difference between consecutive non-identical values	Accurate fuel mass
2	0	12.6	0	0	0	12.6
3	1	12.6	1	0	-0.028571429	12.57142857
4	2	12.6	2	0	-0.057142857	12.54285714
5	3	12.6	3	0	-0.085714286	12.51428571
6	4	12.6	4	0	-0.114285714	12.48571429
7	5	12.6	5	0	-0.142857143	12.45714286
8	6	12.6	6	0	=IF(C9=0,D9/(C8+1)*C8,E9/(C8+1)*C8)	12.42857143
9	7	12.4	0	-0.2	0	12.4

Figure 3.14 - Calculating the DBCNIV just before a new mass value

If the calculated $DBCNIV_i$ of a fuel mass value precedes an identical fuel mass value as shown in Figure 3.15, the case will be that of the previously calculated ($DBCNIV_{i+1} = -0.171428571$) multiplied with the current number of repetitions $nr_5 = 5$ and divided by the total number of occurrences up until this point ($nr_5 + 1 = 6$).

SUM						
=IF(C8=0,D8/(C7+1)*C7,E8/(C7+1)*C7)						
	A	B	C	D	E	F
1	Minute	Fuel mass	Number of repetitions	Consecutive difference	Difference between consecutive non-identical values	Accurate fuel mass
2	0	12.6	0	0	0	12.6
3	1	12.6	1	0	-0.028571429	12.57142857
4	2	12.6	2	0	-0.057142857	12.54285714
5	3	12.6	3	0	-0.085714286	12.51428571
6	4	12.6	4	0	-0.114285714	12.48571429
7	5	12.6	5	0	=IF(C8=0,D8/(C7+1)*C7,E8/(C7+1)*C7)	12.45714286
8	6	12.6	6	0	-0.171428571	12.42857143
9	7	12.4	0	-0.2	0	12.4

Figure 3.15 - Calculating the DBCNIV for a fuel mass equalling the next

After the DBCNIV has been calculated, the accurate fuel mass can be determined through the relation (3.14):

$$afm_i = fm_i + DBCNIV_i \quad (3.14)$$

To obtain the fuel power used by the machine, the relation (3.15) was used. The lower heating value of the fuel was taken from previous works (Bouvenot, 2014), which included a lower heating value analysis of the fuel performed by a third-party laboratory.

$$P_{fuel} = LHV_{fuel} \cdot fm_{fuel} \quad (3.15)$$

The thermal and power efficiencies were calculated with the relations (3.16) and (3.17).

$$\eta_{th} = \frac{P_{th}}{P_{fuel}} = \frac{\frac{V_{water}}{60} \cdot \rho_{water} \cdot c_{p_{water}} (T_6 - T_5)}{P_{fuel}} \quad (3.16)$$

$$\eta_{el} = \frac{P_{el}}{P_{fuel}} \quad (3.17)$$

An overview of the μ CHP to user circuit is presented in Figure 3.13. The thermal power was calculated according to temperatures in point 6 and point 5 of the diagrams presented below, as also shown in the relation (3.16). In calculating the total efficiency of the system, the thermal losses occurred between points 6 and 7 were considered and included in the final efficiency of the μ CHP unit. The reason of this inclusion was that the machine itself is being described in this article and not the circuit connecting it to the user. The thermal losses occurred depend on distance from the machine to the heat exchanger with the user, isolation of the pipes and other parameters that are variable from one case to the other. Therefore, the thermal losses are calculated with the relation (3.18) and the total efficiency is calculated with the relation (3.19).

$$\%th_{loss} = \frac{\frac{V_{water}}{60} \cdot \rho_{water} \cdot c_{p_{water}} (T_7 - T_6)}{P_{fuel}} \quad (3.18)$$

$$\eta_{total} = (\eta_{th} + \eta_{th_{loss}}) + \eta_{el} \quad (3.19)$$

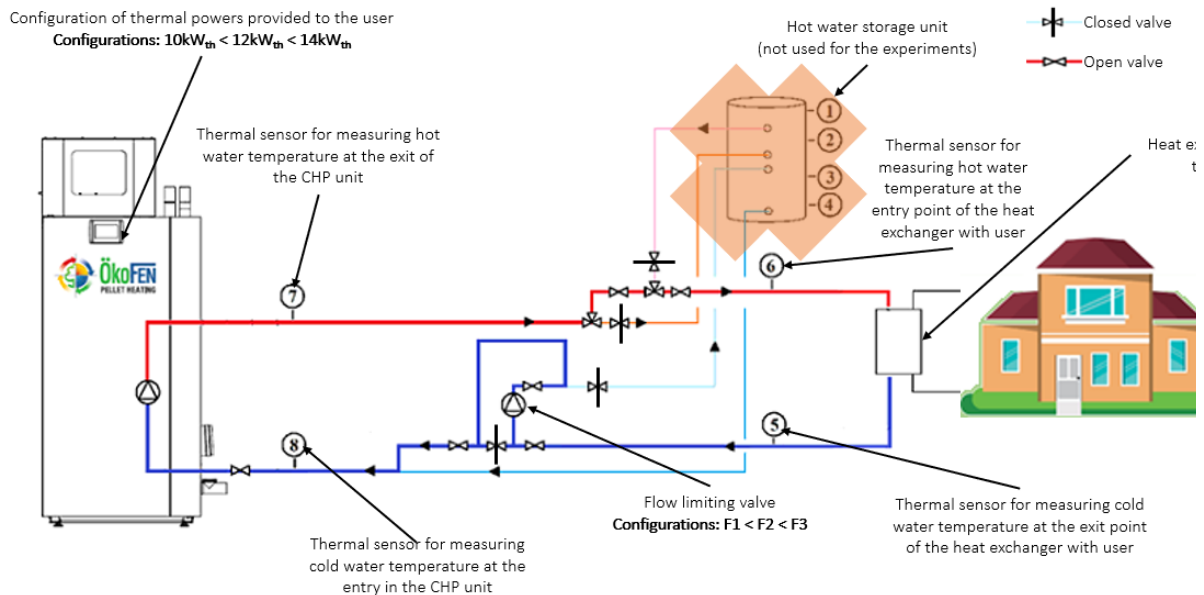


Figure 3.16 - The overview of the μ CHP to user circuit and the points of temperature measurement

3.3. RESULTS

The 9 configurations shown in Table 3.8 were conducted in 2 sessions. In the 1st session of experiments the thermal agent flow was measured through the dedicated flow meters.

3.3.1. Flow rate results

As shown in the relation (3.1), the thermal power output of the cogeneration unit depends on the difference between the high temperature (T_{hot}) and the low temperature (T_{cold}), as well as the flow of the thermal agent conducting heat.

The nominal temperature for hot water is 60 °C and the machine has an inner safeguard, which lowers the thermal output power automatically once the temperature of 75 °C is reached. In certain configurations, the temperature rises above 60 °C, because of a flow inferior to the one needed to evacuate heat from the cogeneration unit.

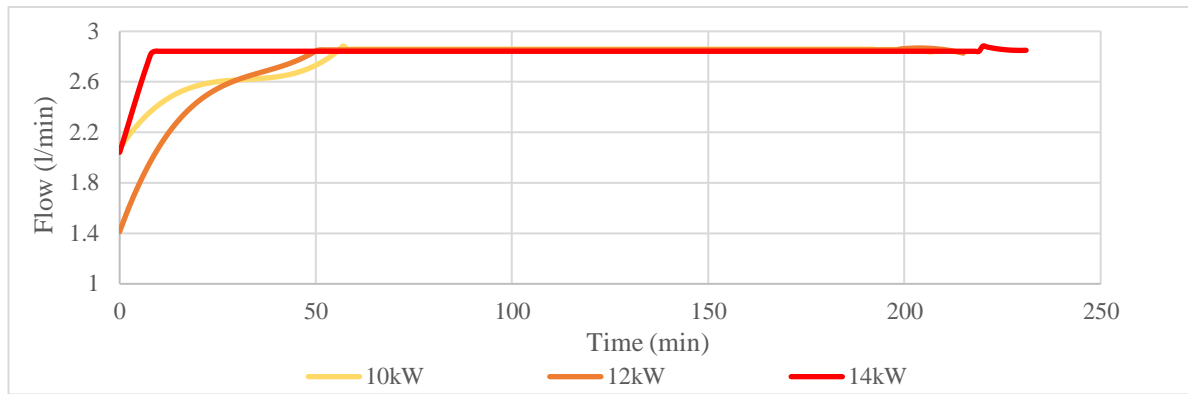


Figure 3.17 - Flow rate results for the F1 setting, for thermal output powers of 10 kW_{th}, 12 kW_{th} and 14kW_{th}

The flow of the thermal agent conducting heat from the machine to the user cannot be precisely set. It depends on the quantity of heat available after powering the Stirling engine.

The flow rises in correlation to the amount of heat to be rejected by the cogeneration unit and its setting influences the maximum flow value attainable.

Figure 3.17 shows that for all scenarios of functioning on the 1st pump setting, the flow reaches a constant value of 2.85 l/min, which is the utmost limit of the F1 setting.

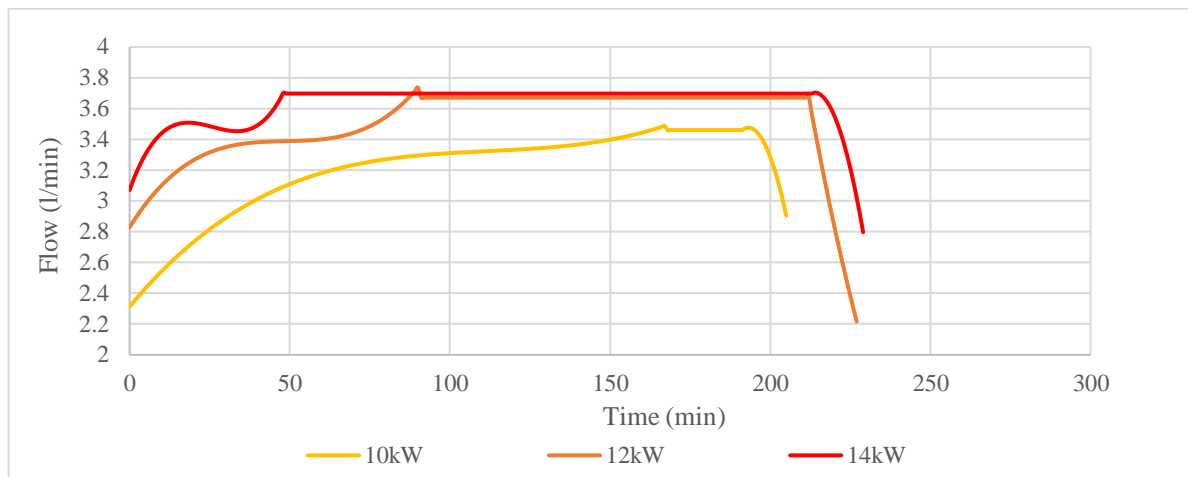


Figure 3.18 - Flow rate results for the F2 setting, for thermal output powers of 10 kW_{th}, 12 kW_{th} and 14 kW_{th}

As the thermal power produced increases, so must the flow of thermal agent which is evacuating heat from the Stirling engine and flue gasses. If this flow is sufficient to evacuate the available heat from the machine, the temperatures of the thermal agent will remain around 60 °C.

Figure 3.18 shows that the machine reaches a constant flow limit of 3.4 l/min after more than 160 minutes for the 10 kW_{th} thermal power output.

For the thermal output power of 14 kW_{th}, the constant flow limit is superior to that of the 10 kW_{th} configuration.

The limit reached is superior, of 3.7 l/min, which is coherent to the superior amount of heat to be evacuated from the μCHP unit. This limit is reached faster for the 14 kW_{th} configuration than for the 12 kW_{th} configuration, in under 50 minutes, in comparison to 90 minutes.

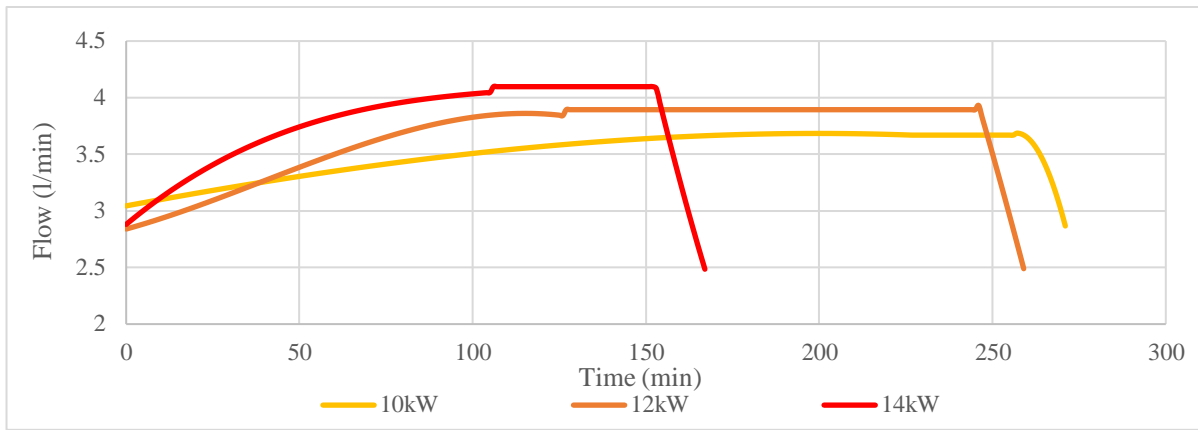


Figure 3.19 - Flow rate results for the F3 setting, for thermal output powers of 10 kW_{th}, 12 kW_{th} and 14 kW_{th}

The 3rd configuration of the flow has the highest limit of flow. As shown in Figure 3.19, it reaches 4.1 l/min in the case of a thermal power output of 14 kW_{th}. The limitative nature of this pump can be observed since the flow remains the approximately the same for the 10 kW_{th} thermal power output, which is 3.5 l/min for F2 and 3.7 l/min for F3, while the same is available for the 12 kW_{th} thermal power output, registering a 3.7 l/min value for F2 and 3.8 l/min for F3.

The 14 kW_{th} thermal power output necessitates the biggest flow of thermal agent evacuating heat from the μCHP unit and it reaches a 4.1 l/min value.

3.3.2. Thermal agent temperature in correlation with the thermal agent flow

As seen in the previous sub-section, the flow of the thermal agent conducting heat from the machine to the user cannot be precisely set, but only limited. Upon stabilizing, the value of the flow depends on the quantity of heat rejected by the Stirling engine. The flow rises in correlation to the amount of heat to be rejected by the cogeneration unit and its setting influences the maximum flow value attainable.

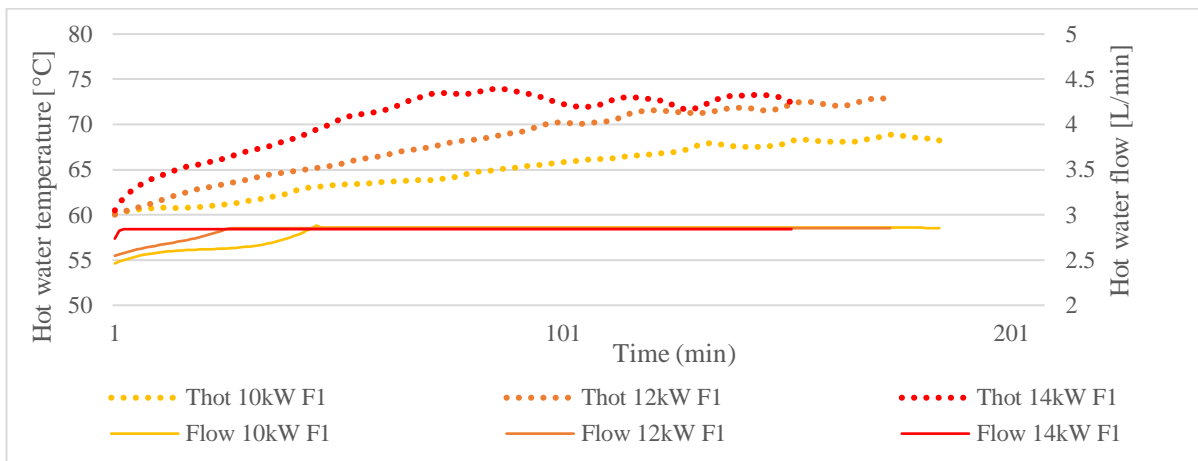


Figure 3.20 - Thermal agent and flow rate result correlation for the F1 setting, for thermal power outputs of 10 kW_{th}, 12 kW_{th} and 14 kW_{th}

Figure 3.20 shows that for all thermal power outputs on the 1st pump setting F1, the flow reaches a constant value limited to 2.85 l/min as previously seen also in Figure 3.17. By correlating the flow values with the temperatures of the thermal agent evacuating heat from the machine, it can be observed that the temperature rises above 60 °C for all configurations. In the case of 14 kW_{th} using Flow 1 (14 kW F1), the temperature (Thot) raises to 74 °C. The machine enables its

safeguard of keeping its temperature below 75 °C and switches to a partial load ratio functioning of the Stirling engine, in order to lower the temperature of its inner thermal agent. The same temperature of the 12 kW_{th} using Flow 1 (12 kW F1) configuration steadily rises to the same temperature of 74 °C as for the 14 kW F1 configuration and the safeguard system of the machine activates the partial load ratio mode.

The temperatures correlated to the functioning in this Flow 2 in Figure 3.21 show that only the 10 kW_{th} configuration temperature (Thot 10 kW F2) stays at a temperature of 61 °C temperature, while the 12 kW_{th} and 14 kW_{th} configurations have 64 °C and 69 °C temperature. These results show that even with a lower thermal power output of 10 kW_{th}, the flow is insufficient to evacuate the heat produced by the machine for the thermal agent to remain at a 60 °C temperature.

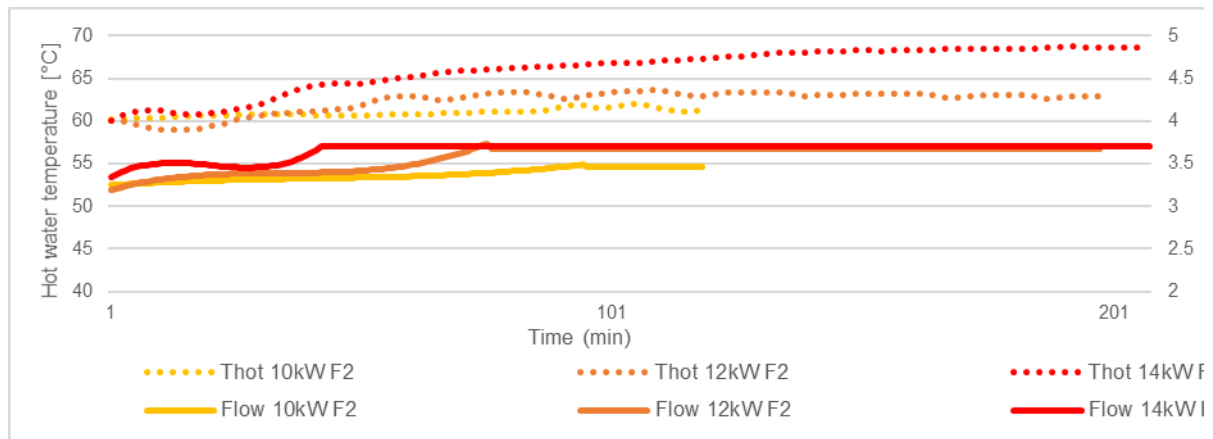


Figure 3.21 - Thermal agent and flow rate result correlation for the F2 setting, for thermal power outputs of 10 kW_{th}, 12 kW_{th} and 14 kW_{th}

In the flow configuration with the highest limit, F3, shown in Figure 3.22, it can be observed that the temperatures still reach values superior to 60 °C, which is the desirable temperature for the domestic hot water arriving at the consumer. The highest temperature attained is for the 14 kW_{th} thermal power output, of 63 °C, while the second temperature is for the 12 kW_{th} thermal power output, of 61 °C and the third is that of the 10 kW_{th} thermal output, of 60 °C.

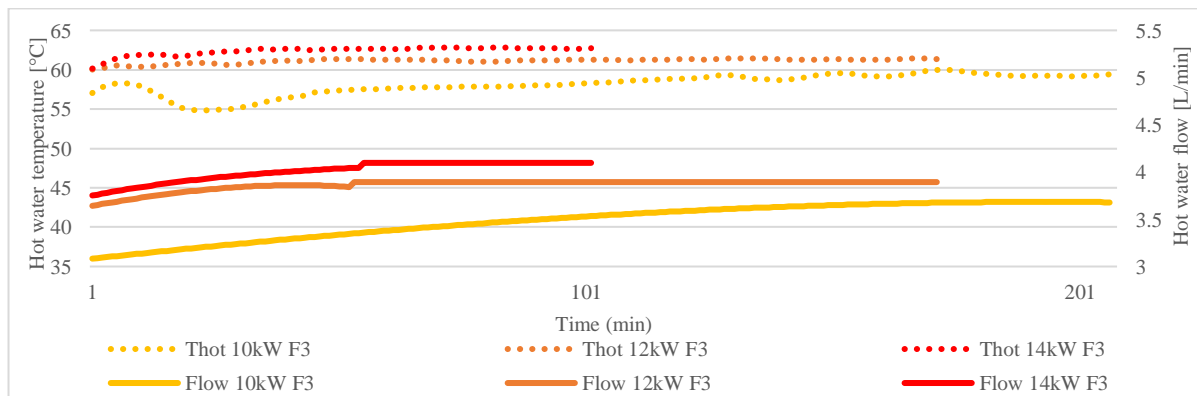


Figure 3.22 - Thermal agent and flow rate result correlation for the F3 setting, for thermal power outputs of 10 kW_{th}, 12 kW_{th} and 14 kW_{th}

Since the flow of the thermal agent influences its temperature, the same thermal power output of 10 kW_{th} has been compared to flows in settings F1, F2 and F3 in Figure 3.23. For the thermal power output of 10 kW_{th}, the F2 and F3 flow configurations have ensured a temperature of the thermal agent between 59 °C to 61 °C. However, for the F1 flow, the temperature rose to nearly

69 °C, which shows that the F1 setting of the flow was insufficient for evacuating heat from the machine.

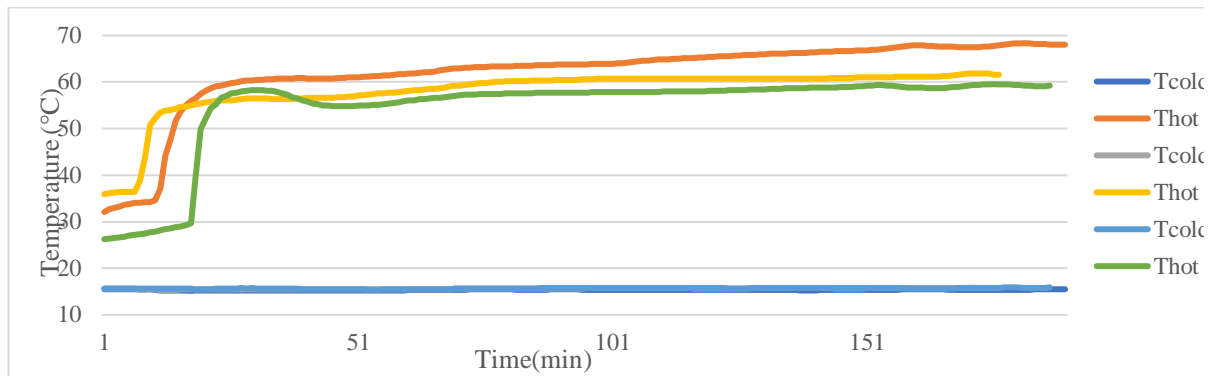


Figure 3.23 - Heat exchanger temperatures for a thermal power output of 10 kW_{th} with the 3 flow settings

As shown in Figure 3.24, in the 12 kW_{th} thermal power output configuration, the temperature of the F2 and F3 configurations have risen to the interval of 60 °C to 62 °C, with 2 °C more than in the 10 kW_{th} thermal output configurations, still remaining in acceptable parameters, near 60 °C. The F1 configuration also registered a rise in the temperature of the thermal agent of 2 °C, reaching 71 °C. This temperature is above the 60 °C threshold that the domestic hot water should have when arriving to the consumer.

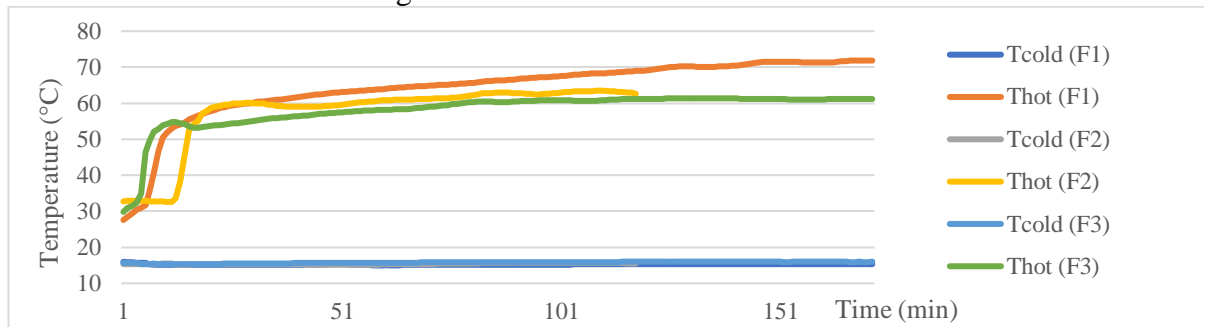


Figure 3.24 - Heat exchanger temperatures for a thermal power output of 12 kW_{th} with the 3 flow settings

For the 14 kW_{th} thermal power output configuration shown in Figure 3.25, the temperatures of the thermal agent rise with 2 °C for the F3 flow setting, with 7°C for the F2 flow setting and with 2 °C for the F1 flow setting.

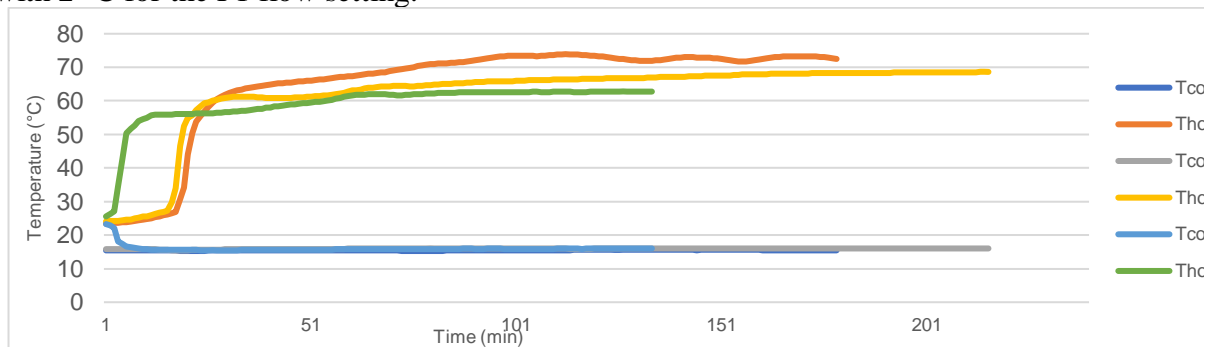


Figure 3.25 - Heat exchanger temperatures for a thermal power output of 14 kW_{th} with the 3 flow settings

The incoherency of these raises is due to the self-guarding mechanism of the machine, because intuitively, there should have been a proportionate raise in temperature for the F1 flow setting, in comparison to the F2 and F3 settings. However, the μ CHP unit starts to automatically run in

the partial-load ratio, to decrease its temperature and not attain the set limit of 75 °C which may damage its components.

3.3.3. Generated power and Stirling engine work fluid temperature

Since in many cases, the μ CHP unit entered in partial load-ratio, it is interesting to observe the power output that was generated, in function of different flow rate settings. The same thermal power output has been grouped with the 3 flow rates, to observe the variation of the power produced due to the machines' safeguarding mechanism.

As seen in Figure 3.26, the temperatures of the working fluid of the μ CHP unit reach similar values, of 420 °C to 440 °C. It can be observed that the 14 kW_{th} thermal output configuration generates the most power, reaching values of 950 W to 1,000 W. This configuration also reaches a stable 900 W value the fastest.

The configurations 10 kW_{th} and 12 kW_{th} reach inferior values in comparison to 14 kW_{th}, halting at 900 W. The difference between the 10 kW_{th} and 12 kW_{th} configurations is that in the case of 12 kW_{th}, the 900 W generated power is stabilized faster than the 10 kW_{th} configuration. However, the F3 configuration has a more constant power generation with less noise.

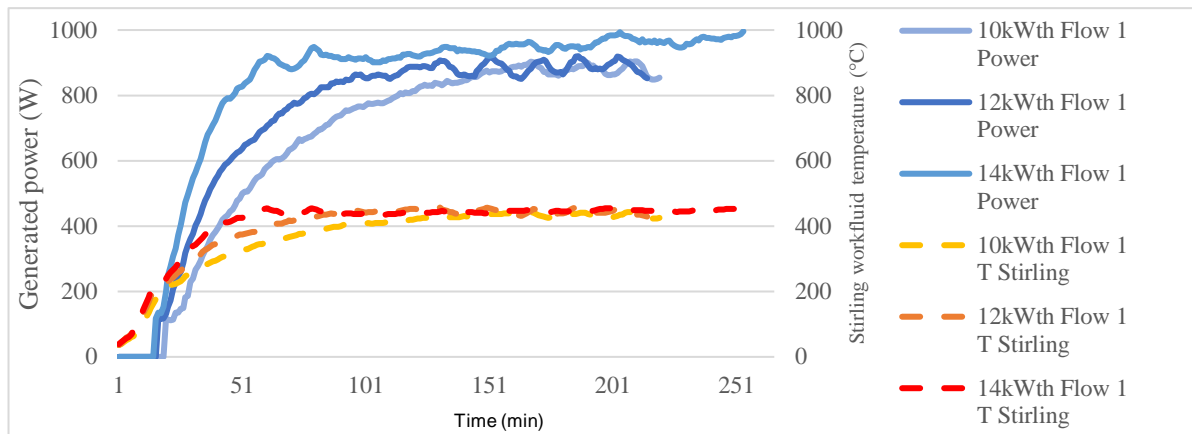


Figure 3.26 - Generated power output and Stirling work fluid temperature for the F1 flow setting

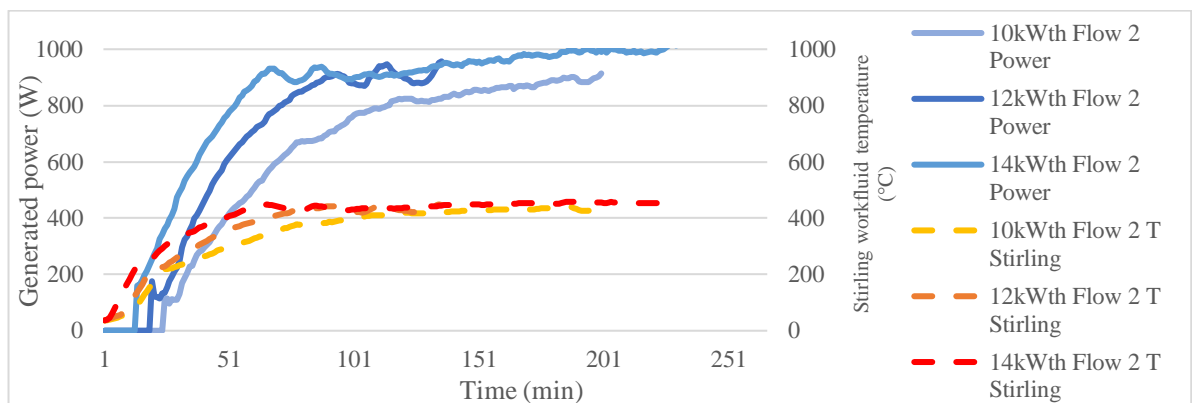


Figure 3.27 - Generated power output and Stirling work fluid temperature for the F2 flow setting

For the flow setting F2, it can be observed in Figure 3.27 that the temperatures of the working fluid of the Stirling engine are similar to those for the flow setting F1. Also, similar to the case of the F1 configuration, the 14 kW_{th} configuration in with F2 achieves the nominal generated power faster than the 10 kW_{th} and 12 kW_{th} configurations.

The generated power for the 14 kW_{th} case is more than 1,000 W_{el} after 220 minutes of functioning, while it reaches 950 W_{el} for the 12 kW_{th} configuration after 140 minutes, value comparable to the 14 kW_{th} configuration at that point in time. The 10 kW_{th} configuration reaches only 900 W_{el} after 200 minutes of functioning.

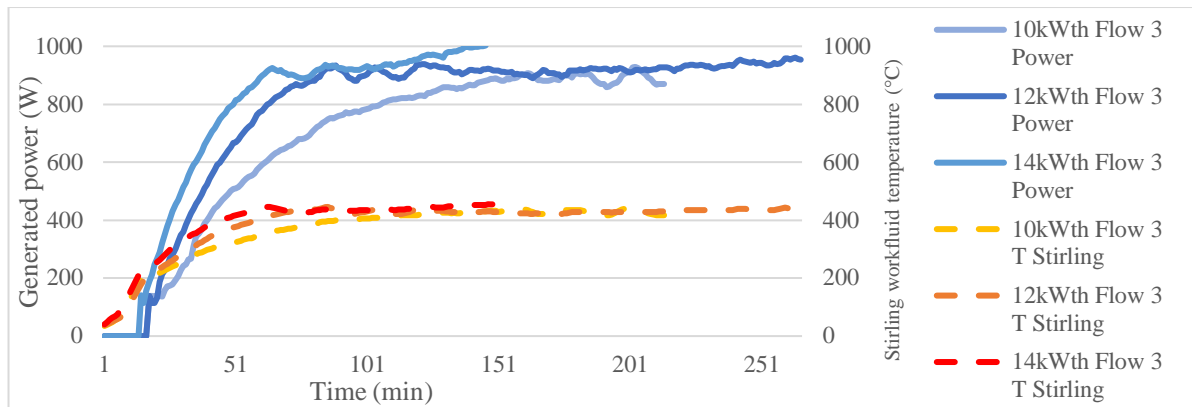


Figure 3.28 - Generated power output and Stirling work fluid temperature for the F3 flow setting

For the F3 flow setting, shown in Figure 3.28, the 14 kW_{th} thermal power output configuration passes the 1000 W_{el} threshold much faster than in the F2 flow setting, after 145 minutes, in comparison to 220 minutes for F2.

The temperatures of the working fluid remain similar, in the 420 °C to 440 °C interval.

The power generated by the 12 kW_{th} thermal power output is relatively stable at 900 W_{el} to 950 W_{el}, reaching this point after 65 minutes of functioning, while for the 14 kW_{th} configuration, this power is reached after 55 minutes of functioning.

In the case of 10 kW_{th}, the generated power reaches the 900 W_{el} value after 150 minutes, the values remaining under 950 W_{el}.

3.3.4. Fuel mass flow consumption and efficiencies

The fuel mass flow has been calculated with the relation (3.8) for all configurations, as suggested in the Table 3.12.

Table 3.12 - Configuration thermal power and agent flow

Configuration [thermal power - agent flow]	Stirling engine start [minute]	Flow limiting pump start [minute]
10kW-F1	30	26
	33	33
10kW-F2	43	59
	36	34
10kW-F3	30	31
	48	69
12kW-F2	42	58
12kW-F3	31	46
	30	40
	26	40
	26	40
14kW-F2	39	62
14kW-F3	116	207

The results are shown in Figure 3.29. The highest consumption of fuel per hour was for the F2 flows for the 3 thermal power outputs (10 kW_{th}, 12 kW_{th} and 14 kW_{th}).

For the 10 kW_{th} and 12 kW_{th} configuration, the F1 flow had a higher rate of consumption, than for the F3 flow, while in the case of 14 kW_{th} it was the opposite.

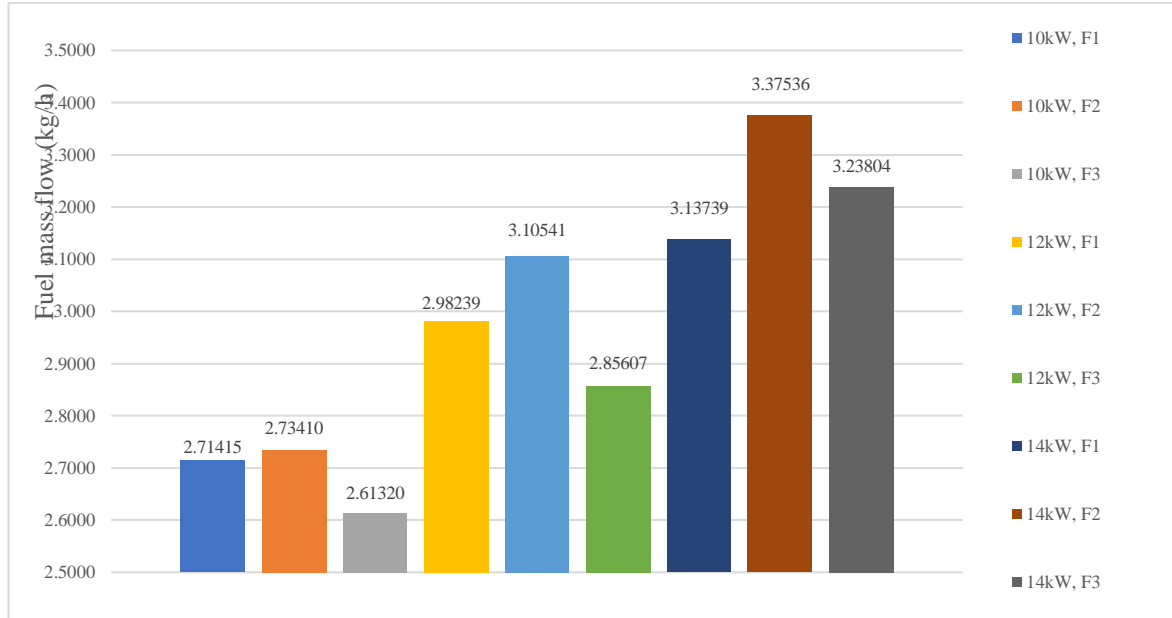


Figure 3.29 - The fuel mass flow consumption of the studied configurations

By using Formulas (3.15), (3.16) and (3.17) the thermal and power efficiencies were calculated. As previously stated, the linear thermal losses were included in the thermal efficiency, since the machine itself is being characterized and not the whole system connecting it to the user.

A ranking of the 9 total efficiencies is shown in the Table 3.13.

It can be observed that the flow of thermal agent evacuating heat from the machine was the defining factor in the total efficiency of configurations. As a general pattern, the greater the flow, the better the total efficiency.

Table 3.13 - Ranking of configuration in function of total efficiency

Configuration	Total efficiency	Thermal efficiency	Linear thermal losses	Power efficiency
12kW, F3	98.60%	89.04%	2.75%	6.82%
10kW, F3	97.83%	88.16%	2.88%	6.79%
14kW, F3	93.38%	84.18%	2.81%	6.40%
10kW, F2	92.83%	83.39%	2.74%	6.70%
14kW, F2	90.70%	82.14%	2.44%	6.12%
12kW, F2	90.10%	81.38%	2.84%	5.88%
10kW, F1	89.00%	79.96%	2.62%	6.43%
12kW, F1	86.95%	78.39%	2.73%	5.84%
14kW, F1	83.56%	75.21%	2.75%	5.61%

The results are graphically represented in the Figure 3.30.

The highest overall efficiency calculated with the relation 3.19 was that of the 12 kW_{th} thermal power output with the flow F3 configuration.

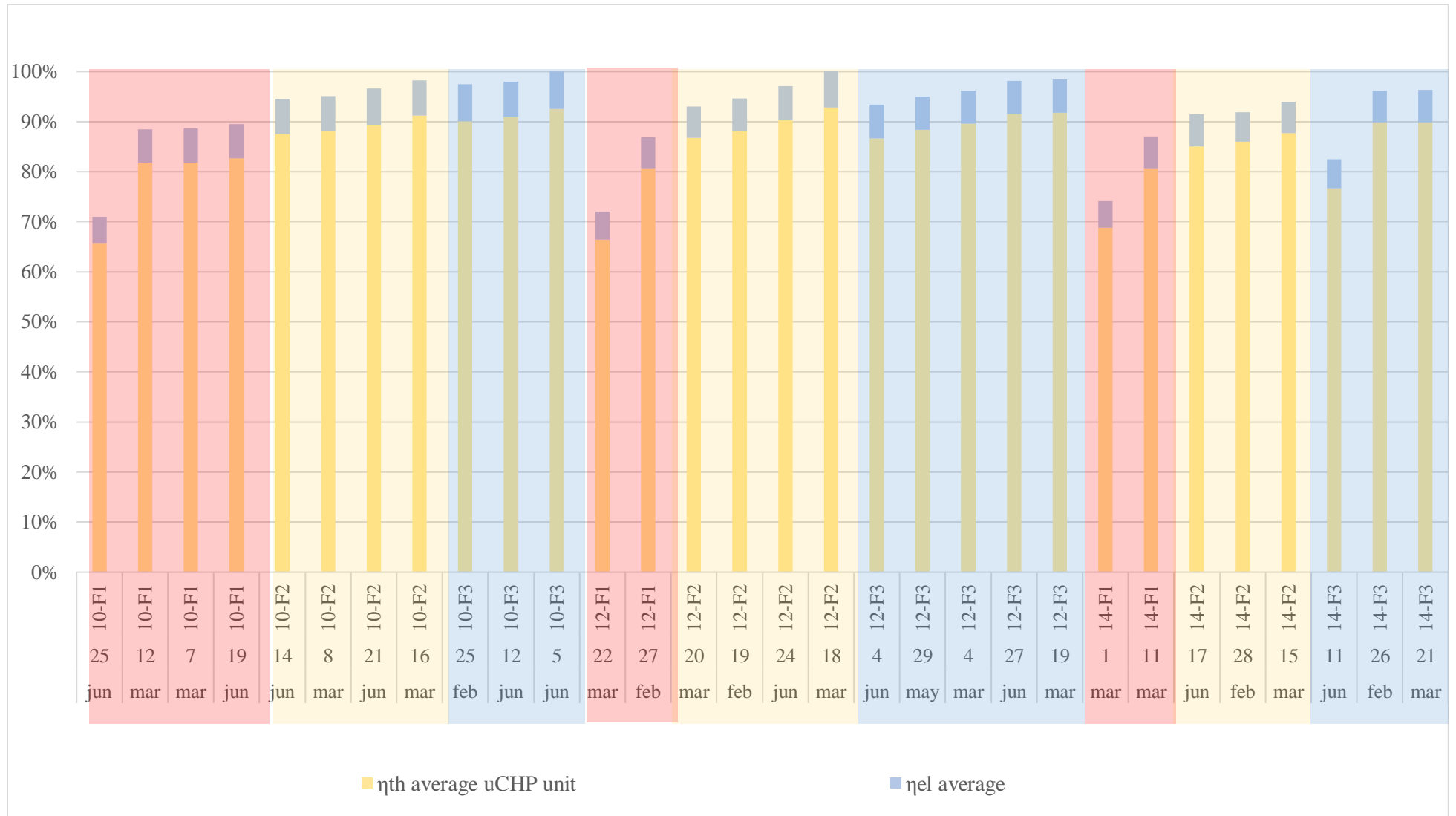


Figure 3.30 - Power and thermal efficiencies, and the thermal losses in all the studied configurations

3.4. CONCLUSIONS AND PERSPECTIVES

A biomass Stirling micro cogeneration device has been tested in order to know its performances. A dynamic model based on experimental investigations has been developed to evaluate its output thermal power and power efficiencies.

In the tests conducted at the INSA Strasbourg, iCube Laboratory, the cogeneration unit made manufactured by ÖkoFEN, model Condens_E, worked in 9 configurations: 3 thermal agent flow rates and 3 thermal power outputs, presented in the Table 3.8.

The temperature of the thermal agent fueling the household end-user with domestic hot water was configured in the studied μ CHP unit to be 60 °C.

Unlike the study where the thermal efficiency raised as domestic hot water temperature rose (Valenti, 2014), in the current case, a rise of temperature of the domestic hot water is correlated with an incapability of the thermal agent flow value to evacuate the amount of thermal power produced by the machine.

This produces accumulation of heat inside the μ CHP unit leads to a rise in temperature, which triggers a self-guarding mechanism of the machine when it reaches 75 °C.

It is to be noted that the thermal agent temperature was measured in point 6 shown in the Figure 3.14, therefore the temperature of the agent inside the μ CHP unit had 1 °C to 2 °C than what was measured.

Table 3.14 - Thermal agent properties and partial load functioning for the configurations

Configuration	Stable temperature [°C]	Time to reach stable temperature [minutes]	Automatic switch to partial load functioning
10kW, F1	69	160	YES
10kW, F2	60	75	NO
10kW, F3	58	75	NO
12kW, F1	71	150	YES
12kW, F2	61	80	YES
12kW, F3	59	80	NO
14kW, F1	74	120	YES
14kW, F2	69	100	YES
14kW, F3	62	60	NO

The linear loss of temperature explains why the partial load mode was enabled when the thermal agent in measuring point 6 had values of 73 °C to 74 °C.

Table 3.14 shows the values of the stable temperatures reached by the thermal agent and the time to reach said values, as well as whether the configuration yielded in an automatic enabling of partial load functioning due to an insufficient heat evacuation.

Generally, for all configurations, the bigger the flow is ($F1 < F2 < F3$), the better the heat evacuation from the μ CHP unit is, therefore the lower the stable temperature is.

With a good heat evacuation, the temperature will ideally stay around 60 °C, with a medium-quality heat evacuation, the temperature will stay below 75 °C and with a poor-quality heat evacuation, the temperature will go over 75 °C, resulting in a partial load functioning.

One of the premises of the current work was that only one configuration would be manually applied at a time, per each test.

However, if this premise were to be modified and the machine could switch from one configuration to another, a higher thermal power output could be configured with a lower thermal agent flow in order to reach the desired temperature as fast as possible, for then to switch to a more stable configuration.

In this case, the 14 kW_{th}, F1 configuration would be best suited to power-up the system as fast as possible, although it has the lowest efficiency.

After reaching the 60 °C value, the configuration could be switched to 12 kW_{th}, F3 for functioning while having the best total efficiency.

In the summer season, the end-user requirement for heat would diminish, therefore a lower thermal power configuration would be better suited.

In this case, a configuration of 10 kW_{th}, F1 would be recommended to get to the nominal temperature of 60 °C, after which the flow rate would be changed to F3.

Table 3.15 shows the time necessary for all configurations to reach 60 °C and 0.8 kW_{el} respectively.

Table 3.15 - Time required to reach the configured temperature of the thermal agent for each configuration

Configuration	Time to reach 60 °C [minutes]	Time to reach 0.8 kW _{el} [minutes]
10kW, F1	25	110
10kW, F2	70	110
10kW, F3	150	110
12kW, F1	20	80
12kW, F2	20	70
12kW, F3	80	60
14kW, F1	20	40
14kW, F2	25	50
14kW, F3	55	50

The value of 60 °C has been chosen because it is the configured end-user domestic hot water temperature.

The value of 0.8 kW_{el} has been chosen as 80 % of the nominal power generation capacity of the Condens_E μCHP unit produced by ÖkoFEN, because not all configurations reach 1 kW_{el} in power generation, while all configurations produce more than 0.8 kW_{el}.

A simple algorithm is proposed in Figure 3.31.

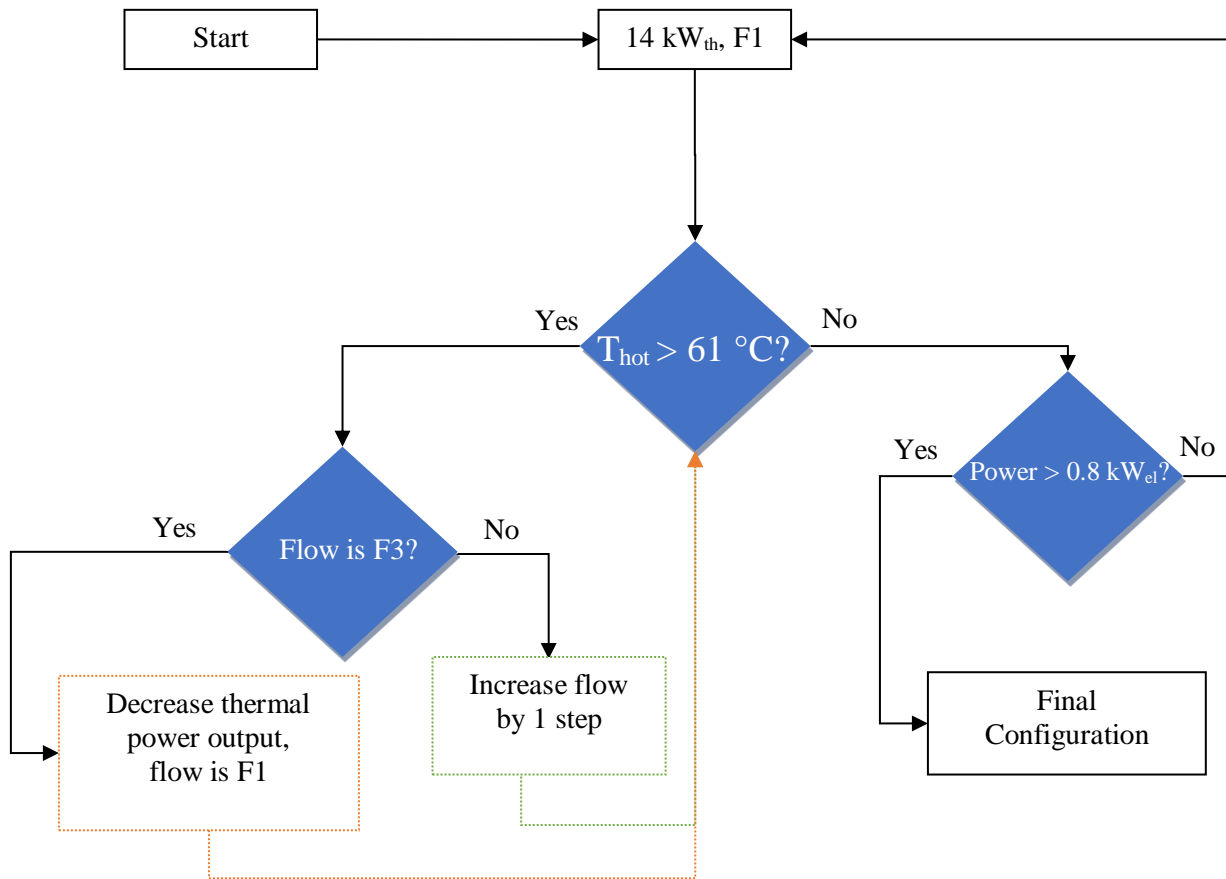


Figure 3.31 - Proposed algorithm for the μ CHP functioning

Since the 14 kW_{th}, F1 configuration is the quickest one to reach both 60 °C and a 0.8 kW_{el}, it could be used to render the machine in constant operation mode as fast as possible.

If the thermal agent transporting heat has a temperature superior to 61 °C, it would be verified if the flow rate is the biggest available (F3).

If it is the case, it is considered that the end-user domestic hot water needs are lower than the thermal power configuration currently in use and a lower thermal power configuration with the lowest flow available (F1) is switched on.

If the flow rate is insufficient to evacuate the residual heat from the μ CHP unit, the flow rate would be increased by 1 step, from F1 to F2 or from F2 to F3, depending on the case.

Ideally, the functioning mode would be 12 kW_{th}, F3 as it has the highest total efficiency of 98.6 % and highest power efficiency of 6.82 %, as shown in Figure 3.30, but the end-user thermal needs may differ from this configuration.

For further studies, it would be interesting to couple the μ CHP unit with a thermal storage unit, in order to see what regime of functioning would be best to heat up a large tank of water and then to maintain its temperature.

The speed of heating up the thermal storage tank would be relevant in function of its dimensions which are dependent on the domestic hot water consumption of the household residents.

An electrical storage unit would also be relevant in the case that the household would have a photovoltaic system.

Since the studied μ CHP unit is supposed to cover the baseload of a household consumption of electricity, a PVT and battery system would be a relevant addition to the goal of energetic self-sufficiency.

A dynamic simulation of a photovoltaic-thermal (PVT) system has been conducted (Barbu, 2019), evaluating the PVT output power coverage of household demands regarding power in Bucharest (58%) and Strasbourg (48%).

The thermal power coverage was conditioned with the use of an auxiliary heater, for meeting the domestic hot water needs in Bucharest (51%) and Strasbourg (41%).

CHAPTER 4

MATHEMATICAL MODEL

4.1. FUEL DESCRIPTION

The mathematical model is based on the process of combustion of 4 different sources of fuel. The first 3 are Oak, Beech and Douglas Fir. The contents of carbon, hydrogen, nitrogen, sulphur, and oxygen present in the sources of fuel as well as the lower heating value are taken from the Phyllis database (TNO Database).

The fuels are dry and therefore the moisture content is null. The Phyllis database does not contain the mass density of the fuel; therefore, this parameter is taken from a different database (Köppen. Since the mass density is given as a range, it has been considered the average of the 2 intervals given. The 4th species of fuel is the one used for experiments at INSA Strasbourg, France.

The volume of the combustion chamber is imposed, in an order of size comparable to that of the ÖkoFEN Pellematic Condens_e cogeneration unit model, present at INSA Strasbourg.

The reference temperature of biomass used in temperature difference calculus has been taken from literature (Altawell, 2014). The input parameters have been centralized in the Table 4.1.

Table 4.1 - Input parameters and their notations

Input Data		
Parameter	Symbol	Unit of measure
Fuel chamber volume	$Vol_{comb\ chamb}$	m^3
Fuel density	ρ_{fuel}	kg/m^3
Fuel lower heating value	LHV_{fuel}	MJ/kg
Fuel Carbon content	%C	%
Fuel Hydrogen content	%H	%
Fuel Nitrogen content	%N	%
Fuel Sulphur content	%S	%
Fuel Oxygen content	%O	%
Fuel Ash content	%A	%
Fuel Moisture content	% W_t	%
Air density	ρ_{air}	kg/m^3_N
Vapor specific volume	v_{vapor}	m^3_N/kg
Atmospheric temperature	T_{atm}	K
Reference temperature	T_{ref}	K
Air humidity	x_{air}	g/kg
Air specific heat coefficient at p=const.	cp_{air}	$kJ/(kg*K)$
Heat loss due to incomplete combustion	$Q_{loss\ inc\ fuel}$	%

The properties of the 4 sources of fuel - the 3 species of wood (Oak, Beech and Douglas Fir) and the Bois d'Or pellets used in experiments at INSA Strasbourg have been centralized in Table A4.1 in Annex 4.

There are different composition configurations because the formulas found analyse the fuel in specific conditions. The properties of the pellets have been analysed by the EIFER Institute laboratory in France (Bouvenot, 2015).

The properties of the air entering the combustion chamber have been centralized in Table A4.2 in Annex 4.

4.2. DETERMINATION OF LOWER HEATING VALUE (LVH) AND COMPARISON WITH LITERATURE

Even the values are given in literature (TNO Database, Bouvenot, 2015), the lower heating value can be recalculated with several relations. This will become relevant especially later in calculus when different fuel moisture configurations will be tested.

The relation (4.1) is found in literature (Yun, 2018) and it considers moisture content but not directly the ash content. The second lower heating value formula (4.2) is a variant of Dulong's formula and it is also found in literature (Mărculescu, 2017), it does not directly account for moisture or ash content of the fuel. The relation (4.3) found in literature (van Loo, 2008) is calculated through the higher heating value. The lower heating value is calculated with the relation (4.4) by subtracting the energy necessary for the water to evaporate.

$$LHV_1 = 4.1868 \cdot (81 \cdot \%C^i + 246 \cdot \%O^i + 26 \cdot (\%S^i - \%O^i)) - 6 \cdot \%W_t^i; \quad (4.1)$$

$$LHV_2 = 32463 \cdot \frac{\%C^i}{100} + 104346 \cdot \frac{(\%W_t^i - \frac{\%O^i}{8})}{100} - 1762 \cdot \frac{\%Cl^i}{100} + 10435 \cdot \frac{\%S^i}{100}; \quad (4.2)$$

$$HHV_3 = 0.3491 \cdot \%C^i + 1.1783 \cdot \%H^i + 0.1050 \cdot \%S^i - 0.0151 \cdot \%N^i - 0.1034 \cdot \%O^i - 0.0211 \cdot \%Ash^i; \quad (4.3)$$

$$LHV_3 = HHV \cdot \left(1 - \frac{\%W_t^i}{100}\right) - 2.444 \cdot \frac{\%W_t^i}{100} - 2.444 \cdot \frac{\%H^i}{100} \cdot 8.936 \cdot \left(1 - \frac{\%W_t^i}{100}\right). \quad (4.4)$$

In literature (van Loo, 2008), the variation of the lower heating value in function of moisture for a biomass fuel is given as shown in Figure 4.1.

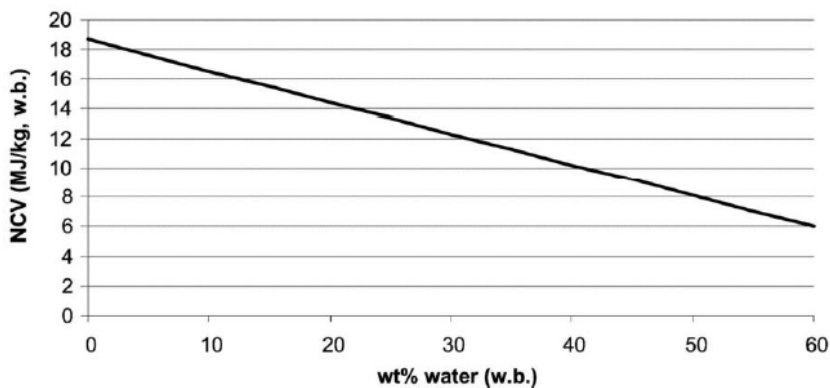


Figure 4.1 - Lower heating value as function of moisture content (van Loo, 2008)

The fuel used has a composition of %C=50, %H=5 and %O=44. In order to validate which formula should be used for correlating values with those in literature, the moisture content should be varied from 0% to 60% and the proportion of the other components (%C, %O, %H, %S, %Cl, %A) should be recalculated to adapt to this new value as shown in the relation (4.5). The notation %X_w represents the variable proportion of the X component in the fuel (Table 4.2).

Table 4.2 - Properties of the air entering combustion

Parameter	Input data	Symbol
Final proportion of the X component in the fuel in function of final moisture		%X _w ^f
Initial proportion of the X component in the fuel		%X _w ⁱ
Initial moisture of the fuel		%W _t ⁱ
Final moisture of the fuel		%W _t ^f

$$\%X_w^f = \frac{\%X_w^i}{(100 - \%W_t^i)} \cdot (100 - \%W_t^f). \tag{4.5}$$

By using the relation (4.5), the new product ratios were determined, and they were introduced in the relations (4.1), (4.2) and (4.3). The new lower heating values are indicated in Table A.4.3 in Annex 4 and are suggested in the Figure 4.2.

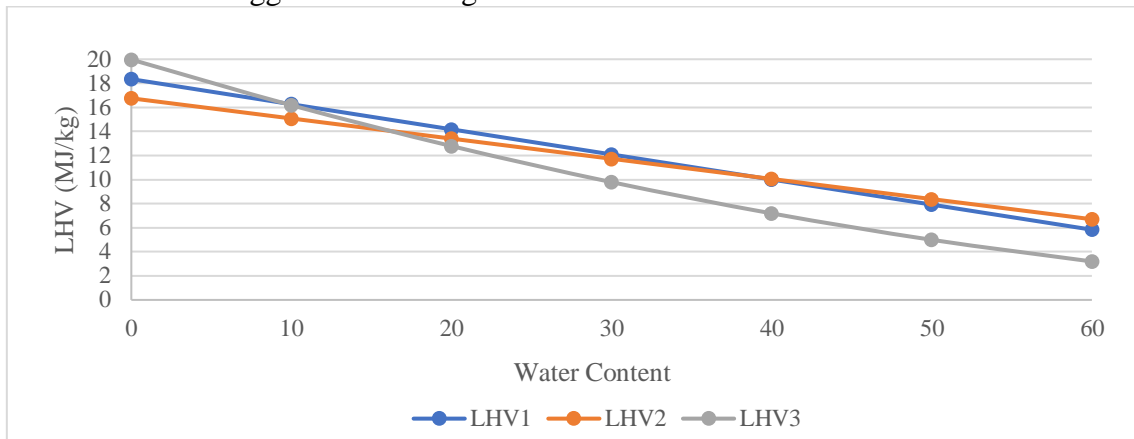


Figure 4.2 - Obtained lower heating values through the 3 formulas

By superposing the Figure 4.1 and Figure 4.2, it results that the relation (4.1) is in the most correlation with the literature results (van Loo, 2008), as shown in Figure 4.3.

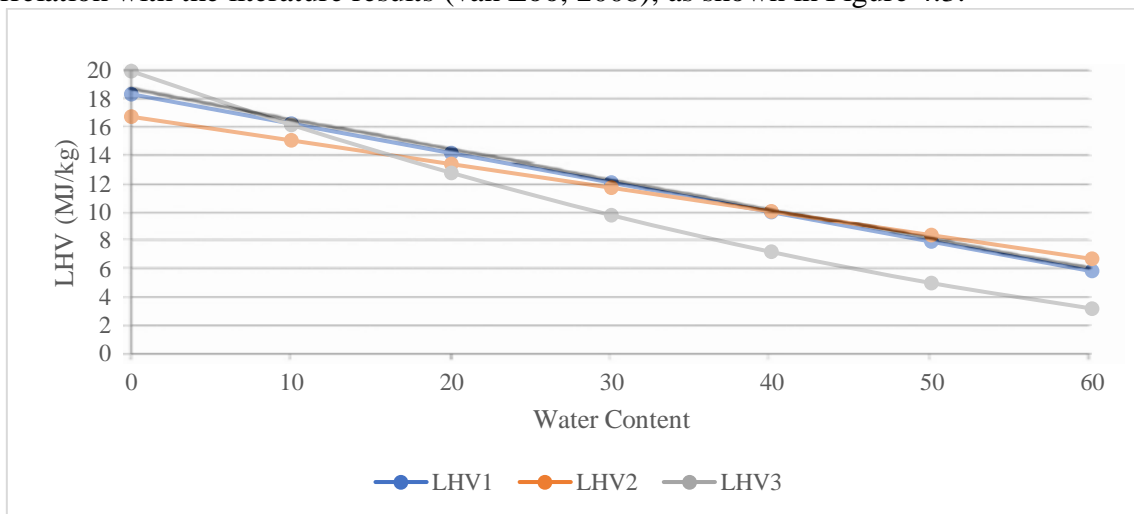


Figure 4.3 - Superposition of Figure 1 (van Loo, 2008) and obtained results

The comparison between the lower heating value for the species given by literature (TNO Database, Bouvenot, 2015) and the lower heating value resulted from the relation (4.1) is shown (Figure 4.4). The corresponding values are presented in Table A4.4 in Annex 4.

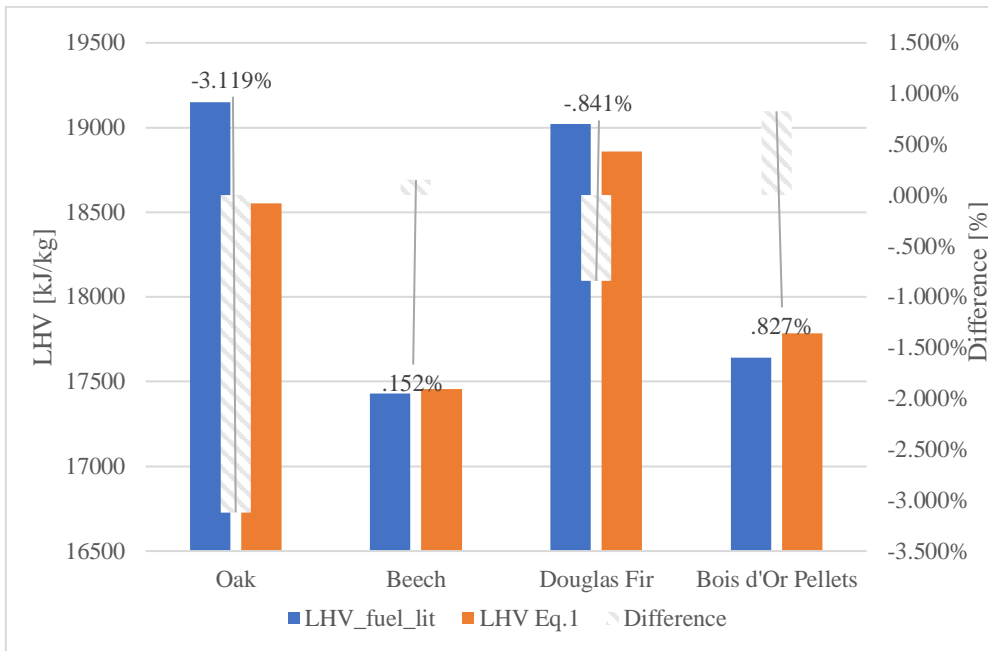


Figure 4.4 - Differences between LHV values obtained through literature and the relation (4.1)

The differences range from -3.12% to 0.83%, the biggest difference being for Oak (-3.12%). This last biggest difference is acceptable, in the context in which a more pessimistic approach towards the fuel quality is taken.

4.3. ENERGY BALANCE IN THE COMBUSTION CHAMBER

The first goal is to calculate the amount of heat produced by the combustion chamber, as shown in the Figure 4.5.

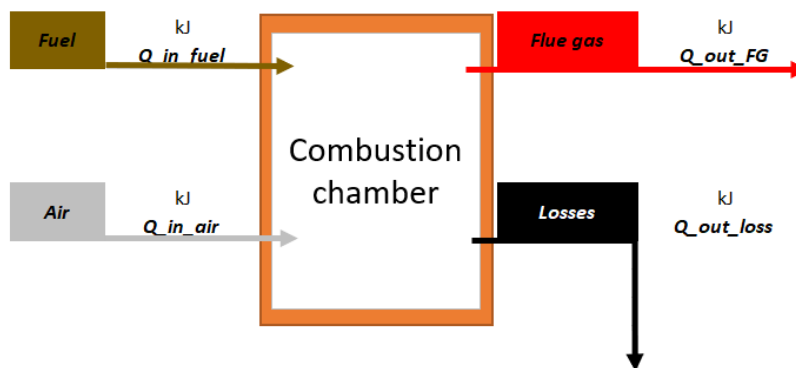


Figure 4.5 - Combustion chamber energy balance

This is done by doing the balance of entering and exiting amounts of energy in the combustion chamber, as shown in the relation (4.6).

$$Q_{in_{fuel}} + Q_{in_{air}} = Q_{out_{FG}} + Q_{out_{loss}} \quad (4.6)$$

Each of the quantities of energy must be determined. The heat entering the combustion chamber is calculated as shown in the relation (4.7).

$$Q_{in_{fuel}} = \rho_{fuel} \cdot V_{fuel} \cdot LHV_{fuel}. \quad (4.7)$$

The density of the fuel (ρ_{fuel}) and the lower heating value of the fuel (LHV_{fuel}^i) are given in the input, while the effective volume of fuel used must be determined.

The heat received through the quantity of air entering the combustion chamber ($Q_{in_{air}}$) is insignificant when compared to the amount of heat of the fuel ($Q_{in_{fuel}}$), because there is no preheating of air and even if it were to be, the house-hold dimension of the system would make the preheated amount of energy gained quite small. Nevertheless, the heat brought in by the air is calculated with the relation (4.8).

$$Q_{in_{air}} = \rho_{air} \cdot c_{p_{air}} \cdot (T_{atm} - T_{ref}). \quad (4.8)$$

The heat released along with the flue gasses is calculated with the relation (4.9) as the useful part of the heat entering the combustion chamber in relation to the combustion efficiency.

$$Q_{out_{FG}} = \eta_{comb} \cdot (Q_{in_{fuel}} + Q_{in_{air}}). \quad (4.9)$$

The heat lost is the remaining part of the total energy entered into the combustion chamber, and it is calculated with the relation (4.10).

$$Q_{out_{loss}} = (1 - \eta_{comb}) \cdot (Q_{in_{fuel}} + Q_{in_{air}}). \quad (4.10)$$

4.3.1. Determination of the flue gas real specific wet volume $v_{real_{wetFG}}$ and the heat amount produced by the fuel entering the combustion chamber $Q_{in_{fuel}}$

To determine the volume of fuel entering in the chamber of combustion it has to be ensured that the entirety of flue gas emanated by the fuel stays in the combustion chamber for 1 second. Therefore, the volume of the fuel (V_{fuel}) is linked to the flue gas real specific wet volume ($v_{real_{wetFG}}$) and to the volume of the combustion chamber ($V_{comb_{chamb}}$).

Table 4.3 - Parameters necessary to calculate the fuel volume

Parameter	Symbol	Unit of measure
Air theoretical dry specific volume	$V_{th_{dry_{air}}}$	m^3_N/kg_{fuel}
Air theoretical wet specific volume	$V_{th_{wet_{air}}}$	m^3_N/kg_{fuel}
Air real dry specific volume	$V_{real_{dry_{air}}}$	m^3_N/kg_{fuel}
Air real wet specific volume	$V_{real_{wet_{air}}}$	m^3_N/kg_{fuel}
CO ₂ theoretical specific volume	$V_{th_{CO_2}}$	m^3_N/kg_{fuel}
SO ₂ theoretical specific volume	$V_{th_{SO_2}}$	m^3_N/kg_{fuel}
N ₂ theoretical specific volume	$V_{th_{N_2}}$	m^3_N/kg_{fuel}
Flue Gas theoretical dry specific volume	$V_{th_{dry_{FG}}}$	m^3_N/kg_{fuel}
H ₂ O theoretical specific volume	$V_{th_{H_2O}}$	m^3_N/kg_{fuel}
Flue Gas real wet specific volume	$V_{real_{wet_{FG}}}$	m^3_N/kg_{fuel}
Fuel volume	V_{fuel}	m^3
Fuel mass	m_{fuel}	kg

To calculate the specific volume of flue gas measured in $\text{m}^3_{\text{N}}/\text{kg}_{\text{fuel}}$, the volume of all the species of gas contained in the flue gas has to be obtained. The parameters to be calculated are presented in Table 4.3. The properties of air and the properties of flue gas were calculated. The formulas were taken from literature (Leca, 1994, Pop, 1987). The parameters in Table 4.3 are given in the order of calculation, aiming at the calculation of flue gas real wet specific volume ($v_{\text{realwetFG}}$). The relations (4.11 – 4.24) were taken from literature (Altawell, 2014, Pop, 1987).

$$V_{\text{fuel}} = \frac{V_{\text{combchamb}}}{\rho_{\text{fuel}} \cdot v_{\text{realwetFG}}}; \quad (4.11)$$

$$v_{\text{thdryair}} = \frac{100}{21} \cdot \left(1.8678 \cdot \frac{\%C^i}{100} + 5.6 \cdot \frac{\%H^i}{100} + 0.7 \cdot \frac{\%S^i}{100} - 0.7 \cdot \frac{\%O^i}{100} \right); \quad (4.12)$$

$$v_{\text{thwetair}} = (1 + 0.00161 \cdot x_{\text{air}}) \cdot v_{\text{thdryair}}; \quad (4.13)$$

$$v_{\text{realdryair}} = \lambda \cdot v_{\text{thdryair}}; \quad (4.14)$$

$$v_{\text{realdryair}} = \lambda \cdot v_{\text{thdryair}}; \quad (4.15)$$

$$v_{\text{thCO}_2} = 1.8678 \cdot \frac{\%C^i}{100}; \quad (4.16)$$

$$v_{\text{thSO}_2} = 0.7 \cdot \frac{\%S^i}{100}; \quad (4.17)$$

$$v_{\text{thN}_2} = 0.79 \cdot v_{\text{thdryair}} + \frac{22.4}{28} \cdot \frac{\%N^i}{100}; \quad (4.18)$$

$$v_{\text{thdryFG}} = v_{\text{thCO}_2} + v_{\text{thSO}_2} + v_{\text{thN}_2}; \quad (4.19)$$

$$v_{\text{thH}_2\text{O}} = 11.2 \cdot \frac{\%H^i}{100} + v_{\text{vapor}} \cdot \frac{\%W_t^i}{100} + 0.00161 \cdot x_{\text{air}} \cdot v_{\text{thdryair}}; \quad (4.20)$$

$$v_{\text{thwetFG}} = v_{\text{thdryFG}} + v_{\text{thH}_2\text{O}}; \quad (4.21)$$

$$v_{\text{realdryFG}} = v_{\text{thdryFG}} + (\lambda - 1) \cdot v_{\text{thdryair}}; \quad (4.22)$$

$$v_{\text{realH}_2\text{O}} = v_{\text{thH}_2\text{O}} + 0.00161 \cdot x_{\text{air}} \cdot (\lambda - 1) \cdot v_{\text{thH}_2\text{O}}; \quad (4.23)$$

$$v_{\text{realwetFG}} = v_{\text{realdryFG}} + v_{\text{realH}_2\text{O}}. \quad (4.24)$$

In the Annex 4, the calculated specific volumes of the air entering the combustion chamber are indicated in Table A4.5 and the specific volumes of the flue gas are presented in Table A4.6.

Using the flue gas real wet specific volume ($v_{\text{realwetFG}}$) obtained through the relation (4.24), the amount of fuel which can enter in the combustion chamber is determined, so that the volume of flue gas obtained can remain inside for at least 1 second at atmospheric pressure.

After having obtained this value, the mass of the fuel (m_{fuel}) through the relation (4.25) is calculated and then the heat introduced into the combustion chamber by the fuel (Q_{in_fuel}) through the relation (4.7).

$$m_{fuel} = \rho_{fuel} \cdot V_{fuel} \quad (4.25)$$

The results are shown in Table A4.7 in Annex 4.

4.3.2. Determination of the mass of air which enters the combustion chamber m_{air} and of heat inlet of air Q_{in_air}

To calculate the mass of air which enters the combustion chamber, the parameters are shown in Table 4.4, in the order of their appearance.

Table 4.4 - Calculated properties of air

Parameter	Calculated Data	
	Symbol	Unit of measure
Oxygen theoretical specific mass	m_{thO_2}	kg/kg _{fuel}
Nitrogen theoretical specific mass	m_{thN_2}	kg/kg _{fuel}
Air theoretical dry specific mass	$m_{thdryair}$	kg/kg _{fuel}
Air theoretical wet specific mass	$m_{thwetair}$	kg/kg _{fuel}
Air real dry specific mass	$m_{realdryair}$	kg/kg _{fuel}
Air real wet specific mass	$m_{realwetair}$	kg/kg _{fuel}
Air mass	m_{air}	kg

All the parameters at the initial state "i" are calculated using the relations (4.26 - 4.32) as found in the literature (Horbaniuc, 2008).

$$m_{th O_2} = \left(\frac{\%C^i}{M_C} + \frac{\%H^i}{4 \cdot M_H} + \frac{\%S^i}{M_S} - \frac{\%O^i}{M_{O_2}} \right) \cdot \frac{M_{O_2}}{100} \quad (4.26)$$

$$m_{th N_2} = \frac{76,8}{23,2} \cdot \left(\frac{\%C^i}{M_C} + \frac{\%H^i}{4 \cdot M_H} + \frac{\%S^i}{M_S} - \frac{\%O^i}{M_{O_2}} \right) \cdot \frac{M_{O_2}}{100} \quad (4.27)$$

The relations (4.26) and (4.27) describe the dry theoretical mass of the components of air: Oxygen and Nitrogen. The specific theoretical dry mass of air is calculated with the relation (4.28) by adding the 2 previous amounts calculated.

$$m_{thdryair} = m_{th O_2} + m_{th N_2} \quad (4.28)$$

The theoretical amount of wet air is calculated through the relation (4.29) by introducing the parameter of air moisture.

$$m_{thwetair} = m_{thdryair} \cdot \left(1 + \frac{x_{air}}{1000} \right) \quad (4.29)$$

The real amount of wet air is calculated through the relation (4.30) by multiplication of the theoretical amount of wet air with the air excess.

$$m_{realwetair} = \lambda \cdot m_{thwetair} \quad (4.30)$$

The mass of air is determined through the relation (4.31) by multiplying the specific mass of air to the mass of fuel used in combustion.

$$m_{\text{air}} = m_{\text{fuel}} * m_{\text{realwetair}} \quad (4.31)$$

The heat resulted from the air component in combustion is calculated through the relation (4.32).

$$Q_{\text{inair}} = m_{\text{air}} \cdot (c_{\text{pair}}^{\text{Tatm}} \cdot T_{\text{atm}} - c_{\text{pair}}^{\text{Tref}} \cdot T_{\text{ref}}) \quad (4.32)$$

The calculated air masses and resulted heat from air are indicated in Table A4.8 in Annex 4.

4.3.3. Determination of the adiabatic combustion temperature by using volumes and enthalpies

The first method of obtaining the combustion temperature is through the relation (4.6), by using volumes, not masses. In Table 4.5 the parameters which are to be calculated are shown.

Table 4.5 - Calculated specific volumes

Parameter	Symbol	Unit of measure
Specific volume of air O ₂	V _{thO₂}	m ³ _N / kg _{fuel}
Specific volume of dry air	V _{thdryair}	m ³ _N / kg _{fuel}
Specific volume of H ₂ O in the air	V _{thH₂O air}	m ³ _N / kg _{fuel}
Specific volume of CO ₂ in the flue gasses	V _{thCO₂ FG}	m ³ _N / kg _{fuel}
Specific volume of SO ₂ in the flue gasses	V _{thSO₂ FG}	m ³ _N / kg _{fuel}
Specific volume of N ₂ in the flue gasses	V _{thN₂ FG}	m ³ _N / kg _{fuel}
Specific volume of H ₂ O in the flue gasses	V _{thH₂O FG}	m ³ _N / kg _{fuel}

Formulas used to calculate them are shown in the relations (4.33) - 4.40) while the results obtained are shown in Table A4.9 in Annex 4.

$$v_{\text{thO}_2} = 1.8678 \cdot \frac{(\%C^i + 0.375 \cdot \%S^i)}{100} + 5.6 \cdot \frac{\%H^i}{100} - 0.7 \cdot \frac{\%O^i}{100} \quad (4.33)$$

$$v_{\text{thdryair}} = \frac{100}{21} \cdot v_{\text{thO}_2} \quad (4.34)$$

$$v_{\text{thH}_2\text{Oair}} = 0.00161 \cdot x_{\text{air}} \cdot v_{\text{thdryair}} \quad (4.35)$$

$$v_{\text{thwetair}} = v_{\text{thdryair}} + v_{\text{thH}_2\text{Oair}} \quad (4.36)$$

$$v_{\text{thCO}_2\text{FG}} = 1.8678 \cdot \frac{\%C^i}{100} \quad (4.37)$$

$$v_{\text{thSO}_2\text{FG}} = 0.7 \cdot \frac{\%S^i}{100} \quad (4.38)$$

$$v_{\text{thN}_2\text{FG}} = 0.79 \cdot v_{\text{thdryair}} + 0.8 \cdot \frac{\%N^i}{100} \quad (4.39)$$

$$v_{\text{thH}_2\text{OFG}} = 11.2 \cdot \frac{\%H^i}{100} + 0.00161 \cdot \lambda \cdot v_{\text{thdryair}} + 1.244 \cdot \frac{\%W_t^i}{100} \quad (4.40)$$

The heat entered in the system is calculated through the relation (4.41).

$$\begin{aligned}
 Q_{in_{th}} &= Q_{in_{fuel}} + Q_{in_{air}} \\
 &= LHV_{fuel}^i + \lambda \cdot v_{th_{dry_{air}}} \cdot (c_{p_{air}} \cdot T_{atm} - c_{p_{air}} \cdot T_{ref}) + \lambda \cdot v_{th_{H_2O_{air}}} \\
 &\quad \cdot (c_{p_{H_2O}} \cdot T_{atm} - c_{p_{H_2O}} \cdot T_{ref})
 \end{aligned} \tag{4.41}$$

After calculating the heat entering the combustion chamber, the useful heat quantity can be determined through the relation (4.42) since the efficiency of the combustion chamber is known.

$$Q_{in_{real}} = \eta_{comb} \cdot (Q_{in_{fuel}} + Q_{in_{air}}) = Q_{out_{FG}} \tag{4.42}$$

The heat exited from combustion can be calculated also with the relation (4.43) through volumes of flue gas components, and not masses as it was in the previous case.

$$\begin{aligned}
 Q_{out_{FG}} &= v_{th_{CO_2_{FG}}} \cdot (c_{p_{CO_2}}^{T_{FG}} \cdot T_{FG} - c_{p_{CO_2}}^{T_{ref}} \cdot T_{ref}) + v_{th_{SO_2_{FG}}} \\
 &\quad \cdot (c_{p_{SO_2}}^{T_{FG}} \cdot T_{FG} - c_{p_{SO_2}}^{T_{ref}} \cdot T_{ref}) + v_{th_{N_2_{FG}}} \cdot (c_{p_{N_2}}^{T_{FG}} \cdot T_{FG} - c_{p_{N_2}}^{T_{ref}} \cdot T_{ref}) \\
 &\quad + v_{th_{H_2O_{air}}} \cdot (c_{p_{H_2O}}^{T_{FG}} \cdot T_{FG} - c_{p_{H_2O}}^{T_{ref}} \cdot T_{ref}) + (\lambda - 1) \cdot v_{th_{dry_{air}}} \\
 &\quad \cdot (c_{p_{wet_{air}}}^{T_{FG}} \cdot T_{FG} - c_{p_{wet_{air}}}^{T_{ref}} \cdot T_{ref}) + (\lambda - 1) \cdot v_{th_{H_2O_{FG}}} \\
 &\quad \cdot (c_{p_{H_2O}}^{T_{FG}} \cdot T_{FG} - c_{p_{H_2O}}^{T_{ref}} \cdot T_{ref})
 \end{aligned} \tag{4.43}$$

The calculation of the heat amounts requires the use of the specific volume heat coefficients reported to volume, not to the mass of the components.

These coefficients were found in literature (Yun, 2018, Pop, 1987, Horbaniuc, 2008, Ražnjević, 1978) and they are displayed in Table A4.10 in Annex 4.

In order to obtain these specific values for any temperature, these coefficients were transformed into a 5th degree regression in Excel through the formulas presented in Table 4.6.

Table 4.6 - Excel functions used to determine the coefficients of the 5th degree regressions for the specific volume heat coefficients

Coefficient	MS Office Excel Function
x^5	=@INDEX(LINEST(known Y's, known X's ^{1,2,3,4,5}),1)
x^4	=INDEX(LINEST(known Y's, known X's ^{1,2,3,4,5}),1,2)
x^3	=INDEX(LINEST(known Y's, known X's ^{1,2,3,4,5}),1,3)
x^2	=INDEX(LINEST(known Y's, known X's ^{1,2,3,4,5}),1,4)
x^1	=INDEX(LINEST(known Y's, known X's ^{1,2,3,4,5}),1,5)
x^0	=INDEX(LINEST(known Y's, known X's ^{1,2,3,4,5}),1,6)

The known Y's are the values of specific heat and the known X's are the temperatures corresponding to each value.

This method is preferable to reading the value of the trendline in an Excel generated graphic, as the program tends to approximate small numbers, producing additional errors.

In Table A4.11 in Annex 4, the obtained coefficients are shown. The values of x^5 , x^4 , x^3 , x^2 and x^1 coefficients are quite small, so an approximation would not have been desirable.

Compared with the values from Table A4.10 in Annex 4, for temperatures in between 100 °C and 2500 °C, the relative errors are varying between -0,90 % and +0,53 %.

The results of theoretical and real heat calculations using the relations (4.41) and (4.42) are shown in Table A4.12 in Annex 4.

The heat exiting the combustion process is calculated with the relation (4.43).

The temperature of flue gas components determines the heat transfer coefficients' value.

The coefficient value of air components at atmospheric and reference temperatures are indicated in Table A4.13 in Annex 4.

The coefficients of the flue gas components at reference temperature have been calculated and are shown in Table A4.14. They will be used to calculate the flue gas temperature through the relation (4.43).

By isolating the flue gas temperature in the relation (4.44) in each of the components, it can be determined. The temperature-depending specific volume heat coefficients of the components however are unknown.

$$\begin{aligned}
 T_{FG(1)} &= \\
 &= \frac{Q_{outFG} + v_{thCO_2FG} \cdot c_{pCO_2}^{T_{ref}} \cdot T_{ref} + v_{thSO_2FG} \cdot c_{pSO_2}^{T_{ref}} \cdot T_{ref} + v_{thN_2FG} \cdot c_{pN_2}^{T_{ref}} \cdot T_{ref} + v_{thH_2Oair} \cdot c_{pH_2O}^{T_{ref}} \cdot T_{ref}}{v_{thCO_2FG} \cdot c_{pCO_2}^{T_{FG(0)}} + v_{thSO_2FG} \cdot c_{pSO_2}^{T_{FG(0)}} + v_{thN_2FG} \cdot c_{pN_2}^{T_{FG(0)}} + v_{thH_2OFG} \cdot c_{pH_2O}^{T_{FG(0)}} + (\lambda - 1) \cdot (v_{thH_2Oair} \cdot c_{pH_2O}^{T_{FG(0)}} + v_{thdryair} \cdot c_{pwetair}^{T_{FG(0)}})} \\
 &+ \frac{(\lambda - 1) \cdot v_{thdryair} \cdot c_{pwetair}^{T_{ref}} \cdot T_{ref} + (\lambda - 1) \cdot v_{thH_2OFG} \cdot c_{pH_2O}^{T_{ref}} \cdot T_{ref}}{v_{thCO_2FG} \cdot c_{pCO_2}^{T_{FG(0)}} + v_{thSO_2FG} \cdot c_{pSO_2}^{T_{FG(0)}} + v_{thN_2FG} \cdot c_{pN_2}^{T_{FG(0)}} + v_{thH_2OFG} \cdot c_{pH_2O}^{T_{FG(0)}} + (\lambda - 1) \cdot (v_{thH_2Oair} \cdot c_{pH_2O}^{T_{FG(0)}} + v_{thdryair} \cdot c_{pwetair}^{T_{FG(0)}})}
 \end{aligned} \tag{4.44}$$

To determine the flue gas temperature, the Seidel - Gauss (Brătianu, 1998) method is used.

By choosing an initial temperature for the flue gas $T_{FG(0)}$, the specific volume heat coefficients of the flue gas at the initial temperature are calculated and the new temperature for the flue gasses $T_{FG(1)}$ is obtained (4.44).

For the next iterations, the relation (4.45) is used and the new temperature $T_{FG(i+1)}$ will be obtained by calculating the specific heat coefficients at $T_{FG(i)}$.

$$\begin{aligned}
 T_{FG(i+1)} &= \\
 &= \frac{Q_{outFG} + v_{thCO_2FG} \cdot c_{pCO_2}^{T_{ref}} \cdot T_{ref} + v_{thSO_2FG} \cdot c_{pSO_2}^{T_{ref}} \cdot T_{ref} + v_{thN_2FG} \cdot c_{pN_2}^{T_{ref}} \cdot T_{ref} + v_{thH_2Oair} \cdot c_{pH_2O}^{T_{ref}} \cdot T_{ref}}{v_{thCO_2FG} \cdot c_{pCO_2}^{T_{FG(i)}} + v_{thSO_2FG} \cdot c_{pSO_2}^{T_{FG(i)}} + v_{thN_2FG} \cdot c_{pN_2}^{T_{FG(i)}} + v_{thH_2Oair} \cdot c_{pH_2O}^{T_{FG(i)}} + (\lambda - 1) \cdot (v_{thH_2OFG} \cdot c_{pH_2O}^{T_{FG(i)}} + v_{thdryair} \cdot c_{pwetair}^{T_{FG(i)}})} \\
 &+ \frac{(\lambda - 1) \cdot v_{thdryair} \cdot c_{pwetair}^{T_{ref}} \cdot T_{ref} + (\lambda - 1) \cdot v_{thH_2OFG} \cdot c_{pH_2O}^{T_{ref}} \cdot T_{ref}}{v_{thCO_2FG} \cdot c_{pCO_2}^{T_{FG(i)}} + v_{thSO_2FG} \cdot c_{pSO_2}^{T_{FG(i)}} + v_{thN_2FG} \cdot c_{pN_2}^{T_{FG(i)}} + v_{thH_2Oair} \cdot c_{pH_2O}^{T_{FG(i)}} + (\lambda - 1) \cdot (v_{thH_2OFG} \cdot c_{pH_2O}^{T_{FG(i)}} + v_{thdryair} \cdot c_{pwetair}^{T_{FG(i)}})}
 \end{aligned} \tag{4.45}$$

The process will be repeated until an acceptable error between 2 successive values of the flue gas temperature is obtained, as shown in Figure 4.6.

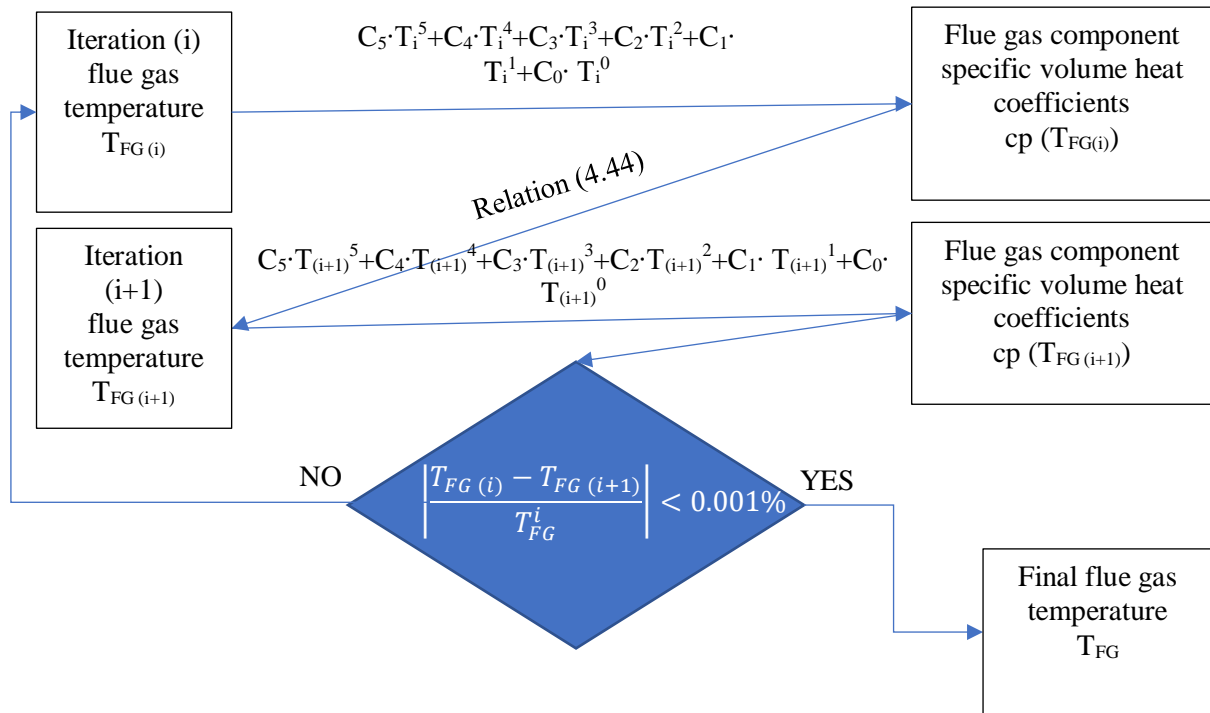


Figure 4.6 - The iteration algorithm used to determine the flue gas temperature

In total, 8 iterations were enough to obtain a very small error (<0.001%).

The initial temperature used for the iteration was the average temperature of the available heat transfer coefficient data.

Since these values range from 273.15 K to 2773.15 K, the average was 1523.15 K.

In Annex 4, Table A4.15 shows the resulted values for the temperature of flue gases, T_{FG} ,

The Figure 4.7, Figure 4.8, Figure 4.9, and Figure 4.10 show the evolution of temperature over one iteration to the other as well as the errors between successive iterations.

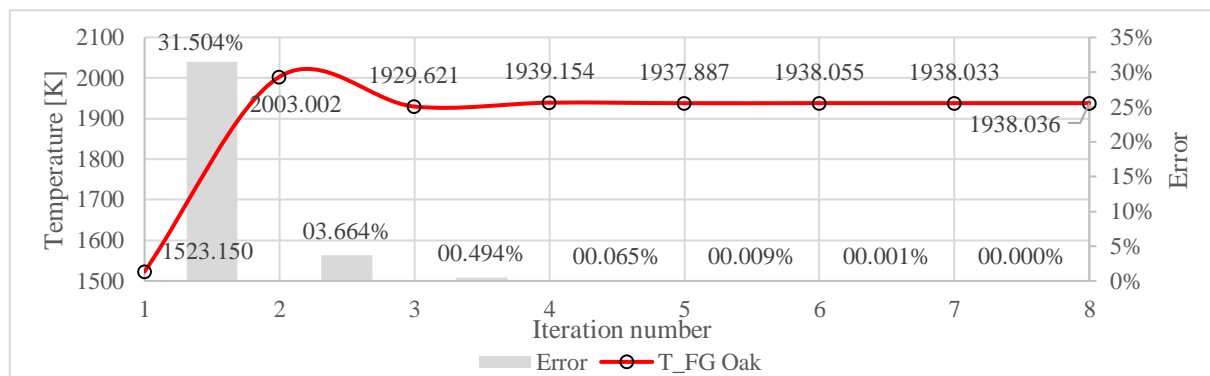


Figure 4.7 - Obtained flue gas temperatures and errors between iterations for Oak specie

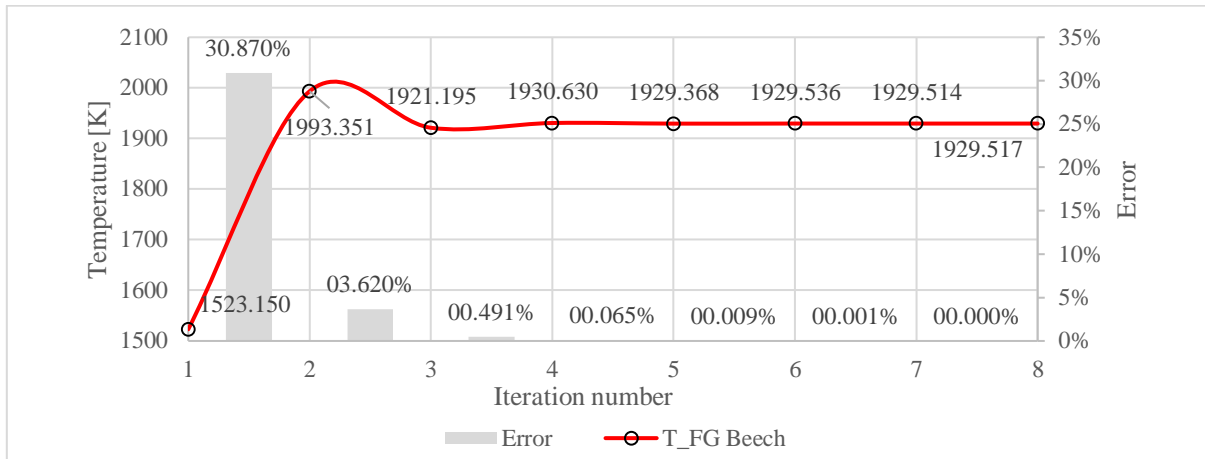


Figure 4.8 - Obtained flue gas temperatures and errors between iterations for Beech specie

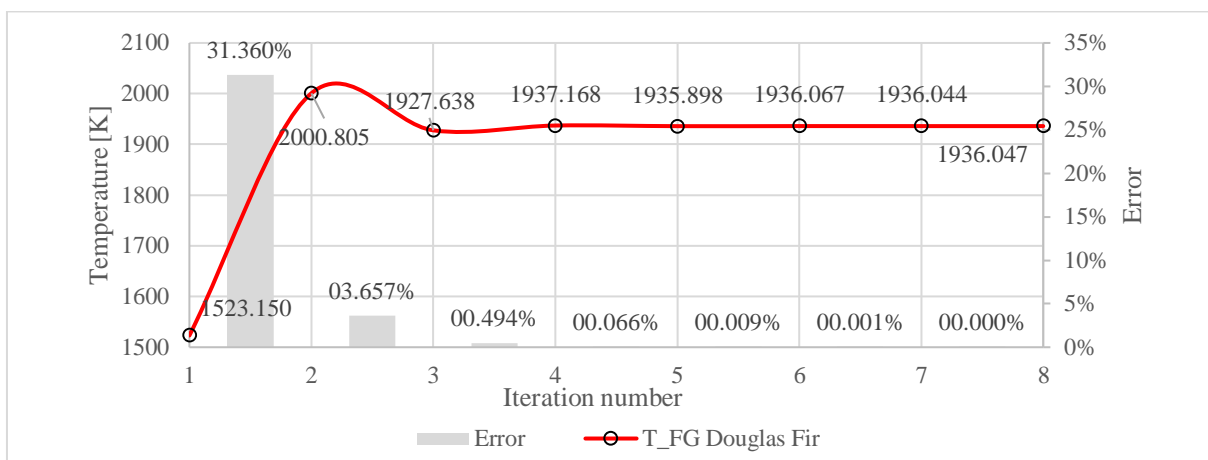


Figure 4.9 - Obtained flue gas temperatures and errors between iterations for Douglas Fir specie

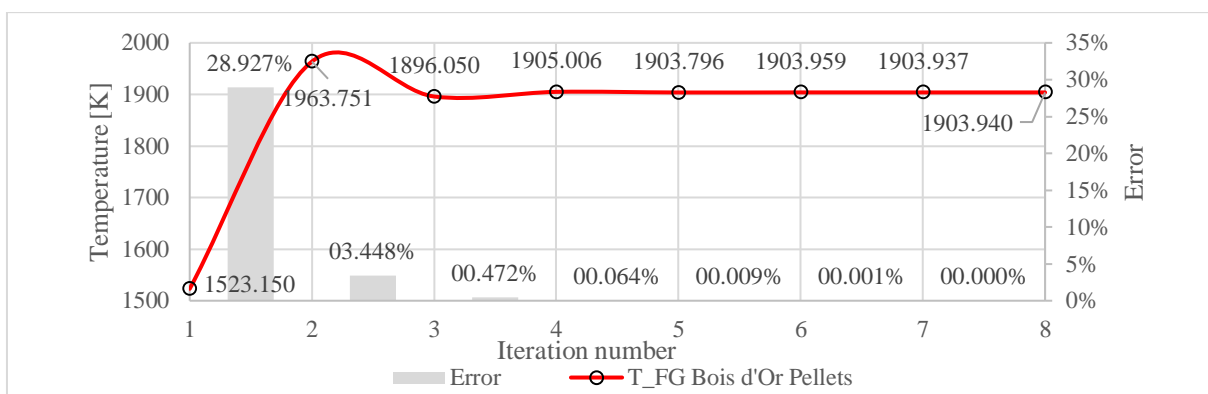


Figure 4.10 - Obtained flue gas temperatures and errors between iterations for Bois d'Or Pellets

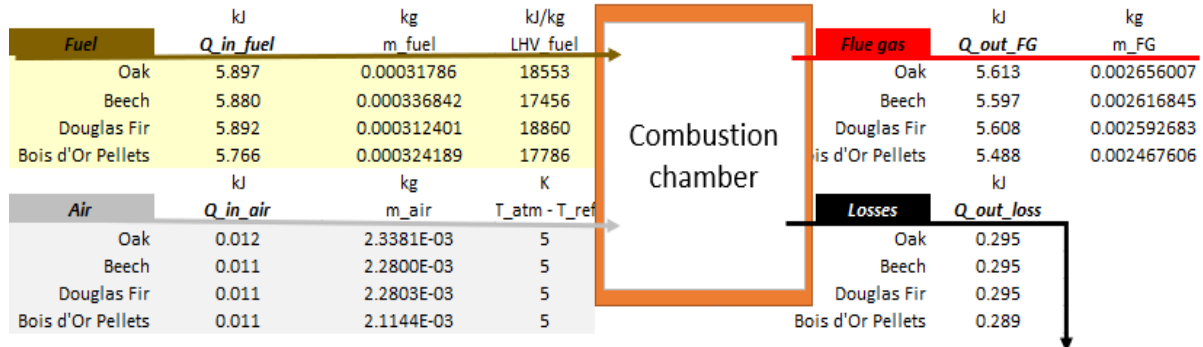
4.3.4. Determination of the adiabatic combustion temperature by using masses and enthalpies

The useful heat of the flue gases exiting from the combustion chamber ($Q_{out\ FG}$) is calculated through the relation (4.9) and the heat loss of the process ($Q_{out\ loss}$) is calculated through the relation (4.10). The results are presented in Table 4.7.

Table 4.7 - Obtained results for output heat and losses after combustion

$Q_{out\ FG}$	kJ	$Q_{out\ loss}$	kJ
Oak	5.614	Oak	0.295
Beech	5.599	Beech	0.295
Douglas Fir	5.608	Douglas Fir	0.295
Bois d'Or		Bois d'Or	0.289
Pellets	5.495	Pellets	

The complete balance of energies of the combustion chamber can be visualized in the Figure 4.11.


Figure 4.11 - Energy balance of combustion

For this second method of the adiabatic temperature of combustion calculation, alternatively the relation (4.9) could have been written as the relation (4.46).

$$\begin{aligned}
 Q_{out_{FG}} &= m_{FG}^i \cdot \delta H_{FG} = m_{FG}^i \cdot \left[H(c_{p_{FG}}^{T_{FG}}, T_{FG}) - H(c_{p_{FG}}^{T_{ref}}, T_{ref}) \right] \\
 &= m_{FG}^i \cdot \left(c_{p_{FG}}^{T_{FG}} \cdot T_{FG} - c_{p_{FG}}^{T_{ref}} \cdot T_{ref} \right)
 \end{aligned} \quad (4.46)$$

At the initial state i , the relation (4.47) – (4.51) found in the literature (Pop, 1987), are used to obtain the flue gases masse.

$$m_{CO_2} = \frac{\%C^i}{100} \cdot \frac{M_{CO_2}}{M_C} \quad (4.47)$$

$$m_{SO_2} = \frac{\%S^i}{100} \cdot \frac{M_{SO_2}}{M_S} \quad (4.48)$$

$$m_{N_2}^{FG} = m_{th\ N_2} + \frac{\%N^i}{100} \quad (4.49)$$

$$m_{H_2O} = \frac{\%H^i}{100} \cdot \frac{M_{H_2O}}{2 \cdot M_H} + \frac{x_{air}}{1000} \cdot m_{th_{dry\ air}} + \frac{\%W_t^i}{100} \quad (4.50)$$

$$m_{FG}^i = m_{CO_2} + m_{SO_2} + m_{N_2}^{FG} + m_{H_2O} + (\lambda - 1) \cdot \left(1 + \frac{x_{air}}{1000} \right) \cdot m_{th_{dry\ air}} \quad (4.51)$$

Based on the results from relations (4.30) and (4.51), the balance equation (4.52) should reflect the correctness of computation (Popa, 1986):

$$1 + m_{real_{wet\ air}} = m_{FG}^i + \frac{\%Ash^i}{100} \quad (4.52)$$

The results of the verifications are showed in Table 4.8.

Table 4.8 - Balance equation results

Balance Equation (4.52)	$1 + m_{\text{realwetair}} - m_{\text{FG}}^i - \frac{\% \text{Ash}^i}{100} =$ $= 0.00 (?)$
Oak	0.00 <input checked="" type="checkbox"/>
Beech	0.00 <input checked="" type="checkbox"/>
Douglas Fir	0.00 <input checked="" type="checkbox"/>
Bois d'Or Pellets	0.00 <input checked="" type="checkbox"/>

Since the value of Q_{outFG} is known, the adiabatic combustion temperature is obtained. The heat capacity of the flue gasses is also unknown, and it varies with temperature. To determine the temperature of the flue gasses the balance equation (4.6) is reformulated as the relation (4.53):

$$m_{\text{realwetair}} \cdot \delta H_{\text{air}} + m_{\text{fuel}} \cdot \text{LHV}_{\text{fuel}}^i = m_{\text{FG}}^i \cdot \delta H_{\text{FG}} - Q_{\text{outloss}} \quad (4.53)$$

Writing the relation (4.10) under the shape of the relation (5.54):

$$Q_{\text{outloss}} = (1 - \eta_{\text{combchamber}}) \cdot (m_{\text{realwetair}} \cdot \delta H_{\text{air}} + m_{\text{fuel}} \cdot \text{LHV}_{\text{fuel}}^i), \quad (4.54)$$

the relation (4.53) becomes the relation (4.55):

$$\begin{aligned} m_{\text{FG}}^i \cdot \delta H_{\text{FG}} &= m_{\text{realwetair}} \cdot \delta H_{\text{air}} + m_{\text{fuel}} \cdot \text{LHV}_{\text{fuel}}^i + Q_{\text{outloss}} \\ &= [1 + (1 - \eta_{\text{combchamber}})] \cdot (m_{\text{realwetair}} \cdot \delta H_{\text{air}} + m_{\text{fuel}} \cdot \text{LHV}_{\text{fuel}}^i) \end{aligned} \quad (4.55)$$

4.3.4.1. Air and Flue Gas masses calculation at wet ash free state

In the literature (van Loo, 2008), an established alternative to the use of initial state to calculate the air masses (§ 4.3.2) and flue gas masses (§ 4.3.4), consists in using the wet ash free state "waf" (Table A4.1, Annex 4). Furthermore, the different methods used to determine the air and flue gas enthalpies are relying on. Towards the enthalpies' calculation, specific masses of components shown in Table 4.9 and molar masses indicated in the Annex 4, Table A4.16, are used.

Table 4.9 - Specific masses of air and flue gas components

Parameter	Calculated data	
	Symbol	Unit of measure
Specific mass of O ₂ used in combustion	$m_{\text{O}_2\text{incomb}}^{\text{waf}}$	kg/kg _{fuel waf}
Specific mass of N ₂ used in combustion	$m_{\text{N}_2\text{incomb}}^{\text{waf}}$	kg/kg _{fuel waf}
Specific mass of Air used in combustion	$m_{\text{airincomb}}^{\text{waf}}$	kg/kg _{fuel waf}
Specific mass of CO ₂ resulted from combustion	$m_{\text{CO}_2\text{outcomb}}^{\text{waf}}$	kg/kg _{fuel waf}
Specific mass of N ₂ resulted from combustion	$m_{\text{N}_2\text{outcomb}}^{\text{waf}}$	kg/kg _{fuel waf}
Specific mass of O ₂ resulted from combustion	$m_{\text{O}_2\text{outcomb}}^{\text{waf}}$	kg/kg _{fuel waf}
Specific mass of SO ₂ resulted from combustion	$m_{\text{SO}_2\text{outcomb}}^{\text{waf}}$	kg/kg _{fuel waf}
Specific mass of H ₂ O resulted from combustion	$m_{\text{H}_2\text{Ooutcomb}}^{\text{waf}}$	kg/kg _{fuel waf}
Specific mass of Flue Gas resulted from combustion	$m_{\text{FG}}^{\text{waf}}$	kg/kg _{fuel waf}

The relations (4.56) - (4.64) taken from literature (van Loo, 2008), are used to calculate the "waf" specific masses of the components from the Table 4.9. The dry ash free "daf" specific masses of the components are also used.

$$m_{\text{O}_2\text{incomb}}^{\text{waf}} = \lambda \cdot \left(\frac{\%C^{\text{daf}}}{M_C} + \frac{\%H^{\text{daf}}}{4 \cdot M_H} + \frac{\%S^{\text{daf}}}{M_S} - \frac{\%O^{\text{daf}}}{M_{\text{O}_2}} \right) \cdot \frac{M_{\text{O}_2}}{100} \cdot \left(1 - \frac{\%W_t^{\text{waf}}}{100} \right) \quad (4.56)$$

$$m_{\text{N}_2\text{incomb}}^{\text{waf}} = \frac{79}{21} \cdot \lambda \cdot \left(\frac{\%C^{\text{daf}}}{M_C} + \frac{\%H^{\text{daf}}}{4 \cdot M_H} + \frac{\%S^{\text{daf}}}{M_S} - \frac{\%O^{\text{daf}}}{M_{\text{O}_2}} \right) \cdot \frac{M_{\text{N}_2}}{100} \cdot \left(1 - \frac{\%W_t^{\text{waf}}}{100} \right) \quad (4.57)$$

$$m_{\text{airincomb}}^{\text{waf}} = m_{\text{O}_2\text{incomb}}^{\text{waf}} + m_{\text{N}_2\text{incomb}}^{\text{waf}} \quad (4.58)$$

$$m_{\text{CO}_2\text{outcomb}}^{\text{waf}} = \frac{\%C^{\text{daf}}}{100} \cdot \frac{M_{\text{CO}_2}}{M_C} \cdot \left(1 - \frac{\%W_t^{\text{waf}}}{100} \right) \quad (4.59)$$

$$m_{\text{N}_2\text{outcomb}}^{\text{waf}} = m_{\text{N}_2\text{incomb}}^{\text{waf}} + \frac{\%N^{\text{daf}}}{100} \cdot \left(1 - \frac{\%W_t^{\text{waf}}}{100} \right) \quad (4.60)$$

$$m_{\text{O}_2\text{outcomb}}^{\text{waf}} = m_{\text{O}_2\text{incomb}}^{\text{waf}} \cdot \frac{\lambda - 1}{\lambda} \quad (4.61)$$

$$m_{\text{SO}_2\text{outcomb}}^{\text{waf}} = \frac{\%S^{\text{daf}}}{100} \cdot \frac{M_{\text{SO}_2}}{M_S} \cdot \left(1 - \frac{\%W_t^{\text{waf}}}{100} \right) \quad (4.62)$$

$$m_{\text{H}_2\text{Ooutcomb}}^{\text{waf}} = \frac{\%H^{\text{daf}}}{100} \cdot \frac{M_{\text{H}_2\text{O}}}{2 \cdot M_H} \cdot \left(1 - \frac{\%W_t^{\text{waf}}}{100} \right) + \frac{\%W_t^{\text{waf}}}{100} \quad (4.63)$$

$$m_{\text{FG}}^{\text{waf}} = m_{\text{CO}_2\text{outcomb}}^{\text{waf}} + m_{\text{N}_2\text{outcomb}}^{\text{waf}} + m_{\text{O}_2\text{outcomb}}^{\text{waf}} + m_{\text{SO}_2\text{outcomb}}^{\text{waf}} + m_{\text{H}_2\text{Ooutcomb}}^{\text{waf}} \quad (4.64)$$

The results are listed in the Annex 4, the Table A4.17 and Table A4.18. The correctness of calculation for the masses of wet ash free flue gas $m_{\text{FG}}^{\text{waf}}$ (Table A4.17) and wet ash free air $m_{\text{airincomb}}^{\text{waf}}$ (Table A4.18) can be verified through the balance equation (4.65) recommended in the literature (van Loo, 2008):

$$m_{\text{FG}}^{\text{waf}} = m_{\text{airincomb}}^{\text{waf}} + 1. \quad (4.65)$$

The results of this verification are shown in the Table 4.10.

Table 4.10 - Balance results for verifying the wet ash free masses

Balance	$m_{\text{FG}}^{\text{waf}} - (m_{\text{airincomb}}^{\text{waf}} + 1)$ = 0.00 (?)
Oak	0.00 <input checked="" type="checkbox"/>
Beech	0.00 <input checked="" type="checkbox"/>
Douglas Fir	0.00 <input checked="" type="checkbox"/>
Bois d'Or Pellets	0.00 <input checked="" type="checkbox"/>

Because of the Lower Heating Value ($\text{LHV}_{\text{fuel}}^i$), which is considered, all along this work, at the initial state (i), the conversion of the wet ash free (waf) specific masses of the components towards the initial state (i) specific masses of the components is needed. The conversion relations (4.66) - (4.72) are further indicated.

$$m_{th\ O_2} = \frac{m^{waf}_{O_2incomb}}{\lambda} \cdot \left(1 - \frac{\%Ash^i}{100}\right) \quad (4.66)$$

$$m_{th\ N_2} = \frac{m^{waf}_{N_2incomb}}{\lambda} \cdot \left(1 - \frac{\%Ash^i}{100}\right) \quad (4.67)$$

$$m_{thdryair} = \frac{m^{waf}_{airincomb}}{\lambda} \cdot \left(1 - \frac{\%Ash^i}{100}\right) \quad (4.68)$$

$$m_{th\ CO_2} = m^{waf}_{CO_2outcomb} \cdot \left(1 - \frac{\%Ash^i}{100}\right) \quad (4.69)$$

$$m_{th\ SO_2} = m^{waf}_{SO_2outcomb} \cdot \left(1 - \frac{\%Ash^i}{100}\right) \quad (4.70)$$

$$m_{th\ N_2}^{FG} = \frac{m^{waf}_{N_2outcomb}}{\lambda} \cdot \left(1 - \frac{\%Ash^i}{100}\right) + \frac{\%N^i}{100} \cdot \frac{\lambda - 1}{\lambda} \quad (4.71)$$

$$m_{H_2O} = \left(m^{waf}_{H_2Ooutcomb} + \frac{x_{air}}{1000} \cdot \frac{m^{waf}_{airincomb}}{\lambda} \right) \cdot \left(1 - \frac{\%Ash^i}{100}\right) \quad (4.72)$$

With the conversion relations from above, the combustion air mass (4.30) becomes:

$$m_{realwetair} = \lambda \cdot \left(1 + \frac{x_{air}}{1000}\right) \cdot \frac{m^{waf}_{airincomb}}{\lambda} \cdot \left(1 - \frac{\%Ash^i}{100}\right) \quad (4.73)$$

and the heat entering in the combustion chamber coming from air (Q_{in_air}) is calculated with the relation (4.74):

$$m_{realwetair} \cdot \delta H_{air} = \lambda \cdot \left(1 + \frac{x_{air}}{1000}\right) \cdot \frac{m^{waf}_{airincomb}}{\lambda} \cdot \left(1 - \frac{\%Ash^i}{100}\right) \cdot \delta H_{air} \quad (4.74)$$

With the previous conversion relations, the flue gas mass at initial state from the relation (4.75):

$$m_{FG}^i = m_{CO_2} + m_{SO_2} + m_{N_2}^{FG} + m_{H_2O} + (\lambda - 1) \cdot \left(1 + \frac{x_{air}}{1000}\right) \cdot m_{thdryair} \quad (4.75)$$

becomes:

$$m_{FG}^i = \left[m^{waf}_{CO_2outcomb} + m^{waf}_{SO_2outcomb} + \frac{m^{waf}_{N_2outcomb}}{\lambda} + \left(m^{waf}_{H_2Ooutcomb} + \frac{x_{air}}{1000} \cdot m^{waf}_{airincomb} \right) + \frac{\lambda - 1}{\lambda} \cdot m^{waf}_{airincomb} \right] \cdot \left(1 - \frac{\%Ash^i}{100}\right) + \frac{\%N^i}{100} \cdot \frac{\lambda - 1}{\lambda} \quad (4.76)$$

and:

$$\begin{aligned}
 m_{FG}^i \cdot \delta H_{FG} = & \left(1 - \frac{\%Ash^i}{100} \right) \\
 & \cdot \left[m_{CO_2outcomb}^{waf} \cdot \delta H_{CO_2} + m_{SO_2outcomb}^{waf} \cdot \delta H_{SO_2} + \frac{m_{N_2outcomb}^{waf}}{\lambda} \right. \\
 & \cdot \delta H_{N_2} + \left(m_{H_2Ooutcomb}^{waf} + \frac{x_{air}}{1000} \cdot m_{airincomb}^{waf} \right) \cdot \delta H_{H_2O} \\
 & \left. + \frac{\lambda - 1}{\lambda} \cdot m_{airincomb}^{waf} \cdot \delta H_{Air} \right] + \frac{\%N^i}{100} \cdot \frac{\lambda - 1}{\lambda} \cdot \delta H_{N_2}
 \end{aligned} \quad (4.77)$$

Under these assumptions, the relation (4.53) becomes:

$$\begin{aligned}
 \lambda \cdot \left(1 + \frac{x_{air}}{1000} \right) \cdot \frac{m_{airincomb}^{waf}}{\lambda} \cdot \left(1 - \frac{\%Ash^i}{100} \right) \cdot \delta H_{air} + m_{fuel} \cdot LHV_{fuel}^i \\
 = \left(1 - \frac{\%Ash^i}{100} \right) \\
 \cdot \left[m_{CO_2outcomb}^{waf} \cdot \delta H_{CO_2} + m_{SO_2outcomb}^{waf} \cdot \delta H_{SO_2} + \frac{m_{N_2outcomb}^{waf}}{\lambda} \right. \\
 \cdot \delta H_{N_2} + \left(m_{H_2Ooutcomb}^{waf} + \frac{x_{air}}{1000} \cdot m_{airincomb}^{waf} \right) \cdot \delta H_{H_2O} \\
 \left. + \frac{\lambda - 1}{\lambda} \cdot m_{airincomb}^{waf} \cdot \delta H_{Air} \right] + \frac{\%N^i}{100} \cdot \frac{\lambda - 1}{\lambda} \cdot \delta H_{N_2} - Q_{outloss}
 \end{aligned} \quad (4.78)$$

and the relation (4.55) is:

$$\begin{aligned}
 m_{CO_2outcomb}^{waf} \cdot \delta H_{CO_2} + m_{SO_2outcomb}^{waf} \cdot \delta H_{SO_2} \\
 + \left(\frac{m_{N_2outcomb}^{waf}}{\lambda} + \frac{\%N^i}{100} \cdot \frac{\lambda - 1}{\lambda} \cdot \frac{1}{1 - \frac{\%Ash^i}{100}} \right) \cdot \delta H_{N_2} \\
 + \left(m_{H_2Ooutcomb}^{waf} + \frac{x_{air}}{1000} \cdot m_{airincomb}^{waf} \right) \cdot \delta H_{H_2O} \\
 + \frac{\lambda - 1}{\lambda} \cdot m_{airincomb}^{waf} \cdot \delta H_{Air} - \eta_{combchamber} \cdot m_{fuel} \cdot \frac{LHV_{fuel}^i}{1 - \frac{\%Ash^i}{100}} \\
 - \eta_{combchamber} \cdot \left(1 + \frac{x_{air}}{1000} \right) \cdot m_{airincomb}^{waf} \cdot \delta H_{air} = 0
 \end{aligned} \quad (4.79)$$

where:

$$m_{airincomb}^{waf} \cdot \delta H_{air} = m_{airincomb}^{waf} \cdot \left(c_{p_{air}}^{T_{atm}} \cdot T_{atm} - c_{p_{air}}^{T_{ref}} \cdot T_{ref} \right) \quad (4.80)$$

4.3.4.2. Gaskell Equation for enthalpy calculation

In the literature (Gaskell, 2003, Shomate, 1954), the enthalpy change associated with a temperature change from T_1 to T_2 for an ideal gas at constant pressure is determined with the relation (4.81):

$$\delta H_{1 \rightarrow 2} = \int_{T_1}^{T_2} C_p dT \quad (4.81)$$

where the ideal gas heat capacity is approximated by Gaskell (Gaskell, 2003), with the relation (4.82):

$$C_p(T) = a + b \cdot T + \frac{c}{T^2} \quad (4.82)$$

By integrating the relation (4.82), the enthalpy change becomes:

$$\delta H_{1 \rightarrow 2} = a \cdot (T_2 - T_1) + \frac{b}{2} \cdot (T_2^2 - T_1^2) - c \cdot \left(\frac{1}{T_2} - \frac{1}{T_1} \right) \quad (4.83)$$

To determine the flue gases adiabatic combustion temperature, with the relation (4.83), the relation (4.46) is re-written under the form of the relation (4.84):

$$\begin{aligned} Q_{outFG} &= m_{FG}^i \cdot \delta H_{FG} = m_{FG}^i \cdot \left[H(c_{pFG}^{T_{FG}}, T_{FG}) - H(c_{pFG}^{T_{ref}}, T_{ref}) \right] = \\ &= \sum_i^n m_i \cdot a_i \cdot (T_{FG} - T_{ref}) + \sum_i^n m_i \cdot \frac{b_i}{2} \cdot (T_{FG}^2 - T_{ref}^2) \\ &\quad - \sum_i^n m_i \cdot c_i \cdot \left(\frac{1}{T_{FG}} - \frac{1}{T_{ref}} \right) \end{aligned} \quad (4.84)$$

The products mass - enthalpy are calculated with specific coefficients (a_i , b_i , c_i) addressing all flue gas components and the amount of flue gases energy is calculated. Some parameters have previously been provided and the results will be compared, along with an error between the previous and current. In the Table 4.11, the components of the combustion adiabatic temperature (T_{FG}) equation are listed.

Table 4.11 - The combustion adiabatic temperature equation's components

Parameter	Calculated data	
	Symbol	Unit of measure
Mass of "i" component	m_i	kg
Specific coefficients	a_i, b_i, c_i	-
Temperature of combustion	T_{FG}	K
Temperature of reference	T_{ref}	K
Flue gas mass	m_{FG}	kg
Flue gas enthalpy difference	δH_{FG}	kJ/(kg·K)

For each term in the relation (4.84), the related expressions used for their calculation are below detailed.

$$\begin{aligned} \sum_i^n m_i \cdot a_i \cdot (T_{FG} - T_{ref}) &= \\ &= \left[m^{waf}_{CO_2outcomb} \cdot a_{CO_2} + m^{waf}_{SO_2outcomb} \cdot a_{SO_2} \right. \\ &\quad + \left(\frac{m^{waf}_{N_2outcomb}}{\lambda} + \frac{\%N^i}{100} \cdot \frac{\lambda - 1}{\lambda} \cdot \frac{1}{1 - \frac{\%Ash^i}{100}} \right) \cdot a_{N_2} \\ &\quad + \left(m^{waf}_{H_2Ooutcomb} + \frac{x_{air}}{1000} \cdot m^{waf}_{airincomb} \right) \cdot a_{H_2O} + \frac{\lambda - 1}{\lambda} \cdot m^{waf}_{airincomb} \\ &\quad \left. \cdot (0.768 \cdot a_{N_2} + 0.232 \cdot a_{O_2}) \right] \cdot (T_{FG} - T_{ref}) \end{aligned} \quad (4.85)$$

$$\begin{aligned}
 \sum_i^n m_i \cdot \frac{b_i}{2} \cdot (T_{FG}^2 - T_{ref}^2) &= \\
 &= \left[m^{waf}_{CO_2out_{comb}} \cdot \frac{b_{CO_2}}{2} + m^{waf}_{SO_2out_{comb}} \cdot \frac{b_{SO_2}}{2} \right. \\
 &+ \left(\frac{m^{waf}_{N_2out_{comb}}}{\lambda} + \frac{\%N^i}{100} \cdot \frac{\lambda-1}{\lambda} \cdot \frac{1}{1-\frac{\%Ash^i}{100}} \right) \cdot \frac{b_{N_2}}{2} \\
 &+ \left(m^{waf}_{H_2Oout_{comb}} + \frac{x_{air}}{1000} \cdot m^{waf}_{airin_{comb}} \right) \cdot \frac{b_{H_2O}}{2} + \frac{\lambda-1}{\lambda} \cdot m^{waf}_{airin_{comb}} \\
 &\left. \cdot \left(0.768 \cdot \frac{b_{N_2}}{2} + 0.232 \cdot \frac{b_{O_2}}{2} \right) \right] \cdot (T_{FG}^2 - T_{ref}^2) \quad (4.86)
 \end{aligned}$$

$$\begin{aligned}
 \sum_i^n m_i \cdot c_i \cdot \left(\frac{1}{T_{FG}} - \frac{1}{T_{ref}} \right) &= \\
 &= \left[m^{waf}_{CO_2out_{comb}} \cdot c_{CO_2} + m^{waf}_{SO_2out_{comb}} \cdot c_{SO_2} \right. \\
 &+ \left(\frac{m^{waf}_{N_2out_{comb}}}{\lambda} + \frac{\%N^i}{100} \cdot \frac{\lambda-1}{\lambda} \cdot \frac{1}{1-\frac{\%Ash^i}{100}} \right) \cdot c_{N_2} \\
 &+ \left(m^{waf}_{H_2Oout_{comb}} + \frac{x_{air}}{1000} \cdot m^{waf}_{airin_{comb}} \right) \cdot a_{H_2O} + \frac{\lambda-1}{\lambda} \cdot m^{waf}_{airin_{comb}} \\
 &\left. \cdot (0.768 \cdot c_{N_2} + 0.232 \cdot c_{O_2}) \right] \cdot \left(\frac{1}{T_{FG}} - \frac{1}{T_{ref}} \right) \quad (4.87)
 \end{aligned}$$

The combustion adiabatic temperature T_{FG} is obtained by resolving the equation (4.88) below indicated:

$$\begin{aligned}
 &\left[m^{waf}_{CO_2out_{comb}} \cdot a_{CO_2} + m^{waf}_{SO_2out_{comb}} \cdot a_{SO_2} + \left(\frac{m^{waf}_{N_2out_{comb}}}{\lambda} + \frac{\%N^i}{100} \cdot \frac{\lambda-1}{\lambda} \cdot \frac{1}{1-\frac{\%Ash^i}{100}} \right) \cdot a_{N_2} + \right. \\
 &\left. \left(m^{waf}_{H_2Oout_{comb}} + \frac{x_{air}}{1000} \cdot m^{waf}_{airin_{comb}} \right) \cdot a_{H_2O} + \frac{\lambda-1}{\lambda} \cdot m^{waf}_{airin_{comb}} \cdot (0.768 \cdot a_{N_2} + 0.232 \cdot a_{O_2}) \right] \cdot T_{FG} + \\
 &\left[m^{waf}_{CO_2out_{comb}} \cdot \frac{b_{CO_2}}{2} + m^{waf}_{SO_2out_{comb}} \cdot \frac{b_{SO_2}}{2} + \left(\frac{m^{waf}_{N_2out_{comb}}}{\lambda} + \frac{\%N^i}{100} \cdot \frac{\lambda-1}{\lambda} \cdot \frac{1}{1-\frac{\%Ash^i}{100}} \right) \cdot \frac{b_{N_2}}{2} + \right. \\
 &\left. \left(m^{waf}_{H_2Oout_{comb}} + \frac{x_{air}}{1000} \cdot m^{waf}_{airin_{comb}} \right) \cdot \frac{b_{H_2O}}{2} + \frac{\lambda-1}{\lambda} \cdot m^{waf}_{airin_{comb}} \cdot \left(0.768 \cdot \frac{b_{N_2}}{2} + 0.232 \cdot \frac{b_{O_2}}{2} \right) \right] \cdot T_{FG}^2 - \\
 &\left[m^{waf}_{CO_2out_{comb}} \cdot c_{CO_2} + m^{waf}_{SO_2out_{comb}} \cdot c_{SO_2} + \left(\frac{m^{waf}_{N_2out_{comb}}}{\lambda} + \frac{\%N^i}{100} \cdot \frac{\lambda-1}{\lambda} \cdot \frac{1}{1-\frac{\%Ash^i}{100}} \right) \cdot c_{N_2} + \right. \\
 &\left. \left(m^{waf}_{H_2Oout_{comb}} + \frac{x_{air}}{1000} \cdot m^{waf}_{airin_{comb}} \right) \cdot a_{H_2O} + \frac{\lambda-1}{\lambda} \cdot m^{waf}_{airin_{comb}} \cdot (0.768 \cdot c_{N_2} + 0.232 \cdot c_{O_2}) \right] \cdot \frac{1}{T_{FG}} - \\
 &\left[m^{waf}_{CO_2out_{comb}} \cdot a_{CO_2} + \right. \quad (4.88)
 \end{aligned}$$

$$\begin{aligned}
 & m_{\text{SO}_2\text{outcomb}}^{\text{waf}} \cdot a_{\text{SO}_2} + \left(\frac{m_{\text{N}_2\text{outcomb}}^{\text{waf}}}{\lambda} + \frac{\%Ni}{100} \cdot \frac{\lambda-1}{\lambda} \cdot \frac{1}{1-\frac{\%Ash^i}{100}} \right) \cdot a_{\text{N}_2} + \left(m_{\text{H}_2\text{Ooutcomb}}^{\text{waf}} + \right. \\
 & \left. \frac{x_{\text{air}}}{1000} \cdot m_{\text{airincomb}}^{\text{waf}} \right) \cdot a_{\text{H}_2\text{O}} + \frac{\lambda-1}{\lambda} \cdot m_{\text{airincomb}}^{\text{waf}} \cdot \left(0.768 \cdot a_{\text{N}_2} + 0.232 \cdot a_{\text{O}_2} \right) \Bigg] \cdot T_{\text{ref}} - \\
 & \left[m_{\text{CO}_2\text{outcomb}}^{\text{waf}} \cdot \frac{b_{\text{CO}_2}}{2} + m_{\text{SO}_2\text{outcomb}}^{\text{waf}} \cdot \frac{b_{\text{SO}_2}}{2} + \left(\frac{m_{\text{N}_2\text{outcomb}}^{\text{waf}}}{\lambda} + \frac{\%Ni}{100} \cdot \frac{\lambda-1}{\lambda} \cdot \frac{1}{1-\frac{\%Ash^i}{100}} \right) \cdot \frac{b_{\text{N}_2}}{2} + \right. \\
 & \left. \left(m_{\text{H}_2\text{Ooutcomb}}^{\text{waf}} + \frac{x_{\text{air}}}{1000} \cdot m_{\text{airincomb}}^{\text{waf}} \right) \cdot \frac{b_{\text{H}_2\text{O}}}{2} + \frac{\lambda-1}{\lambda} \cdot m_{\text{airincomb}}^{\text{waf}} \cdot \left(0.768 \cdot \frac{b_{\text{N}_2}}{2} + 0.232 \cdot \right. \right. \\
 & \left. \left. \frac{b_{\text{O}_2}}{2} \right) \right] \cdot T_{\text{ref}}^2 + \left[m_{\text{CO}_2\text{outcomb}}^{\text{waf}} \cdot c_{\text{CO}_2} + m_{\text{SO}_2\text{outcomb}}^{\text{waf}} \cdot c_{\text{SO}_2} + \left(\frac{m_{\text{N}_2\text{outcomb}}^{\text{waf}}}{\lambda} + \frac{\%Ni}{100} \cdot \frac{\lambda-1}{\lambda} \cdot \right. \right. \\
 & \left. \left. \frac{1}{1-\frac{\%Ash^i}{100}} \right) \cdot c_{\text{N}_2} + \left(m_{\text{H}_2\text{Ooutcomb}}^{\text{waf}} + \frac{x_{\text{air}}}{1000} \cdot m_{\text{airincomb}}^{\text{waf}} \right) \cdot c_{\text{H}_2\text{O}} + \frac{\lambda-1}{\lambda} \cdot m_{\text{airincomb}}^{\text{waf}} \cdot \right. \\
 & \left. \left(0.768 \cdot c_{\text{N}_2} + 0.232 \cdot c_{\text{O}_2} \right) \right] \cdot \frac{1}{T_{\text{ref}}} - \eta_{\text{combchamber}} \cdot m_{\text{fuel}} \cdot \frac{\text{LHV}_{\text{fuel}}^i}{1-\frac{\%Ash^i}{100}} - \eta_{\text{combchamber}} \cdot \left(1 + \frac{x_{\text{air}}}{1000} \right) \cdot \\
 & m_{\text{airincomb}}^{\text{waf}} \cdot \left(c_{\text{pair}}^{\text{Tatm}} \cdot T_{\text{atm}} - c_{\text{pair}}^{\text{Tref}} \cdot T_{\text{ref}} \right) = 0
 \end{aligned}$$

The specific coefficients (a_i , b_i , c_i) for each of the components of flue gases are presented in Annex 4, Table A4.19.

The sums of products between coefficients (a_i , b_i , c_i) and flue gas component masses (m_{CO_2} , m_{N_2} , m_{O_2} , m_{SO_2} , $m_{\text{H}_2\text{O}}$) have been calculated in Annex 4, Table A4.20.

The values of terms from the equation (4.88) containing the unknown variable T_{FG} (T_{FG}^2 , T_{FG}^1 , $T_{\text{FG}}^{(-1)}$) and the free term (T_{FG}^0) have been determined and they are indicated in Annex 4, Table A4.21.

The way to find a solution to this equation (4.88) was to give values to T_{FG} , until the Equation's calculated value would become 0, therefore valid.

An approximate way to find this temperature was to observe when the function described by the equation would intersect the 0 axis, as shown in Figure 4.12 and Figure 4.13.

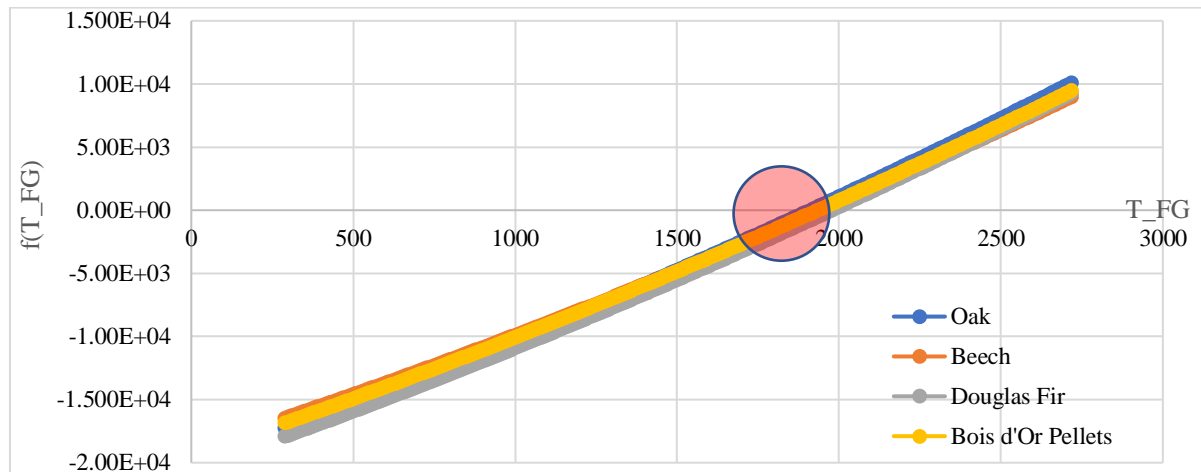


Figure 4.12 - Flue gas temperature function with a step of 10 K

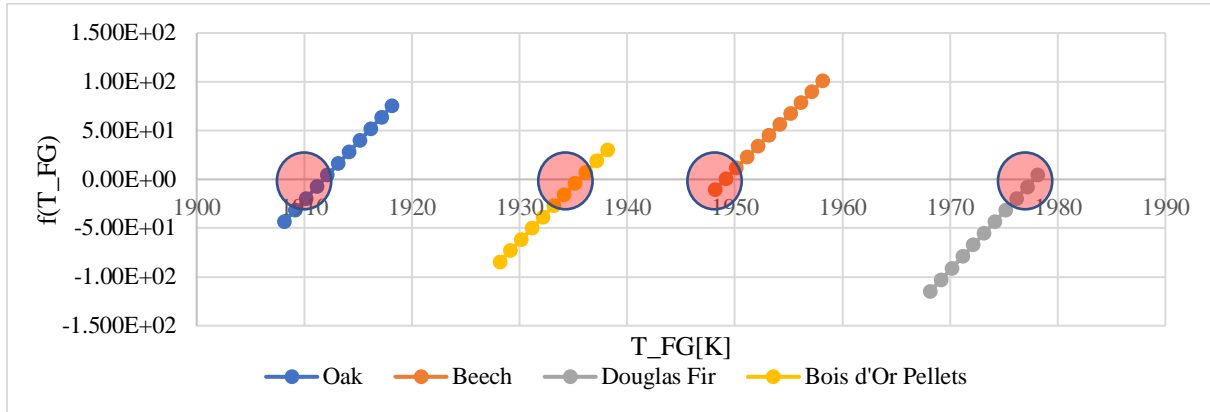


Figure 4.13 - Flue gas temperature function with a step of 1K

This was done by calculating the result for each temperature in the equation (4.88) starting from 273 K with a step of 10 K and a function in Excel was used to determine if from one result to the other the function intersected the 0 axis (table 4.12).

Table 4.12 - The equation (4.88) function

T_{FG} [K]	$[273 \div 2713, \text{step: } 10]$
$f(T_{FG})$	$C_1 \cdot T_{FG}^2 + C_2 \cdot T_{FG}^1 + C_3 \cdot T_{FG}^0 + C_4 \cdot T_{FG}^{(-1)}$
Found?	$IF(OR((AND(f(T_{FG_i}) < 0; f(T_{FG_{i+1}}) > 0); (AND(f(T_{FG_i}) > 0; f(T_{FG_{i+1}}) > 0))))); T_{FG_i}; "no")$

The Excel function named “Found” is presented in relation (4.89). If it detects that the result of 2 successive functions has passed from negative to positive or the opposite, it equals in the first of the 2 values of T_{FG} .

$$= IF(OR((AND(f(T_{FG_i}) < 0; f(T_{FG_{i+1}}) > 0); (AND(f(T_{FG_i}) > 0; f(T_{FG_{i+1}}) > 0))))); T_{FG_i}; "no") \quad (4.89)$$

The relation (4,90) finds the maximum of all “found” functions to determine the point in which the relation (4.88) calculated value passed through the 0 axis, as shown in Figure 4.13. Since the value of the temperature found is the only numerical value in the column, it will be the result yielded by the function of (4.90).

$$= MAX(Found_i; Found_n) \quad (4.90)$$

In Annex 4, the Table A4.22, the considered extract of the wooden species tables of the equation (4.88) function containing temperatures, results and "found" function (step:10) are indicated.

After finding the temperature for which the function passes from negative to positive, thus intersecting the 0 axis, the temperatures inside the previously used 10K step interval can be tested to further refine the result, by reducing the step to 1, as shown in Table 4.13.

Table 4.13 - Refining the result of the equation (4.88) function

T_{FG} [K]	$[T_{FG_{found}} \div T_{FG_{found}} + 10, \text{step: } 1]$
$f(T_{FG})$	$C_1 \cdot T_{FG}^2 + C_2 \cdot T_{FG}^1 + C_3 \cdot T_{FG}^0 + C_4 \cdot T_{FG}^{(-1)}$
Found?	$IF(OR((AND(f(T_{FG_i}) < 0; f(T_{FG_{i+1}}) > 0); (AND(f(T_{FG_i}) > 0; f(T_{FG_{i+1}}) > 0))))); T_{FG_i}; "no")$

The same function “Found?” applies to this interval, to find with more precision [1 K] the temperature for which the function passes from negative to positive results. The obtained refined results are suggested in the Figure 4.13 and are shown in the Annex 4, Table A4.23. A comparison of these results with those obtained by using MSOffice Excel SOLVER function is included in Annex 4, the Table A4.24. It is to be remarked that the precision of FOUND? function results is affected by relative errors smaller than 0.038%.

4.3.4.3. Howard Shomate Equation and JANAF coefficients for enthalpy calculation

In the literature (Shomate, 1954), the enthalpy change associated with a temperature change from T_1 to T_2 for an ideal gas at constant pressure is determined with the relation (4.91) identical with (4.81):

$$\delta H_{1 \rightarrow 2} = \int_{T_1}^{T_2} C_p \, dT \quad (4.91)$$

where the ideal gas heat capacity is approximated by the Howard Shomate relation (4.92):

$$C_p(t) = A + B \cdot t + C \cdot t^2 + D \cdot t^3 + \frac{E}{t^2} \left[\frac{J}{\text{mol} \cdot K} \right], \quad t = \frac{T[K]}{1000} \quad (4.92)$$

By integrating the relation (4.91), the enthalpy change becomes:

$$\delta H_{1 \rightarrow 2} = A \cdot (t_2 - t_1) + \frac{B}{2} \cdot (t_2^2 - t_1^2) + \frac{C}{3} \cdot (t_2^3 - t_1^3) + \frac{D}{4} \cdot (t_2^4 - t_1^4) - E \cdot \left(\frac{1}{t_2} - \frac{1}{t_1} \right) \quad (4.93)$$

Taking into consideration the relation (4.93), to determine the flue gases adiabatic combustion temperature T_{FG} , the right member of the relation (4.46) must be re-written under the form of the relation (4.94):

$$\begin{aligned} m_{FG}^i \cdot \delta H_{FG} = & \sum_i^n \frac{m_i}{M_i} \cdot A_i \cdot (t_{FG} - t_{ref}) + \sum_i^n \frac{m_i}{M_i} \cdot \frac{B_i}{2} \cdot (t_{FG}^2 - t_{ref}^2) \\ & + \sum_i^n \frac{m_i}{M_i} \cdot \frac{C_i}{3} \cdot (t_{FG}^3 - t_{ref}^3) + \sum_i^n \frac{m_i}{M_i} \cdot \frac{D_i}{4} \cdot (t_{FG}^4 - t_{ref}^4) \\ & - \sum_i^n \frac{m_i}{M_i} \cdot E_i \cdot \left(\frac{1}{t_{FG}} - \frac{1}{t_{ref}} \right), \end{aligned} \quad (4.94)$$

$$t_{FG} = \frac{T_{FG}[K]}{1000}; \quad t_{ref} = \frac{T_{ref}[K]}{1000}$$

which is more explicit under the form of the relation (4.95):

$$\begin{aligned} m_{FG}^i \cdot \delta H_{FG} = & \sum_i^n \frac{m_i}{M_i} \cdot A_i \cdot t_{FG} + \sum_i^n \frac{m_i}{M_i} \cdot \frac{B_i}{2} \cdot t_{FG}^2 + \sum_i^n \frac{m_i}{M_i} \cdot \frac{C_i}{3} \cdot t_{FG}^3 + \sum_i^n \frac{m_i}{M_i} \cdot \frac{D_i}{4} \cdot t_{FG}^4 \\ & - \sum_i^n \frac{m_i}{M_i} \cdot E_i \cdot \frac{1}{t_{FG}} + \sum_i^n \frac{m_i}{M_i} \cdot F_i - \sum_i^n \frac{m_i}{M_i} \cdot H_i - \sum_i^n \frac{m_i}{M_i} \cdot A_i \cdot t_{ref} \\ & - \sum_i^n \frac{m_i}{M_i} \cdot \frac{B_i}{2} \cdot t_{ref}^2 - \sum_i^n \frac{m_i}{M_i} \cdot \frac{C_i}{3} \cdot t_{ref}^3 - \sum_i^n \frac{m_i}{M_i} \cdot \frac{D_i}{4} \cdot t_{ref}^4 \\ & + \sum_i^n \frac{m_i}{M_i} \cdot E_i \cdot \frac{1}{t_{ref}} - \sum_i^n \frac{m_i}{M_i} \cdot F_i + \sum_i^n \frac{m_i}{M_i} \cdot H_i \end{aligned} \quad (4.95)$$

Within the relation (4.95), the following relations (4.96) - (4.103) are used:

$$\begin{aligned}
 \sum_i^n \frac{m_i}{M_i} \cdot A_i &= \frac{m^{\text{waf}}_{\text{CO}_2\text{outcomb}}}{M_{\text{CO}_2}} \cdot A_{\text{CO}_2} + \frac{m^{\text{waf}}_{\text{SO}_2\text{outcomb}}}{M_{\text{SO}_2}} \cdot A_{\text{SO}_2} \\
 &\quad + \frac{\left(\frac{m^{\text{waf}}_{\text{N}_2\text{outcomb}}}{\lambda} + \frac{\%N^i}{100} \cdot \frac{\lambda - 1}{\lambda} \cdot \frac{1}{1 - \frac{\%Ash^i}{100}} \right)}{M_{\text{N}_2}} \cdot A_{\text{N}_2} \\
 &\quad + \frac{\left(m^{\text{waf}}_{\text{H}_2\text{Ooutcomb}} + \frac{x_{\text{air}}}{1000} \cdot m^{\text{waf}}_{\text{airincomb}} \right)}{M_{\text{H}_2\text{O}}} \cdot A_{\text{H}_2\text{O}} + \frac{\lambda - 1}{\lambda} \cdot m^{\text{waf}}_{\text{airincomb}} \\
 &\quad \cdot \left(\frac{0,768}{M_{\text{N}_2}} \cdot A_{\text{N}_2} + \frac{0,232}{M_{\text{O}_2}} \cdot A_{\text{O}_2} \right)
 \end{aligned} \tag{4.96}$$

$$\begin{aligned}
 \sum_i^n \frac{m_i}{M_i} \cdot \frac{B_i}{2} &= \frac{m^{\text{waf}}_{\text{CO}_2\text{outcomb}}}{M_{\text{CO}_2}} \cdot \frac{B_{\text{CO}_2}}{2} + \frac{m^{\text{waf}}_{\text{SO}_2\text{outcomb}}}{M_{\text{SO}_2}} \cdot \frac{B_{\text{SO}_2}}{2} \\
 &\quad + \frac{\left(\frac{m^{\text{waf}}_{\text{N}_2\text{outcomb}}}{\lambda} + \frac{\%N^i}{100} \cdot \frac{\lambda - 1}{\lambda} \cdot \frac{1}{1 - \frac{\%Ash^i}{100}} \right)}{M_{\text{N}_2}} \cdot \frac{B_{\text{N}_2}}{2} \\
 &\quad + \frac{\left(m^{\text{waf}}_{\text{H}_2\text{Ooutcomb}} + \frac{x_{\text{air}}}{1000} \cdot m^{\text{waf}}_{\text{airincomb}} \right)}{M_{\text{H}_2\text{O}}} \cdot \frac{B_{\text{H}_2\text{O}}}{2} + \frac{\lambda - 1}{\lambda} \cdot m^{\text{waf}}_{\text{airincomb}} \\
 &\quad \cdot \left(\frac{0,768}{M_{\text{N}_2}} \cdot \frac{B_{\text{N}_2}}{2} + \frac{0,232}{M_{\text{O}_2}} \cdot \frac{B_{\text{O}_2}}{2} \right)
 \end{aligned} \tag{4.97}$$

$$\begin{aligned}
 \sum_i^n \frac{m_i}{M_i} \cdot \frac{C_i}{3} &= \frac{m^{\text{waf}}_{\text{CO}_2\text{outcomb}}}{M_{\text{CO}_2}} \cdot \frac{C_{\text{CO}_2}}{3} + \frac{m^{\text{waf}}_{\text{SO}_2\text{outcomb}}}{M_{\text{SO}_2}} \cdot \frac{C_{\text{SO}_2}}{3} \\
 &\quad + \frac{\left(\frac{m^{\text{waf}}_{\text{N}_2\text{outcomb}}}{\lambda} + \frac{\%N^i}{100} \cdot \frac{\lambda - 1}{\lambda} \cdot \frac{1}{1 - \frac{\%Ash^i}{100}} \right)}{M_{\text{N}_2}} \cdot \frac{C_{\text{N}_2}}{3} \\
 &\quad + \frac{\left(m^{\text{waf}}_{\text{H}_2\text{Ooutcomb}} + \frac{x_{\text{air}}}{1000} \cdot m^{\text{waf}}_{\text{airincomb}} \right)}{M_{\text{H}_2\text{O}}} \cdot \frac{C_{\text{H}_2\text{O}}}{3} + \frac{\lambda - 1}{\lambda} \cdot m^{\text{waf}}_{\text{airincomb}} \\
 &\quad \cdot \left(\frac{0,768}{M_{\text{N}_2}} \cdot \frac{C_{\text{N}_2}}{3} + \frac{0,232}{M_{\text{O}_2}} \cdot \frac{C_{\text{O}_2}}{3} \right)
 \end{aligned} \tag{4.98}$$

$$\begin{aligned}
 \sum_i^n \frac{m_i}{M_i} \cdot \frac{D_i}{4} &= \frac{m^{\text{waf}}_{\text{CO}_2\text{outcomb}}}{M_{\text{CO}_2}} \cdot \frac{D_{\text{CO}_2}}{4} + \frac{m^{\text{waf}}_{\text{SO}_2\text{outcomb}}}{M_{\text{SO}_2}} \cdot \frac{D_{\text{SO}_2}}{4} \\
 &\quad + \frac{\left(\frac{m^{\text{waf}}_{\text{N}_2\text{outcomb}}}{\lambda} + \frac{\%N^i}{100} \cdot \frac{\lambda - 1}{\lambda} \cdot \frac{1}{1 - \frac{\%Ash^i}{100}} \right)}{M_{\text{N}_2}} \cdot \frac{D_{\text{N}_2}}{4} \\
 &\quad + \frac{\left(m^{\text{waf}}_{\text{H}_2\text{Ooutcomb}} + \frac{x_{\text{air}}}{1000} \cdot m^{\text{waf}}_{\text{airincomb}} \right)}{M_{\text{H}_2\text{O}}} \cdot \frac{D_{\text{H}_2\text{O}}}{4} + \frac{\lambda - 1}{\lambda} \cdot m^{\text{waf}}_{\text{airincomb}} \\
 &\quad \cdot \left(\frac{0,768}{M_{\text{N}_2}} \cdot \frac{D_{\text{N}_2}}{4} + \frac{0,232}{M_{\text{O}_2}} \cdot \frac{D_{\text{O}_2}}{4} \right)
 \end{aligned} \tag{4.99}$$

$$\begin{aligned}
 \sum_i^n \frac{m_i}{M_i} \cdot E_i = & \frac{m^{waf}_{CO_2outcomb}}{M_{CO_2}} \cdot E_{CO_2} + \frac{m^{waf}_{SO_2outcomb}}{M_{SO_2}} \cdot E_{SO_2} \\
 & + \frac{\left(\frac{m^{waf}_{N_2outcomb}}{\lambda} + \frac{\%N^i}{100} \cdot \frac{\lambda - 1}{\lambda} \cdot \frac{1}{1 - \frac{\%Ash^i}{100}} \right)}{M_{N_2}} \cdot E_{N_2} \\
 & + \frac{\left(m^{waf}_{H_2Ooutcomb} + \frac{x_{air}}{1000} \cdot m^{waf}_{airincomb} \right)}{M_{H_2O}} \cdot E_{H_2O} \\
 & + \frac{\lambda - 1}{\lambda} \cdot m^{waf}_{airincomb} \cdot \left(\frac{0,768}{M_{N_2}} \cdot E_{N_2} + \frac{0,232}{M_{O_2}} \cdot E_{O_2} \right)
 \end{aligned} \tag{4.100}$$

$$\begin{aligned}
 \sum_i^n \frac{m_i}{M_i} \cdot F_i = & \frac{m^{waf}_{CO_2outcomb}}{M_{CO_2}} \cdot F_{CO_2} + \frac{m^{waf}_{SO_2outcomb}}{M_{SO_2}} \cdot F_{SO_2} \\
 & + \frac{\left(\frac{m^{waf}_{N_2outcomb}}{\lambda} + \frac{\%N^i}{100} \cdot \frac{\lambda - 1}{\lambda} \cdot \frac{1}{1 - \frac{\%Ash^i}{100}} \right)}{M_{N_2}} \cdot F_{N_2} \\
 & + \frac{\left(m^{waf}_{H_2Ooutcomb} + \frac{x_{air}}{1000} \cdot m^{waf}_{airincomb} \right)}{M_{H_2O}} \cdot F_{H_2O} \\
 & + \frac{\lambda - 1}{\lambda} \cdot m^{waf}_{airincomb} \cdot \left(\frac{0,768}{M_{N_2}} \cdot F_{N_2} + \frac{0,232}{M_{O_2}} \cdot F_{O_2} \right)
 \end{aligned} \tag{4.101}$$

$$\begin{aligned}
 \sum_i^n \frac{m_i}{M_i} \cdot H_i = & \frac{m^{waf}_{CO_2outcomb}}{M_{CO_2}} \cdot H_{CO_2} + \frac{m^{waf}_{SO_2outcomb}}{M_{SO_2}} \cdot H_{SO_2} \\
 & + \frac{\left(\frac{m^{waf}_{N_2outcomb}}{\lambda} + \frac{\%N^i}{100} \cdot \frac{\lambda - 1}{\lambda} \cdot \frac{1}{1 - \frac{\%Ash^i}{100}} \right)}{M_{N_2}} \cdot H_{N_2} \\
 & + \frac{\left(m^{waf}_{H_2Ooutcomb} + \frac{x_{air}}{1000} \cdot m^{waf}_{airincomb} \right)}{M_{H_2O}} \cdot H_{H_2O} \\
 & + \frac{\lambda - 1}{\lambda} \cdot m^{waf}_{airincomb} \cdot \left(\frac{0,768}{M_{N_2}} \cdot H_{N_2} + \frac{0,232}{M_{O_2}} \cdot H_{O_2} \right)
 \end{aligned} \tag{4.102}$$

The free term is calculated with the relation (4.103).

$$\begin{aligned}
 - \sum_i^n \frac{m_i}{M_i} \cdot A_i \cdot t_{ref} - \sum_i^n \frac{m_i}{M_i} \cdot \frac{B_i}{2} \cdot t_{ref}^2 - \sum_i^n \frac{m_i}{M_i} \cdot \frac{C_i}{3} \cdot t_{ref}^3 - \sum_i^n \frac{m_i}{M_i} \cdot \frac{D_i}{4} \cdot t_{ref}^4 + \sum_i^n \frac{m_i}{M_i} \cdot E_i \cdot \frac{1}{t_{ref}} \\
 - \sum_i^n \frac{m_i}{M_i} \cdot F_i + \sum_i^n \frac{m_i}{M_i} \cdot H_i - \eta_{combchamber} \cdot m_{fuel} \cdot \frac{LHV_{fuel}^i}{1 - \frac{\%Ash^i}{100}} - \eta_{combchamber} \\
 \cdot \left(1 + \frac{x_{air}}{1000} \right) \cdot m^{waf}_{airincomb} \cdot \left(c_{pair}^{T_{atm}} \cdot T_{atm} - c_{pair}^{T_{ref}} \cdot T_{ref} \right)
 \end{aligned} \tag{4.103}$$

The left member of the relation (4.46) can be rewritten under the relation (4.96):

$$\begin{aligned}
 & m^{waf}_{CO_{2outcomb}} \cdot \delta H_{CO_2} + m^{waf}_{SO_{2outcomb}} \cdot \delta H_{SO_2} \\
 & + \left(\frac{m^{waf}_{N_{2outcomb}}}{\lambda} + \frac{\%N^i}{100} \cdot \frac{\lambda - 1}{\lambda} \cdot \frac{1}{1 - \frac{\%Ash^i}{100}} \right) \cdot \delta H_{N_2} \\
 & + \left(m^{waf}_{H_2Ooutcomb} + \frac{x_{air}}{1000} \cdot m^{waf}_{airincomb} \right) \cdot \delta H_{H_2O} \\
 & + \frac{\lambda - 1}{\lambda} \cdot m^{waf}_{airincomb} \cdot \delta H_{Air} - \eta_{combchamber} \cdot m_{fuel} \cdot \frac{LHV_{fuel}^i}{1 - \frac{\%Ash^i}{100}} \\
 & - \eta_{combchamber} \cdot \left(1 + \frac{x_{air}}{1000} \right) \\
 & \cdot m^{waf}_{airincomb} \cdot \left(c_{p_{air}}^{T_{atm}} \cdot T_{atm} - c_{p_{air}}^{T_{ref}} \cdot T_{ref} \right) = 0
 \end{aligned} \tag{4.104}$$

For each of the flue gas components, the coefficients A_i , B_i , C_i , D_i , E_i , F_i and H_i (Gaskell, 2003, Shomate, 1954), are indicated in Annex 4, Table A4.25. In the same Annex 4, the molar masses are indicated in Table A4.16, the masses m_i are taking in consideration the results from Table A4.17 and Table A4.18 and the conversion relations (4.66) – (4.72).

For the Gaskell equation, the related coefficients a_i , b_i and c_i are constant (Mărculescu, 2017). Because in the Howard Shomate equation, the coefficients A_i , B_i , C_i , D_i , E_i , F_i and H_i are temperature - dependent, only the components of the free term (relation 4.103) at the reference temperature T_{ref} are determined and indicated in the Annex 4, the Table A4.26.

The values of terms from the relation (4.103) containing the constant T_{ref} (T_{ref}^4 , T_{ref}^3 , T_{ref}^2 , T_{ref}^1 , T_{ref}^0 , $T_{ref}^{(-1)}$) have been determined and they are indicated in Table A4.27 in Annex 4. Based on the coefficients indicated in Table A4.27, the free term represented by the relation (4.103) gets the values shown in Annex 4, the Table A4.28.

Because the coefficients A_i , B_i , C_i , D_i , E_i , F_i and H_i are temperature - dependent as shown in the Annex 4, the Table A4.25 and suggested by the relation (4.105) in which T_{FG} is unknown:

$$\begin{aligned}
 \sum_i^n \frac{m_i}{M_i} \cdot \frac{D_i}{4} = f_1(T_{FG}); \quad \sum_i^n \frac{m_i}{M_i} \cdot \frac{C_i}{3} = f_2(T_{FG}); \quad \sum_i^n \frac{m_i}{M_i} \cdot \frac{B_i}{2} = f_3(T_{FG}); \\
 \sum_i^n \frac{m_i}{M_i} \cdot A_i = f_4(T_{FG}); \quad \sum_i^n \frac{m_i}{M_i} \cdot F_i - \sum_i^n \frac{m_i}{M_i} \cdot H_i = f_5(T_{FG}); \quad \sum_i^n \frac{m_i}{M_i} \cdot E_i = f_6(T_{FG});
 \end{aligned} \tag{4.105}$$

an iterative calculation is required.

The resulting values of the relations (4.96) – (4.102), namely $C_{1FG}(T_{FG})$, $C_{2FG}(T_{FG})$, $C_{3FG}(T_{FG})$, $C_{4FG}(T_{FG})$, $C_{5FG}(T_{FG})$, and $C_{6FG}(T_{FG})$ in Table 4.14, cannot be specified as it was done in the case of Gaskell equation (i.e., Table A4.20 and Table A4.21 in Annex 4).

Table 4.14 - The equation function (4.95) and (4.103) right member and (4.104) left member

T_{FG} [K]	[273 ÷ 2713, step: 10]
$f(T_{FG})$	$C_1(t_{FG}) \cdot t_{FG}^4 + C_2(t_{FG}) \cdot t_{FG}^3 + C_3(t_{FG}) \cdot t_{FG}^2 + C_3(t_{FG}) \cdot t_{FG}^1 + C_4(t_{FG}) \cdot t_{FG}^0 + C_5(t_{FG}) \cdot t_{FG}^{(-1)}$
Found?	IF (OR((AND($f(T_{FG}_i) < 0$; $f(T_{FG}_{i+1}) > 0$); (AND($f(T_{FG}_i) > 0$; $f(T_{FG}_{i+1}) > 0$))); T_{FG}_i ; "no")

Applying in this case the same relations (4.89) and (4.90), and considering both, the relation (4.95) and (4.103) as the right member and the relation (4.104) as the left member, of the same

relation (4.46), with the values from Table A4.28 in Annex 4, the corresponding results are suggested in the Figure 4.14 and indicated in Annex 4, the Table A4.29.

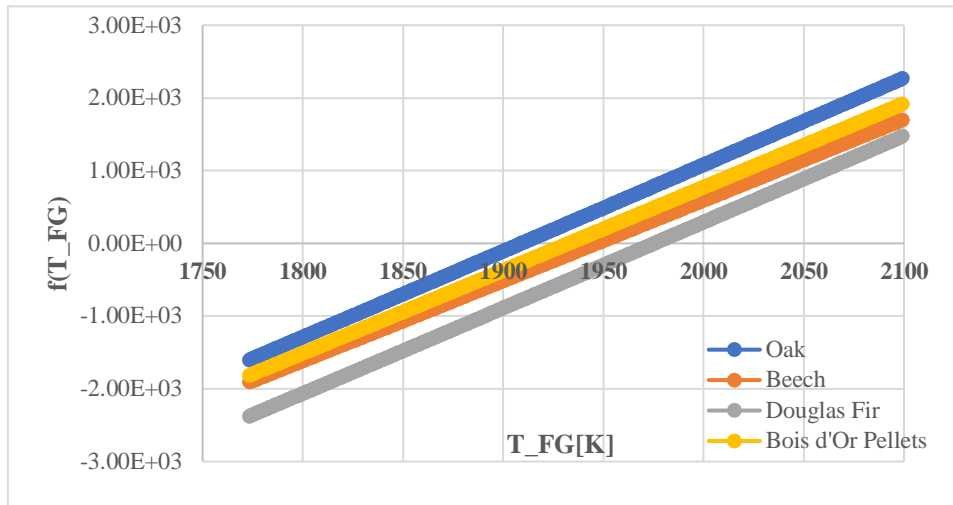


Figure 4.14 - Flue gas temperature results

After finding the temperature for which the function passes from negative to positive, thus intersecting the 0 axis, the temperatures inside the previously used 10K step interval can be tested to further refine the result, by reducing the step to 1, as shown in the Table 4.15.

Table 4.15 - Refining the result of the equation function (4.95) and (4.103) right member and (4.104) left member

T_{FG} [K]	$[T_{FG_{found}} \div T_{FG_{found}} + 10, \text{step: } 1]$
$f(T_{FG})$	$C_1(t_{FG}) \cdot t_{FG}^4 + C_2(t_{FG}) \cdot t_{FG}^3 + C_3(t_{FG}) \cdot t_{FG}^2 + C_3(t_{FG}) \cdot t_{FG}^1 + C_4(t_{FG}) \cdot t_{FG}^0 + C_5(t_{FG}) \cdot t_{FG}^{(-1)}$
Found?	$IF(OR((AND(f(T_{FG_i}) < 0; f(T_{FG_{i+1}}) > 0); (AND(f(T_{FG_i}) > 0; f(T_{FG_{i+1}}) > 0))))); T_{FG_i}; "no"$

The same function “Found?” applies to this interval, to find with more precision [1 K] the temperature for which the function passes from negative to positive results. The obtained refined results are suggested in the Figure 4.15 and are shown in the Annex 4, Table A4.30.

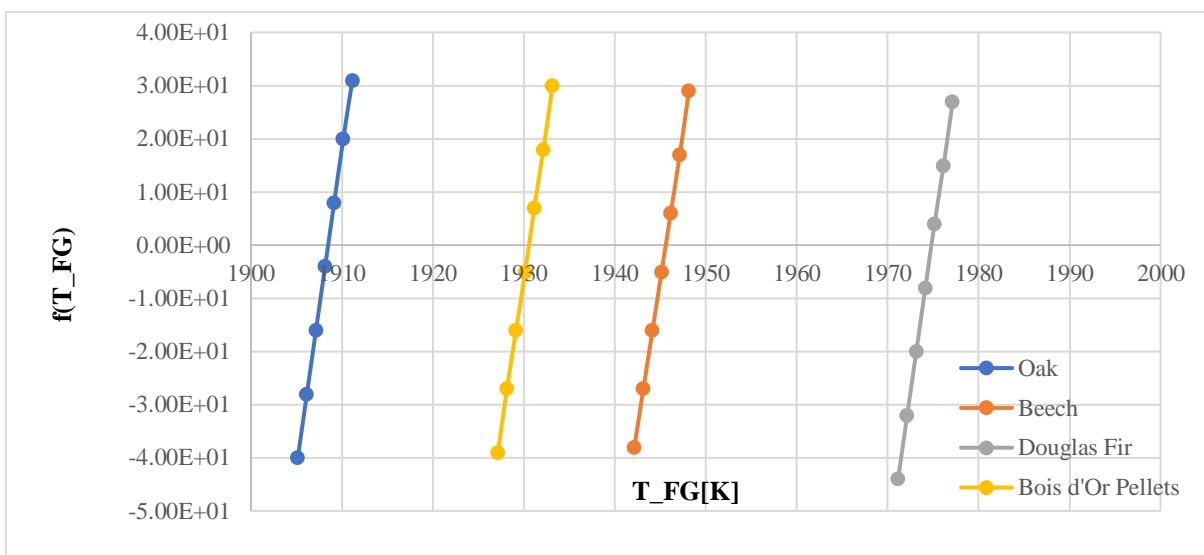


Figure 4.15 - Flue gas temperature refined results

A comparison of these results with those obtained by using MSOffice Excel SOLVER function is showed in Annex 4, the Table A4.31. It is to be remarked that the precision of FOUND? function results is affected by relative errors smaller than 0.035%.

4.3.4.4. Combustion adiabatic temperature, comparison of results

The results from Table A4.15, Table A4.24 and Table A4.31, all included in Annex 4, are compared in Table 4.16.

Table 4.16 - Comparison of results obtained for three different methods of calculation

Method used	Combustion Adiabatic Temperature					
	Method of Iterative Calculus		Gaskell Equation and Constant Coefficients		Shomate Howard Equation and JANAF Temperature - Dependent Coefficients	
	8 th Iteration		FOUND? [step: 0.01]		FOUND? [step: 1]	
Wooden Species	T [K]	ε_r (%)	[K]	ε_r (%)	[K]	ε_r (%)
Oak	1937.96	0.00	1911.79	1.350%	1908.15	1.538%
Beech	1929.01	0.00	1949.08	-1.040%	1945.15	-0.837%
Douglas Fir	1936.05	0.00	1977.79	-2.156%	1974.15	-1.968%
Bois d'Or Pellets	1902.30	0.00	1935.52	-1.746%	1930.15	-1.464%

Compared to the results obtained with the method of iterative calculus and considered reference, the results of Gaskell Equation with constant coefficients give relative errors varying in between -2.156 % and +1.350 %. By using the Shomate Howard Equation with JANAF temperature - dependent coefficients the relative errors varying in between -1.464 % and +1.538 %. In this second case, the relative error - spread is with 0.5% smaller than in the first case.

Given these remarks, the convergence of solutions obtained is excellent and all three methods are valid for further exploitation.

4.4. COMBUSTION POWER CALCULUS

A fuel mass flow rate of 2.8 kg/h is proposed, equal to that measured through experiments (configuration 12kW - F3) on the ÖkoFEN Pellematic Condens_E cogeneration unit at INSA Strasbourg. The parameters introduced are centralized in Table 4.17.

Table 4.17 - Parameters used for power calculus in combustion

Parameter	Input data	
	Symbol	Unit of measure
Fuel mass flow entering combustion	\dot{m}_{fuel}	kg/h
Air mass flow entering combustion	\dot{m}_{air}	kg/h
Flue gas flow exiting combustion	\dot{m}_{FG}	kW
Thermal power from air entering combustion	$P_{in,air}$	kW
Thermal power from flue gas exiting combustion	$P_{out,FG}$	kW
Thermal power losses of combustion	$P_{out,loss}$	kW
Thermal power from fuel entering combustion	$P_{in,fuel}$	kW

Since the parameters calculated until now all depend on the fuel mass (specific masses measured in kg/kg_{fuel}), it is accessible to calculate the air mass flow and the flue gas flow, as

well as the thermal powers entering and exiting the combustion process. The relations (4.106) and (4.107) describe the flows of air and flue gasses.

The specific masses are those calculated in Method 1, with the relation (4.73) for the specific mass of air, and with the relation (4.76) for the specific mass of flue gas.

The relation (4.108) describes the balance of thermal powers in combustion, while the relations (4.109) - (4.111) are used to determine the thermal powers entering and exiting combustion, in order to calculate the thermal power of flue gas resulted from the combustion process through the relation (4.112).

$$fm_{air} = fm_{fuel} \cdot m_{realwet,air} \quad (4.106)$$

$$fm_{FG} = fm_{fuel} \cdot m_{FG}^i \quad (4.107)$$

$$P_{in,fuel} + P_{in,air} = P_{out,FG} + P_{out,loss} \quad (4.108)$$

$$P_{in,fuel} = fm_{fuel} \cdot LHV_{fuel} \quad (4.109)$$

$$P_{in,air} = fm_{air} \cdot [T_{atm} \cdot cp_{air}(T_{atm}) - T_{ref} \cdot cp_{air}(T_{ref})] \quad (4.110)$$

$$P_{out,loss} = \eta_{comb, chamber} \cdot (P_{in,fuel} + P_{in,air}) \quad (4.111)$$

$$P_{out,FG} = P_{in,fuel} + P_{in,air} - P_{out,loss} \quad (4.112)$$

The values of the parameters used in the calculation of powers as well as the powers are centralized in Table 4.18.

Table 4.18 - Results of mass flows and powers entering and exiting the combustion process

Fuel		Air		Losses		Flue gas	
fm_{fuel}	kg/h	$fm_{air} (fm_{fuel})$	kg/h	$P_{out,loss}$	kW	fm_{FG}	kg/h
Oak	2.8	Oak	20.60	Oak	0.72	Oak	23.40
Beech	2.8	Beech	18.95	Beech	0.68	Beech	21.75
Douglas Fir	2.8	Douglas Fir	20.44	Douglas Fir	0.74	Douglas Fir	23.24
Bois d'Or Pellets	2.8	Bois d'Or Pellets	18.26	Bois d'Or Pellets	0.69	Bois d'Or Pellets	21.31
$P_{in,fuel}$	kW	$P_{in,air} (fm_{air})$	kW			$P_{out,FG}$	kW
Oak	14.43	Oak	0.03			Oak	13.74
Beech	13.58	Beech	0.03			Beech	12.93
Douglas Fir	14.67	Douglas Fir	0.03			Douglas Fir	13.97
Bois d'Or Pellets	13.83	Bois d'Or Pellets	0.03			Bois d'Or Pellets	13.17

4.5. STIRLING ENGINE KEY POINTS, POWER AND ENERGY CALCULUS

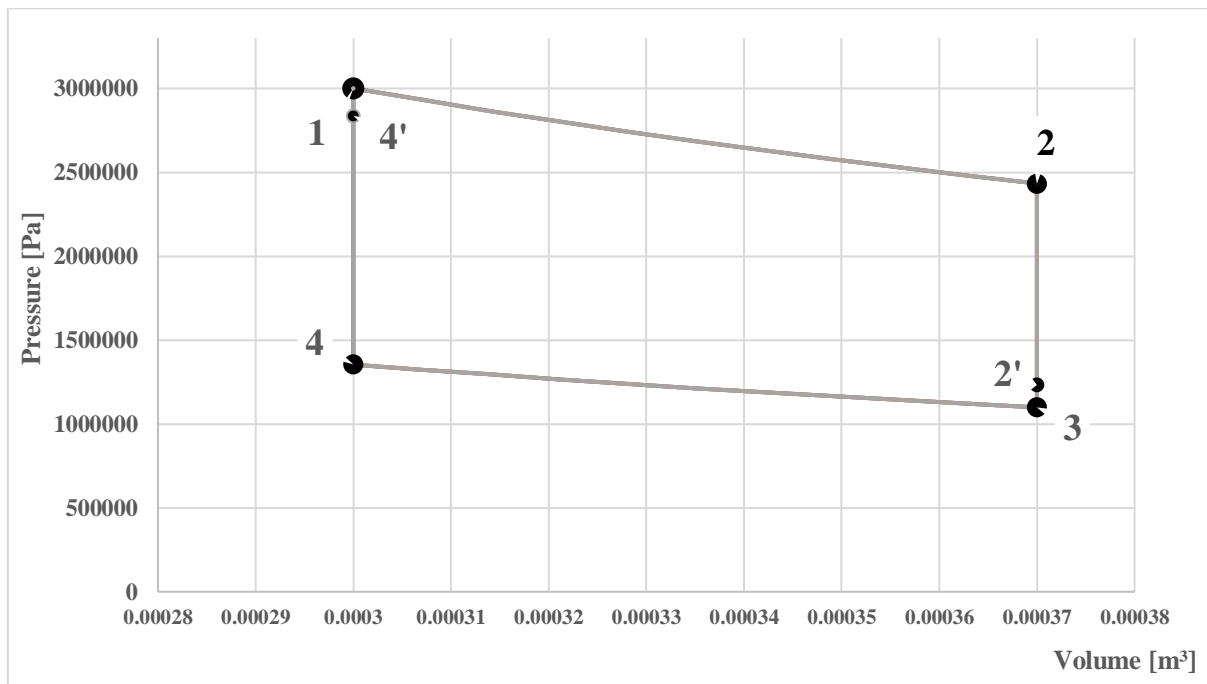
The Stirling engine has been modelled in accordance to the theoretical model of a Stirling engine, with formulas found in literature (Damirchi, 2016, Arashnia, 2015, Dobre, 2012). The input data is presented in Table 4.19.

The Stirling engine is modelled to have the same points of temperature, volume and pressure for all species and it is an important element of the installation, since power is more valuable than thermal power in terms of price. Therefore, it is ideal that it runs at full load for the same for all types of wood.

Table 4.19 - Input parameters and their values for the Stirling engine

Input data			
Parameter	Symbol	Value	Unit of measure
Piston swept volume	$V_{\max} - V_{\min}$	0.000070	m^3
Unswept volume	V_{\min}	0.000300	m^3
Charge pressure	p_{\max}	3000000	Pa
Hot side temperature	T_{hot}	693.15	K
Cold side temperature	T_{cold}	40	K
Frequency	f	50	Hz
Number of rotations per second	n	50	rot/s
Universal gas constant	RM	8.3143	$\text{kJ}/(\text{kmol}\cdot\text{K})$
Molar mass	M_{He}	4.003	g/mol
Gas constant of Helium	R_{He}	2.077017237	$\text{kJ}/(\text{kg}\cdot\text{K})$
Heat transfer coefficient at constant pressure of Helium at 300K	$c_{p\text{He}}(300\text{K})$	5.1926	$\text{kJ}/(\text{kg}\cdot\text{K})$
Heat transfer coefficient at constant volume of Helium at 300K	$c_{v\text{He}}(300\text{K})$	3.1156	$\text{kJ}/(\text{kg}\cdot\text{K})$
Compression ratio	ε	1.233333333	-
Stirling engine regenerator efficiency	$\eta_{\text{regenStir}}$	90.00%	%
Stirling engine internal efficiency	η_{intStir}	26.00%	%
Stirling engine mechanical efficiency	η_{mec}	90.00%	%
Stirling engine electrical efficiency	η_{elec}	98.00%	%
Power consumed by the electrical burner	P_{burner}	0.2	kW_{el}

There are 4 points of interest in the theoretical Stirling cycle, regarding volume, pressure and temperature (Figure 4. 16).


Figure 4.16 - Stirling Cycle pressure - Volume diagram

The 1-2'-2 and 3-4'-4 processes are considered isothermal, while 2-3 and 4-1 processes are considered isochore. Starting from the point of maximum pressure and temperature, point 1, and using the relations (4.113) – (4.126), the volume and pressure of each point of the cycle can be calculated.

$$R_{\text{He}} = \frac{RM}{M_{\text{He}}} \quad (4.113)$$

$$\varepsilon = \frac{V_{\text{max}}}{V_{\text{min}}} \quad (4.114)$$

$$V_1 = V_{4'} = V_4 = V_{\text{min}} \quad (4.115)$$

$$V_2 = V_{2'} = V_3 = V_{\text{max}} \quad (4.116)$$

$$T_1 = T_2 = T_{\text{hot}} \quad (4.117)$$

$$T_3 = T_4 = T_{\text{cold}} \quad (4.118)$$

$$p_1 = p_{\text{max}} \quad (4.119)$$

$$p_2 = p_1 \cdot \frac{V_1}{V_2} \quad (4.120)$$

$$p_3 = p_2 \cdot \frac{T_3}{T_2} \quad (4.121)$$

$$p_4 = p_3 \cdot \frac{T_3}{T_4} \quad (4.122)$$

$$T_{2'} = (1 - \eta_{\text{regenStir}}) \cdot (T_2 - T_3) + T_3 \quad (4.123)$$

$$p_{2'} = p_2 \cdot \frac{T_{2'}}{T_2} \quad (4.124)$$

$$T_{4'} = T_1 - (1 - \eta_{\text{regenStir}}) \cdot (T_1 - T_4) \quad (4.125)$$

$$p_{4'} = p_4 \cdot \frac{T_{4'}}{T_4} \quad (4.126)$$

The results of the 6 points are shown in Table 4.20. Since the same values apply for all species of fuel, the results are the same for all fuels.

Table 4.20 - Thermodynamic values of pressure and volume within the theoretical Stirling cycle

Parameter Unit	Pressure Pa	Volume m ³	Temperature K
Point 1	3000000	0.0003	693.15
Point 2	2432432	0.00037	693.15
Point 2'	1129933	0.00037	359.15
Point 3	985211	0.00037	313.15
Point 4	1215094	0.0003	313.15
Point 4'	2821509	0.0003	727.15

In order to calculate the powers and quantities of energy in the Stirling engine, the mass of Helium (m_{He}) inside the Stirling engine must be determined. The law of perfect gasses is applied in the relation (4.127).

$$m_{He} = \frac{P_1 \cdot V_1}{T_1 \cdot [R(He) \cdot 1000]} \quad (4.127)$$

Once the mass of Helium has been determined, all parameters which are necessary to calculate the thermal power and thermal energy are known. In this respect, the relations (4.128) - (4.137) are used:

$$P_{thSt_{in}} = m_{He} \cdot R(He) \cdot T_1 \cdot \ln\left(\frac{V_3}{V_4}\right) \cdot n \quad (4.128)$$

$$P_{thSt_{out}} = m_{He} \cdot R(He) \cdot T_3 \cdot \ln\left(\frac{V_3}{V_4}\right) \cdot N \quad (4.129)$$

$$Q_{St_{out}} = P_{thSt_{out}} \cdot \frac{3600}{2.89} \quad (4.130)$$

$$Q_{St_{in}} = P_{thSt_{in}} \cdot \frac{3600}{2.89} \quad (4.131)$$

$$P_{th} = P_{thSt_{in}} - P_{thSt_{out}} \quad (4.132)$$

$$P_{int} = \eta_{int_{st}} \cdot P_{th} \quad (4.133)$$

$$P_{mec} = \eta_{mec} \cdot P_{int} \quad (4.134)$$

$$P_{elec_{gross}} = \eta_{elec} \cdot P_{mec} \quad (4.135)$$

$$P_{elec_{net}} = P_{elec_{gross}} - P_{burner} \quad (4.136)$$

$$P_{thSt_{out_{real}}} = P_{thSt_{in}} - P_{int} \quad (4.137)$$

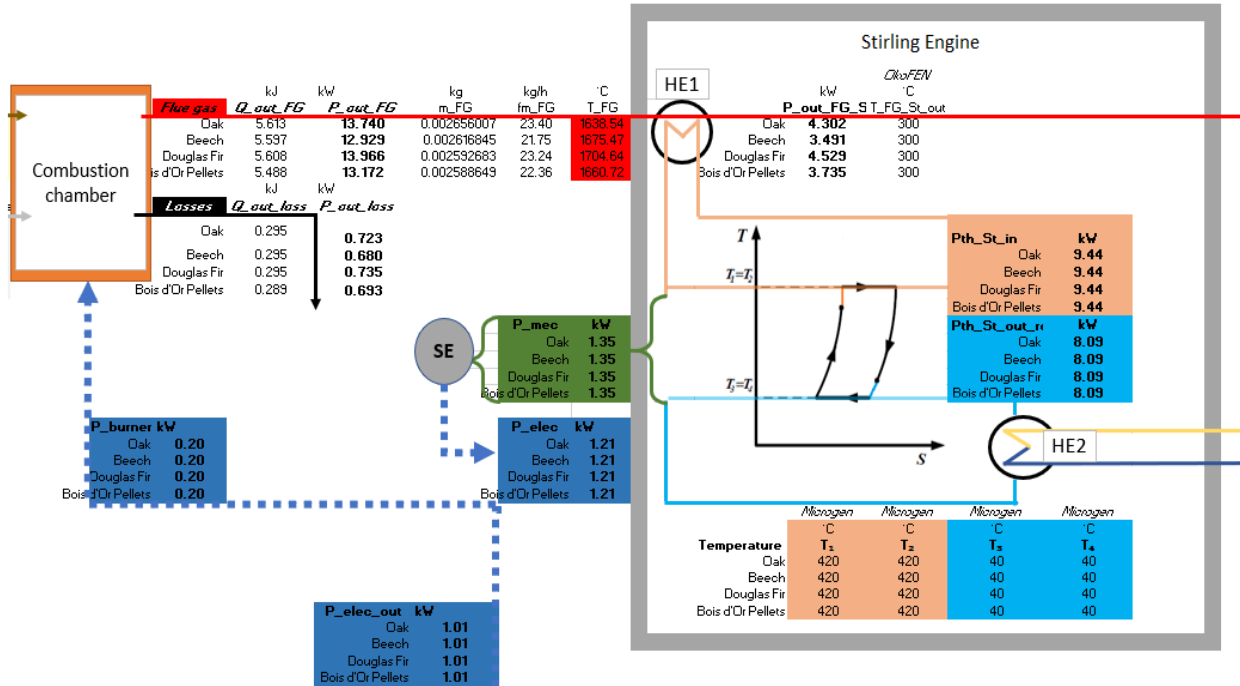


Figure 4.17 - Operational performances of the Stirling cycle related to the Combustion process

The calculated vales of all the Stirling cycle operational performances are suggested in the Figure 4.17 and indicated in the Table 4.21.

Table 4.21 - Ingoing and outgoing powers within the Stirling cycle

Parameter	Value	Unit	Parameter	Value	Unit
P_{thStin}	9.44	kW_{th}	$P_{elecgross}$	1.19	kW_{el}
$P_{thStout}$	4.26	kW_{th}	P_{burner}	0.20	kW_{el}
P_{int}	1.35	kW_{th}	$P_{elecnet}$	0.99	kW_{el}
P_{mec}	1.21	kW	$P_{thStoutreal}$	8.09	kW_{th}

4.6. USEFUL THERMAL POWER DELIVERED TO THE END USER

As seen in Figure 4.18, the thermal power input (P_{thStin}) and output ($P_{thStoutreal}$) of the Stirling cycle are known, as well as the power of the flue gasses transferring the heat to the Stirling engine (P_{outFG}) through heat exchanger HE1.

The water is initially heated through heat exchanger HE2 by the thermal power leaving the Stirling cycle ($P_{thStoutreal}$) and in a second phase, the thermal power of flue gasses that remains ($P_{outFGSt}$) is transferred through heat exchanger HE3 to the water fuelling the consumer before the flue gasses are exhausted into the atmosphere.

The power of the flue gasses which have passed through the heat exchanger of the Stirling engine is added to the thermal power output of the Stirling engine.

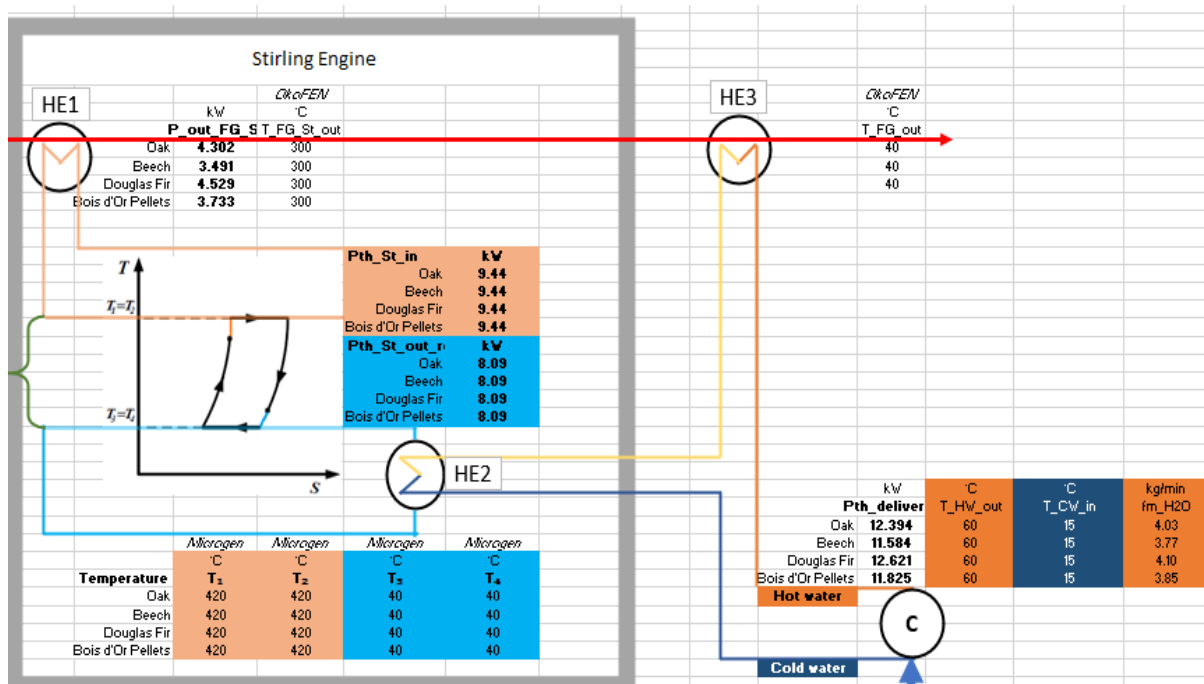


Figure 4.18 - The Stirling cycle outgoing heat recovery through the consumer's hot water delivery system

At INSA Strasbourg, where the experiment on the Bois d'Or Pellets was conducted, the cold water entering the heat exchanger HE2 had a temperature of 15 °C and the domestic hot water exiting the heat exchanger HE3 had a temperature of 60 °C. Consequently, these will be values imposed as norm for the mathematical model.

Table 4.22 - Parameters used for the calculation of the thermal power delivered to the end user

Temperature of cold water entering in the system	TCW_{in}	$^{\circ}C$
Temperature of hot water exiting from the system	THW_{out}	$^{\circ}C$
Thermal power delivered to the consumer	$P_{th_{delivered}}$	kW
Mass flow of water carrying heat to the consumer	fm_{H2O}	kg/min
Intermediate temperature of water after heat exchange with SE	T_{int}	$^{\circ}C$
Heat capacity at constant pressure of hot water	$c_p(T_{HW})$	$kJ/(kg \cdot K)$
Heat capacity at constant pressure of cold water	$c_p(T_{CW})$	$kJ/(kg \cdot K)$

The beforementioned powers are expressed with the relations (4.138) - (4.140).

$$P_{th_{delivered}} = P_{th_{St_{out\ real}}} + P_{out_{FGSt}} \quad (4.138)$$

$$P_{th_{delivered}} = fm_{H2O} \cdot [T_{HW} \cdot c_p(T_{HW}) - T_{CW} \cdot c_p(T_{CW})] \quad (4.139)$$

$$P_{th_{St_{out\ real}}} = fm_{H2O} \cdot [(T_{int} \cdot c_p(T_{int})) - T_{CW} \cdot c_p(T_{CW})] \quad (4.140)$$

By rearranging the relation (4.139), the mass flow of water carrying heat to the consumer can be determined by using the relation (4.141).

$$fm_{H2O} = \frac{P_{th_{delivered}}}{T_{HW} \cdot c_p(T_{HW}) - T_{CW} \cdot c_p(T_{CW})} \cdot 60 \quad (4.141)$$

In order to determine the heat capacities of the hot and cold water, a 2nd degree equation is formed by following the heat capacities of water from 0.01 $^{\circ}C$ to 100 $^{\circ}C$, after converting these values into Kelvin degrees, as seen in Annex 4, the Table A4.32.

By using formulas like those presented in Table 4.6, the 2nd degree equation is determined as shown in Table 4.23.

Table 4.23 - Excel functions used to determine the coefficients of the 2nd degree regressions for heat capacity

Coefficient	MS Office Excel Function
x^2	=@INDEX(LINEST(known Y's, known X's^{1,2}),1)
x^1	=INDEX(LINEST(known Y's, known X's^{1,2}),1,2)
x^0	=INDEX(LINEST(known Y's, known X's^{1,2}),1,3)

After calculating the heat coefficients for the hot water and cold water, the flow of water carrying heat to the consumer can be calculated through the relation (4.141).

The results are presented in Annex 4, the Table A4.33. The results of the flow are presented in both kg/min (as obtained at INSA Strasbourg) and kg/h for ease of further calculus.

It is interesting to know the intermediary temperature of water after having received heat from the Stirling Engine. This can be done by rearranging (4.140) into the relation (4.142) and then (4.143).

$$T_{int} \cdot c_p(T_{int}) = \frac{P_{th_{St_{out\ real}}}}{fm_{H2O}} + T_{CW} \cdot c_p(T_{CW}) \quad (4.142)$$

$$T_{int} = \frac{\frac{P_{th_{St_{out\ real}}}}{fm_{H2O}} + T_{CW} \cdot c_p(T_{CW})}{c_p(T_{int})} \quad (4.143)$$

$$P_{th_check_i} = fm_{H_2O} \cdot [T_{int_i} \cdot c_p(T_{int_i}) - T_{CW} \cdot c_p(T_{CW})] \quad (4.144)$$

The issue is that the intermediary temperature (T_{int}) and the heat capacity of water corresponding to this temperature $c_p(T_{int})$ are both unknown. This will be solved in a similar way as for the temperature of the flue gasses through the “Found?” function. A thermal power called “ P_{th_check} ” will be calculated through the relation (4.144), for values of T_{int} from 15°C to 60°C, after converting these values to degree Kelvin and calculating the heat transfer coefficient afferent to each value of T_{int} .

The aim of the “Found?” function is to once again verify if the difference between the “ P_{th_check} ” thermal power and the “ $P_{th_Stoutreal}$ ” thermal power passes from negative to positive, or vice-versa, signifying that the function has passed through the 0 point on the abscissa (Table 4.24).

Table 4.24 - Found function for the intermediary temperature of the water fuelling the consumer with thermal power

T_{int} [K]	[273 ÷ 2713, step: 10]
$f(T_{int})$	Difference = $P_{th_Stoutreal} - P_{th_check_i}$
Found?	IF (OR((AND($f(T_{int_i}) < 0$; $f(T_{int_{i+1}}) > 0$); (AND($f(T_{int_i}) > 0$; $f(T_{int_{i+1}}) > 0$))))); T_{int_i} ; "no")

In Annex 4, Table A4.34, the solutions of the “Found?” function for the species, with a step of 1 are indicated.

After finding the intermediary temperatures of water for each species, the results can furtherly be refined by dividing the step to 10 and restarting the search from the found value. This is done by selecting the maximum value from the “Found?” column when starting a new iteration. For the 0.1 step, the first value of T_{int} will be the maximum of the “Found?” values in the 1 step and for the 0.01 step, the first value of T_{int} will be the maximum of the “Found?” values in the 0.01 step. The results are presented in Annex 4, Table A4.35.

The found intermediary temperatures are shown in Table 4.25.

Table 4.25 - Intermediary hot water temperature values

T_{int}	°C	$c_p(T_{int})$	kJ/(kg·°C)
Oak	44.86	Oak	4.1789
Beech	46.88	Beech	4.1789
Douglas Fir	44.34	Douglas Fir	4.1790
Bois d'Or Pellets	46.25	Bois d'Or Pellets	4.1789

To verify that these values are correct, the relation (4.145) should be applied.

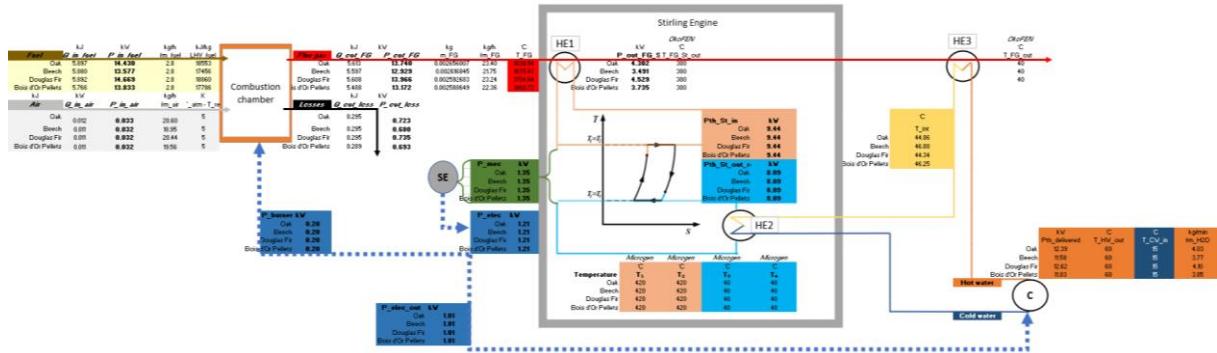
$$P_{out_FG_St} = fm_{H_2O} \cdot [T_{HW_out} \cdot c_p(T_{HW_out}) - T_{int} \cdot c_p(T_{HW_out})] \quad (4.145)$$

The results of the verification are shown in Table 4.26.

Table 4.26 - Balance test of the flue gas power exiting the Stirling cycle

Balance	$P_{out_FG_St} - fm_{H_2O} \cdot [T_{HW_out} \cdot c_p(T_{HW_out}) - T_{int} \cdot c_p(T_{HW_out})] = 0$ (?)
Oak	0.00 <input checked="" type="checkbox"/>
Beech	0.00 <input checked="" type="checkbox"/>
Douglas Fir	0.00 <input checked="" type="checkbox"/>
Bois d'Or Pellets	0.00 <input checked="" type="checkbox"/>

With several relevant values being found, an overview of the system in terms of powers is now available and it is shown in Figure 4.19.



- | | | | |
|---------------------|---|----------------------|---|
| $f_{m_{air}}$ | Mass flow of air entering combustion | $P_{out_{loss}}$ | Loss of thermal power in combustion |
| $f_{m_{FG}}$ | Mass flow of flue gas resulted after combustion | $P_{th_{delivered}}$ | Thermal power delivered to consumer |
| $f_{m_{fuel}}$ | Mass flow of fuel entering combustion | $P_{th_{stin}}$ | Thermal power entering in SE |
| $f_{m_{H_2O}}$ | Mass flow of water carrying heat to consumer | $P_{th_{stoutreal}}$ | Thermal power exiting the SE |
| LHV _{fuel} | Fuel Lower Heating Value | $Q_{in_{air}}$ | Heat of air entering combustion |
| m_{FG} | Specific mass of flow gas per kg of fuel | $Q_{in_{fuel}}$ | Heat of fuel entering combustion |
| P_{burner} | Power supplied to burner | $Q_{out_{FG}}$ | Heat of flue gas exiting combustion |
| $P_{electross}$ | Power produced by Stirling engine (SE) | $Q_{out_{loss}}$ | Heat losses of combustion |
| $P_{electnet}$ | Power delivered to user | $T_{atm} - T_{ref}$ | Difference of temperature of air |
| $P_{in_{air}}$ | Thermal power of air entered in combustion | TCW_{in} | Temperature of cold-water entering μCHP |
| $P_{in_{fuel}}$ | Thermal power of fuel entered in combustion | T_{FG} | Temperature of flow gas after combustion |
| P_{mec} | Mechanical power produced by the Stirling engine | TFG_{out} | Temperature of flow gas at the exit of μCHP |
| $P_{out_{FG}}$ | Thermal power carried by the flue gasses after combustion | TFG_{Stout} | Temperature of flow gas after HE with SE |
| $P_{out_{FGSt}}$ | Thermal power carried by the flue gasses after HE with SE | THW_{out} | Temperature of hot water exiting CHP |

Figure 4.19 - Overview of the μCHP system

4.7. COMPARISON BETWEEN DIFFERENT FUEL MOISTUERS AND AIR EXCESSES

It is necessary to see how the fuels behave in non - ideal cases. While the moisture of pellets is by DINplus standard, more exactly prEN 14961 (Alkangas, 2010, Heigl, 2009), inferior to 10%, if harvested directly from the forest and not treated, biomass can reach a 50% moisture. Configurations of 0%, 10%, 20%, 30%, 40% and 50% moisture (%W) have been mathematically tested. The air excess is used to facilitate a better combustion, towards forming less ash and char. Configurations of excess of air of 1.0, 1.5, 2, 2.5 and 3.0 have been tested. In total, 30 configurations have been tested and they are shown in Table 4.27.

Table 4.27 - The configurations of the biomass species studied

		Fuel moisture (%W _t)					
		0%	10%	20%	30%	40%	50%
Air excess (λ)	1.0	λ=1.0,	λ=1.0,	λ=1.0,	λ=1.0,	λ=1.0,	λ=1.0,
		W=0%	W=10%	W=20%	W=30%	W=40%	W=50%
	1.5	λ=1.5,	λ=1.5,	λ=1.5,	λ=1.5,	λ=1.5,	λ=1.5,
		W=0%	W=10%	W=20%	W=30%	W=40%	W=50%
	2.0	λ=2.0,	λ=2.0,	λ=2.0,	λ=2.0,	λ=2.0,	λ=2.0,
		W=0%	W=10%	W=20%	W=30%	W=40%	W=50%
	2.5	λ=2.5,	λ=2.5,	λ=2.5,	λ=2.5,	λ=2.5,	λ=2.5,
		W=0%	W=10%	W=20%	W=30%	W=40%	W=50%
	3.0	λ=3.0,	λ=3.0,	λ=3.0,	λ=3.0,	λ=3.0,	λ=3.0,
		W=0%	W=10%	W=20%	W=30%	W=40%	W=50%

These configurations are relevant to see how the system behaves when functioning with lower or higher qualities of the same composition of fuel. The same 4 species have been tested in these 30 configurations and the results will be presented in the following.

The adiabatic temperature of combustion obtained in literature (van Loo, 2008) by variation of the moisture of fuel and air excess entering combustion is shown in Figure 4.20.

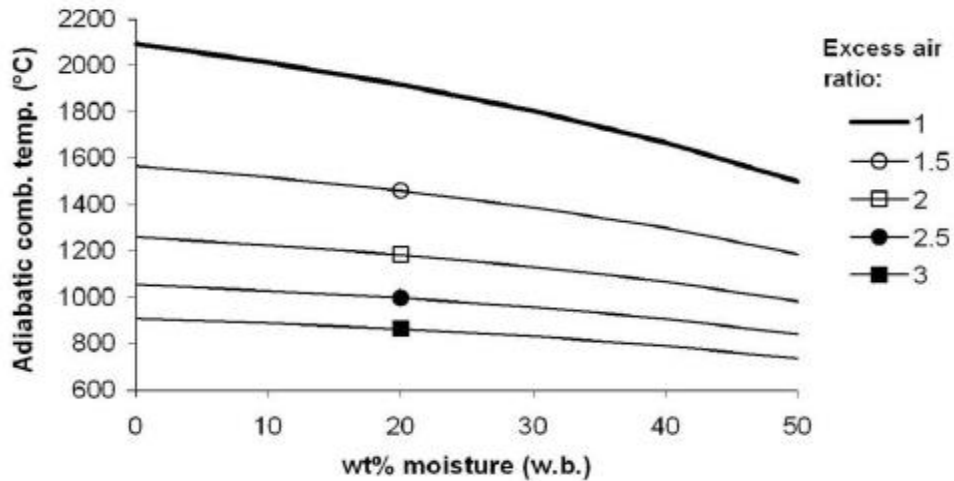


Figure 2.4 Adiabatic combustion temperature as a function of moisture content (w.b.) and excess air ratio for a continuous combustion process

Note: Fuel composition: 50wt% C, 6wt% H and 44wt% O, d.b.

Figure 4.20 - Adiabatic temperature of combustion found in literature (van Loo, 2008)

The results obtained by applying the algorithm described in this chapter are shown in Figure 4.21. The temperatures found in literature are slightly higher (maximum 200°C or 10% at 0 moisture and 1 excess air ratio) than those found in the current chapter.

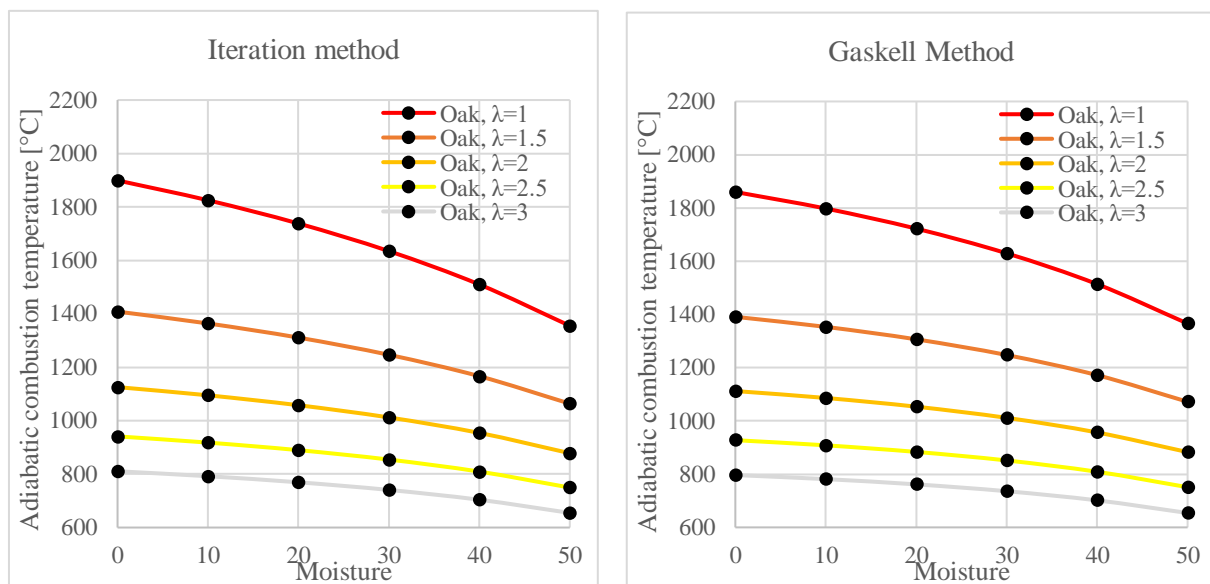


Figure 4.21 - Adiabatic combustion temperatures for the 4 species

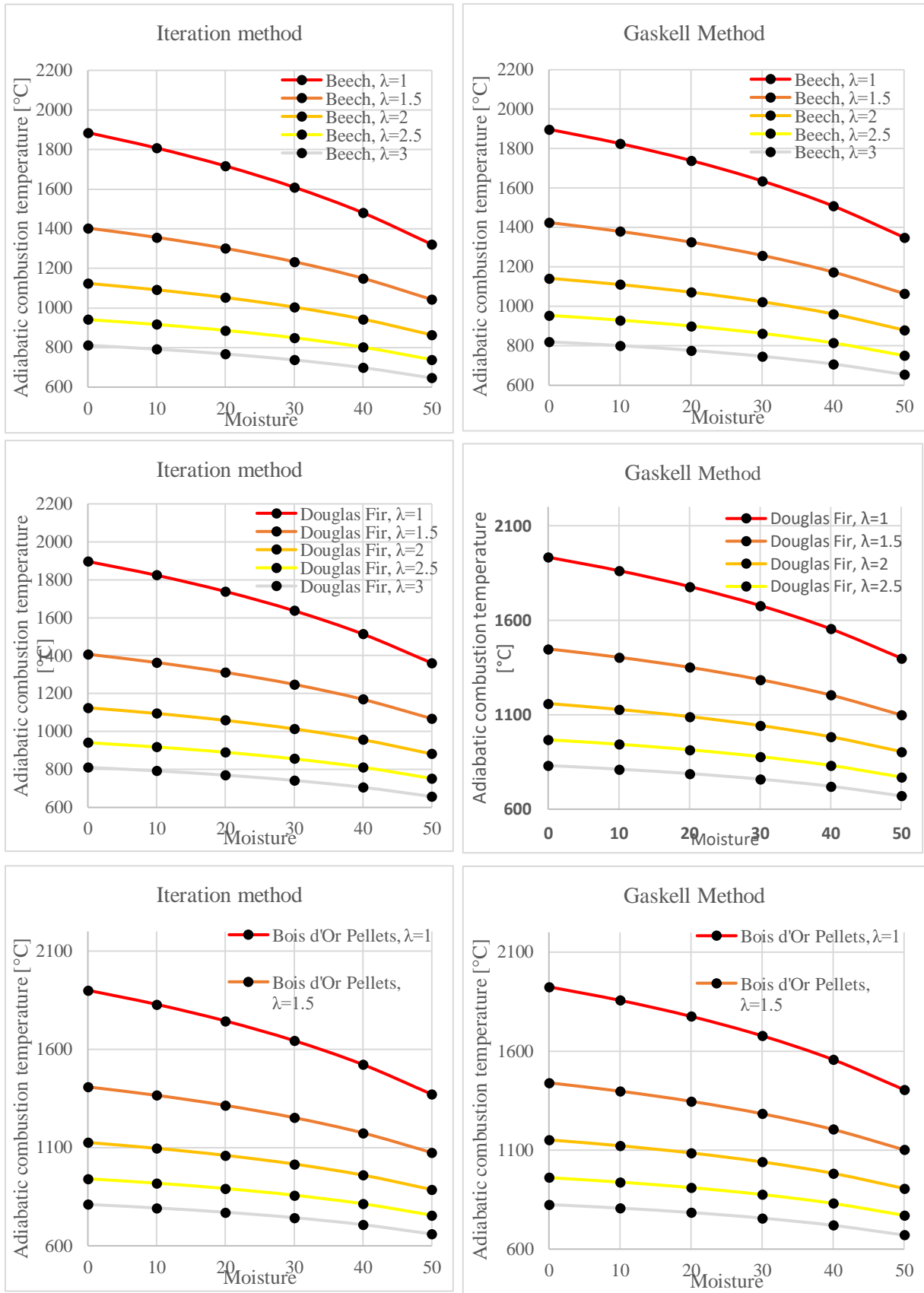


Figure 4.21 - Adiabatic combustion temperatures for the 4 species (continuation)

The results are presented in Annex 4, the Table A4.36.

The thermal power of the flue gas resulted from combustion (P_{FG}) is important for determining the functioning performance of the Stirling engine. The thermal power necessary for the Stirling to function at nominal load ($P_{th_{Stin}}$) has been calculated through the relation (4.129) and in Table 4.21 the value has been shown to be 9.44 kW_{el}.

Any value of the flue gas thermal power (P_{FG}) under the value of 9.44 kW_{el} will result in a partial load functioning of the Stirling engine, since not enough thermal power entering the engine is available to have a nominal load functioning, as shown in Figure 4.22 and in Annex 4, in the Table A4.38.

Consequently, because the cases in which the thermal power is insufficient for a nominal load functioning of the Stirling engine, an adjustment in the modelling of the Stirling engine had to be made. A new set of parameters was put into place, with conditional clauses. The parameters are shown in Table 4.28.

Table 4.28 - Partial load functioning of the Stirling engine input parameters

Parameter	Symbol	Unit of measure
Real thermal power entered in the Stirling engine	$P_{th_{Stinreal}}$	kW _{th}
Real thermal power exited from the Stirling engine in partial load	$P_{th_{StoutrealP}}$	kW _{th}
Real internal power of the Stirling engine	$P_{intreal}$	kW
Real mechanical power generated by the Stirling engine	$P_{mecreal}$	kW
Real power generated by the Stirling engine	$P_{elecreal}$	kW _{el}
Real power sent to the consumer	$P_{elecnetreal}$	kW _{el}

The relations corresponding to these parameters are (4.146) - (4.151).

$$P_{th_{Stinreal}} = \text{if}(P_{FG} > P_{th_{Stin}}, P_{th_{Stin}}, P_{FG}) \quad (4.146)$$

$$P_{intreal} = P_{th_{Stinreal}} - P_{th_{Stout}} \quad (4.147)$$

$$P_{mecreal} = \eta_{Stinternal} \cdot P_{intreal} \quad (4.148)$$

$$P_{th_{StoutrealP}} = P_{th_{Stinreal}} - P_{mecreal} \quad (4.149)$$

$$P_{elecgrossreal} = \eta_{mec} \cdot P_{mecreal} \quad (4.150)$$

$$P_{elecnetreal} = P_{elecgrossreal} - P_{burner} \quad (4.151)$$

The relation (4.146) describes an “IF” function in Excel, that means that if the $P_{th_{Stinreal}}$ has the value of $P_{th_{Stin}}$ equal to 9.44 kW_{th}, if the thermal power of the flue gas (P_{FG}) is superior to the necessary thermal power of the Stirling to function at nominal load ($P_{th_{Stin}}$).

If the thermal power of the flue gas is inferior to $P_{th_{Stin}}$, the value of the actual thermal power available for the Stirling ($P_{th_{Stinreal}}$) will have the value of the flue gas thermal power, considering that the entirety of this power goes in the Stirling engine.

Two new elements have been added in the mathematical model overview, showing the functioning of the engine at partial load. The added elements are highlighted with circles in Figure 4.24.

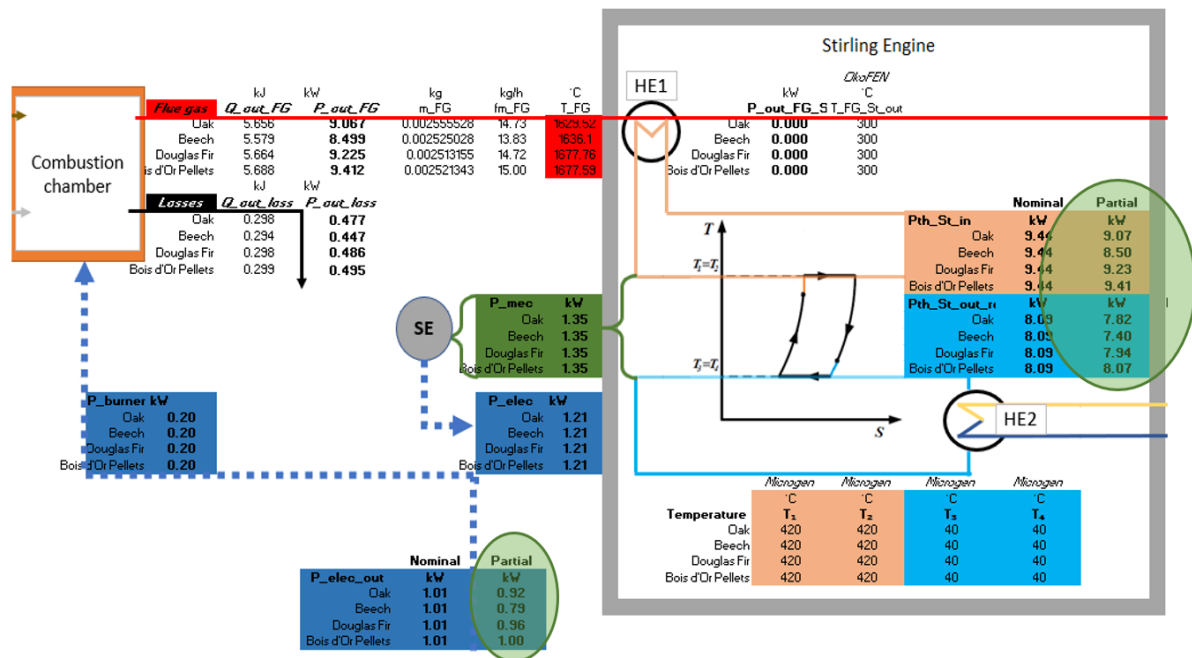


Figure 4.24 - The overview of the Stirling engine with the partial load functioning parameters

The values of the power sent to the consumer can be observed in Figure 4.25.

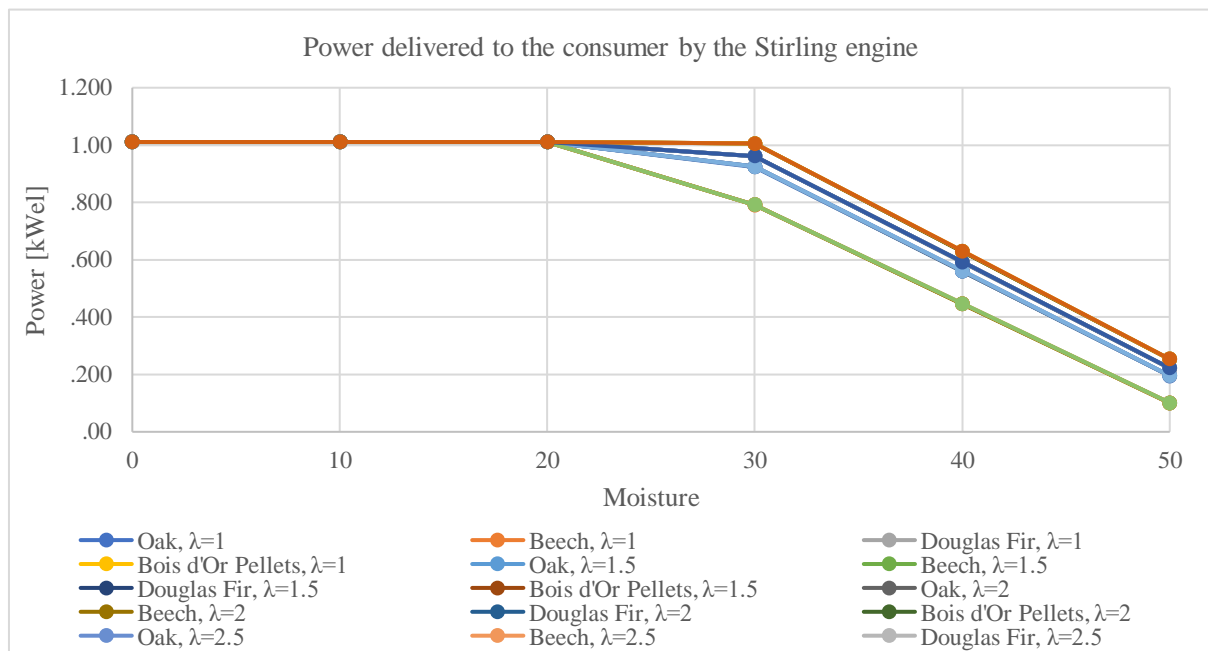


Figure 4.25 - The power delivered to the consumer by the Stirling engine

For all air excess configurations, the functioning of the Stirling engine starts to be in a partial load from a fuel moisture of 20%, with the exception of pellets which still offer a functioning at nominal load at a fuel moisture of 30%. The results are found in Annex 4, in the Table A4.39.

The thermal power delivered to the Stirling engine also affects the mass flow of water delivered to the consumer. Since a lower amount of power enters the Stirling engine in partial load, a lower power will exit it to heat up the domestic hot water.

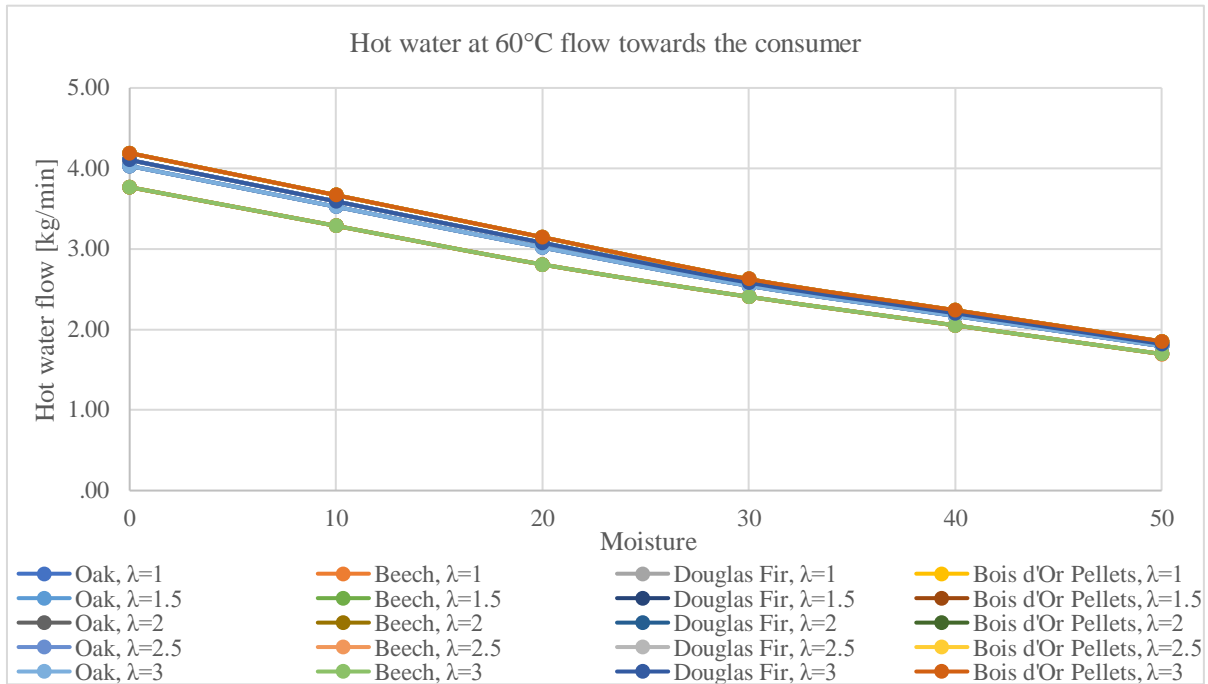


Figure 4.26 - The domestic hot water mass flow delivered to the consumer

The mass flow dependency of domestic hot water (heated from 15°C to 60°C) to the fuel moisture is shown in Figure 4.26 and the results are shown in Annex 4, in the Table A4.40. The thermal power delivered to the user is also strongly influenced by the fuel moisture.

It halves from fuel moisture 0% to 50%, as shown in Figure 4.27 and in Annex4, in the Table A4.41.

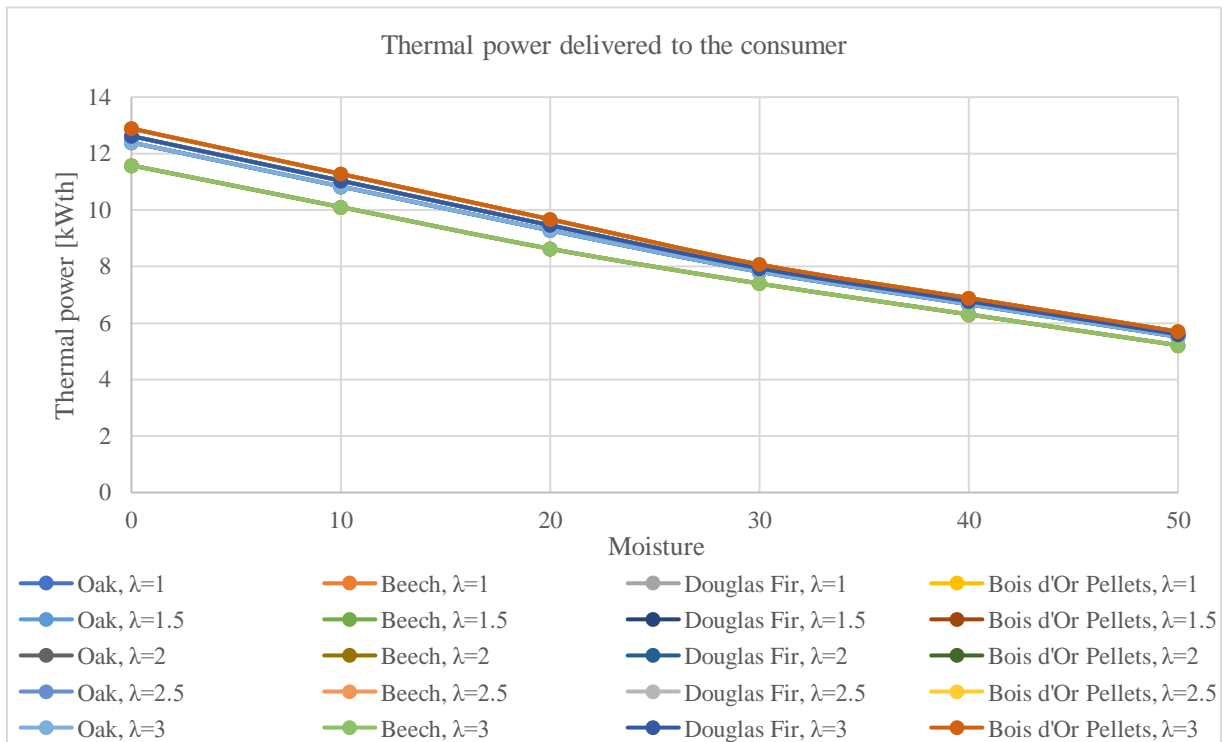


Figure 4.27 - Thermal power delivered to the consumer

4.8. COMPARISON OF EFFICIENCIES IN DIFFERENT CONFIGURATIONS ($\lambda=I, W=J$)

In terms of thermal efficiency, it can be first calculated by reporting the useful powers: thermal ($P_{th\text{delivered}}$) and power ($P_{elec\text{netreal}}$) to the power generated by the fuel (P_{fuel}) for each configuration, as shown in the relations (4.152) - (4.154). Secondly, it is necessary to report the useful powers of each configuration to the dry configuration of the same air excess, as shown in the relations (4.155) - (4.157).

$$\eta_{th}^{\lambda=i,w=j} = \frac{P_{th\text{delivered}}^{\lambda=i,w=j}}{P_{fuel}^{\lambda=i,w=j}} \quad (4.152)$$

$$\eta_{el}^{\lambda=i,w=j} = \frac{P_{elec\text{netreal}}^{\lambda=i,w=j}}{P_{fuel}^{\lambda=i,w=j}} \quad (4.153)$$

$$\eta_{total}^{\lambda=i,w=j} = \frac{P_{th\text{delivered}}^{\lambda=i,w=j} + P_{elec\text{netreal}}^{\lambda=i,w=j}}{P_{fuel}^{\lambda=i,w=j}} \quad (4.154)$$

$$\eta_{th\text{to dry}}^{\lambda=i,w=j} = \frac{P_{th\text{delivered}}^{\lambda=i,w=j}}{P_{fuel}^{\lambda=i,w=0}} \quad (4.155)$$

$$\eta_{el\text{to dry}}^{\lambda=i,w=j} = \frac{P_{elec\text{netreal}}^{\lambda=i,w=j}}{P_{fuel}^{\lambda=i,w=0}} \quad (4.156)$$

$$\eta_{total\text{to dry}}^{\lambda=i,w=j} = \frac{P_{th\text{delivered}}^{\lambda=i,w=j} + P_{elec\text{netreal}}^{\lambda=i,w=j}}{P_{fuel}^{\lambda=i,w=0}} \quad (4.157)$$

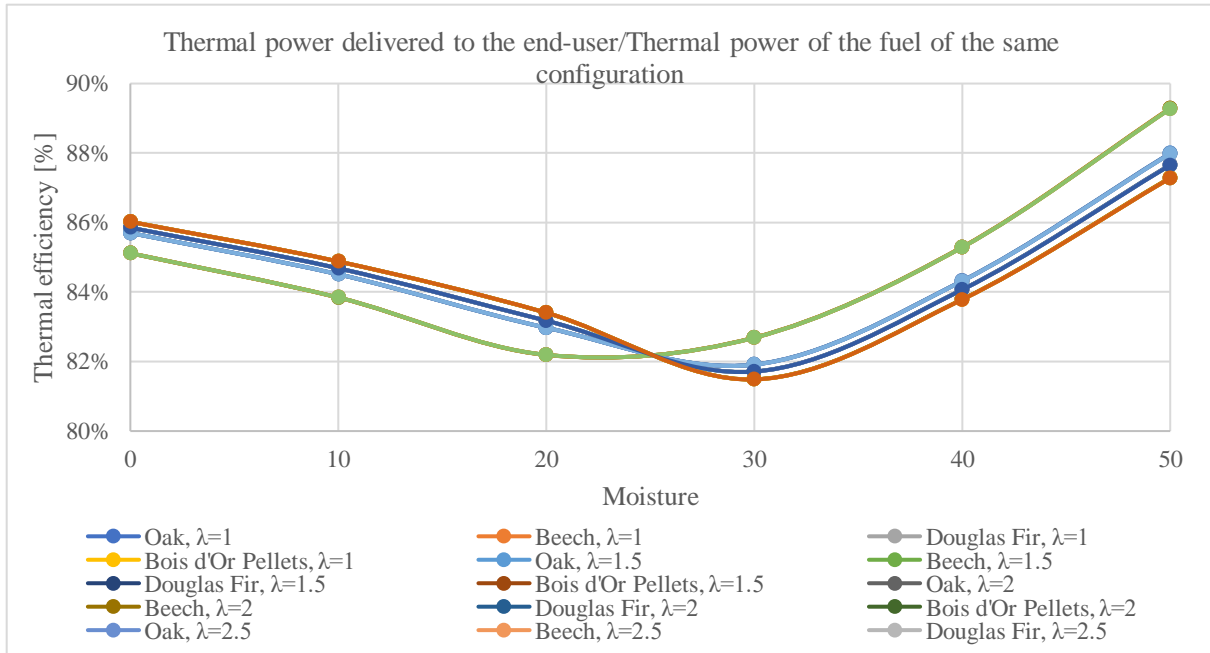


Figure 4.28 - Thermal efficiency of the μ CHP system, reported to the wet fuel thermal power of the same configuration

As shown in Figure 4.28, the thermal power efficiency calculated with the relation (4.152) decreases from 85%-86% in the 0% fuel moisture zone to 82%-83% in the 30% fuel moisture zone and increases to 87-89% in the 50% fuel moisture zone. The results are shown in Annex 4, in the Table A4.42. At first sight these results seem counter-intuitive, because the thermal power efficiency is supposed to constantly drop, as in non-CHP systems.

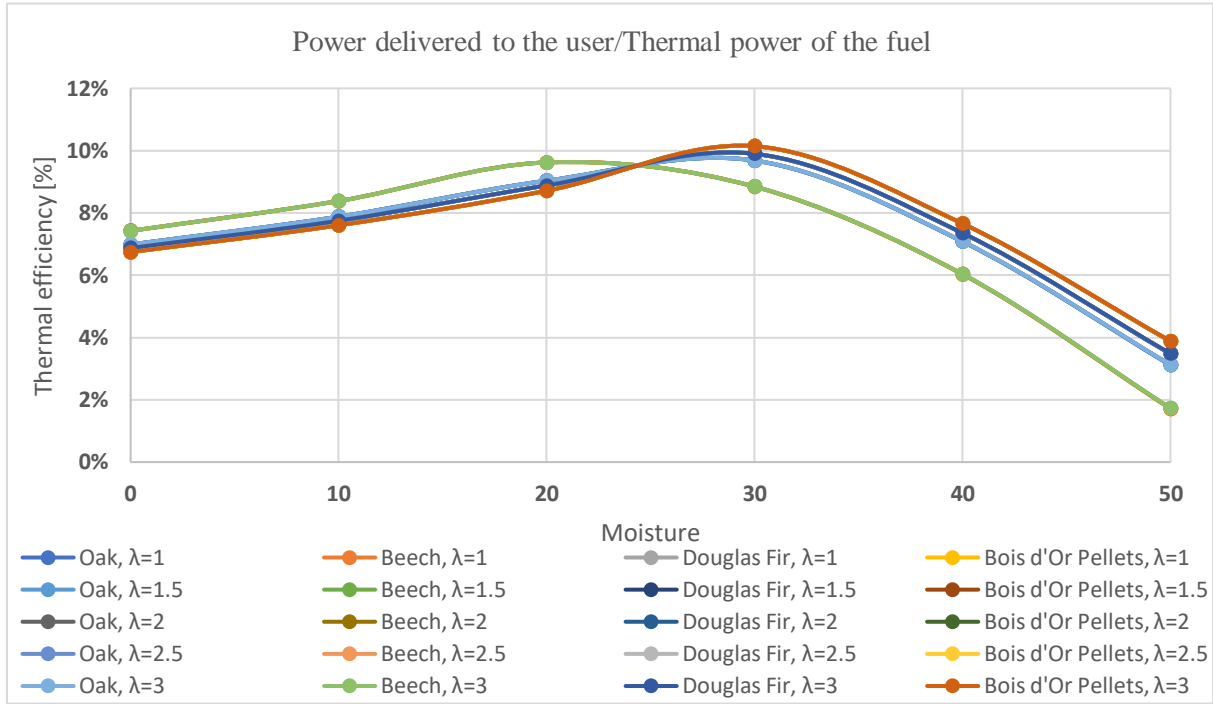


Figure 4.29 - Power efficiency reported to the fuel thermal power of the same configuration

Nevertheless, if the correlation of this data with the power efficiency data obtained through the relation (4.153) and shown in Figure 4.29, with results in Annex 4, in the Table A4.43 is made, it can be observed that the decrease in thermal efficiency is correlated with an increase in power efficiency, because a bigger ratio of the available fuel power is redirected to the Stirling engine thermal necessities.

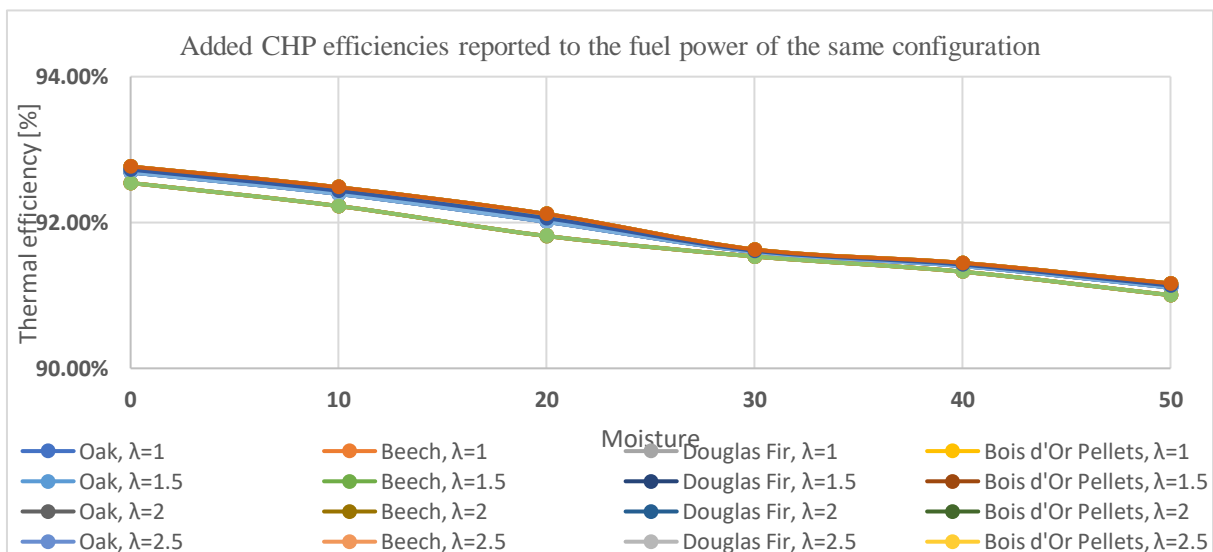


Figure 4.30 - Added μCHP efficiencies reported to the fuel power of the same configuration

While the absolute value of the thermal fuel power drops, the needs of the Stirling engine for nominal load functioning remain the same (9.44 kW_{th}).

Therefore, starting from the fuel moisture of 30%, more thermal power is produced from the lower values of fuel power, since the Stirling engine requirements are not met, and it functions in a partial load (Figure 4.30 and the Table A4.44 in Annex 4).

It is inaccurate to state that for a better thermal efficiency, fuel with moisture over 30% should be used, because these efficiencies have been calculated by dividing a decreasing absolute value of thermal power to a decreasing absolute value of fuel thermal power.

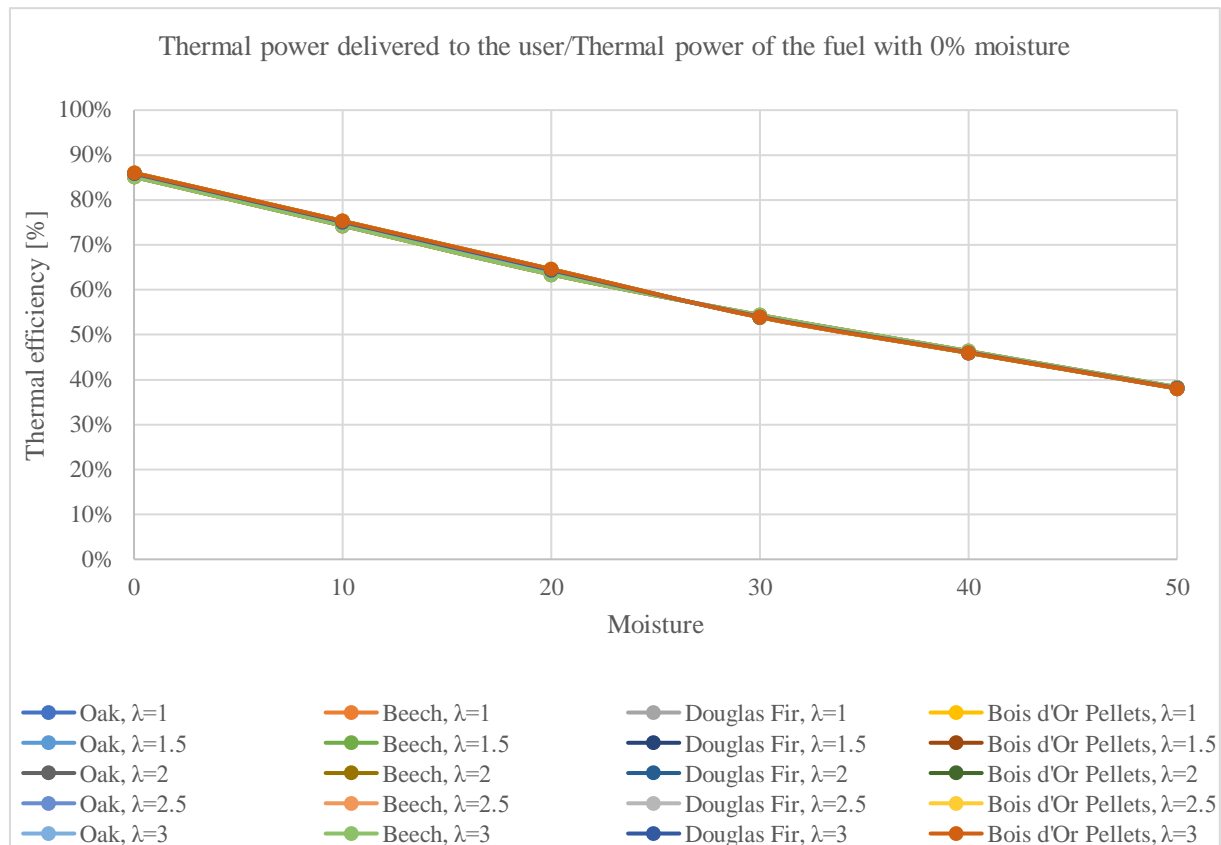


Figure 4.31 - The thermal efficiencies of the configurations reported to the fuel power with “zero” fuel moisture

The inability of the Stirling engine to function at nominal load is the main problem in over 30% fuel moisture cases since the whole purpose of a μCHP system is to ensure power primarily and then thermal power.

The total efficiency, calculated with the relation (4.154), is relevant to seeing how the system behaves in overall to the percentual raising of moisture levels of the fuel.

Still, a more interesting approach is to compare the performances obtained through wet fuels to the fuel power obtained by using a dry fuel, as shown in the relations (4.155) - (4.157).

By using the relations (4.155) - (4.157), the efficiency of the μCHP system reported to the ideal case of 0 fuel moisture for each air excess case can be determined.

The efficiency calculus using Equations η_1 to η_3 considered the thermal power generated by fuels with moisture, showing the efficiency of the μ CHP system itself, with the given fuel.

The relations (4.155) - (4.157) show the efficiency of the system regarding the deteriorating thermal quality of the fuel as the moisture percentage elevates.

In Figure 4.31 it can be observed that the thermal efficiency decreases in an almost linear way, from 85%-86% at a fuel moisture of 0% to 38% at a fuel moisture of 50%, more than halving its value. The results are shown in Annex 4, in the Table A4.45.

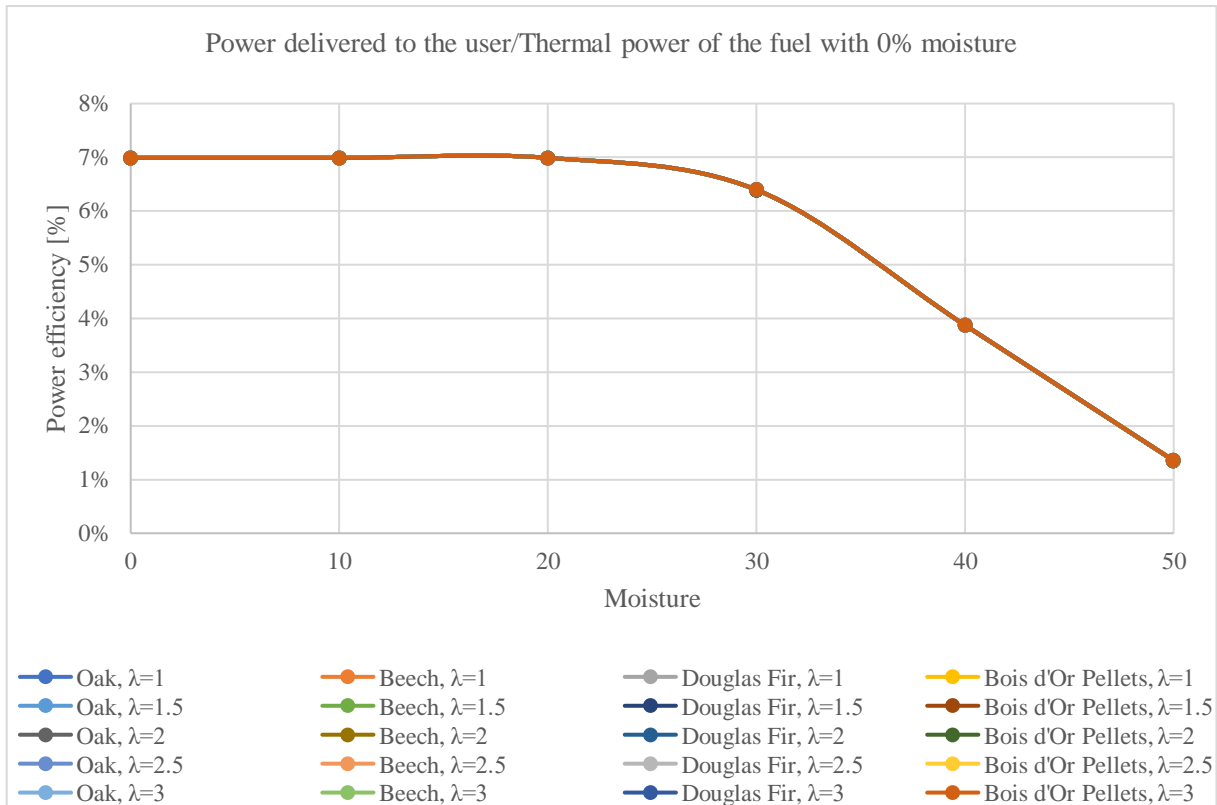


Figure 4.32 - The power efficiencies of the configurations reported to the fuel power with “zero” fuel moisture

In Figure 4.32 it is shown that the power efficiency is maintained constant until a fuel moisture of 20%, meaning that the Stirling engine still has enough thermal power from the flue gas to function at a nominal load.

The power efficiency is maintained to 7% until the 20% fuel moisture, then it drops to 1.35% at 30% fuel moisture, reducing itself by more than 5 times.

In the context where the power generated by the μ CHP would ensure a base load of power auto-consumption of the consumer, having a reduced power efficiency and a reduced power generation is counter-productive.

If the thermal power produced is not entirely needed as it is in the case of the summer season, the fuels used can be of a higher moisture, provided that their moisture does not negatively impact the μ CHP system.

The power efficiency results are shown in Annex 4, Table A4.46.

In Figure 4.33 the μ CHP total efficiency is shown and the corresponding results are showed in Annex 4, in the Table A4.47.

It decreases in an almost linear way, from 92% to 93% values at 0% fuel moisture, to 39% to 40% values at 50% fuel moisture, more than halving its value.

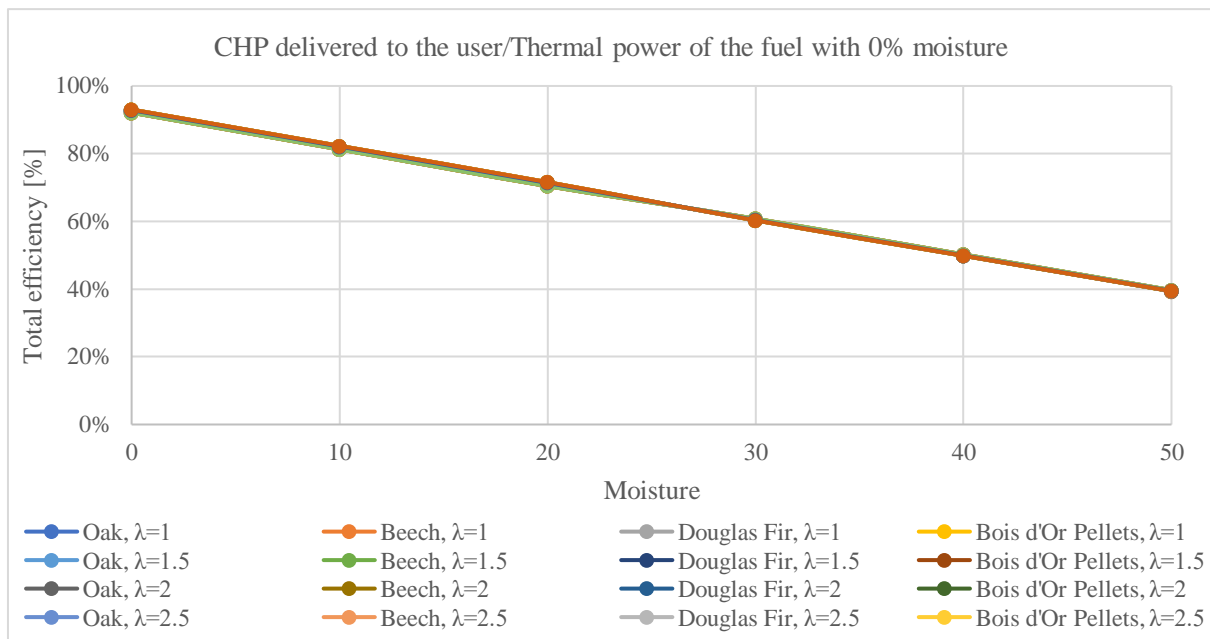


Figure 4.33 - The μ CHP efficiencies of the configurations reported to the fuel power with “zero” fuel moisture

4.9. CONCLUSIONS

In the mathematical model, different wood species have been fully described and the determination of the lower heating value in each case led to results in excellent agreement with those found in the literature. This is an important issue because the lower heating values were inputs for all subsequent calculus of the model.

When considering the energy balance in the combustion chamber, the mass of air which enters the combustion chamber and of heat inlet of air, respectively the flue gas real specific wet volume and the heat amount generated by the fuel entering the combustion chamber have been duly calculated.

For each wood specie, the adiabatic combustion temperature calculated by using volumes and enthalpies were obtained. Additionally, the adiabatic combustion temperature by using masses and enthalpies have been calculated.

Three different methods were deployed: use of air and flue gas masses calculation at wet ash free state, use of Gaskell equation, and use of Howard Shomate Equation and JANAF coefficients. The comparison of results has showed an excellent agreement between the Combustion adiabatic temperature calculated values.

Combustion power calculus to determine the thermal powers entering and exiting combustion and the thermal power of flue gas resulted from the combustion process have been performed.

In terms of Stirling Engine key points, power and energy calculus, the Stirling engine has been modelled in accordance to the theoretical model of a Stirling engine, based on formulas found in literature.

The Stirling engine model had the same points of temperature, volume and pressure for all species and it is an important element of the installation, since power is more valuable than thermal power in terms of price. Therefore, it was found as ideal that it runs at full load for the same for all types of wood. All the Stirling cycle operational performances were carried out.

In the mathematical model has been also considered that the useful thermal power delivered to the end user should be calculated based on the thermal power input and output of the Stirling cycle, which are known, as well as the power of the flue gasses transferring the heat to the Stirling engine.

The water is initially heated by the thermal power leaving the Stirling cycle and, in a second phase, the thermal power of flue gasses that remains is transferred to the water fuelling the consumer before the flue gasses are exhausted into the atmosphere.

For all air excess configurations, it was observed that the functioning of the Stirling engine and the power generation starts to be in a partial load from a maximum limit, which smaller that in the case of pellets which still keep a functioning at nominal load at a greater fuel moisture.

For different fuel moistures has revealed the mass flow dependency of domestic hot water to the fuel moisture and that the thermal power delivered to the user is also strongly influenced by the fuel moisture.

The comparison of efficiencies in different configurations ($\lambda=i$, $w=j$) has pointed out that the efficiencies describing the overall performances of the solid biomass micro-cogeneration unit with Stirling motor are appropriate for a dry fuel in order to get the best useful power outputs.

The efficiencies describing the overall performances of the solid biomass micro-cogeneration unit with Stirling motor aim to show that using a dry fuel is recommended for the best useful power outputs.

If thermal power is not entirely needed, the fuel may have a moisture of up to 20% for the Stirling engine to function at nominal load.

The beforementioned case is intuitively the one of summer season, where the thermal energy need is lower than that of the winter season.

It is therefore crucial to use dry fuel in the cold seasons, to obtain the maximum thermal power available, provided that the system has not been over-dimensioned for the consumer home.

If it is the case, lower quality fuels in terms of moisture can be used, because their thermal output will not create a surplus of thermal power.

The current chapter concludes that a study of the consumer needs is necessary, to better determine the fit of fuel quality to the μ CHP system in function of the consumer's necessities, work which will be done in the following chapter.

CHAPTER 5

MATHEMATICAL MODEL FOR THE SIMULATION OF TRANSIENT REGIMES

5.1. TESTS FOR TRANSIENT REGIMES

In order to assess the behaviour of the micro-cogeneration unit in various transient regimes of operation, 32 laboratory tests were performed. The micro-cogeneration unit, consisting in a condensing boiler and a Stirling engine, produces electricity and / or heat, according to the simulated transient regime. It has been considered that:

- for 22 out of 32 tests, the production of electrical energy has a longer duration than that of the production of thermal energy;
- for 6 out of 32 tests, the production of electrical energy started earlier than the production of thermal energy but stopped more quickly, so that in the end the cogeneration unit produced exclusively thermal energy;
- for 3 out of 32 tests, the production of thermal energy started earlier than the production of electrical energy, but stopped faster, so that at the end of the cogeneration unit produced exclusively electrical energy;
- for 1 out of 32 test, the production of thermal energy lasted longer than that of the production of electrical energy.

Most of the measurements done were only affected by the errors of the equipment used, adhering to their class of precision. The exception to the above consideration is the manner of measuring the fuel consumption, which represented a major source of incertitude.

5.2. MATHEMATICAL MODEL FOR TRANSIENT REGIMES

5.2.1. Introduction

The fuel mass flow was determined as described in Chapter 3 - Experimental study on the biomass micro-cogeneration unit with a Stirling engine, by measuring the weight of the entire μ CHP unit, since the fuel reservoir was placed inside the machine.

During the starting phase of the firing process, an amount of thermal agent (water) would also enter in the machines' circuits, leading to uncertainties in the weighing. In Table 5.1 the stages of the experimental studies are described.

Table 5.1 - The 5 stages of the experimental study

Stage	Description
1. Boot	combustion process has started
2. Start	thermal power evacuation process has started
3. Constant	thermal power production is constant
4. Stop	thermal power production is stopping
5. End	thermal power production ended

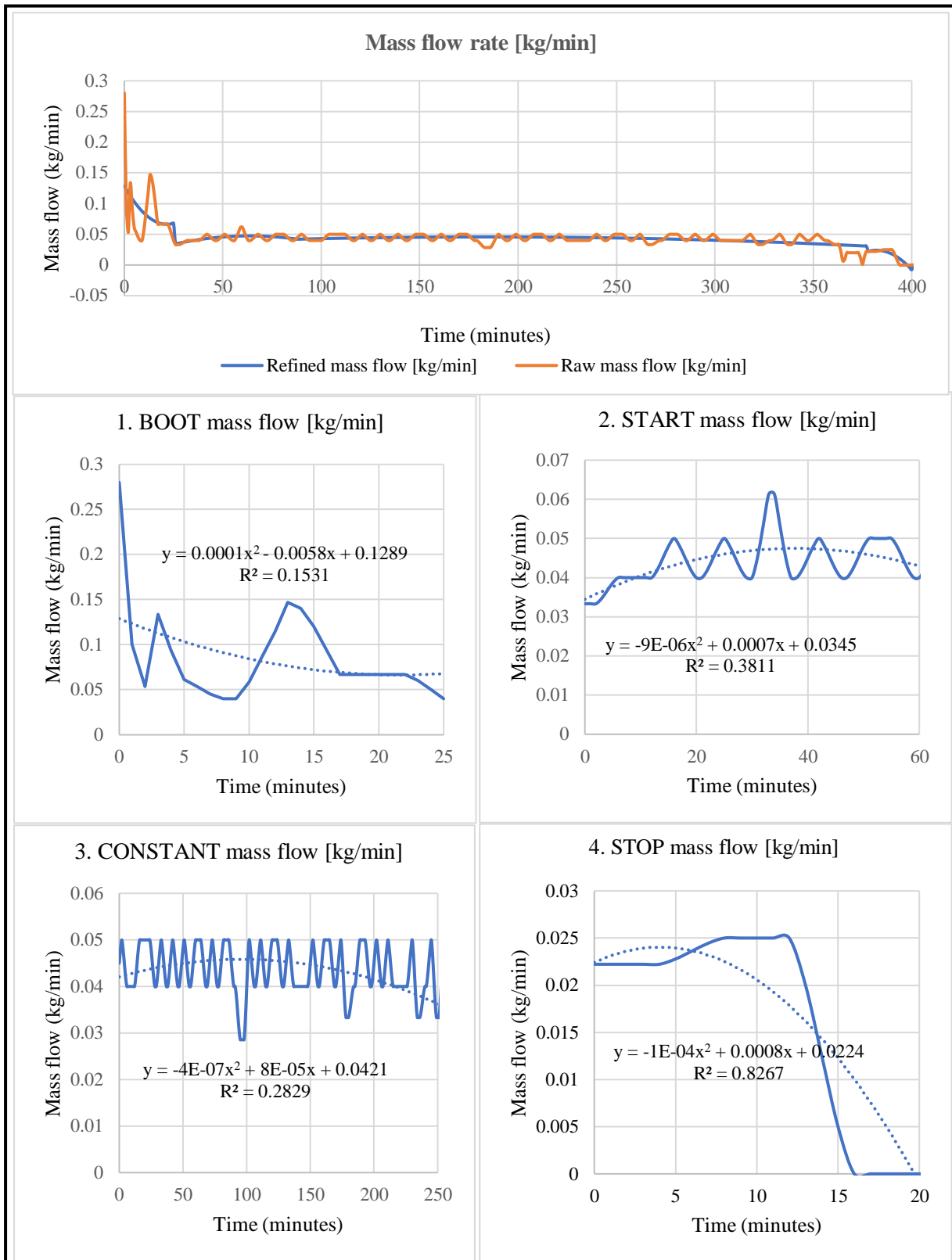


Figure 5.1 - Raw and refined mass flow recorded during an experiment

Due to a low correlation between the functions found (Figure 5.1) and the measured data of the fuel mass flow, a transitory mathematical model of the fuel mass flow was found to be necessary. The model was applied to 32 tests conducted in the iCube laboratory “Climatherm”. There are

showed the division of the fuel mass flow into 4 different functions based on the phases of the micro-cogeneration unit: “1. Boot”, “2. Start”, “3. Constant” and “4. Stop”. In the “End” phase, the fuel mass flow is null. The regression was calculated for each of these 4 functions using relation (5.1).

$$R = \frac{n[\sum_{i=1}^{n=t_{\max}}(x_i \cdot y_i) - \sum_{i=1}^{n=t_{\max}} x_i \cdot \sum_{i=1}^{n=t_{\max}} y_i]}{\sqrt{[n \cdot \sum_{i=1}^{n=t_{\max}} x_i^2 - (\sum_{i=1}^{n=t_{\max}} x_i)^2] \cdot [n \cdot \sum_{i=1}^{n=t_{\max}} y_i^2 - (\sum_{i=1}^{n=t_{\max}} y_i)^2]}} \quad (5.1)$$

Table 5.2 - Parameters used in determining the accuracy of the fuel mass flow function

Parameter	Notation	Unit of measurement
Time in the "i" minute	t_i	minute
Fuel mass flow	$y_i = fm_i$	kg/minute

The model was applied to 32 tests conducted in the iCube laboratory “Climatherm”. The simulations of transient regimes have showed that the uncertainty related to the consumption of fuel in the form of wood pellets is significant.

Considering the above, the mathematical model used was that of an inverse algorithm, in which for each of the 32 tests the following were considered:

- the input data considered was the production of power, the production of thermal power, the temperatures measured by the sensors inside the micro-cogeneration unit, on the path of the flue gas, from the combustion chamber to the exhaust, as well as different points of the circuit connecting the unit to the consumer;
- the calculated output was the corresponding consumption of fuel, under the form of wooden pellets.

The difficulties linked to the nonlinearities induced by the variation of different physical properties, in accordance to temperature (namely the specific heat of at constant pressure of the combustion air and the components of the flue gas and the specific heat of the agent - water), used in simulation to determine the enthalpies, were overcome using the Gauss - Seidel method (Brătianu, 1998).

The Gauss-Seidel method is an improved form of the Jacobi method, also known as the successive displacement method.

5.2.2. The power generation simulation

5.2.2.1. Stirling cycle calculus

The Stirling cycle calculus was done to determine the consumption of fuel under the form of wooden pellets, for power production.

In all tests, the calculus was done considering a cycle with partial heat recovery, considering the heat transfer at a finite difference of temperature at the hot source and losses of pressure due to the finite process speed and friction within the Stirling engine (Dobre, 2012), the efficiency being calculated with relation (5.2).

The parameters centralized in Table 5.3.

Table 5.3 - Parameters used in the power generation simulation

Parameter	Notation and value	Source
Expansion volume	$V_3 = 37 \text{ cm}^3$	Hypothesis
Compression volume	$V_4 = 30 \text{ cm}^3$	Hypothesis
Compression ratio	$\varepsilon = \frac{V_3}{V_4} = 1.2333$	Calculus
Hot head Stirling engine temperature	$T_1 = T_{\text{inlet}}^{\text{Stir}}$	μ CHP measurement
Cold head Stirling engine temperature	T_4	μ CHP measurement
Hot source temperature	T_H	μ CHP measurement
Cold source temperature	$T_C = T_4$	Hypothesis
Regeneration efficiency	$\eta_{\text{reg}} = 0.99$	Hypothesis
Regeneration losses	$X = 1 - \eta_{\text{reg}} = 0.01$	Calculus
Adiabatic exponent of Helium	$k = 1.6666$	Hypothesis
Ratio of the μ CHP internal power consumption	$\varepsilon_{\text{SI}} = 0.1$	Hypothesis
Mechanical efficiency	$\eta_m = 0.99$	Hypothesis
Generator efficiency	$\eta_g = 0.99$	Hypothesis
Internal irreversibility efficiency	$\eta_{\text{II,ir}}$	Calculus
Partial heat regeneration efficiency	$\eta_{\text{II,ir ext } \Delta T}$	Calculus
Finite temperature difference efficiency	$\eta_{\text{II,ir int x}}$	Calculus
Pressure loss efficiency	$\eta_{\text{II,ir int } \Delta p} = 0.95$	Hypothesis
Flue gas enthalpy entering the Stirling engine	$H_{\text{inlet}}^{\text{ST}}$	Calculus
Minutely heat entering the Stirling engine	$Q_{\text{inlet}}^{\text{Stir}}$	Calculus
Thermal power entering the Stirling engine	$p_{\text{inlet}}^{\text{Stir}}$	Calculus
Thermal power exiting the Stirling engine	$p_{\text{outlet}}^{\text{Stir}}$	Calculus
Thermal power used by the Stirling engine	$p_{\text{intern}}^{\text{Stir}}$	Calculus
Fuel mass flow reversly calculated from power	m_{fuel}	Hypothesis
Calculated fuel mass flow	m_{fuel}	Calculus
Measured power	$p_{\text{electric}}^{\text{measured}}$	μ CHP measurement
Calculated power	$p_{\text{electric}}^{\text{calculated}}$	Calculus

$$\eta_{\text{II,ir}} = \eta_{\text{II,ir ext } \Delta T} \cdot \eta_{\text{II,ir int x}} \cdot \eta_{\text{II,ir int } \Delta p} \quad (5.2)$$

In a partial heat recovery cycle (Figure 5.2), the internal irreversibility's efficiency (Dobre, 2012) is described with relation (5.3).

$$\eta_{\text{II,ir int x}} = \frac{1}{1 + \frac{X}{(k-1) \cdot \ln \varepsilon} \cdot \eta_{\text{II,ir ext } \Delta T}} \quad (5.3)$$

In Stirling cycles that consider the heat transfer from the hot source a finite difference (Dobre, 2012), the hot source temperature is calculated with relation (5.4) and the equivalent theoretical Carnot efficiency is calculated with relation (5.5).

$$T_H = \frac{T_1^2}{T_4} \quad (5.4)$$

$$\eta_{\text{II,ir ext } \Delta T} = 1 - \sqrt{\frac{T_C}{T_H}} \quad (5.5)$$

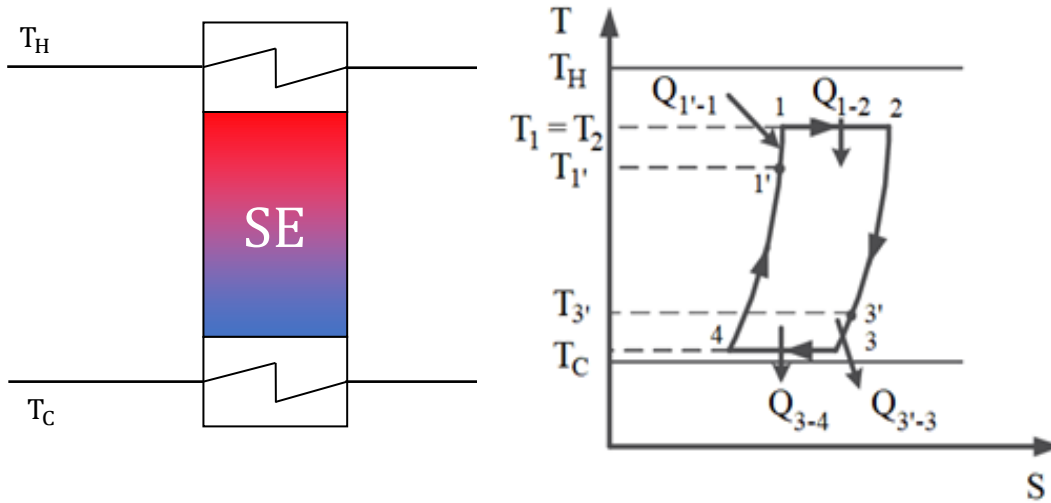


Figure 5.2 - Stirling engine and Stirling cycle temperature - entropy diagram

The internal irreversibility efficiency caused by pressure losses due to the finite speed of the process and to the friction inside the Stirling engine ($\eta_{II,ir \text{ int } \Delta p}$) was presumed to be 95%, due to the lack of information which could have led to its calculation.

The calculus of the Stirling engine power afferent to the micro-cogeneration unit was done using relation (5.6).

$$P_{\text{electric}}^{\text{calculated}} = \eta_{II,ir} \cdot (1 - \varepsilon_{SI}) \cdot \eta_m \cdot \eta_g \cdot P_{\text{inlet}}^{\text{Stir}} \quad (5.6)$$

5.2.2.2. Thermal power delivered to the Stirling hot source and Equivalent Inlet Enthalpy calculation

Using the measured temperature values at the Stirling hot head and the sum of the products of the masses and specific heats at constant pressure depending on temperature for all components of the flue gas, the enthalpy values are calculated for each of the beforementioned measured values, as shown in relation (5.7).

$$H_{\text{inlet}}^{\text{Stir}}(T_{\text{inlet}}^{\text{Stir}}) \left[\frac{\text{kJ}}{\text{kg}_{\text{fuel}}} \right] = \sum_i [m_i \cdot c_i(T_{\text{inlet}}^{\text{Stir}})] \cdot T_{\text{inlet}}^{\text{Stir}} \quad (5.7)$$

To simulate a distribution in time of the fuel consumption, the minutely heat transfer is calculated through relation (5.8), being converted in thermal power through relation (5.9).

$$Q_{\text{inlet}}^{\text{Stir}} \left[\frac{\text{kJ}}{\text{min}} \right] = m_{\text{fuel}} \cdot H_{\text{inlet}}^{\text{Stir}}(T_{\text{inlet}}^{\text{Stir}}) \quad (5.8)$$

$$P_{\text{inlet}}^{\text{Stir}} [\text{W}] = \frac{1000}{60} \cdot Q_{\text{inlet}}^{\text{Stir}} \quad (5.9)$$

5.2.2.3. Outlet thermal power and internal thermal power of the Stirling engine calculation

By determining the inlet thermal power in the Stirling engine, it becomes possible to calculate the outlet thermal power in the Stirling engine through relation (5.10) and the internal power retained by the Stirling engine through relation (5.11).

$$P_{\text{outlet}}^{\text{Stir}} [\text{W}] = (1 - \eta_{\text{II,ir}}) \cdot P_{\text{inlet}}^{\text{Stir}} \quad (5.10)$$

$$P_{\text{intern}}^{\text{Stir}} [\text{W}] = \eta_{\text{II,ir}} \cdot P_{\text{inlet}}^{\text{Stir}} \quad (5.11)$$

5.2.2.4. Distribution in time of the mass flow consumption of fuel

Determining the distribution in time of the fuel used in power production is done by multiplying the randomly chosen fuel mass flow with the report of the measured power and the calculated power, through relation (5.12).

$$m_{\text{fuel}}^{\text{power}} \left[\frac{\text{kg}}{\text{min}} \right] = m_{\text{fuel, random}}^{\text{power}} \cdot \frac{P_{\text{electric}}^{\text{measured}}}{P_{\text{electric, random}}^{\text{calculated}}} \quad (5.12)$$

5.2.3. The thermal power generation simulation

5.2.3.1. Calculus of the thermal power sent to end - user

The calculus of the thermal power sent to the user ($P_{\text{calculated}}^{\text{flow}}$) was done to determine the consumption of fuel for thermal power generation.

In all 32 tests, the simulation of thermal power inside the micro-cogeneration was done by taking into consideration the thermal power evacuated by the Stirling engine ($P_{\text{outlet}}^{\text{Stir}}$), the thermal power recovered from the flue gasses ($P_{\text{FG}}^{\text{Stir HE}}$), and the thermal power recovered through condensation of the water vapor from the flue gasses before their exhaust (P_{condens}). In a limited number of tests, there were moments in which, for the chosen model, lacked the possibility of evacuating the thermal power from the Stirling engine, in the cases in which the thermal agent flow was null.

Table 5.4 - Parameters used in the thermal power generation simulation

Parameter	Notation and value	Source
Regeneration efficiency	$\eta_{\text{reg}} = 0.99$	Hypothesis
Stirling engine thermal power outlet	$P_{\text{outlet}}^{\text{Stir}}$	Calculus
Flue gas – water heat exchanger efficiency	$\eta_{\text{FG-H2O}}^{\text{HE}} = 0.97$	Hypothesis
Flue gas temperature in combustion chamber	$T_{\text{FRT Ist}}^{\text{PE1}}$	μCHP measurement
Vapor – agent heat exchanger efficiency	$\eta_{\text{vap-ag}}^{\text{HE}} = 0.97$	Hypothesis
Vapor from flue gas temperature	$T_{\text{KT}}^{\text{PE1}}$	μCHP measurement
Measured thermal power produced by the unit	$P_{\text{measured}}^{\text{flow}}$	μCHP measurement
Calculated thermal power produced by the unit	$P_{\text{calculated}}^{\text{flow}}$	Calculus
Thermal power evacuated by the Stirling engine	$P_{\text{outlet}}^{\text{Stir}}$	Calculus
Thermal power recovered from the flue gasses	$P_{\text{FG}}^{\text{Stir HE}}$	Calculus
Thermal power recovered from water vapor	P_{condens}	Calculus
Water latent heat of vaporisation	LVH	Calculus
Fuel consumption	m_{fuel}	Calculus
Fuel consumption reversly calculated from heat	$m_{\text{fuel}}^{\text{heat}}$	Calculus

The calculated thermal power generated by the micro-cogeneration unit is calculated using relation (5.13).

$$P_{\text{calculated}}^{\text{flow}} [\text{W}] = \eta_{\text{reg}} \cdot P_{\text{outlet}}^{\text{Stir}} + \eta_{\text{sch}} \cdot P_{\text{FG}}^{\text{Stir HE}} + \eta_{\text{FG}} \cdot P_{\text{condens}} \quad (5.13)$$

5.2.3.2. Calculus of the thermal power recovered from flue gases

Using the measured values of the flue gas temperature in the combustion chamber ($T_{FRT\ Ist}^{PE1}$) and the sum of all masses and specific heats at constant pressure, depending on temperature of all flue gas components, the enthalpies of the flue gas are calculated, for each of the beforementioned values of the flue gas temperature, as shown in relation (5.14).

$$H_{FG}^{Stir\ HE}(T_{FRT\ Ist}^{PE1}) \left[\frac{kJ}{kg_{fuel}} \right] = \sum_i [m_i \cdot c_i(T_{FRT\ Ist}^{PE1})] \cdot T_{FRT\ Ist}^{PE1} \quad (5.14)$$

5.2.3.3. Calculus of the thermal power recovered from water vapor condensation

Using the measured values of water vapor temperature from the flue gasses ($T_{FRT\ Ist}^{PE1}$), the latent heat of vaporisation of water is calculated, depending on temperature $LVH(T_{KT}^{PE1})$. For a distribution in time of the fuel consumption (m_{fuel}^{heat}), chosen randomly, the thermal power recovered from water vapor condensation is calculated using relation (5.15).

$$P_{condens} = \frac{1000}{60} \cdot m_{fuel}^{heat} \cdot LVH(T_{KT}^{PE1}) \quad (5.15)$$

5.2.4. Time - distribution for the fuel mass consumption

Determining the distribution in time of the fuel mass consumption afferent to the thermal energy production is through the following algorithm:

1. Calculus of the report between the measured thermal power produced by the micro-cogeneration unit ($P_{measured}^{flow}$) and the calculated thermal power produced by the micro-cogeneration unit ($P_{calculated}^{flow}$);
2. The randomly chosen values of fuel consumption (m_{fuel}^{heat}) are given the values following the calculus of relations (5.13) to (5.15);
3. Relations (5.6) to (5.15) are recalculated.

The process is repeated until the results from 2 successive iterations are equal, as shown in Figure 5.3

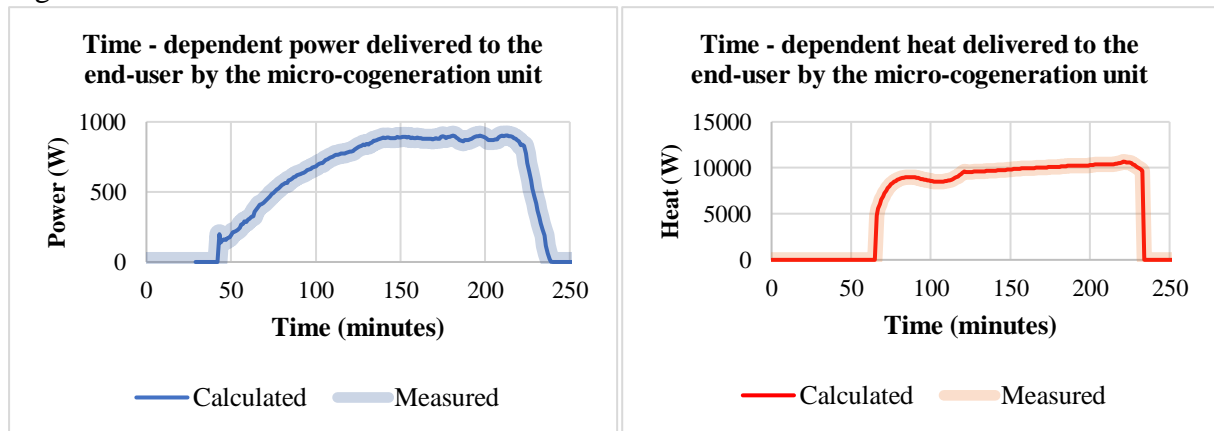


Figure 5.3 - An example of measured and calculated power and heat delivered to end - user

5.2.5. Simulation results

In Table 5.5, the calculated values for the total amount of generated electricity, the fuel mass consumed and the efficiency of power generation for all 32 transient tests are indicated.

Table 5.5 - Efficiency of power generation and the related fuel mass consumption determined for all 32 transient tests

No.	LHV _{fuel} MJ/kg _{fuel} 17,64020676	Start	Stop	Electricity				
		First	Last	Start	Stop	Amount	Fuel	Efficiency
				(min)	(min)	(kJ)	(kg)	(%)
1	VN MASTER 10-1 mar 07	Power	Power	43	240	8153.04	3.617	12.78
2	VN MASTER 10 -1 mar 12	Power	Power	42	269	9524.22	4.265	12.66
3	VN MASTER 10-2 mar 08	Power	Heat	27	240	9128.70	4.064	12.73
4	VN MASTER 10-2 mar 16	Power	Power	37	255	9036.36	4.029	12.71
5	VN MASTER 10-3 feb 25	Power	Power	25	283	1213.04	4.936	12.88
6	VN MASTER 12-1 feb 27	Power	Power	25	247	9945.18	4.210	13.39
7	VN MASTER 12-1 mar 22	Power	Power	44	143	3762.12	1.735	12.29
8	VN MASTER 12-2 feb 19	Power	Power	0	269	13161.96	5.227	14.27
9	VN MASTER 12-2 mar 18	Power	Power	27	320	13218.11	5.646	13.27
10	VN MASTER 12-2 mar 20	Power	Power	46	289	11333.94	4.686	13.71
11	VN MASTER 12-3 mar 04	Power	Power	27	267	11066.16	4.557	13.77
12	VN MASTER 12-3 mar 19	Power	Power	30	299	13068.06	5.272	14.05
13	VN MASTER 14-1 mar 01	Power	Power	27	145	4864.32	2.122	12.99
14	VN MASTER 14-1 mar 11	Power	Power	31	289	12260.52	4.982	13.95
15	VN MASTER 14-2 feb 28	Power	Power	27	263	11489.64	4.588	14.20
16	VN MASTER 14-2 mar 15	Power	Power	33	287	12845.22	5.027	14.49
17	VN MASTER 14-3 feb 26	Power	Power	29	307	14272.68	5.510	14.68
18	VN MASTER 14-3 mar 21	Power	Power	26	201	8380.50	3.346	14.20
19	VN MASTER 10 -1 jun 19	Heat	Power	30	389	16627.44	7.164	13.16
20	VN MASTER 12-3 jun 04	Power	Power	31	254	10375.86	4.254	13.83
21	VN-MASTER-10-3 jun 05	Power	Power	30	267	10358.22	4.536	12.95
22	VN MASTER 10-1 jun 18	Heat	Power	25	347	15939.90	6.328	14.28
23	VN MASTER 10-1 jun 25	Heat	Heat	33	270	7992.84	3.900	11.62
24	VN MASTER 10-2 jun 14	Power	Power	43	342	13208.16	5.769	12.98
25	VN MASTER 10-2 jun 21	Heat	Power	36	309	11840.52	5.150	13.03
26	VN MASTER 10-3 jun 12	Power	Heat	48	280	9783.30	4.359	12.72
27	VN MASTER 12-2 jun 24	Power	Power	42	216	7893.42	3.287	13.61
28	VN MASTER 12-3 jun 27	Power	Power	30	297	12938.64	5.273	13.91
29	VN MASTER 12-3 may 28	Power	Heat	26	270	11475.36	4.720	13.78
30	VN MASTER 12-3 may 29	Power	Heat	26	270	11475.36	4.720	13.78
31	VN MASTER 14-2 jun 17	Power	Heat	39	225	9023.10	3.581	14.28
32	VN MASTER 14-3 jun 11	Power	Heat	116	297	9366.54	3.579	14.84

The efficiency of power generation varies between 11.62% and 14.84%. The small value is for a transient test (code VN MASTER 10-1 jun 25), in which the beginning of heat generation has occurred before the power generation start and the heat generation stopped after the stop of the power generation. The greatest value is for a transient test (code VN MASTER 14-3 jun 11), in

which the power generation has started considerably earlier than the heat generation (91 minutes) despite the fact that the heat generation stop has occurred later than the power generation stop (71 minutes).

The calculated values for the total amount of generated heat, the fuel mass consumed and the efficiency of heat generation for all 32 transient tests are showed in Table 5.6.

Table 5.6 - Efficiency of heat generation and the related fuel mass consumption determined for all 32 transient tests

No.	LHV _{fuel} MJ/kg _{fuel} 17,64020676	Start	Stop	Heat				
		First	Last	Start (min)	Stop (min)	Amount (kJ)	Fuel (kg)	Efficiency (%)
1	VN MASTER 10-1 mar 07	Power	Power	66	234	95989.68	7.752	70.20
2	VN MASTER 10 -1 mar 12	Power	Power	56	264	119628.15	9.726	69.73
3	VN MASTER 10-2 mar 08	Power	Heat	33	245	102243.73	10.017	57.86
4	VN MASTER 10-2 mar 16	Power	Power	42	248	120864.78	10.144	67.54
5	VN MASTER 10-3 feb 25	Power	Power	49	278	134240.96	11.182	68.06
6	VN MASTER 12-1 feb 27	Power	Power	28	244	128772.55	10.117	72.16
7	VN MASTER 12-1 mar 22	Power	Power	53	138	48032.52	4.033	67.52
8	VN MASTER 12-2 feb 19	Power	Power	65	267	136497.77	10.222	75.70
9	VN MASTER 12-2 mar 18	Power	Power	43	315	169055.63	13.779	69.55
10	VN MASTER 12-2 mar 20	Power	Power	58	286	154284.03	12.264	71.32
11	VN MASTER 12-3 mar 04	Power	Power	47	259	142077.97	10.988	73.30
12	VN MASTER 12-3 mar 19	Power	Power	32	292	173944.35	13.319	74.03
13	VN MASTER 14-1 mar 01	Power	Power	32	141	63667.05	5.044	71.55
14	VN MASTER 14-1 mar 11	Power	Power	50	282	151546.38	11.711	73.36
15	VN MASTER 14-2 feb 28	Power	Power	32	256	159316.15	12.048	74.96
16	VN MASTER 14-2 mar 15	Power	Power	52	282	173952.21	13.163	74.92
17	VN MASTER 14-3 feb 26	Power	Power	32	301	196105.29	14.620	76.04
18	VN MASTER 14-3 mar 21	Power	Power	28	196	117377.35	9.265	71.82
19	VN MASTER 10 -1 jun 19	Heat	Power	26	384	203275.51	16.252	70.90
20	VN MASTER 12-3 jun 04	Power	Power	46	249	133977.16	11.019	68.93
21	VN-MASTER-10-3 jun 05	Power	Power	31	261	132386.14	11.232	66.82
22	VN MASTER 10-1 jun 18	Heat	Power	0	339	198395.99	15.725	71.52
23	VN MASTER 10-1 jun 25	Heat	Heat	32	295	140387.02	13.286	59.90
24	VN MASTER 10-2 jun 14	Power	Power	59	336	168782.88	14.176	67.49
25	VN MASTER 10-2 jun 21	Heat	Power	34	303	152214.46	12.375	69.73
26	VN MASTER 10-3 jun 12	Power	Heat	69	293	137307.39	12.459	62.48
27	VN MASTER 12-2 jun 24	Power	Power	58	199	89712.53	6.785	74.95
28	VN MASTER 12-3 jun 27	Power	Power	40	293	169496.82	12.993	73.95
29	VN MASTER 12-3 may 28	Power	Heat	40	274	150928.70	12.520	68.34
30	VN MASTER 12-3 may 29	Power	Heat	40	274	150928.70	12.520	68.34
31	VN MASTER 14-2 jun 17	Power	Heat	62	376	209439.57	25.466	46.62
32	VN MASTER 14-3 jun 11	Power	Heat	207	368	120685.12	14.401	47.51

The efficiency of heat generation varies between 46.62% and 76.04%. The small value is for a transient test (code VN MASTER 14-2 jun 17), in which the beginning of heat generation has occurred after the power generation start and the heat generation stopped after the stop of the

power generation (151 minutes). The greatest value is for a transient test (code VN MASTER 14-3 feb 26), in which the power generation has started slightly earlier than the heat generation (3 minutes) and the fact that the heat generation stop has occurred slightly earlier than the power generation stop (6 minutes). For this transient test, the power and heat generation have practically simultaneously occurred.

Table 5.7 contains the calculated values of the fuel mass consumption for power generation, the fuel mass consumed for heat generation for the total amount of generated heat, the fuel mass consumed and the efficiency of heat generation for all 32 transient tests.

Table 5.7 - Comparison between the measured values and calculated values for the fuel mass consumption for all 32 transient tests

No.	LHV _{fuel} MJ/kg _{fuel} 17,64020676	Start	Stop	Measured fuel mass (kg)	Calculated fuel mass			Relative error (%)
		First	Last		Power (kg)	Heat (kg)	Overall (kg)	
1	VN MASTER 10-1 mar 07	Power	Power	16.600	3.617	7.752	11.369	-31.51%
2	VN MASTER 10 -1 mar 12	Power	Power	13.800	4.265	9.726	13.991	1.38%
3	VN MASTER 10-2 mar 08	Power	Heat	11.600	4.064	10.017	14.081	21.39%
4	VN MASTER 10-2 mar 16	Power	Power	13.600	4.029	10.144	14.173	4.21%
5	VN MASTER 10-3 feb 25	Power	Power	11.800	4.936	11.182	16.118	36.59%
6	VN MASTER 12-1 feb 27	Power	Power	12.600	4.210	10.117	14.327	13.71%
7	VN MASTER 12-1 mar 22	Power	Power	13.400	1.735	4.033	5.768	-56.96%
8	VN MASTER 12-2 feb 19	Power	Power	23.000	5.227	10.222	15.449	-32.83%
9	VN MASTER 12-2 mar 18	Power	Power	15.000	5.646	13.779	19.425	29.50%
10	VN MASTER 12-2 mar 20	Power	Power	16.800	4.686	12.264	16.950	0.89%
11	VN MASTER 12-3 mar 04	Power	Power	13.400	4.557	10.988	15.545	16.01%
12	VN MASTER 12-3 mar 19	Power	Power	16.800	5.272	13.319	18.591	10.66%
13	VN MASTER 14-1 mar 01	Power	Power	8.000	2.122	5.044	7.166	-10.43%
14	VN MASTER 14-1 mar 11	Power	Power	15.400	4.982	11.711	16.693	8.40%
15	VN MASTER 14-2 feb 28	Power	Power	14.000	4.588	12.048	16.636	18.83%
16	VN MASTER 14-2 mar 15	Power	Power	14.400	5.027	13.163	18.190	26.32%
17	VN MASTER 14-3 feb 26	Power	Power	15.600	5.510	14.620	20.130	29.04%
18	VN MASTER 14-3 mar 21	Power	Power	11.600	3.346	9.265	12.611	8.72%
19	VN MASTER 10 -1 jun 19	Heat	Power	17.000	7.164	16.252	23.416	37.74%
20	VN MASTER 12-3 jun 04	Power	Power	12.400	4.254	11.019	15.273	23.17%
21	VN-MASTER-10-3 jun 05	Power	Power	11.400	4.536	11.232	15.768	38.32%
22	VN MASTER 10-1 jun 18	Heat	Power	16.600	6.328	15.725	22.053	32.85%
23	VN MASTER 10-1 jun 25	Heat	Heat	14.200	3.900	13.286	17.186	21.03%
24	VN MASTER 10-2 jun 14	Power	Power	14.000	5.769	14.176	19.945	42.46%
25	VN MASTER 10-2 jun 21	Heat	Power	18.000	5.150	12.375	17.525	-2.64%
26	VN MASTER 10-3 jun 12	Power	Heat	12.400	4.359	12.459	16.818	35.63%
27	VN MASTER 12-2 jun 24	Power	Power	9.600	3.287	6.785	10.072	4.92%
28	VN MASTER 12-3 jun 27	Power	Power	13.600	5.273	12.993	18.266	34.31%
29	VN MASTER 12-3 may 28	Power	Heat	16.800	4.720	12.520	17.240	2.62%
30	VN MASTER 12-3 may 29	Power	Heat	16.800	4.720	12.520	17.240	2.62%
31	VN MASTER 14-2 jun 17	Power	Heat	12.000	3.581	25.466	29.047	142.06%
32	VN MASTER 14-3 jun 11	Power	Heat	40.800	3.579	14.401	17.980	-55.93%

As it can easily be observed in the Table 5.3, the simulations of transient regimes have showed that the uncertainty related to the consumption of fuel in the form of wood pellets is significant.

The relative errors vary from 8.40% to 142.06% (the calculated value exceeds the measured value) and from -56.96% to -10.43% (the calculated value is smaller the measured value), when considering as reference the values of the measured fuel mass. The transient tests not affected by the fuel mass measurement uncertainty are showed in Table 5.8.

Table 5.8 - Transient tests in which the relative error stays under the acceptable value of $\pm 5\%$

Test number	Transient test code	Efficiencies			Fuell mass relative error
		Power	Heat	Overall	
27	VN MASTER 12-2 jun 24	13.61%	74.95%	54.94%	4.92%
4	VN MASTER 10-2 mar 16	12.71%	67.54%	51.92%	4.21%
29	VN MASTER 12-3 may 28	13.78%	68.34%	53.40%	2.62%
30	VN MASTER 12-3 may 29	13.78%	68.34%	53.40%	2.62%
2	VN MASTER 10 -1 mar 12	12.66%	69.73%	52.33%	1.38%
10	VN MASTER 12-2 mar 20	13.71%	71.32%	55.39%	0.89%
25	VN MASTER 10-2 jun 21	13.03%	67.73%	53.07%	-2.64%

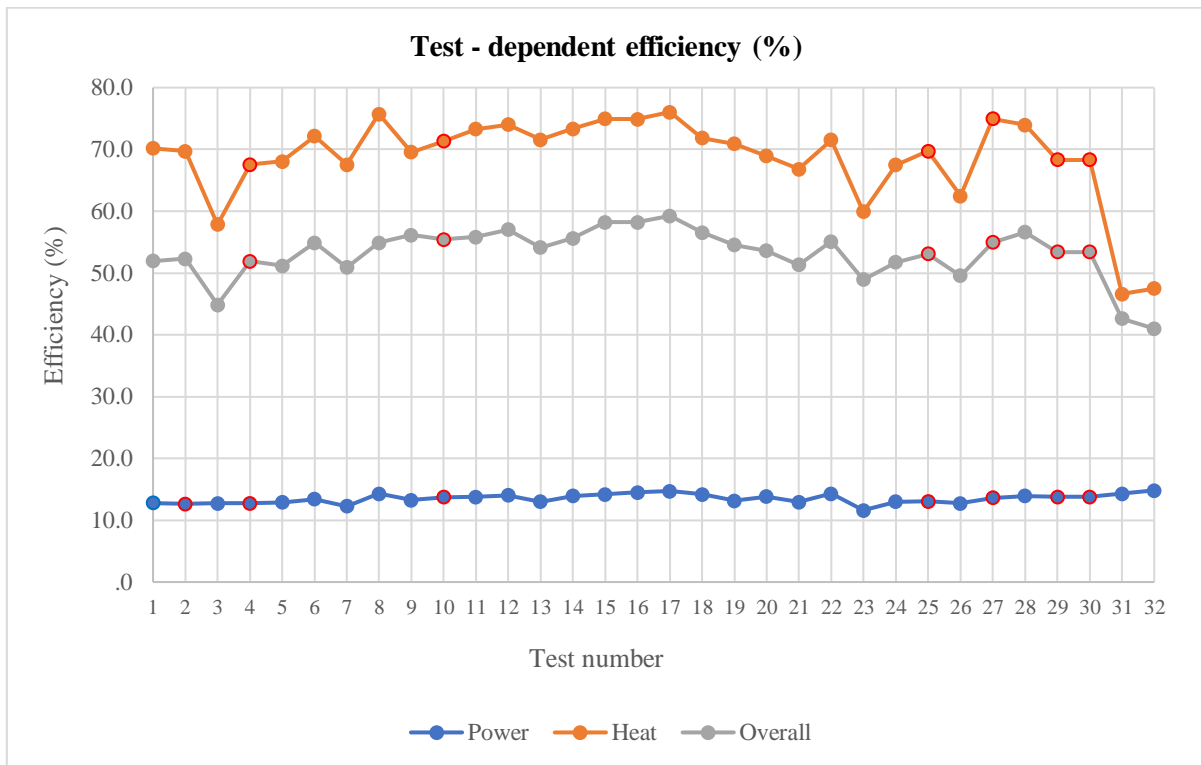


Figure 5.4 - The test - dependent efficiency for the power generation, the heat generation and overall

In the Figure 5.4, the values for power generation, heat generation and micro-cogeneration unit efficiencies are represented.

As it was expected, the efficiency overall has as upper limit the efficiencies for heat generation and as lower limit the efficiency for power generation. It can be observed that the heat generation efficiency has a stronger influence on the efficiency overall than the efficiency of power generation.

If the efficiencies within Table 5.4 are observed, the values for the power generation efficiency vary from 12.66% to 13.78%, the efficiency of heat generation varies within the interval 67.54% - 74.95%, and the efficiency overall varies between 51.92% and 55.39%.

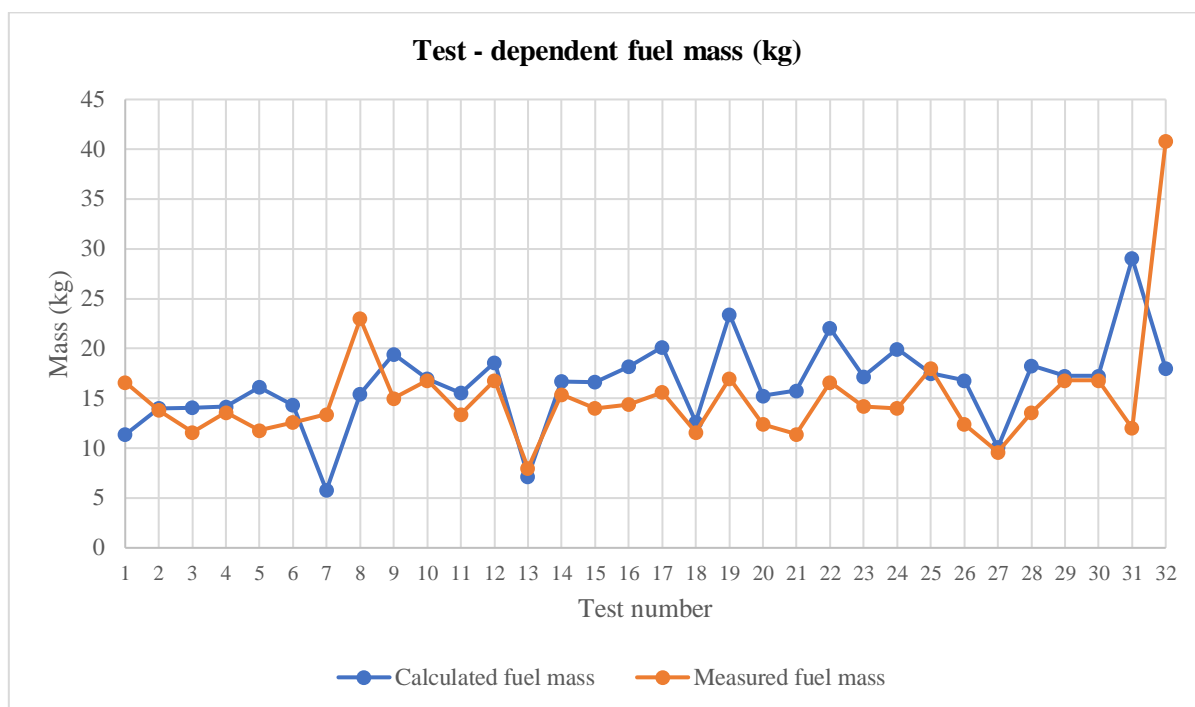


Figure 5.5 - Comparison between the test - dependent fuel mass calculated and measured values

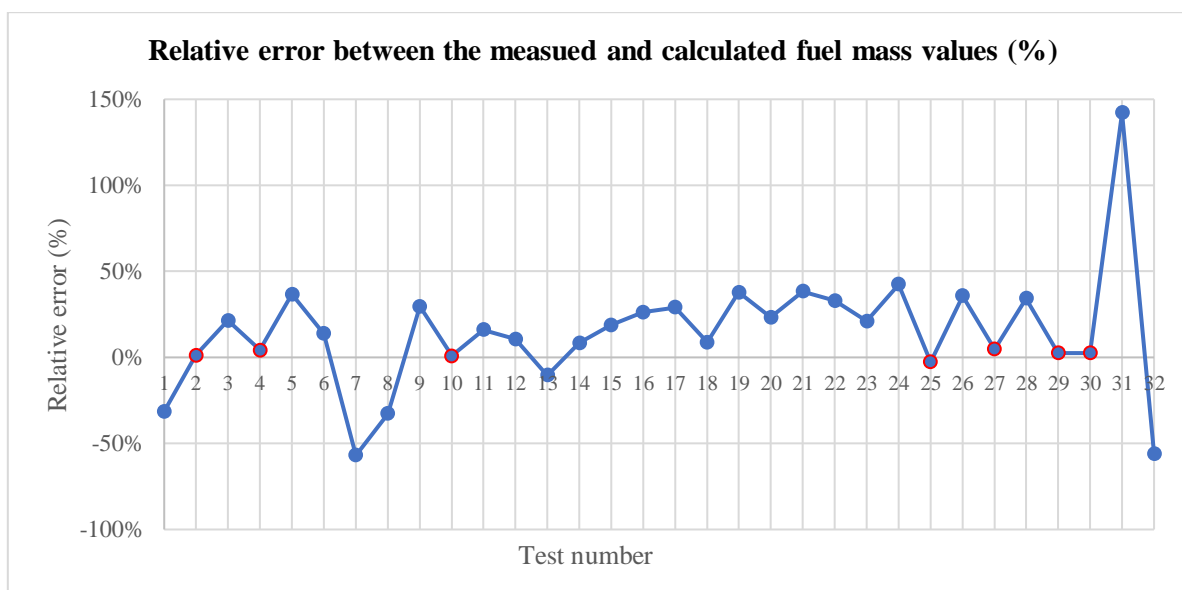


Figure 5.6 - The test - dependent relative errors for fuel mass calculated values and measured values (considered as reference)

Figures 5.5 and 5.6 suggest how much the fuel mass measurement uncertainty affected the transient tests. This is the reason for which further laboratory tests should be deployed only after the needed actions to limit the errors affecting the fuel mass measurements were carried out.

5.3. INVESTMENT PROJECT PROFITABILITY INDICES

In general, the annual cash flow (CF_h) is determined with the relation (5.16), by deducting from the annual income (Inc_h) the annual operating expenditures (Exp_h) and investments (Inv_h):

$$CF_h = Inc_h - (Inv_h + Exp_h) \quad (5.16)$$

The discount method is currently used to discount the annual cash flow. Discounting (Tomiță, 2004, Malamatenios, 2007), which can ensure the comparison of expenses and revenues at the beginning of the investment, is the method by which the identified and estimated economic benefits (including cash flow) are updated to present value, using, a discount rate.

The discount rate d (%) results from the sum of the cost of capital used to make that investment (c), the business risk rate (r) and the security rate (s). The discounting involves an explicit forecast period and a residual value (El Ghayaly, 2005, Malamatenios, 2007).

The main steps required to apply the discount method (Frăsineanu, 2005) are:

- the adoption of the hypotheses regarding the evolution of the investment's sponsor, choosing the key variables that will influence its further activity and the general limits of the company's dynamic behaviour;
- choosing the forecast duration; the choice of the explicit period is based on elements such as the lifespan of the equipment and installations that are the object of the investment, the normal investment cycle, the duration of operation of the investment's sponsor;
- establishing the evolution scenarios of the investment's sponsor at macroeconomic level and respectively, at the level of the economic sector in which it operates;
- the estimation of the residual value of the investment; in the case of an investment in the energy field with a finite lifetime, the liquidation value will be used to estimate the residual value of the investment.

The discounted annual cash flow is used to determine the main profitability indices of the investment project.

5.3.1. Profitability indices, calculation and applicability

The main profitability indices of an investment are:

- static indices: specific investment, gross payback, economic efficiency coefficient, economic efficiency, recalculated expenses etc. ;
- dynamic indices, which quantify the influence of the time factor: cash flow, discounted net present value, internal rate of return, profitability break-even point, discounted payback time, discounted economic efficiency, discounted specific expenses etc.

The main profitability indices used in the procedures of the International Bank for Reconstruction and Development (IBRD) in evaluating feasibility studies (Romănu, 1993), their calculation methods and applicability are presented below.

The ratio (R) between the discounted annual income (benefits) and the discounted annual costs expresses the annual income, in monetary units, resulting from a financial effort, in that monetary unit, made with the investment and the operation (Romănu, 1993). The ratio R can be calculated with the relation (5.17):

$$R = \frac{\sum \text{Inc}_h \frac{1}{(1+d)^h}}{\sum (\text{Inv}_h + \text{Exp}_h) \frac{1}{(1+d)^h}} > 1, \quad (5.17)$$

where d is the discount rate, h is the year in which the expense is made or the income is obtained, t is the duration of the investment, T is the lifetime of the further investment, Inc_h is the annual income in year h , Exp_h are the annual operating expenses for year h and Inv_h is the annual investment for year h . It is preferable that the indicator R to get supraunitary values, situations in which $R < 1$, being unacceptable. In case the R is equal to the unit, other criteria such as the social one may intervene in the decision on the investment opportunity.

The discounted annual cash flow (CF_h) expresses the statement of income and expenses for each year in the interval $1, t + T$. It is calculated with the relation (5.18):

$$\text{CF}_h = [\text{Inc}_h - (\text{Inv}_h + \text{Exp}_h)] \frac{1}{(1+d)^h}. \quad (5.18)$$

The discounted Net Present Value (dNPV) expresses the discounted net income over the entire period of time $1, t + T$, and is calculated with the relation (5.19):

$$\text{dNPV} = \sum \text{CF}_h > 0, \quad (5.19)$$

or by summing up all the discounted annual cash flows over the entire time period $1, t + T$:

$$\text{dNPV} = \sum_{h=1}^{t+T} \frac{\text{Inc}_h}{(1+d)^h} - \sum_{h=1}^{t+T} \frac{\text{Inv}_h + \text{Exp}_h}{(1+d)^h} > 0. \quad (5.20)$$

The dNPV indicator, used both in the financial analysis and in the economic analysis of the investment, must take as many positive values as possible, negative values for dNPV being unacceptable. To tackle this situation or the positive term should be increased (revenues) or somehow, the expenditures should diminish.

The Internal Rate of Return (IRR) expresses the economic power of the further objective and represents that value of the discount rate for which the discounted Net Present Value is null ($\text{dNPV} = 0$). The determination of the Internal Rate of Return can be done analytically using the relation (5.21):

$$\text{IRR} = d_{\min} + (d_{\max} - d_{\min}) \cdot \frac{\text{dNPV}_+}{\text{dNPV}_+ + |\text{dNPV}_-|}, \quad (5.21)$$

or graphically (Malamatenios, 2007, El Ghayaly, 2005, Romănu, 1993), like suggested in Figure 5.7.

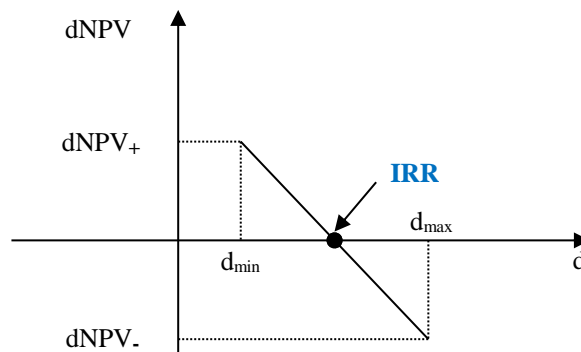


Figure 5.7 - Graphic method for the determination of the Internal Rate of Return
 (source: Malamatenios, Ch., Vezirigianni, G., Grepmeier, K., Renewable Energy & Energy Efficiency: Trainig Course, NicVox, ISBN (13) 978-973-8489-37-0, Bucharest, 2007).

The determination of the two coefficients, a_{\min} and a_{\max} , will be done by successive iterations (it is desirable that the difference between the two values is not greater than 5%), so as to obtain a positive value for dNPV and a negative value for the same dNPV.

For the economic analysis, the indicator is called the Internal Rate of Economic Return, and for the financial analysis it is called the Internal Rate of Financial Return.

The Gross Payback Time (GPT) is the operating period at the end of which the generated cash flow fully recovers the investment. The relation from which this indicator can be obtained is:

$$\sum_{h=1}^{GPT} [\text{Inc}_h - (\text{Inv}_h + \text{Exp}_h)] = 0. \quad (5.22)$$

If the annual cash flow is constant, the Gross Payback Time is obtained with the relation (5.23):

$$GPT = \frac{\text{Inv}}{\text{Inc} - \text{Exp}}. \quad (5.23)$$

The use of the Gross Payback Time of the investment requires the definition of the initial moment of time, this being usually considered as the moment of commissioning of the installations and equipment that have been the object of the investment.

The Discounted Payback Time (DPT) is the operating period at the end of which the discounted cash flow generated fully recovers the investment and there is also the possibility to obtain a cash flow that corresponds to the discount rate:

$$\sum_{h=1}^{GPT} \frac{\text{Inc}_h - (\text{Inv}_h + \text{Exp}_h)}{(1 + d)^h} = 0. \quad (5.24)$$

If the annual cash flows are constant then the Discounted Payback Time term can be determined using the Gross Payback Time, based on the relation (5.25):

$$DPT = - \frac{\ln(1 - GPT * d)}{\ln(1 + d)}. \quad (5.25)$$

The use of the gross return on investment requires the definition of the initial moment of time, this being usually considered as the moment of commissioning of the installations and equipment that have been the object of the respective investment.

In general, the indices in the case of economic analysis are more favorable than those determined in the financial analysis.

Static indicators are more favorable than dynamic ones, which quantify the influence of the time factor, take into account the importance of money and in general, investments / expenses are made now when money has a higher economic value, and profit is obtained later when the economic importance of money decreases.

The discounted net income is a basic index with which all other indices can be determined, being the most conclusive in estimating the profitability of an investment project in the field of energy efficiency. The information provided is absolute values of a quantitative nature (Malamatenios, 2007), which is why the other indices presented in this chapter are used alongside this index. The internal rate of return can be determined without knowing the discount rate, but when estimating the efficiency of the investment, the comparison of these two rates is relevant. It is not recommended to use the internal rate of return when comparing several solutions because the conclusions obtained could be false and the most economically efficient

solution is not necessarily characterized by a maximum value of the internal rate of return (Malamatenios, 2007).

The gross return on investment is easy to calculate and can be used in a first selection of an investment project, simplifying as much as possible the decision-making process regarding its realization. The updated term of return on investment has the same advantages in use as the gross term of recovery, the information provided having an easy-to-understand meaning (Malamatenios, 2007).

5.3.2. Input data for the economic simulation of the transient tests

For the economic simulations of the results obtained in the case of four transient tests, the input data which have been chosen are showed in Table 5.9. The annual operation of the μ CHP, the fuel price, the heat price (without subsidies) and the electricity price are those specific for Romania, a country with temperate continental climate. The total size of investment and the lifespan of the μ CHP unit are defined.

Table 5.9 - Input data for the economic simulation of the transient tests

Operation hours/year	Fuel price €/MWh	Heat Price €/MWh	Electricity Price €/MWh	μ CHP Price €	μ CHP Lifespan years
4000	28.57	84.11	303.92	15000	20

5.3.3. Economic simulation of the Test code VN MASTER 10-1 mar 07

For the Test code VN MASTER 10-1 mar 07, the power and heat generation within the μ CHP and the fuel consumption decomposition are indicated in Figure 5.8.

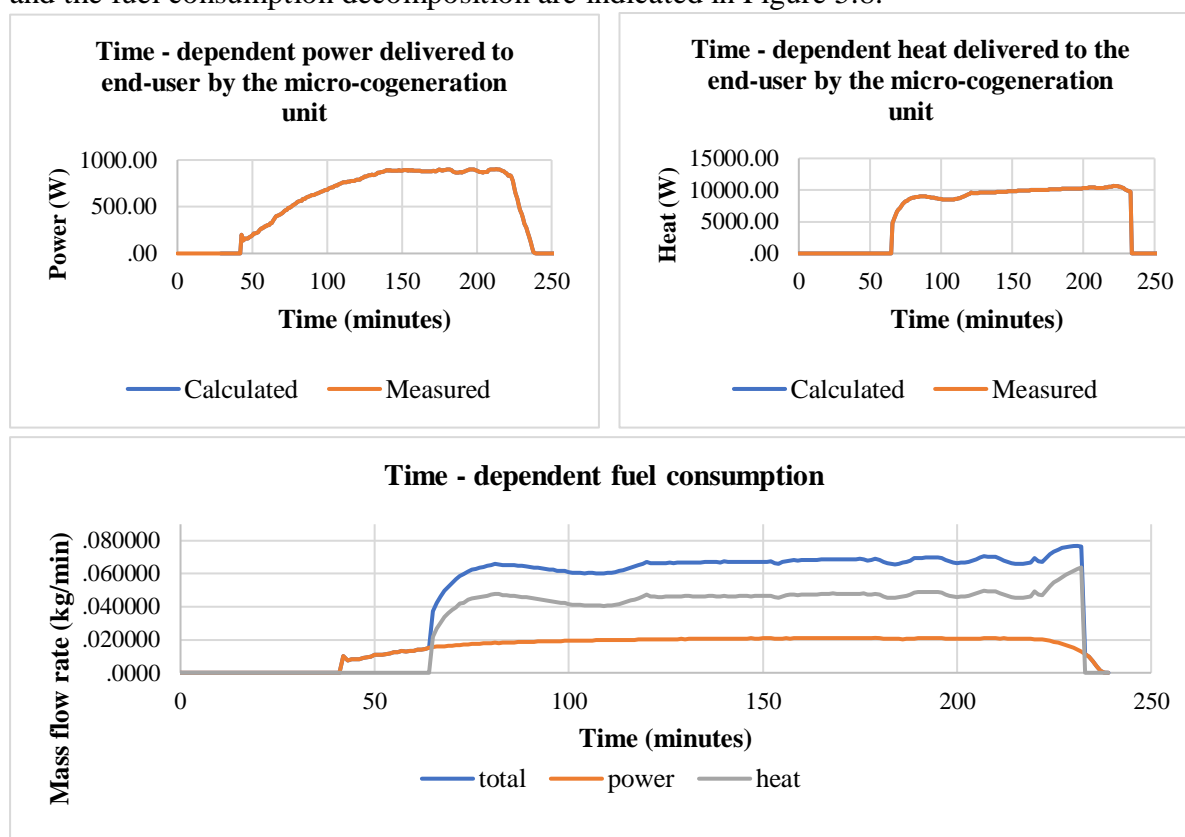


Figure 5.8 - A test (code VN MASTER 10-1 mar 07) whose power generation lasts longer than the heat generation

Based on the total amounts of electricity and thermal energy generated within the μ CHP and with the fuel mass consumption decomposition as showed in Figure 5.8, the average values for the power and the heat generated within the μ CHP and the related total fuel consumption are indicated in Table 5.10.

Table 5.10 - Performances of the μ CHP for the Test code VN MASTER 10-1 mar 07

Electricity	Power	Thermal Energy	Heat	Fuel
kJ	kW	kJ	kW	kW
8153	0.686	95990	9.466	18.857

Considering the input data indicated in Table 5.9 and the calculated values showed in Table 5.10, the financial performances of the μ CHP for the Test code VN MASTER 10-1 mar 07 are indicated in Table 5.11.

Table 5.11 - Financial performances of the μ CHP for the Test code VN MASTER 10-1 mar 07

Type of energy units	Before			After			Savings	
	Power kW	Energy MWh/year	Expenditures €/year	Power kW	Energy MWh/year	Ependitures €/year	Energy MWh/year	Earnings €/year
Fuel	0	0	0	18.857	75.43	2155.02	-75.43	-2155.02
Heat	9.47	37.87	3184.83	9.47	37.87	0	0	3184.83
Electricity	0.69	2.75	834.29	0.69	2.75	0	0	834.29
Total			4.019.11			2155.02		1864.09

Based on the financial earning in Table 5.11 and on the gross cash - flow projection over the lifespan of the μ CHP (Annex 5, Table A5.1), the investment performances for the results of mathematical model in the case of the Test code VN MASTER 10-1 mar 07 are showed in Table 5.12. The values for IRR and dNPV are fulfilling the requirements stated in §5.3.1.

Table 5.12 - Investment performances of the μ CHP for the Test code VN MASTER 10-1 mar 07

Discount Rate	Gross Payback Time	Discounted Payback Time	Internal Rate of Return (IRR)	Discounted Net Present Value (dNPV)
%	years	years	%	€
5	8.0	10.5	10.8	8.231

In Figure 5.9, the Gross and Discounted Payback Time are showed.

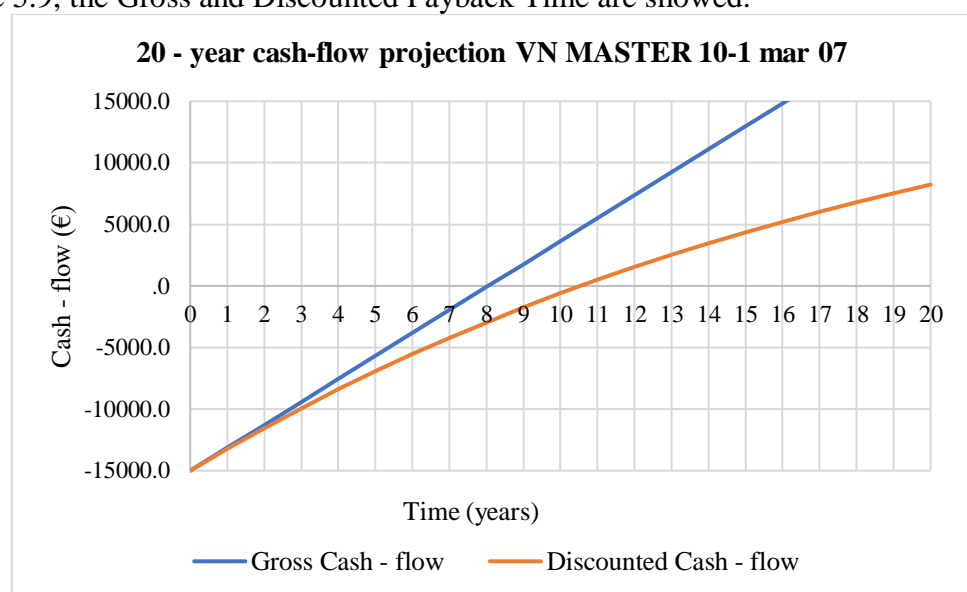


Figure 5.9 - Gross and Discounted Payback Time (code VN MASTER 10-1 mar 07)

5.3.4. Economic simulation of the Test code VN MASTER 14-3 jun 11

For the Test code VN MASTER 14-3 jun 11, the power and heat generation within the μ CHP and the fuel consumption decomposition are indicated in Figure 5.10.

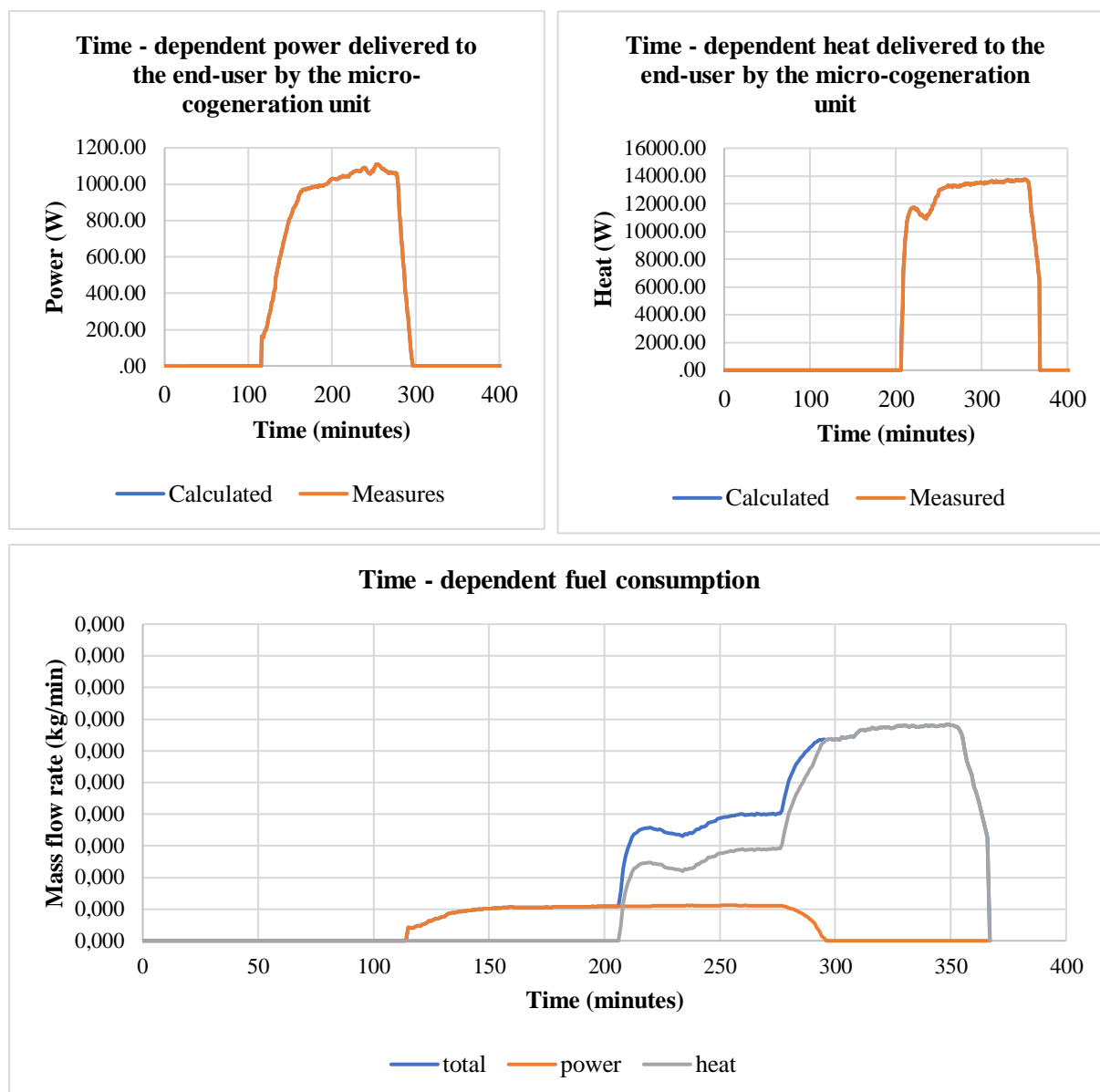


Figure 5.10 - A test (code VN MASTER 14-3 jun 11) whose power generation starts earlier than the heat generation but stops quicker, so that in the end, the micro-cogeneration unit produces heat exclusively

Based on the total amounts of electricity and thermal energy generated within the μ CHP and with the fuel mass consumption decomposition as shown in Figure 5.10, the average values for the power and the heat generated within the μ CHP and the related total fuel consumption are indicated in Table 5.13.

Table 5.13 - Performances of the μ CHP for the Test code VN MASTER 14-3 jun 11

Electricity	Power	Thermal Energy	Heat	Fuel
kJ	kW	kJ	kW	kW
9367	0.858	120685	12.416	31.916

Considering the input data indicated in Table 5.9 and the calculated values showed in Table 5.13, the financial performances of the μ CHP for the Test code VN MASTER 14-3 jun 11 are indicated in Table 5.14.

Table 5.14 - Financial performances of the μ CHP for the Test code VN MASTER 14-3 jun 11

Type of energy units	Before			After			Savings	
	Power kW	Energy MWh/year	Expenditures €/year	Power kW	Energy MWh/year	Ependitures €/year	Energy MWh/year	Earnings €/year
Fuel	0	0	0	31.92	127.66	3647.53	-127.66	-3647.53
Heat	12.42	49.66	4177.21	12.42	49.66	0	0	4177.21
Electricity	0.86	3.43	1042.73	0.86	3.43	0	0	1042.73
Total			5219.94			3647.53		1572.41

Based on the financial earnings showed in Table 5.14 and on the gross cash - flow projection over the lifespan of the μ CHP (Annex 5, Table A5.2), the investment performances for the results of mathematical model in the case of the Test code VN MASTER 14-3 jun 11 are showed in Table 5.15. The values for IRR and dNPV are fulfilling the requirements stated in §5.3.1.

Table 5.15 - Investment performances of the μ CHP for the Test code VN MASTER 14-3 jun 11

Discount Rate	Gross Payback Time	Discounted Payback Time	Internal Rate of Return	Discounted Net Present Value
%	years	years	%	€
5	9.5	13.5	8.4	4,596

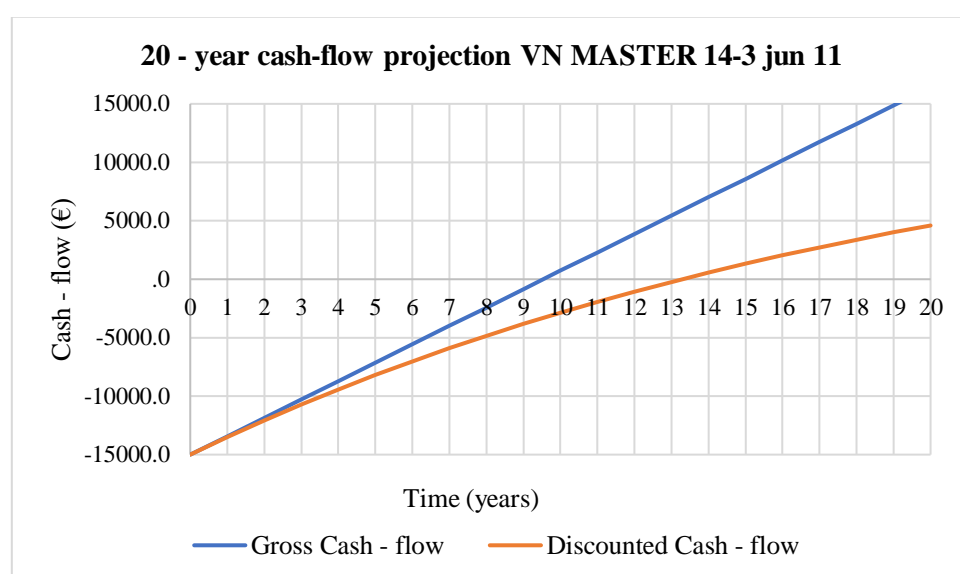


Figure 5.11 - Gross and Discounted Payback Time (code VN MASTER 14-3 jun 11)

5.3.5. Economic simulation of the Test code VN MASTER 10-1 jun 25

For the Test code VN MASTER 10-1 jun 25, the power and heat generation within the μ CHP and the fuel consumption decomposition are indicated in Figure 5.12.

Based on the total amounts of electricity and thermal energy generated within the μ CHP and with the fuel mass consumption decomposition as showed in Figure 5.12, the average values

for the power and the heat generated within the μ CHP and the related total fuel consumption are indicated in Table 5.16.

Table 5.16 - Performances of the μ CHP for the Test code VN MASTER 10-1 jun 25

Electricity	Power	Thermal Energy	Heat	Fuel
kJ	kW	kJ	kW	kW
7993	0.560	140387	8.863	19,614

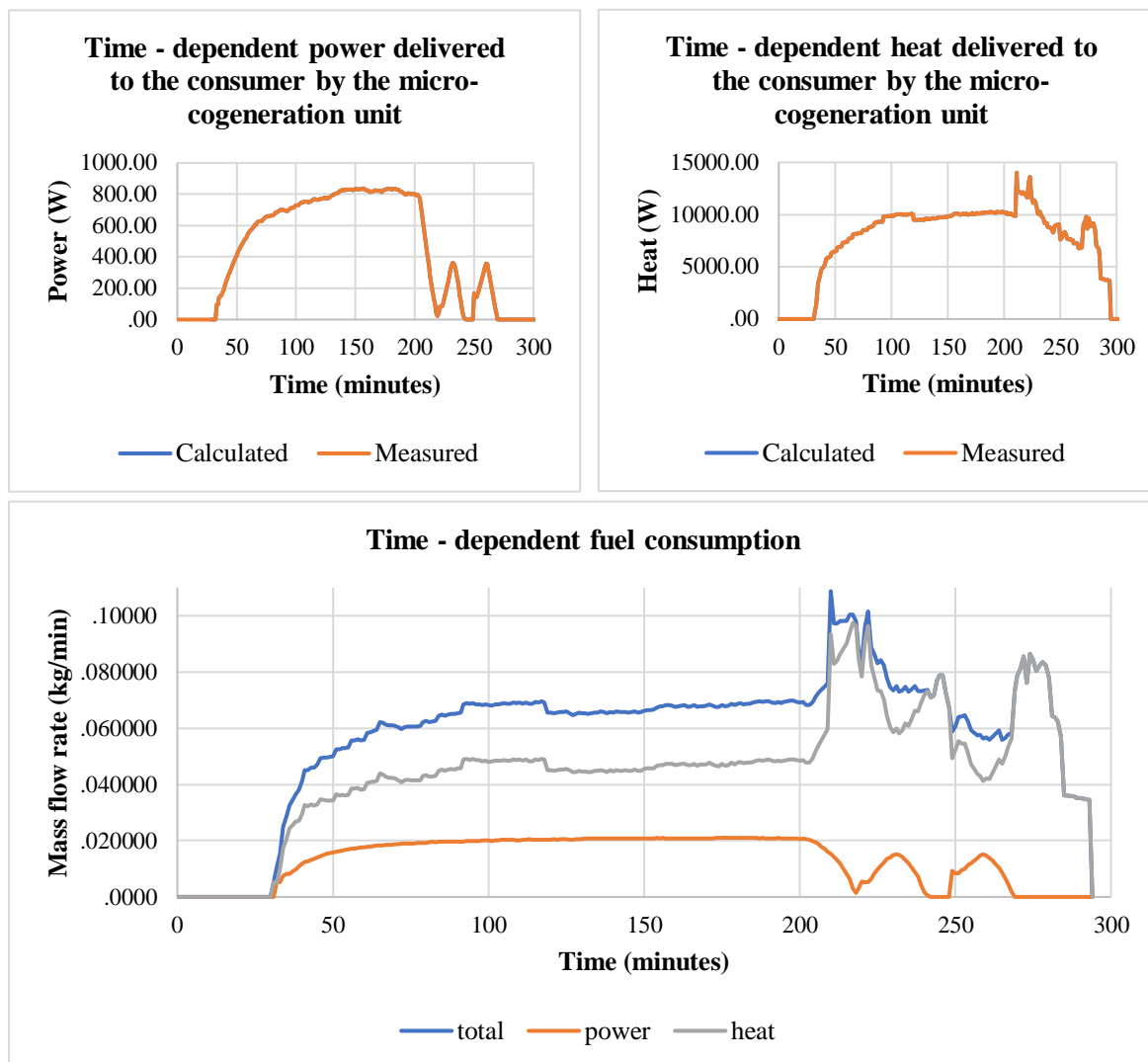


Figure 5.12 - A test (code VN MASTER 10-1 jun 25) whose heat generation lasts longer than the power generation

Considering the input data indicated in Table 5.9 and the calculated values showed in Table 5.16, the financial performances of the μ CHP for the Test code VN MASTER 10-1 jun 25 are indicated in Table 5.17.

Table 5.17 - Financial performances of the μ CHP for the Test code VN MASTER 10-1 jun 25

Type of energy units	Before			After			Savings	
	Power kW	Energy MWh/year	Expenditures €/year	Power kW	Energy MWh/year	Ependitures €/year	Energy MWh/year	Earnings €/year
Fuel	0	0	0	19.61	78.46	2241.55	-78.46	-2241.55
Heat	8.86	35.45	2981.75	8.86	35.45	0	0	2981.75
Electricity	0.56	2.24	6809.43	0.56	2.24	0	0	680.43
Total			3662.18			2241.55		1420.63

Based on the financial earnings showed in Table 5.17 and on the gross cash - flow projection over the lifespan of the μ CHP (Annex 5, Table A5.3), the investment performances for the results of mathematical model in the case of the Test code VN MASTER 10-1 jun 25 are showed in Table 5.18. The values for IRR and dNPV are fulfilling the requirements stated in §5.3.1.

Table 5.18 - Investment performances of the μ CHP for the Test code VN MASTER 10-1 jun 25

Discount Rate	Gross Payback Time	Discounted Payback Time	Internal Rate of Return	Discounted Net Present Value
%	years	years	%	€
5	10.5	15.5	7.0	2,704

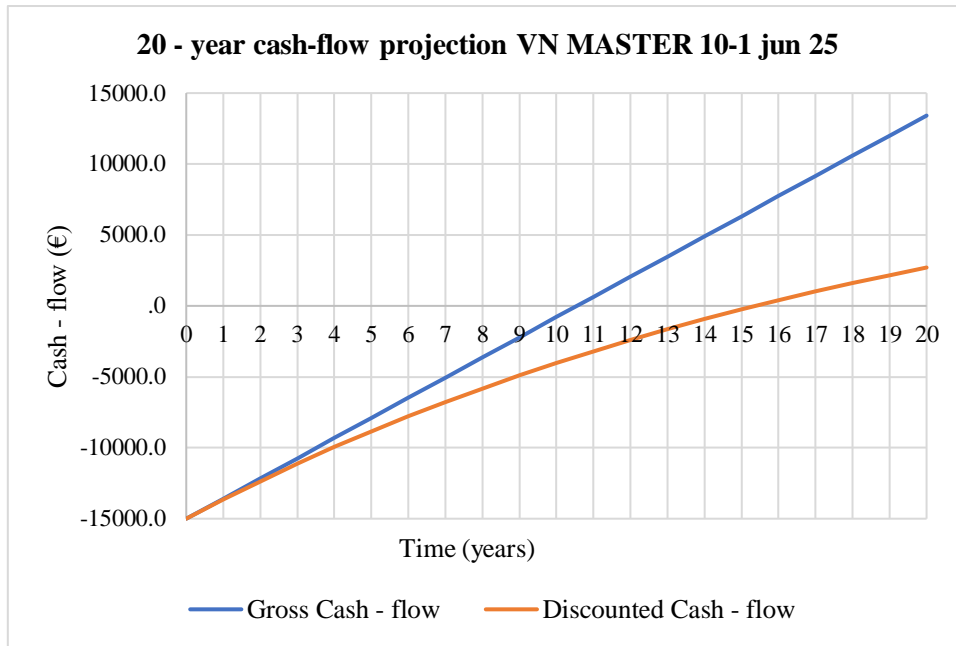


Figure 5.13 - Gross and Discounted Payback Time (code VN MASTER 10-1 jun 25)

5.3.6. Economic simulation of the Test code VN MASTER 10-1 jun 18

For the Test code VN MASTER 10-1 jun 18, the power and heat generation within the μ CHP and the fuel consumption decomposition are indicated in Figure 5.14.

Based on the total amounts of electricity and thermal energy generated within the μ CHP and with the fuel mass consumption decomposition as showed in Figure 5.14, the average values for the power and the heat generated within the μ CHP and the related total fuel consumption are indicated in Table 5.19.

Table 5.19 - Performances of the μ CHP for the Test code VN MASTER 10-1 jun 18

Electricity	Power	Thermal Energy	Heat	Fuel
kJ	kW	kJ	kW	kW
15940	0.822	198396	9.725	19.358

Considering the input data indicated in Table 5.9 and the calculated values showed in Table 5.19, the financial performances of the μ CHP for the Test code VN MASTER 10-1 jun 18 are indicated in Table 5.20.

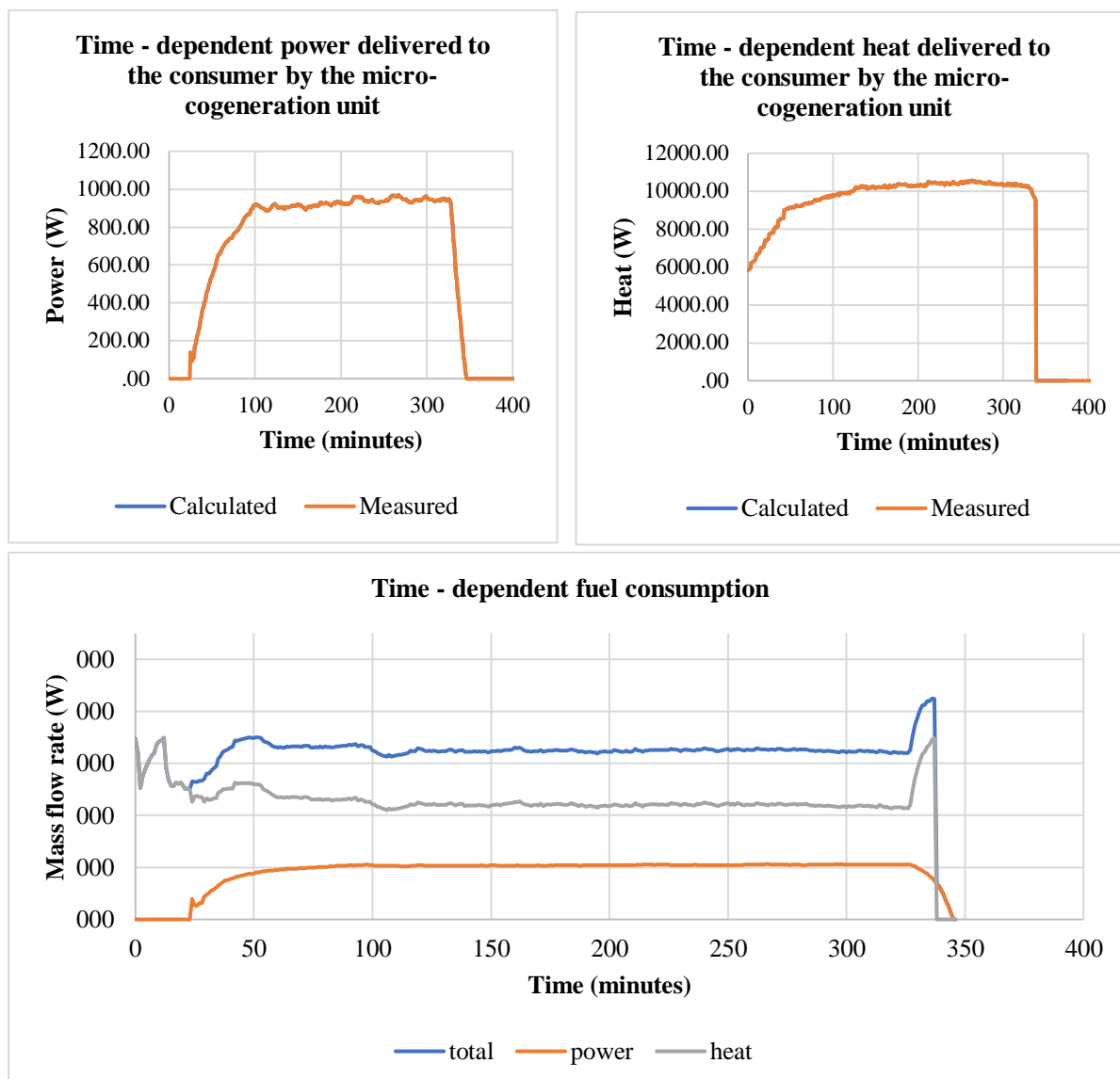


Figure 5.14 - A test (code VN MASTER 10-1 jun 18) whose heat generation starts earlier than the power generation but stops earlier, so that the micro - cogeneration unit produces power exclusively

Table 5.20 - Financial performances of the μ CHP for the Test code VN MASTER 10-1 jun 18

Type of energy units	Before			After			Savings	
	Power kW	Energy MWh/year	Expenditures €/year	Power kW	Energy MWh/year	Ependitures €/year	Energy MWh/year	Earnings €/year
Fuel	0	0	0	19.36	77.43	2212.28	-77.43	-2212.28
Heat	9.73	38.90	3.271.91	9.73	38.90	0	0	3271.91
Electricity	0.82	3.29	999.87	0.82	3.29	0	0	999.87
Total			4271.79			2212.28		2059.51

Based on the financial earnings showed in Table 5.20 and on the gross cash - flow projection over the lifespan of the μ CHP (Annex 5, Table A5.4), the investment performances for the results of mathematical model in the case of the Test code VN MASTER 10-1 jun 18 are showed in Table 5.21. The values for IRR and dNPV are fulfilling the requirements stated in §5.3.1.

Table 5.21 - Investment performances of the μ CHP for the Test code VN MASTER 10-1 jun 18

Discount Rate	Gross Payback Time	Discounted Payback Time	Internal Rate of Return	Discounted Net Present Value
%	years	years	%	€
5	7.2	9.3	12.4	10,666

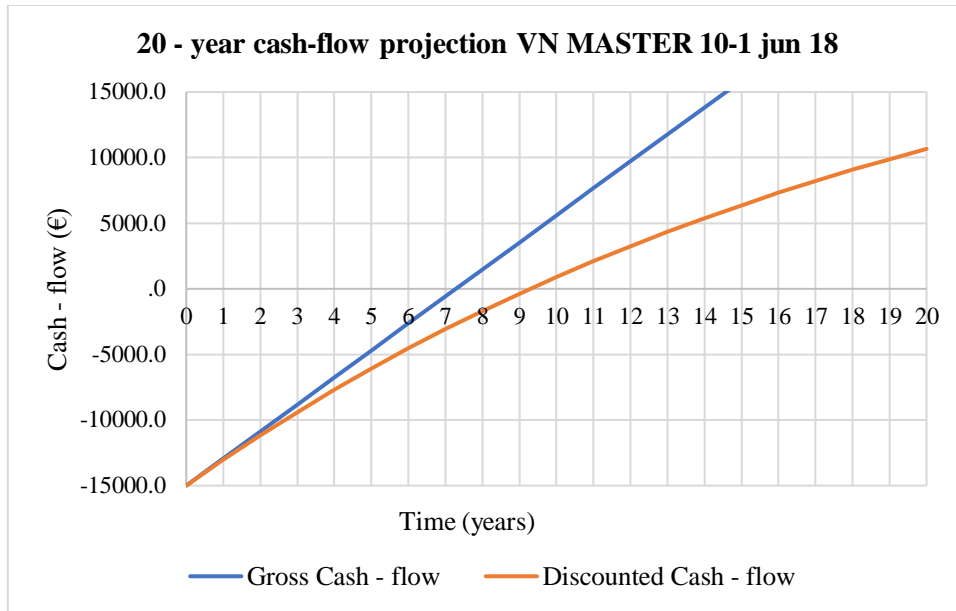


Figure 5.14 - Gross and Discounted Payback Time (code VN MASTER 10-1 jun 18)

5.4. CONCLUSIONS

In order to assess the behaviour of the micro-cogeneration unit in various transient regimes of operation, 32 laboratory tests were performed. Most of the measurements done were only affected by the errors of the equipment used, adhering to their class of precision. The exception to the above consideration is the manner of measuring the fuel consumption, which represented a major source of incertitude.

Due to a low correlation between the regression functions found and the measured data of the fuel mass flow, a transitory mathematical model of the fuel mass flow was carried out. The model was applied to 32 tests conducted in the iCube laboratory “Climatherm”. The simulations of transient regimes have showed that the uncertainty related to the consumption of fuel in the form of wood pellets is significant.

The mathematical model used was that of an inverse algorithm, in which for each of the 32 tests the following were considered:

- the input data considered was the production of power, the production of thermal power, the temperatures measured by the sensors inside the micro-cogeneration unit, on the path of the flue gas, from the combustion chamber to the exhaust, as well as different points of the circuit connecting the unit to the consumer;
- the calculated output was the corresponding consumption of fuel, under the form of wooden pellets.

The difficulties linked to the nonlinearities induced by the variation of different physical properties, in accordance to temperature (namely the specific heat of at constant pressure of the

combustion air and the components of the flue gas and the specific heat of the agent - water), used in simulation to determine the enthalpies, were overcome using the Gauss - Seidel method.

The financial performances of investments have been detailed. Considerations regarding the indices used to economically assess the profitability of an investment have been defined and analysed.

Based on the results of the mathematical model used to simulate the transient regimes of the μ CHP operation, for the selected transient tests, the overall fuel consumptions of the μ CHP and the related generated amounts of electricity and heat delivered from the μ CHP to the end user have been determined and are indicated in Table 5.22.

Table 5.22 - Fuel consumption and generated power and heat for the selected transient tests

Test code	Electricity	Power	Thermal Energy	Heat	Fuel
-	kJ	kW	kJ	kW	kW
VN MASTER 10-1 jun 18	15,940	0.822	198,396	9.725	19.358
VN MASTER 10-1 mar 07	8,153	0.686	95,990	9.466	18.857
VN MASTER 14-3 jun 11	9,367	0.858	120,685	12.416	31.916
VN MASTER 10-1 jun 25	7,993	0.560	140,387	8.863	19.614

For the concerned tests, the results of the mathematical model have been used to determine the investment performances which are indicated in Table 5.23.

Table 5.23 - Investment performances for the selected transient tests.

Test code	Gross Payback Time	Discounted Payback Time	Internal Rate of Return	Discounted Net Present Value
-	years	years	%	€
VN MASTER 10-1 jun 18	7.2	9.3	12.4	10,666
VN MASTER 10-1 mar 07	8.0	10.5	10.8	8,231
VN MASTER 14-3 jun 11	9.5	13.5	8.4	4,596
VN MASTER 10-1 jun 25	10.5	15.5	7.0	2,704

In correlation with the proposed input data showed in Table 5.9, the results of the economic simulation of the chosen tests have revealed that, in transient regimes of operation, the load factor of the micro-cogeneration unit is an important factor when the same investment conditions are assured. Among the analysed transient tests, the results of the test code VN MASTER 10-1 jun 18 and the test code VN MASTER 10-1 mar 07 are supporting this conclusion.

CONCLUSIONS

The European Commission commitment regarding the emission reduction with 55% by 2030, ask for a concert of actions and measures among which the promotion of the decarbonisation of heating and cooling plays a central role.

This is due to the current situation in which heating and cooling account for about 80% of the total energy consumed in residential buildings, out of which two thirds of this energy came from fossil fuels, respectively 76,5%.

At European Union level, the biomass energy potential within the Member States with a significant importance varies between 500 and 1000 GWh/year (respectively, 1800 - 3600 TJ/year), and in few cases, more. In the concerned countries for this doctoral thesis, the solid biomass represented 42.3% of primary renewable energy production in France (2017), and in Romania, about 65% from the country's potential in renewable energy production.

In both countries, if it overwhelmingly serves more as a source of heat, it is also used for the production of electricity: the steam generated by combustion drives turbines generating power.

Because the stand-alone systems account for 88% from the European Union overall heat supply market, the production of heat from solid biomass and, additionally, the simultaneous generation of electricity within such systems was taken into consideration.

Various bibliographic references related to theoretical and applicative works recently carried out have revealed that biomass, the micro-cogeneration and the Stirling engine represent altogether an opportunity to be capitalised.

This is exactly what the present doctoral thesis was supposed to deliver. Because an extended use of a technical approaches relying on the solid biomass combustion micro-cogeneration system equipped with a Stirling engine towards the fulfilment of European Commission requirements, such technology is experimentally and theoretically investigated.

To frame this work, in the first phase heat transfer notions were presented, the ideal Carnot and Stirling cycles are overviewed, the types of Stirling engines are listed, several specific parameters and properties are mentioned, and calculus related to the Stirling engine irreversible cycle with regenerator were provided.

The second phase considers the solid biomass as a viable replacement fuel for coal, even if the lower heating values are superior to lignite (14,654 - 19,305 kJ/kg or less) and somewhat comparable to the sub-bituminous B (22,097 - 24,423 kJ/kg) and comparable to the sub-bituminous C (19,306 - 22,097 kJ/kg), for example.

Additionally, it was taken into account the situation where the solid biomass fuel was to be purchased from a supplier. If the resource is available on-site, the transportation costs are avoided, increasing the profit.

Considering the biomass, the micro-cogeneration and the Stirling engine to put these all together, it is in line with the provisions of the new strategy to boost renovation called 'A Renovation Wave for Europe - Greening our buildings, creating jobs, improving lives', which are strongly considering the decarbonisation and the integration of renewables, and are considering that to generating energy from renewable sources produced on-site or nearby is vital.

A Romanian furniture company already used an O.R.C. cogeneration system to transform its wood biomass from waste to heat and power. A perspective to be investigated is the addition of an electric truck which would serve a cheap means of transport and an energy buffer to be charged by the O.R.C. facility.

Simple economics demonstrate that investing in the promotion of biomass towards the decarbonisation of district and individual heating is feasible. In certain situations, when taking into consideration the European common biomass market, particularities among the EU citizens in terms of annual income, could require additional public support in order to preserve this heat supply available, accessible, affordable and profitable.

When looking deeper into the domain of stand-alone heating systems which account for 88% out of EU total systems delivering heat, the promotion of cogeneration on biomass at individual level makes a lot of sense due to the favourable effect of transforming the power and heat consumers into prosumers.

The solid biomass combustion micro-cogeneration could contribute to tackle the challenges for the energy demand in the residential sector. The premises are presently attractive because the biomass-based micro-cogeneration systems are becoming increasingly popular.

To remain technologically simple and effective, the thermochemical conversion of biomass through a direct grid combustion technology and the micro-cogeneration systems equipped with Stirling engines are considered.

The solid biomass is a viable replacement for coal, because its lower heating values are superior to lignite and somewhat comparable to the sub-bituminous B and comparable to the sub-bituminous C. It was taken into account the situation where the biomass fuel was to be purchased from a supplier.

If the resource is available on-site, the transportation costs are avoided, increasing the profit. This is in line with the provisions of the new EC strategy to boost building renovation, which are strongly considering the decarbonisation and the integration of renewables, this referring to energy from renewable sources produced on-site or nearby are vital. In the case of purchasing biomass, fuel availability could be solved by coupling a biomass fired cogeneration unit to an electric vehicle. A furniture company used an O.R.C. to transform its wood biomass from waste to heat and power. A perspective to be further investigated is the addition of an electric truck which would serve a cheap means of transport and an energy buffer to be charged by the O.R.C. facility.

Simple economics demonstrate that investing the use of biomass towards the decarbonisation of district and individual heating is feasible. In certain situations, when taking into consideration the European common biomass market, particularities among the EU citizens in terms of annual

income, could require additional public support in order to preserve this heat supply available, accessible, affordable and profitable.

The promotion of cogeneration on biomass at individual level makes a lot of sense due to the favourable effect of transforming the power and heat consumers into prosumers. The domain of stand-alone heating systems which account for 88% of the EU total systems delivering heat should be further targeted.

Towards the achievement of the decarbonisation and the integration of renewables to the stand-alone heating systems level, a biomass Stirling micro cogeneration device has been tested in order to assess its performances.

A dynamic model based on experimental investigations has been developed to evaluate its output thermal power and power efficiencies. For the tests conducted at the INSA Strasbourg, iCube Laboratory, the ÖkoFEN micro-cogeneration unit, a total of 9 configurations have been chosen: 3 thermal agent flow rates times 3 thermal power outputs. The temperature of the thermal agent fuelling the household end-user with domestic hot water was configured in the studied μ CHP unit to be 60 °C.

It has been observed that the rise of temperature of the domestic hot water must be correlated with an incapability of the thermal agent flow value to take over and to evacuate the amount of thermal power produced by the machine. This determines the accumulation of heat inside the μ CHP unit and leads to a rise in temperature, which triggers a self-guarding mechanism of the machine when it reaches 75 °C.

It is to be noted that the compared to the thermal agent temperature measured at the outlet to the machine, the temperature of the agent inside the μ CHP unit had 1 °C to 2 °C more than what was measured. The linear loss of temperature explains why the partial load mode was enabled when the thermal agent at the outlet had values of 73 °C to 74 °C.

The values of the stable temperatures reached by the thermal agent and the time to reach said values, as well as whether the configuration yielded in an automatic enabling of partial load functioning due to an insufficient heat evacuation have been obtained. Generally, for all configurations, the bigger the flow was, the better the heat evacuation from the μ CHP unit was, therefore the lower the stable temperature was.

With a good heat evacuation, the temperature will ideally stay around 60 °C, with a medium-quality heat evacuation, the temperature will stay below 75 °C and with a poor-quality heat evacuation, the temperature will go over 75 °C, resulting in a partial load functioning.

One of the premises of the delivered work was that only one configuration would be manually applied at a time, per each test. However, if this premise were to be modified and the machine could switch from one configuration to another, a higher thermal power output could be configured with a lower thermal agent flow in order to reach the desired temperature as fast as possible, for then to switch to a more stable configuration.

The best suited configuration to power-up the system as fast as possible, although it has the lowest efficiency, has been identified. After reaching the 60 °C value, the configuration could be switched to the maximum flow rate for functioning while having the best total efficiency.

For the summer season, when the end-user requirement for heat would diminish a lower thermal power configuration has been observed. Similarly, for this configuration, the start at the minimum flow rate would be recommended to get to the nominal temperature of 60 °C, after which the flow rate would be changed to maximum.

The value of 60 °C has been chosen because it is the configured end-user domestic hot water temperature. On the power generation side, the value of 0.8 kW_{el} has been chosen as 80 % of the nominal power generation capacity of the μCHP unit, because not all configurations reach 1 kW_{el} in power generation, while all configurations produce more than 0.8 kW_{el}.

Based on these operational characteristics, an effective algorithm for the operation of the micro-cogeneration unit has been carried out and thorough explanations about how it works have been provided.

Further studies may be investigate coupling the μCHP unit with a thermal storage unit, in order to see what regime of functioning would be best to heat up a large tank of water and then to maintain its temperature.

The speed of heating up the thermal storage tank would be relevant in function of its dimensions which are dependent on the domestic hot water consumption of the household residents.

An electrical storage unit would also be relevant in the case that the household would have installed a rooftop photovoltaic system.

Since the studied μCHP unit is supposed to cover the baseload of a household demand of electricity, a photovoltaic-thermal (PVT) and battery system would be a relevant addition to the goal of energy self-sufficiency.

In the mathematical model, different wood species have been fully described and the determination of the lower heating value in each case led to results in excellent agreement with those found in the literature.

This is an important issue because the lower heating values were inputs for all subsequent calculus of the model.

When considering the energy balance in the combustion chamber, the mass of air which enters the combustion chamber and of heat inlet of air, respectively the flue gas real specific wet volume and the heat amount generated by the fuel entering the combustion chamber have been duly calculated.

For each wood specie, the adiabatic combustion temperature calculated by using volumes and enthalpies were obtained.

Additionally, the adiabatic combustion temperature by using masses and enthalpies have been calculated.

Three different methods were deployed: use of air and flue gas masses calculation at wet ash free state, use of Gaskell equation, and use of Howard Shomate Equation and JANAF coefficients.

The comparison of results has showed an excellent agreement between the combustion adiabatic temperature calculated values.

Combustion power calculus to determine the thermal powers entering and exiting combustion and the thermal power of flue gas resulted from the combustion process have been performed. In terms of Stirling Engine key points, power and energy calculus, the Stirling engine has been modelled in accordance to the theoretical model of a Stirling engine, based on formulas found in literature.

The Stirling engine model had the same points of temperature, volume and pressure for all species and it is an important element of the installation, since power is more valuable than thermal power in terms of price.

Therefore, it was found as ideal that it runs at full load for the same for all types of wood. All the Stirling cycle operational performances were carried out.

In the mathematical model has been also considered that the useful thermal power delivered to the end user should be calculated based on the thermal power input and output of the Stirling cycle, which are known, as well as the power of the flue gasses transferring the heat to the Stirling engine.

The water is initially heated by the thermal power leaving the Stirling cycle and, in a second phase, the thermal power of flue gasses that remains is transferred to the water fuelling the consumer before the flue gasses are exhausted into the atmosphere.

For all air excess configurations, it was observed that the functioning of the Stirling engine and the power generation starts to be in a partial load from a maximum limit, which smaller that in the case of pellets which still keep a functioning at nominal load at a greater fuel moisture.

For different fuel moistures has revealed the mass flow dependency of domestic hot water to the fuel moisture and that the thermal power delivered to the user is also strongly influenced by the fuel moisture.

The comparison of efficiencies in different configurations ($\lambda=i$, $w=j$) has pointed out that the efficiencies describing the overall performances of the solid biomass micro-cogeneration unit with Stirling motor are appropriate for a dry fuel in order to get the best useful power outputs.

If thermal power is not entirely needed, the fuel may have the observed high moisture level for the Stirling engine to function at nominal load.

The beforementioned case is intuitively the one of summer season, where the thermal energy need is lower than that of the winter season.

It is therefore crucial to use dry fuel in the cold seasons, to obtain the maximum thermal power available, provided that the system has not been over-dimensioned for the consumer home.

If it is the case, lower quality fuels in terms of moisture can be used, because their thermal output will not create a surplus of thermal power.

A study of the consumer needs is necessary, to better determine the fit of fuel quality to the μ CHP system in function of the consumer's necessities, work which will be done in the following chapter. In order to assess the behaviour of the micro-cogeneration unit in various transient regimes of operation, 32 laboratory tests were performed.

Most of the measurements done were only affected by the errors of the equipment used, adhering to their class of precision. Therefore, the manner of measuring the fuel mass consumption represented a major source of uncertainty. To limit this uncertainty, regression functions for the fuel consumption have been used but due to a low correlation with the measured data, a transitory mathematical model of the fuel mass flow was carried out.

The simulations of transient regimes applied to 32 tests conducted in the iCube laboratory "Climatherm" have confirmed the significant uncertainty related to the consumption of fuel in the form of wood pellets.

In each of the 32 tests performed, an inverse algorithm based mathematical model was used.

The model input data were considered the production of power, the production of thermal power, the temperatures measured by the sensors inside the micro-cogeneration unit, on the path of the flue gas, from the combustion chamber to the exhaust, as well as different points of the circuit connecting the unit to the consumer. The calculated output was the corresponding consumption of fuel, under the form of wooden pellets.

The difficulties linked to the nonlinearities induced by the variation of different physical properties, in accordance to used in simulation to determine the enthalpies, were overcome using the Gauss - Seidel method.

To deliver elements of economic assessment of the μ CHP operation in transient regimes, the financial performances of investments have been detailed. Considerations regarding the indices used to economically assess the profitability of an investment have been defined and analysed.

Based on the results of the mathematical model used to simulate the transient regimes of the μ CHP operation, for the selected transient tests, the overall fuel consumptions of the μ CHP and the related generated amounts of electricity and heat delivered from the μ CHP to the end user have been determined. For the concerned tests, the results of the mathematical model have been further used to calculate the investment performances of the μ CHP.

In correlation with the proposed input data, the results of the economic simulation of the chosen tests have revealed that, in transient regimes of operation, the load factor of the micro-cogeneration unit is an important factor when the same investment conditions are assured. Among the analysed transient tests, the results of two out of four are supporting this conclusion.

As perspectives, the continuation of this work may explore different other directions of research, the immediate possible being:

- coupling the micro-cogeneration unit with thermal and electrical storage devices;
- realization of a 100% renewable hybrid system: biomass micro-cogeneration and solar collectors;
- the system exergetic analysis.

ABBREVIATIONS

μ CHP	micro - combined heat and power
ASTM	American Society for Testing and Materials
BIGCHP	biomass integrated gasification combined heat and power
BIOBIB	Database for Biofuels
CHP	combined heat and power
COM	Communication
EC	European Commission
EN	European Norm
EU	European Union
IKA	Janke & Kunkel GmbH & Co.
INSA	Institut National des Sciences Appliquées
ISO	International Organization for Standardization
JANAF	Joint, Army, Navy, Air Force
NI	National Instruments
ORC	Organic Rankine Cycle
PC	Personal Computer
PVT	photovoltaic - thermal
SI	International System of Units
SKM	Standard Keramik Muffel mit Klapptür
SLW	Suszarka Laboratoryjna
TBT	Technical Barriers to Trade
TNO	Nederlandse Organisatie voor Toegepast Natuurwetenschappelijk Onderzoek
TPES	Total Primary Energy Supply
TRNSYS	Transient System Simulation Tool
USB	Universal Serial Bus
WTO	World Trade Organization

BIBLIOGRAPHY

Books, Articles, Legislation, Standards, Regulations, Methodologies

1. * * *, *A Renovation Wave for Europe – greening our buildings, creating jobs, improving lives*, Communication from the Commission to the European Parliament, the Council, the European Economic and Social Committee and the Committee of the Regions, Com (2020) 662 final, European Commission, Brussels, 14 October 2020.
2. * * *, ASTM E871-82(2019), *Standard Test Method for Moisture Analysis of Particulate Wood Fuels*, ASTM International, West Conshohocken, PA, 2019, <https://www.astm.org/Standards/E871.htm>.
3. * * *, Database for the physico-chemical composition of (treated) lignocellulosic biomass, micro- and macroalgae, various feedstocks for biogas production and biochar, TNO, <https://phyllis.nl/Browse/Standard/ECN-Phyllis#biomass>.
4. * * *, *ISO 589:2008 Hard coal - Determination of total moisture*, International Organization for Standardization Switzerland, 2008, <https://www.iso.org/standard/45370.html>.
5. * * *, *NIST Chemistry WebBook*, SRD 69, National Institute for Standards and Technology, U.S. DOC, <https://webbook.nist.gov/chemistry/name-ser/>.
6. * * *, *ÖkoFEN Pellematic Condens_e Technical Data* (accessed on 20 August 2020) http://www.ÖkoFEN-e.com/en/pellematic_smart_e/, 2017.
7. * * *, Solid Biofuels Barometer, A study carried out by the EURObserv'er, december 2020, <https://www.eurobserv-er.org/category/all-solid-biomass-barometers/>.
8. Alakangas, E., *New European Pellets Standard-EN 14961-1*, Finland, 2010, http://www.infobio.ru/sites/default/files/Alakangas_Pellet_standard_EN14961-1.pdf.
9. Altawell, N., *The Selection Process of Biomass Materials for the Production of Bio-Fuels and Co-firing*, IEEE Press - Wiley, John Wiley & Sons Inc, ISBN: 978-1-118-54266-8, New York, 2014.
10. Aoun, B., *Micro combined heat and power operating on renewable energy for residential*, Thèse de doctorat, France: École Nationale Supérieure des Mines de Paris, 2008.
11. Arashnia, I., Najaf, G., Ghobadian, B., Yusaf, T., Mamat, R., Kettner, M., *Development of micro-scale biomass-fuelled CHP system using Stirling Engine*, Energy Procedia, vol. 75, pp. 1108-1113, 2015.
12. Badea, A., Necula, H., ș.a., *Surse regenerabile de energie*, Editura Agir, ISBN 978-973-720-469-1, București, Romania, 2013.

13. Barbu, M., Darie, G., Siroux, M., *Analysis of a Residential Photovoltaic-Thermal (PVT) System in Two Similar Climate Conditions*, Energies 2019, Volume 12.
14. Bartela, Ł., Kotowicz, J., & Dubiel-Jurgaś, K., *Investment risk for biomass integrated gasification combined heat and power unit with an internal combustion engine and a Stirling engine*. Energy, 2018, Volume 150, pp. 601–616.
15. Bartela, Ł., Kotowicz, J., Remiorz, L., Skorek-Osikowska, A., Dubiel, K.. *Assessment of the economic appropriateness of the use of Stirling engine as additional part of a cogeneration system based on biomass gasification*, Renewable Energy 2017, Volume 112, pp. 425-443.
16. Bernotat, K., Sandberg, T., Biomass fired small-scale CHP in Sweden and the Baltic States: a case study on the potential of clustered dwellings, Biomass and Bioenergy, vol. 27, pp. 521-530, 2004.
17. Bianchi, M., De Pascale, A., Melino, F., Performance analysis of an integrated CHP system with thermal and Electric Energy Storage for residential application, Applied Energy, vol. 112, pp. 928-938, 2013.
18. Biedermann, F., Carlsen, H., Obernberger, I., Schöch, M., *Small-scale CHP Plant based on a 75 kWel Hermetic Eight Cylinder Stirling Engine for Biomass Fuels - Development, Technology and Operating Experiences*, 2nd World Conference and Exhibition on Biomass for Energy, Industry and Climate Protection 10-14 May 2004, Rome, Italy.
19. Bouvenot J-B., Andlauer B., Stabat P., Marchio D., Flament B., Latour B., Siroux M., *Gas Stirling engine μ CHP boiler experimental data driven model for building energy simulation*, Energy and Buildings, 84, 113-117 (2014).
20. Bouvenot, J.-B., Etudes expérimentales et numériques de systèmes de micro-cogénération couplés aux bâtiments d'habitation et au réseau électrique, Thèse de Doctorat, École Doctorale MSII, Laboratoire ICube – Département Mécanique (D-M), Université de Strasbourg, 2015.
21. Brătianu, C., Voronca, M.-M., Cojocia, L., *METODE NUMERICE •APLICAȚII•*, Editura TENSOR, București, ISBN 973 - 98203 - 2 - 8, 1998.
22. Brou, S., Modélisation et commande d'un système de cogénération utilisant des énergies renouvelables pour le bâtiment, Thèse de doctorat, France : Université Paris Saclay, 2015.
23. Cardozo, E., & Malmquist, A., *Performance comparison between the use of wood and sugarcane bagasse pellets in a Stirling engine micro-CHP system*, Applied Thermal Engineering, 2019, Volume 159, 113945.
24. Cardozo, E., Erlich, C., Malmquist, A., & Alejo, L., *Integration of a wood pellet burner and a Stirling engine to produce residential heat and power*, Applied Thermal Engineering 2014, Volume 73(1), pp. 671 - 680.
25. Cardozo, E., Erlich, C., Malmquist, A., Alejo, L., *Integration of a wood pellet burner and a Stirling engine to produce residential heat and power*, Applied Thermal Engineering, vol. 73, pp. 671-680, 2014.
26. Chase, M.W., Jr., *NIST-JANAF Thermochemical Tables*, 4th Edition, Journal of Physical and Chemical Reference Data Monographs, Monograph 9, 1998, 1-1951,

- <https://www.nist.gov/srd/journal-physical-and-chemical-reference-data-monographs-or-supplements>.
27. Cruceru, M., Dragostin, C., Voronca, M-M., Voronca, S.-L., *Analysis of a biomass fuelled cogeneration plant with ORC technology*, Proceedings of the Fourth International Symposium on Energy from Biomass and Waste, 12-15.11, ISBN 978-88-6265-006-9, San Servolo, Venice, Italy, pp. 329-326, 2012.
 28. Cruceru, M., Voronca, M-M., Voronca, S.-L., *Promotion of Energy Efficiency and Renewable Energy Sources at Local Level. Case Study: Municipal Public Outdoor Lighting System*, Advances in Environment Technologies, Agriculture, Food & Animal Science, Proceedings of the 2th International Conference on Energy and Environment Technologies and Equipment, ISSN 2227-4359, ISBN 978-1-61804-188-3, WSEAS Press, Braşov, România, pp. 162-167, 2013.
 29. Damien, A., *La biomasse énergie : Définition, Ressources et Usages*, Dunod, Paris, 2008.
 30. Damirchi, H., Najafi, G., Alizadehnia, S., Mamat, R., Nor Azwadi, C. S., Azmi, W. H., Noor, M.M., *Micro Combined Heat and Power to provide heat and electrical power using biomass and Gamma-type Stirling engine*, Applied Thermal Engineering 2016, Volume 103, pp. 1460–1469.
 31. Damirchi, H., Najafi, G., Alizadehnia, S., Mamat, R., Sidik, N. A. C. C., Azmi, W. H., Noor, M. M., *Micro Combined Heat and Power to provide heat and electrical power using biomass and Gamma-type Stirling engine*, Applied Thermal Engineering, vol. 103, pp. 1460-1469, 2016.
 32. Deetlefs, I.N., *Design, simulation, manufacture and testing of a free-piston Stirling engine*, Master Thesis, Department of Mechanical and Mechatronic Engineering, Stellenbosch University, South Africa, 2014.
 33. Deglise, X., *Les conversions thermochimiques du bois*, Revue Forestière Française, pp. 249-270, 1982.
 34. Derviş, E., Çalışkan, S., *The examination of performance characteristics of a beta-type Stirling engine with a rhombic mechanism: The influence of various working fluids and displacer piston material*, International Journal of Energy Research 45(9), March 2021, pp. 13726–13747, <https://doi.org/10.1002/er.6702>.
 35. Dobre, C.G, *Contribuții la dezvoltarea unor Metode ale Termodinamicii Ireversibile Inginerești, aplicate în studiul analitic și experimental al mașinilor Stirling și cvasi-Carnot*, Teză de doctorat, Universitatea Politehnica București, Université Paris Ouest Natterre La Défense, 2012.
 36. Dong, Sh., Shen, G. Xu, M. Zhang, Sh., An, L., *The effect of working fluid on the performance of a large-scale thermoacoustic Stirling engine*, Energy, Volume 181, Elsevier, 2019, pp. 378-386.
 37. Drake, B.G., *Rising sea level, temperature, and precipitation impact plant and ecosystem responses to elevated CO2 on a Chesapeake Bay wetland: review of a 28-year study*, Global Change Biology, Volume 20, Issue 11, pp. 3329 - 3343, 2014, <https://doi.org/10.1111/gcb.12631>
 38. Egas, J., Clucas, D. M., *Stirling Engine Configuration Selection*, Energies 2018, 11, pp. 584, doi:10.3390/en11030584

-
39. Eggleston, H.S., Buendia, L., Miwa, K., Ngara, T. and Tanabe, K. (eds), *2006 IPCC Guidelines for National Greenhouse Gas Inventories*, IPCC National Greenhouse Gas Inventories Programme, IGES, Kanagawa, Japan, 2008, <https://www.ipcc-nggip.iges.or.jp/>
 40. El Ghayaly, Z. M., Stoian, M. (conducător științific), *Evaluarea eficienței economice a proiectelor de investiții în industria mobilei în Egipt*, Teză de doctorat, Academia de Studii Economice, Catalog online, <http://www.biblioteca.ase.ro/catalog/>, București, pp. 86 - 120, 2005.
 41. Evans, A., Strezov, V., Evans, T.J., *Sustainability considerations for electricity generation from biomass*, Renewable and Sustainable Energy Reviews, vol. 14, pp. 1419-1427, 2010.
 42. Frăsineanu, C., *Perfecționarea metodelor de evaluare a patrimoniului*, Curs digital, Academia de Studii Economice, Biblioteca Digitală, <http://www.ase.ro/biblioteca/>, București, 2005.
 43. Garcia-Maraver, A., Perez-Jimenez, J.A., *Biomass Pelletization. Standards and Production*, ISBN. 978-1-78466-062-8. ISBN. 978-1-78466-063-5, Granada, Spain, 2015.
 44. Garnier, J.-Y., *Energy Statistics Manual*, International Energy Agency, Organisation for Economic Co-operation and Development, 2004, https://ec.europa.eu/eurostat/ramon/statmanuals/files/Energy_statistics_manual_2004_EN.pdf.
 45. Gaskell, D.R., *Introduction to the Thermodynamics of Materials*, 4th Edition, Taylor & Francis Books, Inc., New York • London, ISBN 1-56032-992-0, 2003, <https://gateformme.files.wordpress.com/2017/04/introduction-to-thermodynamics-of-materials-by-david-r-gaskel.pdf>.
 46. Giordano, N., *College Physics: Reasoning and Relationships*, Cengage Learning, 2009, pp. 510, ISBN 978-0-534-42471-8.
 47. Gliński M., Bojesen C., Rybiński W., Bykuć S., *Modelling of the Biomass μ CHP Unit for Power Peak Shaving in the Local Electrical Grid*, Energies, 12(3), 458 (2019)
 48. Gras, P., *Les moteurs à air chaud ou moteurs a apport de chaleur externe*, Ambérieu en Bugey, France, 2015, ISBN : 978-2-9537338-1-5
 49. Hargreaves, C.M., *The Philips Stirling engine*, Amsterdam, New York, Elsevier, New York, NY, U.S.A., 1991, ISBN-13: 978-0444884633, ISBN-10: 0444884637.
 50. Hiegl, W., Janssen, R., Pichler, W., *Advancement of pellets-related European Standards*, EIE programme (EIE/06/020/SI2.448557) Development and promotion of a transparent European Pellets Market Creation of a European real-time Pellets Atlas, Munich, Vienna, 2009, <http://bape.com.pl/wp-content/uploads/2014/09/Advancement-of-pellets-related-European-standards.pdf>.
 51. Horbaniuc, B, Dumitrașcu, Gh., *Procese de ardere*, Editura Politehniun, Iași, 2008.
 52. Invernizzi, C.M, *Stirling engines using working fluids with strong real gas effects*, Applied Thermal Engineering, Elsevier, 30, 2010, pp. 1703-1710.
-

53. Jones S. R., Beardmore J., Gillott M., Boukhanouf R., Walker G., *A Control Methodology for Building Energy Management Systems (BEMS)*, Heat Networks with Distributed Generation. Energy Procedia, 153, 2018, pp.295–302.
54. Katona, B., Laza, T., *The technical applicability of Stirling engines in a Hungarian village*, Chemical Papers 2018. Volume 72, pp. 3093–3103.
55. Kimming, M., Sundberg, C., Nordberg, Å., Baky, A., Bernesson, A., Norén, O., Hansson, A. P., *Biomass from agriculture in small-scale combined heat and power plants - A comparative life cycle assessment*, Biomass and Bioenergy, vol. 35, pp. 1572-1581, 2011.
56. Kirillin, V. A., Sychev, V. V., Sheindlin, A. E., *Engineering thermodynamics*, Mir Publishers · Moscow, 1976.
57. Kolin, I, *Stirling Motor: History-Theory-Practice*, Inter University Center, Dubrovnik, Croatia, 1991, pp. 200.
58. Köppen, J., *Toquenatch Creek Cedar Kayak*, Powell River BC, Canada, <http://www.cedar-strip.com/>, <https://cedarstripkayak.wordpress.com/lumber-selection/162-2/>
59. Leca, A., Prisecaru, I., *Proprietăți termofizice și termodinamice • Solide, lichide, gaze*, volumul II, Editura Tehnică, București, 1994.
60. Lee, S.J., *Clarifying the uses of heating values*, edited by Professor Anthony K. Lau, Chemical and Biological Engineering, Canadian Journal of Chemical Engineering, 2016, <https://open.library.ubc.ca/media/download/pdf/42591/1.0343474/4>.
61. Malamatenios, Ch. (coordonator), Vezirigianni, G., Grepmeier, K., *Energii regenerabile & Eficiența energetică: ghid de instruire*, Editura NicVox, ISBN (13) 978-973-8489-37-0, București, 2007.
62. Mameri, F., *Caractérisation multi-physique et multi-échelle d'une installation de conversion d'énergie : application à une unité de cogénération biomasse*, Thèse de doctorat, France : Université Polytechnique Hauts-de France Valenciennes, 2018.
63. Maraver, D., Sin, A., Royo, J., Sebastián, F., *Assessment of CHP systems based on biomass combustion for small-scale applications through a review of the technology and analysis of energy efficiency parameters*, Applied Energy, vol. 102, pp. 1303-1313, 2013.
64. Mărculescu, C., *Valorificarea energetică a combustibililor de suprafață • curs*, suport de curs în format electronic, 102p, Universitatea Politehnica București, 2017.
65. Martinez S., *Etudes expérimentales et numériques d'un micro-cogénérateur solaire - Intégration à un bâtiment résidentiel*, Thèse de doctorat, Université de la Rochelle, France, 2018.
66. Monteiro, E., Moreira, A. N., Ferreira, S., *Planning of micro-combined heat and power systems in the Portuguese scenario*, Applied Energy, vol. 86, pp. 290-298, 2009.
67. Motta, L. I., Miranda, T. N., Regin, F. R., *Biomass gasification in fluidized beds: A review of biomass moisture content and operating pressure effects*, Renewable and Sustainable Energy Reviews, vol. 94, pp. 998-1023, 2018.

-
68. Otepka, P., *Guidebook on Local Bioenergy Supply Based on Woody Biomass*, Training material by BE2020+; Metla and VTT, Promotion of Regional Bioenergy Initiatives IEE/10/470/SI2.593725, Co-funded by the Intelligent Energy Europe Programme of the European Union, ISBN: 978-1-938681-99-8, Scientific & Academic Publishing, USA, 2013, pp. 60, <http://www.sapub.org/book/978-1-938681-98-1.html>.
 69. Park, B.-S., Usman, M., Imran, M., & Pesyridis, A., *Review of Organic Rankine Cycle experimental data trends*, Energy Conversion and Management 2018, Volume 173, pp. 679–691.
 70. Peacock, A.D., Newborough, M., *Impact of micro-CHP systems on domestic sector CO2 emissions*, Applied Thermal Engineering, vol. 25, pp. 2653-2676, 2005.
 71. Pop, M. G., Leca, A., Prisecaru, I., *Tabele, nomograme și formule termotehnice • Îndrumar*, Editura Tehnică, București, 1987.
 72. Popa, B., (coordinator), *Manualul Inginerului Termotehnician*, volumul I, Editura Tehnică, București, 1986.
 73. Qiu, S., Gao, Y., Rinker, G., & Yanaga, K., *Development of an advanced free-piston Stirling engine for micro combined heating and power application*, Applied Energy 2019, Volume 235, pp. 987–1000.
 74. Radovič, L., *Chemistry and Physics of Carbon*, Volume 30, CRC Press, 2007, ISBN (Electronic) 9781420042993, <https://doi.org/10.1201/9781420042993>.
 75. Ražnjević, K., Ștefănescu, D. (adaptare și traducere), *Tabele și diagrame termodinamice*, Editura Tehnică, București, 1978.
 76. Reisinger, K., Haslinger, C., Herger, M. Hofbauer H., *BIOBIB - A database for biofuels*, Institute of Chemical Engineering, Fuel and Environmental Technology, University of Technology Vienna, Austria, 1996, <http://cdmaster2.vt.tuwien.ac.at/biobib/wood.html>
 77. Rohsenow, W.M., *Handbook of Heat Transfer*, Edited by Warren M. Rohsenow & James P. Hartnett, McGraw - Hill, 1973, ISBN 10: 0070535760 / ISBN 13: 9780070535763
 78. Românu, I., Vasilescu, I., *Eficiența economică a investițiilor și a capitalului fix*, Editura Didactică și Pedagogică, București, pp. 125 - 127, 1993.
 79. Saidura, R. Abdelaziz, E. A., Demirbas, A., Hossain, M. S., and Mekhilef, S., *A review on biomass as a fuel for boilers*, Renewable and Sustainable Energy Reviews, vol. 15, pp. 2262-2289, 2011, <https://doi.org/10.1016/j.rser.2011.02.015>.
 80. Sarkar, D., *Thermal Power Plant · Design and Operation*, 1st Edition, Elsevier, 2015, pp. 1 - 37, doi:10.1016/b978-0-12-801575-9.00001-9/e978-0-12-801755-5.
 81. Sartor, K., Dewallef, P., *Integration of heat storage system into district heating networks fed by a biomass CHP plant*, Journal of Energy Storage, vol. 15, pp. 350-358, 2018.
 82. Sartor, K., Quoilin, S., Dewallef, P., *Simulation and optimization of a CHP biomass plant and district heating network*, Applied Energy, vol. 130, pp. 474-483, 2014.
-

83. Shomate Howard, C., *A Method for Evaluation and Correlating Thermodynamic Data*, The Journal of Physical Chemistry 1954, Vol. 58 No. 4 April, pp. 368-372, DOI: 10.1021/j150514a018
84. Tomiță, T., Paraipan, L., Gurmăzescu, A., Vanghelescu, A., *Dicționarul de Management al Riscului*, BRM Business Consulting, ISBN: 973-0-03700-0, București, 2004.
85. Torres García, M., Carvajal Trujillo, E., José Antonio Vélez Godiño, J.A., Sánchez Martínez, D., *Thermodynamic Model for Performance Analysis of a Stirling Engine Prototype*, Energies 2018, 11(10), 2655; <https://doi.org/10.3390/en11102655>.
86. Ulloa, C., Míguez, J.L., Porteiro, J., Eguía, P., Cacabelos, A., *Development of a Transient Model of a Stirling-Based CHP System*, Energies 2013, Volume 6, pp. 3115-3133.
87. Urciuolo, M., Chirone, R., Saverio Marra, F., Solimene, R., *Power generation by Stirling engine during fluidized bed combustion of wood pellets*, Combustion Science and Technology 2018, pp. 263–274.
88. Valenti, G., Silva, P., Fergnani, N., Di Marcoberardino, G., Campanari, S., Macchi, E., *Experimental and Numerical Study of a Micro-cogeneration Stirling Engine for Residential Applications*, Energy Procedia, 2014, Volume 45, pp. 1235–1244.
89. van Loo, S., Koppejan, J., (editors), *The Handbook of Biomass Combustion and Cofiring*, Earthscan, ISBN: 978-1-84407-249-1, London • Sterling, VA, 2008, <https://boilersinfo.com/the-handbook-of-biomass-combustion-and-cofiring/>.
90. Voronca Ș-D., Pop, E., Siroux, M., Darie G., *Analysis of Wooden Biomass Use as Renewable Source of Energy in Romania*, 9th International Conference on ENERGY and ENVIRONMENT (CIEM2019), DOI: 10.1109/CIEM46456.2019.8937617, Date Added to IEEE Xplore: Dec 2019, INSPEC Accession Number: 19228480, Publisher: IEEE, Electronic ISBN: 978-1-7281-1532-0.
91. Voronca, M.-M., *Modelarea numerică cu elemente finite a comportării în exploatare a echipamentelor energetice, cu aplicații la aparatele bazate pe transferul de căldură*, Teză de Doctorat, Universitatea 'POLITEHNICA' București, 1997.
92. Voronca, M-M., Voronca, S.-L., Cruceru, M., *Promotion of the Organic Rankine Cycle based Cogeneration: Opportunities and Challenges*, Journal of Sustainable Energy, Volume III - nr. 1, ISSN: 2067-5534, Editura Universității din Oradea, pp. 32 - 38, 2012.
93. Voronca, Ș.-D., Darie, G., Pătrașcu, R., *Biomass O.R.C. Cogeneration - A Case Study*, ISBN 978-1-5386-3943-6/17 ©2017 IEEE, Bucuresti, Romania.
94. Voronca, Ș-D., Pătrașcu, R., Darie G., *Biomass O.R.C. cogeneration - A case study*, 8th International Conference on ENERGY and ENVIRONMENT (CIEM2017), DOI: 10.1109/CIEM.2017.8120777, Date Added to IEEE Xplore: Dec 2017, INSPEC Accession Number: 17412263, Publisher: IEEE, Electronic ISBN: 978-1-5386-3943-6.
95. Voronca, Ș-D., Voronca, M-M., *Promotion of the Organic Rankine Cycle based Cogeneration: A Case Study (C108)*, Proceedings of the 2th CIGRÉ Regional South-

- East European Conference - RSEEC 2014 "Innovation for efficient and effective management, solutions for power system of the future!", October 8th - 10th, 2014, ISSN 2392 - 716X, The Academy of Romanian Scientists Publishing House, Timișoara, România, pp. 259 - 266, 2014.
96. Wolf, J. P., Dong, *Biomass combustion for power generation: an introduction*, Woodhead Publishing, Philadelphia, United States of America, 2013.
97. Wright, L., Boundy, B., Badger, P.C., Perlack, B., Davis, S., *Biomass Energy Data Book: Edition 2*, Oak Ridge National Laboratory, Oak Ridge, Tennessee, U.S. Department of Energy, 2009, <https://www.co.shasta.ca.us/docs/libraries/>
98. Yun, Y. (editor), *Gasification for Low-grade Feedstock*, Institute for Advanced Engineering, IntechOpen Ltd., ISBN: 978-1-78923-288-2, London, 2018.

Internet Pages

- <http://bape.com.pl/wp-content/uploads/2014/09/Advancement-of-pellets-related-European-standards.pdf>.
- <http://cdmaster2.vt.tuwien.ac.at/biobib/wood.html>
- <http://maps.heatroadmap.eu/berndmoller/maps/31157/Renewable-Resources-Map-for-EU28?#>
- http://www.infobio.ru/sites/default/files/Alakangas_Pellet_standard_EN14961-1.pdf.
- http://www.ÖkoFEN-e.com/en/pellematic_smart_e/, 2017.
- <https://boilersinfo.com/the-handbook-of-biomass-combustion-and-cofiring/>
- <https://doi.org/10.1002/er.6702>.
- <https://doi.org/10.1016/b978-0-12-801575-9.00001-9/e978-0-12-801755-5>.
- <https://doi.org/10.1016/j.rser.2011.02.015>
- <https://doi.org/10.1021/j150514a018>
- <https://doi.org/10.1111/gcb.12631>
- <https://doi.org/10.1201/9781420042993>
- <https://doi.org/10.3390/en11030584>
- <https://doi.org/10.3390/en11102655>
- https://ec.europa.eu/clima/policies/eu-climate-action/2030_ctp_en.
- https://ec.europa.eu/energy/topics/energy-efficiency/energy-efficient-buildings/renovation-wave_en.
- https://ec.europa.eu/eurostat/ramon/statmanuals/files/Energy_statistics_manual_2004_EN.pdf.
- https://ec.europa.eu/info/strategy/priorities-2019-2024/european-green-deal_en.
- <https://gateformme.files.wordpress.com/2017/04/introduction-to-thermodynamics-of-materials-by-david-r-gaskell.pdf>.
- <https://phyllis.nl/Browse/Standard/ECN-Phyllis#biomass>.
- <https://webbook.nist.gov/chemistry/name-ser/>
- <https://www.astm.org/Standards/E871.htm>
- <https://www.astm.org/Standards/E871.htm>.
- <https://www.co.shasta.ca.us/docs/libraries/>
- <https://www.eurobserv-er.org/category/all-solid-biomass-barometers/>.
- <https://www.interregeurope.eu/agrores/news/news-article/9613/untapped-potential-of-biomass-energy-in-romania/>
- <https://www.ipcc-nggip.iges.or.jp/>
- <https://www.iso.org/standard/45370.html>.

<https://www.la Tribune.fr/entreprises-finance/la-tribune-de-l-energie-avec-enedis/tout-savoir-sur-la-filiere-biomasse-en-france-814572.html>

<https://www.nist.gov/srd/journal-physical-and-chemical-reference-data-monographs-or-supplements>.

DISSEMINATION OF RESEARCH RESULTS

Published Works

1. Kallio, S., Siroux, M., Voronca, S.-D., *Energy and exergy analysis of a biomass-fuelled micro-CHP unit*, Proceedings of 34th International Conference on Efficiency, Cost, Optimisation, Simulation and Environmental Impact of Energy Systems ECOS-2021, Taormina, Italia, 2021
2. Voronca Ş-D., Pop, E., Siroux, M., Darie G., *Analysis of Wooden Biomass Use as Renewable Source of Energy in Romania*, 9th International Conference on ENERGY and ENVIRONMENT (CIEM2019), DOI: 10.1109/CIEM46456.2019.8937617, Date Added to IEEE Xplore: Dec 2019, INSPEC Accession Number: 19228480, Publisher: IEEE, Electronic ISBN: 978-1-7281-1532-0.
3. Voronca Ş-D., Pop, E., Siroux, M., Darie G., *Technical and economical analysis of wooden biomass use as renewable source of energy for cogeneration purposes in Romania*, Colloque Francophone sur l'Energie COFRET'18, Strasbourg, France, 2018.
4. Voronca, Ş.-D., Darie, G., Pătraşcu, R., *Biomass O.R.C. Cogeneration - A Case Study*, ISBN 978-1-5386-3943-6/17 ©2017 IEEE, Bucuresti, Romania.
5. Voronca, Ş-D., Pătraşcu, R., Darie G., *Biomass O.R.C. cogeneration - A case study*, 8th International Conference on ENERGY and ENVIRONMENT (CIEM2017), DOI: 10.1109/CIEM.2017.8120777, Date Added to IEEE Xplore: Dec 2017, INSPEC Accession Number: 17412263, Publisher: IEEE, Electronic ISBN: 978-1-5386-3943-6.
6. Voronca, Ş-D., Voronca, M-M., *Promotion of the Organic Rankine Cycle based Cogeneration: A Case Study (C108)*, Proceedings of the 2th CIGRÉ Regional South-East European Conference - RSEEC 2014 "Innovation for efficient and effective management, solutions for power system of the future!", October 8th - 10th, 2014, ISSN 2392 - 716X, The Academy of Romanian Scientists Publishing House, Timișoara, România, pp. 259 - 266, 2014.

ANNEXES

Annex 1: Bibliographic study

Annex 1.1 Solid Biofuels Barometer, A study carried out by the EURObserv'er, december 2020, <https://www.eurobserv-er.org/category/all-solid-biomass-barometers/>.



+2.2%
The evolution of inland consumption from solid biofuels in the EU 28 between 2018 and 2019


SOLID BIOFUELS BAROMETER

A study carried out by EuroObserv'ER

106.0 TWh
The electricity production from solid biofuels in the EU 28 in 2019

80.4 Mtoe
The heat consumption from solid biofuels in the EU 28 in 2019

Solid biofuels energy consumption was 2.2% higher in 2019, reaching 102.6 Mtoe in the EU28 countries, according to EuroObserv'ER. Leaving aside the UK, the consumption figure was 94.5 Mtoe and posted a 8% growth. The increment can be ascribed to both a significant rise in the electricity output of several countries and also to about 1.1% of additional heat consumption with or without the UK's consumption.

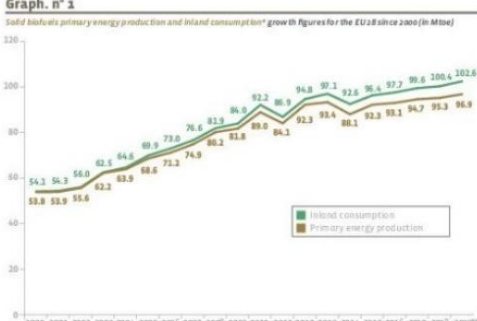


Solid biofuels is an umbrella term for all solid organic components to be used as fuels. They include wood, timber industry by products (wood chips, sawdust, etc.), wood pellets, black liquor from the paper industry, straw, bagasse, animal waste and other substitutable residues including the renewable portion of solid industrial waste. Energy recovery from solid biofuels is mainly used to produce heat and electricity. Charcoal is also an element of solid biomass but is accounted for separately and is not included in the indicators of this barometer; thus, they cover solid biofuels, excluding charcoal. By way of illustration, about 400 kilo of final charcoal energy is consumed in the European Union. Lignocellulosic biomass (cereal straw, forest waste, etc.) can also be converted into 2nd-generation liquid biofuel or gas, such as hydrogen or methane. Biogas output from thermal processes is currently monitored in four European Union countries (Finland, Spain, Italy, and Belgium), amounting to about 1 Gt of gas in 2019. This output is associated with that of biogas and is therefore excluded from the solid biomass energy indicators.

THE CONSUMPTION TREND IS INFLUENCED BY THE CLIMATE CONTEXT

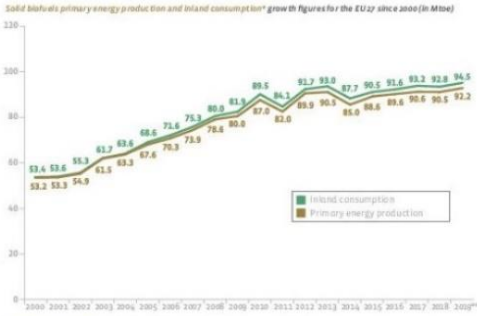
Heat and electricity supply shape the European Union's solid biofuels energy consumption trend. Developments in the main outlet for biomass energy, heat supply, are particularly climate sensitive during the heating season. In recent years, climate change has made a particularly strong impact on the solid biofuels sector and will continue to do so for the foreseeable future. This clouds the readability of governments' actions to encourage the use of solid biofuels for heating purposes. Additionally, the heat energy production indicators do not give due credit to the technological progress made to improve efficiency, domestic heating appliances' combustion efficiency and also that of plants and boiler houses supplying district heating networks. The World Meteorological Organization reports that climate change pursued its

Graph. n° 1
Solid biofuels primary energy production and inland consumption* growth figures for the EU 28 since 2000 (in Mtoe)



Year	Inland consumption (Mtoe)	Primary energy production (Mtoe)
2000	54.2	53.8
2001	54.3	53.9
2002	56.0	55.6
2003	62.7	62.3
2004	62.5	63.9
2005	64.6	65.9
2006	69.9	73.0
2007	70.6	71.3
2008	81.3	74.9
2009	80.2	81.8
2010	86.0	80.6
2011	92.3	84.1
2012	86.9	84.1
2013	94.8	89.4
2014	97.1	88.1
2015	92.6	86.4
2016	97.7	90.8
2017	93.1	84.7
2018	95.3	89.3
2019	102.6	94.9

Solid biofuels primary energy production and inland consumption* growth figures for the EU 27 since 2000 (in Mtoe)



Year	Inland consumption (Mtoe)	Primary energy production (Mtoe)
2000	53.4	53.6
2001	53.3	53.9
2002	55.3	55.9
2003	61.3	61.3
2004	63.3	63.6
2005	63.3	67.6
2006	68.6	71.6
2007	71.3	73.9
2008	75.9	75.9
2009	80.9	80.9
2010	81.9	87.6
2011	84.7	84.7
2012	89.9	90.1
2013	85.0	85.0
2014	87.7	87.7
2015	90.5	91.6
2016	94.6	94.6
2017	90.6	86.6
2018	92.6	90.6
2019	94.6	92.6

relessness march through 2020 and 2021. It says that in 2020 is on track to become one of the three warmest years ever observed and that the last six years since 2015 are the hottest on record. The WMO's provisional report on the State of the Global Climate, shows that despite COVID-19 related lockdowns, GHG concentrations continue to rise. Thus, many generations to come will be subjected to additional warming because of the long atmospheric lifetime of CO₂. Across Europe, the winter of 2020 was another mild one. Apart from the month of January 2020, which saw seasonal norms, temperatures were

much higher than average as early as February and maintained their highs through the winter. The European programme Copernicus report states that four seasons in Europe were warmer than usual in 2020, with three exceptionally warm periods in February, June, and July. Unfortunately, the winter of 2019-2020 was even milder. The Copernicus Climate Change Service reports that it was the warmest on record in Europe, especially in the north and east, 1.4°C warmer than the average winter between 1981 and 2010. Except for mild and highly abnormal temperatures were recorded in the Baltic. This bodes for a sharp drop in solid biofuels consumption for heating purposes for 2020, all the more so as temperatures remained particularly warm in Europe towards the end of the year. The month of November was on average one of the two warmest ever observed in Europe. Therefore, the Member States' 2020 renewable energy targets are likely to be knocked off course, in an energy context that will no doubt be severely affected by the spring and autumn waves of COVID-19.

EU28 CONSUMPTION EXCEEDS 100 MTOE
EuroObserv'ER concludes from the official data available early in December 2020, that at 102.6 Mtoe, primary energy consumption from solid biofuels in the EU28 exceeded 100 Mtoe in 2020, showing an annual increase of 2.3% over 2019. Consolidated statistics released by some countries (including Germany, the UK, Denmark, and the Netherlands) indicate that at the end of the day, the 100 Mtoe figure had been narrowly missed in 2018 as consumption was measured at 100.4 Mtoe. Incidentally, consumption rose in all the top seven solid biofuels consumer countries. The biggest increases can be credited to the UK (50% ktoe), the Netherlands (11% ktoe), Sweden (22% ktoe), Poland (14% ktoe), Italy (20% ktoe), the Czech Republic (6% ktoe), Germany (11% ktoe) and Finland (11% ktoe), often resulting from increased electricity production. Leaving aside the UK, which officially left the EU on 31 January 2020, Member States' consumption settled at 84.6 Mtoe in 2019 (vs 2 Mtoe in 2018),

which is a 1.8% increase over 2018. Primary energy production from solid biofuels, namely solid biofuels (taken from European Union soil), also increased, albeit at slower pace than its consumption. It rose to 96.9 Mtoe in the EU28 (1.7% more than in 2019) and to 2.1 Mtoe in the EU27 (1.8% more than in 2018). The difference, which

accounts for net imports, plus or minus stock variations, was primarily driven by wood pellet and wood chip imports from the USA, Canada, and Russia. EuroObserv'ER distinguishes the two types of final energy use from solid biofuels, namely electricity (table 2) and heat for space heating or process heat). Solid biofuels heat is further

broken down depending on whether it comes from the processing sector, i.e., distribute via district heating networks (table 3) or used directly by the end consumer (in the residential or industrial sectors) (table 4). According to EuroObserv'ER, consumption of solid

Tabl. n° 1
Primary energy production and gross inland consumption of solid biofuels* in the European Union in 2018 and in 2019** (in Mtoe)

	2018		2019**	
	Production	Consumption	Production	Consumption
Germany	12.430	12.796	11.798	11.922
France***	10.248	10.311	10.294	10.411
Sweden	9.229	9.312	9.468	9.553
Finland	8.821	8.831	8.940	9.065
Italy	7.666	8.111	7.936	8.741
United Kingdom	4.765	7.589	4.720	8.099
Poland	6.347	6.367	6.308	6.595
Spain	5.444	5.443	5.128	5.128
Austria	4.627	4.433	4.611	4.558
Romania	3.443	3.443	3.443	3.447
Czechia	3.070	2.991	3.170	3.147
Denmark	2.921	2.921	2.924	2.940
Portugal	2.648	2.429	2.550	2.527
Hungary	2.332	2.331	2.058	2.069
Belgium	2.128	2.000	2.198	1.884
Netherlands	1.942	1.999	1.460	1.553
Bulgaria	1.874	1.443	1.800	1.514
Latvia	1.445	1.496	1.451	1.489
Croatia	1.495	1.259	1.371	1.331
Lithuania	1.286	1.285	1.247	1.261
Estonia	1.148	1.195	1.189	1.201
Slovakia	0.998	0.839	0.874	0.874
Greece	0.782	0.814	0.711	0.816
Slovenia	0.857	0.857	0.955	0.955
Ireland	0.250	0.273	0.237	0.252
Luembourg	0.106	0.207	0.118	0.114
Cyprus	0.023	0.024	0.023	0.024
Malta	0.000	0.001	0.000	0.001
Total EU 28	95.191	100.371	91.816	102.570
Total EU 27 (from 2020)	90.540	91.921	91.216	91.468

* Production from solid biofuels (including wood chips and wood pellets) and from other biomass (including agricultural residues, manure, etc.). ** Provisional data for 2019. *** Data for 2019 are preliminary. Source: EuroObserv'ER data.

Tabl. n° 2
Gross electricity production from solid biofuels* in the European Union in 2018 and 2019** (in TWh)

	2018			2019**		
	Electricity only plant	CHP plant	Total	Electricity only plant	CHP plant	Total
United Kingdom	23.115	0.935	24.050	20.045	0.889	20.934
Finland	1.439	10.150	11.589	1.248	10.099	11.347
Sweden	0.000	10.100	10.100	0.000	11.110	11.110
Germany	5.590	5.760	11.350	5.300	6.000	11.300
Poland	1.000	3.830	4.830	1.084	4.640	5.724
Denmark	0.000	4.427	4.427	0.000	4.133	4.133
Italy	2.268	2.024	4.291	2.120	2.068	4.187
Spain	1.289	0.932	2.221	1.009	0.876	1.885
France***	0.557	3.140	3.696	0.505	3.177	3.684
Austria	0.985	2.081	3.066	0.793	2.933	3.726
Belgium	1.277	1.207	2.484	1.990	1.202	3.192
Netherlands	0.424	1.078	1.502	0.878	1.950	2.828
Portugal	0.800	2.127	2.927	1.848	1.791	3.639
Czechia	0.003	2.118	2.121	0.002	2.197	2.199
Hungary	1.102	0.665	1.767	1.004	0.560	1.564
Bulgaria	0.711	0.559	1.270	0.377	0.679	1.056
Estonia	0.712	0.921	1.633	0.710	0.981	1.691
Slovakia	0.000	1.070	1.070	0.000	0.861	0.861
Latvia	0.000	0.570	0.570	0.000	0.575	0.575
Croatia	0.000	0.313	0.313	0.000	0.487	0.487
Romania	0.023	0.368	0.391	0.023	0.375	0.398
Ireland	0.323	0.013	0.336	0.320	0.017	0.337
Lithuania	0.000	0.335	0.335	0.000	0.311	0.311
Luembourg	0.627	0.095	0.722	0.627	0.109	0.736
Slovenia	0.000	0.163	0.163	0.000	0.151	0.151
Greece	0.013	0.000	0.013	0.000	0.016	0.016
Total EU 28	46.004	55.707	101.711	40.843	50.975	91.818
Total EU 27 (from 2020)	21.370	15.913	37.283	20.910	19.087	39.997

* Including electricity produced by biomass cogeneration combined heat and power. ** Provisional data for 2019. *** Data for 2019 are preliminary. Source: EuroObserv'ER data.



biofuels heat used directly by the end consumer across the EU28, increased slightly (by 0.6% over 2018) to 61.9 Mtoe in 2019. Its EU27 level is similar (rising by 0.1% to 58.0 Mtoe). Much of this increase can be ascribed to rising wood pellet consumption (see below). The amount of solid biofuels heat sold to district heating networks (operated by the processing sector) increased by more than half a million toe to 21.5 Mtoe in 2019 in the EU28 and 19.4 Mtoe in the EU27, thanks largely to the commissioning of new combined heat and power (CHP) plants (in the Netherlands and France) and a pick-up in activity in Finland and Denmark. As for the solid biofuels electricity production trend, it is mainly driven by a few Member States' policies to expand coal by converting or adapting all or some of their power (or CHP) plants to use solid biofuels (pellets, pellets, wood chips, etc.). This trend is also by variations in demand in Northern Europe (at peak pressure CHP plants. Solid biofuels electricity output across

the European Union of 28, was put at 106 TWh in 2019, which is a 3.9% year-on-year increase (by 3.8 TWh). The biggest increases were posted by the UK (1.2 TWh), the Netherlands (1.3 TWh), Sweden (0.9 TWh), Poland (0.9 TWh) and Finland (0.5 TWh). Leaving out the UK, which is the most active biomass electricity producer country, output by the EU27 settled at 80.1 TWh (1.3 TWh rise, which equates to a 0.9% annual growth).

RISING WOOD PELLET CONSUMPTION
Data published by the EPC (European Pellet Council) in the 2020 Bioenergy Europe Statistical Report focusing on the wood pellet sector, shows that EU28 wood pellet consumption in 2019 continued to increase, reaching 27 million tonnes (Mt), i.e., an additional 1.8 Mt of consumption (6.7% growth between 2018 and 2019). The report asserts that the EU28 is the world's biggest user of pellets, putting global consumption at 37.2 Mt, a 7% increase. The EU28 produced 17 Mt of pellets, distributed at

follows: 2.8 Mt in Germany (14.9% rise), 1.6 Mt in Sweden (11.4% fall), 1.6 Mt in Latvia (1.9% rise) and 1.6 Mt in France (6.7% rise). Most of the imports from outside the EU28 come from the USA, Canada, Russia, and other European countries. The top five European wood pellet consumer countries are the UK, with 3.8 Mt (9.2% rise), Italy with 2.4 Mt (5.8% rise), Denmark with 1 Mt (0.4% fall), Germany with 2.3 Mt (5% rise) and France with 1.8 Mt (15.4% rise).

Growth in pellet consumption in the residential and commercial sectors was down on its 2018 level for two main reasons: in most of Europe, energy needs in the 2019-2020 heating season. Secondly, according to the report, European sales of pellets burning stoves did not increase by leaps and bounds, yet Italy and France have the two most proactive residential/commercial market segments. Wood pellet consumption for heating needs (residential and commercial)

sector, and heat produced in CHP plants) increased by 6% between 2018 and 2019 to reach 16.4 Mt. The main consumer countries in 2019, in the EU28, consumption increased by 8.3% to 13.2 million tonnes. UK consumption alone stands at about 8.1 Mt (8.9% more than in 2018), and France, most of it used for residential heating, a little less than 6% is earmarked for CHP plants in Denmark, with just under 4% for residential heating. In Germany more than 70% is used for residential heating and just under 30% for commercial heating. Sweden spreads wood pellet use more evenly between

residential, commercial and CHP plants. The report claims that industrial use of wood pellets (electricity and heat) has surged again. In the EU28, consumption increased by 8.3% to 13.2 million tonnes. UK consumption alone stands at about 8.1 Mt (8.9% more than in 2018), and France, most of it used for residential heating, a little less than 6% is earmarked for CHP plants in Denmark, with just under 4% for residential heating. In Germany more than 70% is used for residential heating and just under 30% for commercial heating. Sweden spreads wood pellet use more evenly between

ELECTRICITY - THE DRIVING FORCE PULLING THE INCREASE IN SOLID BIOFUELS CONSUMPTION
THE NETHERLANDS ENJOYED A SHARP RISE IN SOLID BIOFUELS CONSUMPTION
In the EU27, the Netherlands spearheaded solid biofuels energy consumption in 2019. According to Statistics Netherlands, solid biofuels consumption increased by 39.5% in Netherlands' consumption figures (plants described later).

Tabl. n° 3
Gross heat production from solid biofuels* in the European Union in 2018 and in 2019** (in Mtoe) in the transformation sector

	2017			2018		
	Heat only plant	CHP plant	Total	Heat only plant	CHP plant	Total
Sweden	0.885	1.799	2.684	0.662	1.828	2.490
Finland	0.691	0.993	1.684	0.767	0.894	1.661
Denmark	0.498	0.866	1.364	0.493	0.927	1.420
France***	0.374	0.551	0.925	0.400	0.813	1.213
Austria	0.111	0.333	0.444	0.181	0.337	0.518
Germany	0.110	0.213	0.323	0.135	0.217	0.352
Lithuania	0.395	0.135	0.530	0.397	0.140	0.537
Italy	0.000	0.458	0.458	0.078	0.445	0.523
Poland	0.000	0.252	0.252	0.000	0.297	0.297
Estonia	0.127	0.189	0.316	0.143	0.215	0.358
Latvia	0.124	0.185	0.309	0.154	0.194	0.348
Netherlands	0.020	0.131	0.151	0.056	0.194	0.250
Czechia	0.010	0.120	0.130	0.018	0.145	0.163
Bulgaria	0.000	0.100	0.100	0.007	0.111	0.118
United Kingdom	0.000	0.000	0.000	0.000	0.000	0.000
Hungary	0.000	0.000	0.000	0.000	0.000	0.000
Slovakia	0.000	0.000	0.000	0.000	0.000	0.000
Croatia	0.000	0.000	0.000	0.000	0.000	0.000
Luembourg	0.000	0.000	0.000	0.000	0.000	0.000
Romania	0.000	0.000	0.000	0.000	0.000	0.000
Slovenia	0.000	0.000	0.000	0.000	0.000	0.000
Belgium	0.000	0.000	0.000	0.000	0.000	0.000
Total EU 28	4.111	8.772	12.883	4.150	7.161	11.311
Total EU 27 (from 2020)	1.111	3.772	4.883	1.150	7.161	11.311

* Including electricity produced by biomass cogeneration combined heat and power. ** Provisional data for 2019. *** Data for 2019 are preliminary. Source: EuroObserv'ER data.

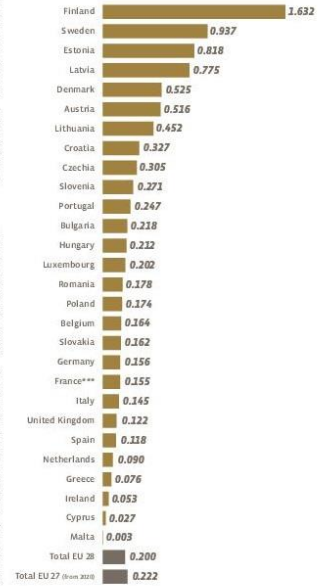
a single year, rising from 1.2 Mtoe in 2018 to just under 1.6 Mtoe in 2020 (by 35.4 ktoe). The main underlying reason for this is that wood pellet imports shot up to 780 000 tonnes in 2019 (26,000 tonnes in 2018), while the country exported 197 000 tonnes in 2019 (18,000 tonnes in 2018). It uses a wide variety of

mainly EU sources for these wood pellet imports such as Latvia (181 000 tonnes), Estonia (128 000 tonnes), Lithuania (18 000 tonnes), Belgium (133 000 tonnes), Portugal (77 000 tonnes) and Germany (52 000 tonnes). Its imports from outside the EU are sourced from Russia (202 000 tonnes), the USA (90 000 tonnes) and Canada (20 000 tonnes). The additional consumption of pellets was solely directed to supply RWZ's two coal-fired power plants, Amers 9 (851 MW) and Femshaven (554 MW) and the 2100-MW Suiper MPP plant (Maasvlakte Power Plant) which have been converted to its biomass cofiring.

plants. The Amers plant can now run on 80% biomass fuel, while the Femshaven and MPP are 50% biomass fueled. According to Statistics Netherlands, solid biofuels electricity production increased by 27.7% between 2018 and 2019 to 2.8 TWh, 1 TWh of which was produced by cogeneration. Heat production from the processing sector also surged by 55.6% to 150 ktoe (including 194 ktoe produced by cogeneration). The Netherlands announced that by 2021 it would shut down all of its remaining coal-fired plant capacities (i.e., 4.8 GW), following the passing of a draft law to prohibit the use of coal for generating electricity in December 2019. The ban will be rolled out in two phases. The oldest plants will close on 1 January 2021 and the more recent plants on 1 January 2023.

THE UK USES AN EXTRA HALF A MILLION TONNE
The UK has led European solid biofuels energy consumption in recent years, and 2019 was no exception. Data released by BEIS, the Department for Business, Energy & Industrial Strategy, shows that the UK's total solid consumption increased to 3.1 Mtoe in 2019 (i.e., 0.4 Mtoe (599 ktoe) more than in 2018). An increase in imports is the only explanation for this rise, as primary energy production from solid biofuels slipped by 9.7% between 2018 and 2019 to 2.7 Mtoe. The reason for the country's sharp increase in solid biofuels energy consumption is its decision to stop using coal for generating power by converting some of its power plants to run on wood fuels. The BEIS states that the electrical capacity of the country's solid biofuels power plants increased slightly in 2019 (by 4.5 MW) and that the high rise in electricity output can be put down to opening the capacity that was newly installed in 2018, over a full year. This new capacity includes the Lynemouth power plant (20 MW), a coal-fired plant that was shut down in 2015 and reopened in 2018 once it had been entirely converted to run on wood pellets. The year 2019 was also the first in which the fourth tranche of the Drax power plant (an additional 700 MW)

Graph 2
Gross inland consumption of solid biofuels* by toe per inhabitant in the European Union in 2019**



Tabl. n° 4
Heat consumption from solid biofuels* in the countries of the European Union in 2018 and 2019**

	Total final energy consumption	Of which solid energy consumption	Of which derived heat***	Total final energy consumption	Of which solid energy consumption	Of which derived heat***
Germany	30.127	9.554	0.573	30.242	9.548	0.592
France****	9.278	8.122	1.126	9.351	8.149	1.121
Sweden	7.576	5.092	2.484	7.625	5.140	2.485
Italy	7.111	6.873	0.518	7.423	6.800	0.523
Finland	7.115	5.511	1.594	7.218	5.587	1.641
Poland	5.276	4.959	0.320	5.272	4.895	0.377
Spain	4.999	4.999	0.000	4.223	4.223	0.000
Austria	3.907	3.014	0.894	3.898	3.005	0.893
Romania	3.424	3.168	0.257	3.417	3.190	0.227
United Kingdom	3.194	3.195	0.001	3.275	3.275	0.000
Czechia	2.485	2.124	0.361	2.605	2.221	0.385
Denmark	2.143	1.179	1.169	2.132	1.162	1.120
Portugal	1.754	1.754	0.000	1.812	1.812	0.000
Hungary	1.578	1.580	0.002	1.599	1.590	0.009
Latvia	1.306	0.995	0.310	1.313	0.965	0.347
Belgium	1.287	1.281	0.006	1.222	1.214	0.008
Croatia	1.113	1.075	0.038	1.185	1.100	0.085
Bulgaria	1.144	1.035	0.109	1.160	1.022	0.138
Lithuania	1.153	0.821	0.332	1.149	0.811	0.337
Netherlands	0.819	0.658	0.161	0.921	0.672	0.250
Greece	0.827	0.827	0.000	0.789	0.789	0.000
Estonia	0.737	0.411	0.316	0.770	0.411	0.358
Slovenia	0.618	0.509	0.109	0.528	0.409	0.119
Slovakia	0.580	0.459	0.121	0.403	0.400	0.003
Ireland	0.203	0.203	0.000	0.185	0.185	0.000
Luxembourg	0.077	0.040	0.038	0.083	0.024	0.059
Cyprus	0.021	0.021	0.000	0.021	0.021	0.000
Malta	0.001	0.001	0.000	0.002	0.002	0.000
Total EU 28	79.504	68.513	16.983	80.418	68.924	17.494
Total EU 27 (from 2020)	76.312	65.427	16.883	77.143	65.749	17.156

* Including chemical. ** 2018 data. *** Derived heat excludes heat included for process. Source: Eurostat & BEIS.

operated over a full year its conversion was finalized (end of 2018). After almost half a century of coal-fired electricity production, the Drax power plant operators announced that they would stop using coal once and for all in March 2021 - an important milestone in the country's aim to become carbon neutral from 2025 through the implementation of carbon sequestering technologies from biomass combustion. The lead factor of the UK's biomass power plants is put at 72.7% in 2019 (72.8% in 2018). Solid biofuels electricity production should increase again in the next two years on the new biomass cogeneration plant at Teeside (299 MW) comes on stream. It was scheduled to start up at the end of 2020 but was delayed by the COVID-19 pandemic.

SWEDEN, WHERE BIOMASS ENERGY BOUNDS
Biomass energy is Sweden's main renewable energy source of final energy. Aconideabish are taken up by solid biofuels. According to Statistics Sweden, solid biofuels consumption approached the 10 Mtoe threshold with 9.6 Mtoe in 2019, which is 2.9% more than in 2018. This additional consumption has essentially been addressed to generate electricity. Output increased by 9.2% to 11.1 TWh in 2019 (9.9 TWh in 2018), produced exclusively in cogeneration plants. This is the third highest output level after the UK (25.9 TWh) and Finland (12.3 TWh). Statistics Finland reports that the country's electrical capacity from solid biofuels fuels decreased slightly between 2018 and 2019 (by 4.4 MW), from 3 028 to 2 984 MW, while the latter had risen by 222 MW between 2017 and 2018. One of the country's most recent installations is the heating network of the municipality of Borås, which was boosted when the Sobaken cogeneration biomass plant (200 MW and 45 MW) came on stream in the spring of 2019. It will produce about 135 GWh of electricity and 395 GWh of heat per annum. Solid biofuels heat from the processing sector is also well established in Sweden, which boasted 25 Mtoe of production in 2019 (no change on its 2018 level). The energy mix of district heating networks is dominated by

biomass. Direct end-user solid biofuels heat consumption only increased by 4% (to 8.6 TWh) in 2019. Sweden pioneered carbon taxing in the 1990s and its low-carbon transition programme is one of the most advanced of any industrialized country. In June 2017, Sweden's Parliament passed a framework law that came into force on 1 January 2021, obliging the government to toe the line by rolling out policies consistent with Parliament's climate target. The law states that part of the emission reduction could be covered by additional measures such as enhancing carbon sinks, namely the forests (by forest extension and better management) and setting up climate projects abroad. Thus, Sweden's forests should contribute more to the country's energy needs while strengthening their role as a carbon sink. When setting its budgets, the government is obliged to publish an accompanying climate report and action plan to support the budget's consistency with the strategy. The law aims to force environmental transition on Swedish society and its business world. Sweden has set targets to achieve carbon neutrality in 2045, five years earlier than recommended by the Paris Accord, and reduce its GHG emissions by 85% from its 1990 level.

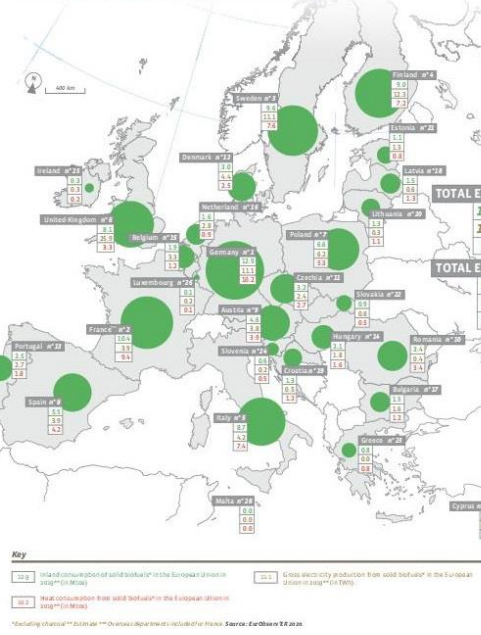
FINLAND'S CONSUMPTION MAKES THE 9-MTAE THRESHOLD
Finland is the most densely forested country in Europe with 80% of its land mass covered with trees and is the biggest per capita consumer of solid biofuels. Statistics Finland reports that annual solid biofuels consumption in 2019 increased by 1.4% to reach the 9.6 Mtoe threshold for the first time. Underpinning this increase are higher demand (25%) for solid biofuels by plants supplying district heating networks, resulting in over 2.6 Mtoe of additional output and a 20% increase in electricity production, primarily by CHP plants, with 12.3 TWh of output in 2019. The UK's departure from the EU hands Finland the top EU biomass electricity producer position. The country's biomass heat production is bound to be boosted in 2020 when a new high-capacity heating plant comes on stream. The operator,

Fortum, announced in May 2020 that the Kivimäki plant (40 MW) in the city of Espoo was entering its commercial phase. The plant, which will produce 30-350 GWh of heat (30-340 Mtoe) will replace one of Fortum's two coal-fired boilers at the Suomenoja plant. In doing so, it will raise the Espoo heating network's "carbon-neutral" share to 50%. Kivimäki's new boiler is a major step in the Espoo Clean Heat programme, that aims to generate fully carbon-neutral urban heating before the end of this decade and stop using coal by 2025.

SOME BIOENERGY OPERATORS ARE AIMING FOR NEGATIVE EMISSIONS

Some bioenergy plant operators, primarily those geared to producing electricity, are contemplating a paradigm shift. Not only do they aim for carbon neutrality of their energy production activity, but also to contribute negatively to GHG emissions. To do so, they are banking on the rollout of new technologies, such as Bioenergy with carbon capture and storage (BECCS) and the production of biochar, an organic solid resulting from biomass pyrolysis that the electricity production process. Biochar production for carbon storage purposes opens up a potentially new activity sector to bioenergy players, provided that they are paid for carbon storage and that it is prioritized by government. More specifically, when the biomass used for energy is converted into biochar, it provides a channel for fixing the carbon and sequestering it in the soil. The Inter-governmental Panel on Climate Change (IPCC) lists this form of biomass energy with carbon capture and storage (BECCS), as a key carbon reduction technology. Biochar production involves partial combustion of the plant matter, when part of the carbon captured by the plant is immediately released as energy, optimally as heat, but also as electricity. 80-90% of more of the carbon may remain in its new form as biochar. There is still energy in the biochar, and its energy value is similar to that of charcoal or coal.

Gross inland consumption, gross electricity production and heat consumption from solid biofuels* in the European Union in 2019**



* Including chemical. ** 2018 data. *** Derived heat excludes heat included for process. Source: Eurostat & BEIS.



The operator, Fortum, announced in May 2020 that the Kivijärvi plant by MWH in the city of Espoo, Finland, was entering its commercial phase. The plant, which will produce 250-260 GWh of heat per year, will raise its gross bearing capacity to 2.5 GWh per year.

Several solid biofuels energy projects are now in the development phase. One that moved into the commercial phase in November 2020, is the Mäsa Power Plant operated by Sigma Power Ariake Corporation (SPAC), a subsidiary of Toshiba ESS (Toshiba Energy Systems & Solutions Corporation), in Omata (Fukuoka Prefecture, Japan). It is Japan's first bioenergy plant to be fitted with a carbon capture and storage system. This coal-fired plant was totally converted to biomass in 2018 and uses palm kernel shells as its main feedstock. Toshiba ESS has operated a pilot installation capable of capturing 30 to 40 tonnes of CO₂ per day since 2009. The new "Demonstration of Sustainable CCS technology" project, whose construction started in February 2018 and as the backing of the country's Environment Ministry, will capture over 500 tonnes of CO₂ every day, i.e., over half the plant's CO₂ emissions. Other projects in development include the Norwegian Full-Chain CCS that seeks to integrate BECCS technology into a cement plant that co-fires 30% biomass and into a household waste-to-energy plant. The DRAX power plant in North Yorkshire (UK) also has a very ambitious project. It already has a pilot running capable of storing a tonne of carbon every day and was the first in the world to store carbon from 100% biomass feedstock. In December 2020, Drax Group Plc announced its aim to become carbon negative by 2030. The plant, whose conversion to biomass is almost complete, produces about 23% of the UK's power. The energy utility Stockholm Energi AB of Sweden, has set itself a new sustainability objective, to be climate positive by 2025. It aims to make Stockholm the world's first climate-positive capital. Stockholm Energi AB announced it was launching a large-scale biochar production project and that furthermore, it was interested in the potential of BECCS technology. The initial long-term environmental target was to make the city of Stockholm's heating network climate neutral by 2030. The new target is to make the company's operations climate positive by 2025.

However, the question of its economic value must be raised. Namely, should full energy recovery be conducted until it is reduced to ashes, leaving little or no carbon, or should the combustion process be stopped, to enable the biochar to be restored to the soil, in the form of stable carbon? Biomass naturally decomposes into GHG, but biochar does

not. When biochar is restored to the soil, carbon from photosynthesis can be stored in the soil while improving and fertilizing it. This option calls for responsible forestry resource management and timber harvesting to meet the need of forest ecosystems. Operators are also seeking to set up

wide-scale bioenergy technologies with carbon capture and storage (BECCS). This process entails trapping the CO₂ molecules before, during or after combustion to prevent their release into the atmosphere and to lock the CO₂ in geological formations. There are three capture processes in development: "pre-combustion" (capture prior to combustion), "post-combustion", capture

after conventional combustion (with air), with little or no change to the combustion process, and "oxycombustion", capture after combustion in the presence of pure oxygen. Until recently, most of the BECCS carbon storage technologies were used in biofuel production plants. According to the Global CCS Institute, Bioenergy

and Carbon Capture and Storage 2020 Perspectives Study, five of the world's plants had BECCS technology (4 plants in the USA and 1 in Canada). Between them, they captured about 1.2 million tonnes of carbon. The biggest of them in Illinois, owned by Archer Daniels Midland, produces ethanol from cereals, and captures up to 1 Mtpa of CO₂.

The Värtan biomass cogeneration plant is currently well placed to be equipped with BECCS technology. A test facility has been operating on the power plant site since December 2019 capable of compressing CO₂ to its liquid state to be stored in rock formations. Stockholm Energi's calculations demonstrate that 800,000 tonnes of CO₂ can be captured per annum on this site alone.

SOLID BIOFUELS FACILITATING CARBON NEUTRALITY

Although the consequences of climate change are now evident to all of us, the declared ambition for the next thirty years is nothing other than to achieve the carbon neutrality of the entire European economy, starting with the decarbonization of the heating, electricity production, and transport sectors. To reach this target, biomass energy technologies, and solid biofuel energy in particular, will be very much

in demand because they are the easiest renewable energy production sectors to substitute fossil energies. They also have the capacity to become a negative emission energy source through the rollout of the new technologies described above, provided that economic incentives are implemented. Still, the future deployment of biomass energy will be subject to new rules following the recasting of the Renewable Energy Directive (2018/2001). The Directive sets out the legal framework applicable to renewable energies from 2021 to 2030 and, in particular, those set in Article 29 relating to sustainability requirements and the GHG reduction criteria of liquid, solid and gaseous fuels. Sustainability criteria now apply to all bioenergy uses (biofuel, electricity, and heat). The Directive's target is to minimize negative environmental risks such as deforestation, biodiversity loss and minimize the risks of negative impacts on forest carbon sinks. As the very annual year draws to a

close, we have to admit that (readability of the 2020 targets assigned by the previous renewable energy directive will be closed). The two major pandemic waves that have hit economic activity and thus the Member States' energy needs, coupled with an unusually mild 2019-2020 winter that reduced heating and electricity needs, have knocked it off its normal path. In the longer term, the future growth of solid biofuels heat and electricity production will depend on the implementation and strategic choices defined in the National Energy and Climate Plans 2020 (NECPs) by each Member State. Bioenergy Europe has made a preliminary analysis of these climate plans in its Statistical Report. Its projections show that bioelectricity as a whole, i.e., not only that sourced from solid biomass, but also biogas, liquid biomass, and renewable household waste will increase by about 30% over the next decade to reach 37.4 Mtoe in 2030 in the EU27 (equating to 20.4 TWh). According

to EuroBSERV'ER, solid biofuels alone accounted for about half of the bioelectricity produced by the EU27 countries in 2019. If biomass electricity production were to grow by 30%, that would imply a level of about 20.4 TWh by 2030. It is harder to forecast the energy contribution of solid biofuels to the heat and cooling targets by the 2030 timeline. The use of solid biofuels heat tends to increase steadily in the industrial and processing sectors. This attests to the operators' and industrialists' willingness to substitute their use of fossil energies. In contrast, the trend in recent years of the residential sector is much less hard and fast. Its energy needs have been more heavily hit by a succession of mild winters. The temperature records made during the winter of 2019-2020 will have added a strong impact on demand for solid biofuels heat in 2020. To recap, the new directive's stated target is that renewable heat and cooling should account for about 40% of renewable energy

consumption by 2030, i.e., roughly twice the current percentage. Furthermore, the new RED directive sets an indicative target of an annual 1.3 percentage point increase in the renewable energy share of final heat consumption, taking the national renewable energy share in the heating and cooling sector in 2020 as the reference point. One caveat applies because the Directive provides for the possibility of integrating into this target the recovery of up to 40% of the mean annual increase as waste heat or cold. According to Bioenergy Europe, however, which has analysed the Member States' renewable energy targets in the heat and cooling sectors through their NECPs, relatively few of them appear to have based their 2030 heat and cooling targets on an annual 1.3 percentage point growth trajectory. Thus, there is uncertainty surrounding the total level of renewable heat production that will be vested in solid biomass by this timeline. Nonetheless, the association recalls that if property

handled, biomass heat offers the EU reliable, easily available, affordable, and efficient solutions to achieve carbon neutrality by 2030. It

Tabl. n° 5

Major European operators of biomass plants in 2019

Operator	Country	Operational capacity (MW)	Biomass and cooling plants	Production (TWh)
Orsted	Denmark	Cooling plants with biomass conversion 216 MWc 218 MWth	Avedøre 3 (Den), Avedøre 2 (Den), Aimes 6 (Den), Herringø (Den), Skarhede 1 (Den), Studstrup (Den)	45 TWh (heat) 8.1 TWh (cold) (8% of total heat and power from biomass in the EU)
Drax Group	United Kingdom	2160 MWc (Renewable biomass power capacity)	Drax power stations (UK)	32.2 TWh (Renewable power in 2019)
Vattenfall	Sweden	CHP biomass plants and heat plants 274 MWc 2214 MWth	Lerjeåsa (SE), Måringsnes Värme (SE) and in Sweden: Gotland, Skövdeborg, Målsjö, Åregrund, Lyckeåsen 1 - Lyckeå, C2-Biomass - Fagersta, Fågelåsåsen 1 - Fågelås, Jönköping, Jönköping Biomass, Kivik, Långåsa, Storvreta, Bollnäs	6.4 TWh (heat)
Pohjolan Voima	Finland	Multifuel (2019-2021, 100% CHP plant) 630 MWc 1472 MWth	Hämeenkyön Voima (FIN), Kymön Voima (FIN), Laajen Voima (FIN), Kauhajoen Voima (FIN), Alavieska K2 (FIN), Pöytä Voima (FIN), Rautan Biomass (FIN)	4.2 TWh (heat) 2.7 TWh (cold) 10% wood-based fuel used
Fortum	Finland	80 CHP 351 MWc, 804 MWth Multifuel (2019-2021, 100% CHP plant) 630 MWc, 1472 MWth	Biomass CHP - Järvenpää (FIN), Joutseno (FIN), Paimio (FIN), Turku (FIN), Riihimäki (FIN), Vammala (FIN), Vammala K2 (FIN), Vammala K3 (FIN), Vammala K4 (FIN), Vammala K5 (FIN), Vammala K6 (FIN), Vammala K7 (FIN), Vammala K8 (FIN), Vammala K9 (FIN), Vammala K10 (FIN), Vammala K11 (FIN), Vammala K12 (FIN), Vammala K13 (FIN), Vammala K14 (FIN), Vammala K15 (FIN), Vammala K16 (FIN), Vammala K17 (FIN), Vammala K18 (FIN), Vammala K19 (FIN), Vammala K20 (FIN)	n.a.
RWE	Germany	300 MWc 350 MWth	Müncheberg CHP biomass plant (GER) Aster biomass and hard-wood fired power plants (NL)	n.a.
Engie	France	270 MWc (2019) 305 MWc (from August 2020)	Bois de Bouffay (FR) Aunis (FR) closed the 31st August 2020	n.a.

Source: EuroBSERV'ER 2020, based on companies annual reports and communication.



This barometer was prepared by EuroBSERV'ER in the scope of the EuroBSERV'ER project, which groups together EuroBSERV'ER (FR), TNO Energy Transition (NL), RENAC (DE), Frankfurt School of Finance and Management (DE), Fraunhofer ISI (DE) and Statista (Netherlands) (NL). This document has been prepared for the European Commission however it reflects the views only of the authors and the Commission cannot be held responsible for any use which may be made of the information contained therein.

Annex 1.2

All about the biomass sector in France

Mainly used to produce heat, solid biomass is not entirely absent from the electricity sector. A French sector still requiring many improvements and innovative projects, solid biomass must also meet the challenge of securing supplies.

The biomass is the leading source of renewable energy consumed in France. In 2017, solid biomass represented 42.3% of primary renewable energy production in France¹. If it serves more as a source of heat, it is also used for the production of electricity: the steam generated by combustion drives turbines creating current. Update on key biomass indicators are:

- 591 MW and 790 MW: these are respectively the figures for installed capacity at the end of October 2018 (maximum capacity of the installations) and the target for 2023;
- 3,150 GWh: the volume of electricity from solid biomass in 2017 in France;
- 45: the number of power plants producing electricity from solid biomass in France at the end of 2018; three factories are present in Martinique and Guyana and three additional sites are under construction in other regions;
- € 1,319 million: this is the turnover of the solid biomass sector in 2017, all energy recovery combined.

The screenshot displays a web browser window with the following content:

- Page Title:** Tout savoir sur la filière biomasse en France
- URL:** <https://www.latribune.fr/entreprises-finance/la-tribune-de-l-energie-avec-enedis/tout-savoir-sur-la-filiere-biomasse-en-france-814572.html>
- Article Text:**

Principalement utilisée afin de produire de la chaleur, la biomasse solide n'est pourtant pas totalement absente du secteur électrique. Filière française nécessitant encore de nombreuses améliorations et des projets innovants, la biomasse solide doit également relever le défi de la sécurisation des approvisionnements.

Article partenaire - Enedis
19 Aoû 2019, 9:53

En 2017, la biomasse solide a représenté en France 42,3 % de la production primaire d'énergies renouvelables*. Si elle sert davantage comme source de chaleur, elle est également utilisée pour la production d'électricité : la vapeur générée par la combustion
- Image:** A photograph showing a pair of hands holding a large quantity of light-colored wood pellets.
- Video Player:** A video player showing a street view of a modern urban area.
- Enedis Logo:** L'ÉLECTRICITÉ EN RÉSEAU
- Text:** La Tribune de l'énergie
- Text:** Pour vous, Enedis construit l'avenir des réseaux électriques

(source: <https://www.latribune.fr/entreprises-finance/la-tribune-de-l-energie-avec-enedis/tout-savoir-sur-la-filiere-biomasse-en-france-814572.html>)

¹ By combustion of plant or animal materials (wood, agricultural waste, organic household waste, etc.) or by methanization (creation of biogas from the fermentation of these materials in biomass plants).

Annex 2: Biomass experimental study

THE DRYING OVEN SLW 53 SIMPLE



tel. (+48) 32 453 91 70

e-mail: info@pol-eko.com.pl
internet: www.pol-eko.com.pl

POL-EKO-APARATURA SP. J.

A. POŁOK – KOWAŁSKA, S. KOWALSKI
44-300 WODZISŁAW ŚLĄSKI, UL. KOKOSZYCKA 172 C

Data sheet

Drying Oven
SLW 53 SIMPLE



The photo above is for reference only, may show additional options not included in standard equipment. The real appearance, particularly color and structure of the material may differ from the ones presented in the photo.



Bank: ING B5 o/Wodzisław: SL
Nr rachunku: 50 1090 1403 1000 0022 0879 5498
Nr rej. W BDO: 000003609

NIP: 647-216-26-87 REGON: 276110984
Sąd Rejonowy w Gliwicach, X Wydział Gospodarczy
KRS: 0000083696

1/3

Figure A2.1 - The drying oven SLW 53 SIMPLE model: Data sheet
(source: <https://www.pol-eko.com.pl/model/drying-oven-slw-simple/simple-drying-oven-slw-simple-53/>)



tel.: (+48) 32 453 91 70

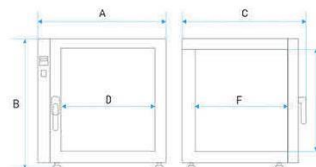
e-mail: info@pol-eko.com.pl
internet: www.pol-eko.com.pl

POL-EKO-APARATURA SP. J.

A. POLOK – KOWALSKA, S. KOWALSKI
44-300 WODZISŁAW ŚLĄSKI, UL. KOKOSZYCKA 172 C

TECHNICAL DATA	
air convection	forced
chamber capacity [l]	56
working capacity [l]	56
controller	microprocessor with external display
display	LCD
TEMPERATURE	
temperature range [°C]	5°C above ambient temperature ... +250°C
temperature resolution every ... [°C]	0,1
over temperature protection	class 1.0 to DIN 12880
CHAMBER	
door	solid
interior	stainless steel to DIN 1.4016
housing	powder coated sheet

overall dims [mm] /1/	
A width	660
B height	590
depth C	620
internal dims [mm]	
width D	390
height E	390
depth F	350



shelves (standard max)	2 5
max shelf workload [kg] /2/	10
max unit workload [kg]	40
weight [kg]	46



Banki ING B5 o/Wodzisław Śl.
Nr rachunku 30 1030 1403 1000 0022 0879 5498
Nr rej. W BDO 000005609

NIP: 647-216-26-87 RECON: 2781198-4
Sąd Rejonowy w Gliwicach, X Wydział Gospodarczy
KRS 0000053696

2/3

Figure A2.1 - The drying oven SLW 53 SIMPLE model: Data sheet (continuation)



tel. (+48) 32 453 91 70 | e-mail: info@pol-eko.com.pl
internet: www.pol-eko.com.pl

POL-EKO-APARATURA SP. J.
A. POL-OK – KOWALSKA, S. KOWALSKI
44-300 WODZISLAW SLASKI, UL. KOKOSZYCKA 172 C

ELECTRICAL PARAMETERS

power supply	230V 50-60Hz
nominal power [W]	1700
warranty	24 months
manufacturer	POL-EKO-APARATURA

all the above technical data refer to standard units (without optional accessories)
* - fluctuation measured in centre of the chamber; in space, variation (K) calculated for chamber as:
 $K = \frac{+/- (T \text{ average max.} - T \text{ average min.})}{2}$
** - other power supplies on request
1 - depth doesn't include 50 mm of power cable

OPTIONS AND ACCESSORIES



Order number: */P INOX

Stainless steel wire shelf INOX



Order number: */PP

Perforated shelf



Order number: BRT*/L or IQ/OQ/PQ

Calibration and IQ, OQ, PQ qualification



Bank: ING B5 o/Wodzisław Sl.
Nr rachunku: 30 1050 1403 1000 0022 0879 5498
Nr rej. W BCO 000005609

NIP: 647-216-26-67 RECON: 2781198-4
Sąd Rejonowy w Gliwicach, X Wydział Gospodarczy
KRS 0000083696

Figure A2.1 - The drying oven SLW 53 SIMPLE model: Data sheet (continuation)

THE CALORIMETER IKA C 200

IKA

designed for scientists



C 200

/// Data Sheet

C 200-System consists of the following components:

Measuring cell C 200

Decomposition vessel C 5010

Oxygen filling station C 248

Consumables for calibrations and installation

Space-saving and low cost combustion calorimeter for determining gross calorific values of liquid and solid samples.

www.ika.com

Subject to technical changes



IKAworlwide



IKAworlwide // #lookattheblue



@IKAworlwide

Figure A2.2 - The calorimeter IKA C 200 model: Data sheet
(source: <https://www.ika.com/en/Products-Lab-Eq/Calorimeters-Oxygen-Bomb-calorimeter-csp-330/C-200-cpdt-8802500/>)

IKA

designed for scientists

Validation according to DIN 51900, ISO 1928, ASTM D240, ASTM D4809, ASTM D5865, ASTM D1989, ASTM D5468, ASTM E711.

Suitable for teaching and training, as well (f.e technical- schools, universities) and for industrial laboratories with less analyses..

Manual handling for water and oxygen filling.

Four different working methods, isoperibolic, dynamic, manual, time controlled makes possible an ideal adjustment of different operating tasks.

Clear and easily explained display which is simply to use .

With an external power pack, "world tension useable" from 100 - 240 V AC, 50/60 Hz. The operating voltage of the calorimeter is 24 V DC low- voltage.

Friendly in aftersales

Manual (teaching mode): ignition and end of the measurement will be done by the operator himself; the temperature increase will be indicated at the display each minute.

All calculations have to be done manually.

At the other three modes ignition and calculation of the gross calorific value will be done automatically.

The gross calorific value will be shown on the display. Acid corrections and calculations of the net calorific value have to be done manually.

The modes have different measuring times:

Isoperibolic: approx: 17 min.

Dynamic : approx. 8 min

Manual : approx. 17 min

(depend on the operator)

Time controlled : 14 min

The decomposition vessel can be equipped in to use an combustible crucibles C 14 (accessory C 5010.4 attachment is necessary)

User-friendly software C 6040 Calwin for controlling the calorimeter and administration of measuring data (assecory).

Transfer of the datas to Excel or Word are possible

Up to eight IKA measuring cells can be controlled by a single PC, using a multiseriial plug in card PCI 8.2 (accessory)

www.ika.com

Subject to technical changes



IKAworldwide



IKAworldwide // #lockattheblue



@IKAworldwide

Figure A2.2 - The calorimeter IKA C 200 model: Data sheet (continuation)

IKA

designed for scientists

Technical Data

Measuring range max. [J]	40000
Measuring mode dynamic 25°C	yes
Measuring mode isoperibol 25°C	yes
Measuring time dynamic approx. [min]	8
Measuring time isoperibol approx. [min]	17
Reproducibility dynamic (1g benzoic acid NBS39i) [%RSD]	0.1
Reproducibility isoperibol (1g benzoic acid NBS39i) [%RSD]	0.1
Working temperature max. [°C]	25
Temperature measurement resolution [K]	0.0001
Interface printer	Centronix
Interface PC	RS232
Decomposition vessel C 5010	yes
Works according to DIN 51900	yes
Works according to DIN EN ISO 1716	yes
Works according to DIN EN ISO 18125	yes
Works according to DIN EN 15400	yes
Works according to DIN CEN TS 14918	yes
Works according to DIN CEN/TS 16023	yes
Works according to DIN SPEC 19524	yes
Works according to ASTM D240	yes
Works according to ASTM D4809	yes
Works according to ASTM D5468	yes
Works according to ASTM D5865	yes
Works according to ISO 1928	yes
Works according to GOST Certified	yes
Dimensions (W x H x D) [mm]	400 x 400 x 400
Weight [kg]	28.912
Permissible ambient temperature [°C]	20 - 25
Permissible relative humidity [%]	80
Protection class according to DIN EN 60529	IP 20
RS 232 interface	yes
Voltage [V]	100 - 240
Frequency [Hz]	50/60
Power input [W]	120

www.ika.com

Subject to technical changes



IKAworlwide



IKAworlwide // #lookattheblue



@IKAworlwide

Figure A2.2 - The calorimeter IKA C 200 model: Data sheet (continuation)

THE NABERTHERM MUFFLE FURNACE L 9/11/SKM



Muffle Furnaces with Embedded Heating Elements in the Ceramic Muffle up to 1100 °C

We particularly recommend the muffle furnace L 9/11/SKM for heat treatment of aggressive substances. The furnace has a ceramic muffle with embedded heating from four sides. The muffle furnace thus combines a very good temperature uniformity with excellent protection of the heating elements from aggressive atmospheres. Another aspect is the smooth, nearly particle free muffle (furnace door made of fiber insulation), an important quality feature.

Standard Equipment

- Tmax 1100 °C
- Muffle heated from four sides
- Furnace chamber with embedded ceramic muffle, high resistance to aggressive gasses and vapours
- Optional flap door (L) which can be used as work platform or lift door (LT) with hot surface facing away from the operator
- Adjustable working air inlet in the door
- Exhaust air outlet in rear wall of furnace
- Controller B410 (5 programs with each 4 segments), alternative controllers see page 75



Muffle furnace L 9/11/SKM with flap door

Additional Equipment

- Chimney, chimney with fan or catalytic converter see page 24
- Over-temperature limiter with adjustable cutout temperature as temperature limiter to protect the oven and load
- Protective gas connection to purge with non-flammable protective or reaction gases (not available in combination with chimney, chimney with fan or catalytic converter) not gas tight
- Manual or automation gas supply system
- Port for thermocouple in the rear wall or in the furnace door
- Please see page 25 for more accessories

Modell	Tmax in °C ¹	Inner dimensions in mm			Volume in l	Outer dimensions ² in mm			Connected load in kW	Electrical connection ³	Weight in kg	Heating time in min ⁴
		w	d	h		W	D	H				
L 9/11/SKM	1100	230	240	170	9	490	505	580	3.4	1-phase	50	75
LT 9/11/SKM	1100	230	240	170	9	490	505	580+320 ⁵	3.4	1-phase	50	75

¹Recommended working temperature for processes with longer dwell times is 1000 °C

²External dimensions vary when furnace is equipped with additional equipment. Dimensions on request.

³Including opened lift door

⁴Heating time of the empty and closed furnace up to Tmax = 100 K (connected to 230 V 1/N/PE)

⁵Please see page 75 for more information about supply voltage



Muffle furnace L 9/11/SKM

Gas supply system for non-flammable protective or reactive gas

Muffle heated from four sides

19

Figure A2.3 - The Nabertherm Muffle furnace L 9/11/SKM with flap door
(Source: <https://www.nabertherm.com/en/products/laboratory/muffle-furnaces>)

Anexa 3: Experimental study on the biomass micro-cogeneration unit with a Stirling engine

Table A3.1 - Polynomial function coefficients of the composing gases densities

Coefficient	kg/m ³ ρ CO ₂	kg/m ³ ρ N ₂	kg/m ³ ρ O ₂	kg/m ³ ρ H ₂ O	kg/m ³ ρ air	kg/m ³ ρ SO ₂	kg/m ³ ρ wet air
x5	-3.3692E-14	-2.4939E-14	-7.87E-15	-1.0547E-09	-6.9304E-15	0	-6.8889E-15
x4	1.1736E-10	1.053E-10	2.4073E-11	2.2417E-06	3.0865E-11	0	3.068E-11
x3	-1.6157E-07	-1.6512E-07	-2.8125E-08	-0.00187103	-5.3564E-08	0	-5.3243E-08
x2	0.00011203	0.00012077	1.5746E-05	0.76364447	4.5862E-05	0	4.5588E-05
x1	-0.04107469	-0.04233886	-0.00434968	-152.709543	-0.02022652	0	-0.02010537
x0	7.50703833	6.52637153	0.54891167	12999.0431	4.33302763	2.6288	4.30707539

Table A3.2 - Polynomial function coefficients of the composing gas heat transfer coefficients

Coefficient	kJ/(m ³ N·K) cp_CO ₂	kJ/(m ³ N·K) cp_N ₂	kJ/(m ³ N·K) cp_O ₂	kJ/(m ³ N·K) cp_H ₂ O	kJ/(m ³ N·K) cp_air	kJ/(m ³ N·K) cp_SO ₂	kJ/(m ³ N·K) cp_wet air
x5	9.7726E-18	-7.9918E-18	-1.4136E-17	-3.8624E-18	-9.3772E-18	3.2299E-17	-8.9337E-18
x4	-9.9232E-14	7.6222E-14	1.1599E-13	4.3542E-14	8.5293E-14	-3.1076E-13	8.5175E-14
x3	4.2072E-10	-2.7852E-10	-3.4433E-10	-1.9294E-10	-2.9438E-10	1.1082E-09	-3.0588E-10
x2	-9.9835E-07	4.5924E-07	4.1063E-07	3.7923E-07	4.5162E-07	-1.8967E-06	4.8396E-07
x1	0.00151425	-0.00021749	-1.357E-05	-6.3841E-05	-0.00017607	0.00189083	-0.00019917
x0	1.25354676	1.32538642	1.28307137	1.48640492	1.3168157	1.32609213	1.3449416

Annex A4: Mathematical model

Table A4. 1 - Fuel properties in different configurations (TNO Database, Bouvenot, 2015)

Fuel properties							
Initial [i]	Dry [dry]		Wet Ash Free [waf]		Dry Ash Free [daf]		
Carbon content	Carbon content		Carbon content		Carbon content		
Oak	49.92%	Oak	49.92%	Oak	51.13%	Oak	51.13%
Beech	48.23%	Beech	48.23%	Beech	48.64%	Beech	48.64%
Douglas Fir	50.64%	Douglas Fir	50.64%	Douglas Fir	50.69%	Douglas Fir	50.69%
Bois d'Or Pellets	47.90%	Bois d'Or Pellets	51.29%	Bois d'Or Pellets	48.11%	Bois d'Or Pellets	51.53%
Hydrogen content	Hydrogen content		Hydrogen content		Hydrogen content		
Oak	5.94%	Oak	5.94%	Oak	6.08%	Oak	6.08%
Beech	5.80%	Beech	5.80%	Beech	5.85%	Beech	5.85%
Douglas Fir	6.18%	Douglas Fir	6.18%	Douglas Fir	6.19%	Douglas Fir	6.19%
Bois d'Or Pellets	5.80%	Bois d'Or Pellets	6.21%	Bois d'Or Pellets	5.83%	Bois d'Or Pellets	6.24%
Nitrogen content	Nitrogen content		Nitrogen content		Nitrogen content		
Oak	0.38%	Oak	0.38%	Oak	0.39%	Oak	0.39%
Beech	0.29%	Beech	0.29%	Beech	0.29%	Beech	0.29%
Douglas Fir	0.06%	Douglas Fir	0.06%	Douglas Fir	0.06%	Douglas Fir	0.06%
Bois d'Or Pellets	0.05%	Bois d'Or Pellets	0.05%	Bois d'Or Pellets	0.05%	Bois d'Or Pellets	0.05%
Sulphur content	Sulphur content		Sulphur content		Sulphur content		
Oak	0.05%	Oak	0.05%	Oak	0.05%	Oak	0.05%
Beech	0.03%	Beech	0.03%	Beech	0.03%	Beech	0.03%
Douglas Fir	0.02%	Douglas Fir	0.02%	Douglas Fir	0.02%	Douglas Fir	0.02%
Bois d'Or Pellets	0.00%	Bois d'Or Pellets	0.01%	Bois d'Or Pellets	0.01%	Bois d'Or Pellets	0.01%
Oxygen content	Oxygen content		Oxygen content		Oxygen content		
Oak	41.34%	Oak	41.34%	Oak	42.35%	Oak	42.35%
Beech	44.80%	Beech	44.80%	Beech	45.19%	Beech	45.19%
Douglas Fir	43.00%	Douglas Fir	43.00%	Douglas Fir	43.04%	Douglas Fir	43.04%
Bois d'Or Pellets	39.20%	Bois d'Or Pellets	41.97%	Bois d'Or Pellets	39.37%	Bois d'Or Pellets	42.17%
Moisture W_t^i	Moisture W_t^i		Moisture W_t^i		Moisture W_t^i		
Oak	0.00%	Oak	0.00%	Oak	0.00%	Oak	0.00%
Beech	0.00%	Beech	0.00%	Beech	0.00%	Beech	0.00%
Douglas Fir	0.00%	Douglas Fir	0.00%	Douglas Fir	0.00%	Douglas Fir	0.00%
Bois d'Or Pellets	6.60%	Bois d'Or Pellets	0.00%	Bois d'Or Pellets	6.63%	Bois d'Or Pellets	0.00%
Ash	Ash		Ash		Ash		
Oak	2.37%	Oak	2.37%	Oak	0.00%	Oak	0.00%
Beech	0.85%	Beech	0.85%	Beech	0.00%	Beech	0.00%
Douglas Fir	0.10%	Douglas Fir	0.10%	Douglas Fir	0.00%	Douglas Fir	0.00%
Bois d'Or Pellets	0.45%	Bois d'Or Pellets	0.47%	Bois d'Or Pellets	0.00%	Bois d'Or Pellets	0.00%

Table A4. 1 - Fuel properties in different configurations (continuation)

Total		Total		Total		Total	
Oak	100.00%	Oak	100.00%	Oak	100.00%	Oak	100.00%
Beech	100.00%	Beech	100.00%	Beech	100.00%	Beech	100.00%
Douglas Fir	100.00%	Douglas Fir	100.00%	Douglas Fir	100.00%	Douglas Fir	100.00%
Bois d'Or Pellets	100.00%	Bois d'Or Pellets	100.00%	Bois d'Or Pellets	100.00%	Bois d'Or Pellets	100.00%
ρ_{fuel}		kg/m ³		LHV_{fuel_literature}		MJ/kg	
Oak		750		Oak		19.15	
Beech		800		Beech		17.43	
Douglas Fir		530		Douglas Fir		19.02	
Bois d'Or Pellets		698		Bois d'Or Pellets		17.64	

Table A4.2 - Properties of the air entering combustion (Bouvenot, 2015, Leca 1994)

Air and vapor properties		
ρ_{air}	1.293	kg/m ³ N
V _{vapor}	1.242	m ³ N/kg
$\eta_{comb_chamber}$	95.00%	-
t _{atm}	20	°C
t _{ref}	15	°C
λ	1.2	-
Q _{loss_inc_fuel}	0	%
X _{air}	10	g/kg
c _p _{water}	1.996	kJ/(kg*K)
c _p _{air}	1.006	kJ/(kg*K)

Table A4.3 - Lower Heating Values using different formulas

LHV [MJ/kg]	Moisture [%W ₁]						
	0	10	20	30	40	50	60
LHV1	18,347	16,261	14,175	12,089	10,003	7,917	5,831
LHV2	16,753	15,078	13,403	11,727	10,052	8,377	6,701
LHV3	19,974	16,179	12,783	9,786	7,190	4,992	3,194

Table A4.4 - Differences between LHV values obtained through literature and the relation (4.1)

LHV _{fuel_lit}	kJ/kg	LHV relation (4.1)	kJ/kg	Difference	%
Oak	19,150	Oak	18,553	Oak	-3.12%
Beech	17,430	Beech	17,456	Beech	0.15%
Douglas Fir	19,020	Douglas Fir	18,860	Douglas Fir	-0.84%
Bois d'Or Pellets	17,640	Bois d'Or Pellets	17,786	Bois d'Or Pellets	0.83%

Table A4.5 - Calculated specific volumes of the air entering the combustion chamber

Air Specific Volumes			
V _{thdryair}	m ³ N/ kg _{fuel}	V _{thwetair}	m ³ N/ kg _{fuel}
Oak	4.64769	Oak	4.72252
Beech	4.34405	Beech	4.41399
Douglas Fir	4.71940	Douglas Fir	4.79538
Bois d'Or Pellets	4.50060	Bois d'Or Pellets	4.57306

Table A4.5 - Calculated specific volumes of the air entering the combustion chamber (continuation)

Air Specific Volumes			
$V_{\text{real,dry,air}}$	$\text{m}^3/\text{kg}_{\text{fuel}}$	$V_{\text{real,wet,air}}$	$\text{m}^3/\text{kg}_{\text{fuel}}$
Oak	5.57723	Oak	5.66703
Beech	5.21286	Beech	5.29678
Douglas Fir	5.66328	Douglas Fir	5.75446
Bois d'Or Pellets	5.40072	Bois d'Or Pellets	5.48767

Table A4.6 - Calculated specific volumes of the flue gas

Flue Gas Specific Volumes			
V_{thCO_2}	$\text{m}^3/\text{kg}_{\text{fuel}}$	$V_{\text{thH}_2\text{O}}$	$\text{m}^3/\text{kg}_{\text{fuel}}$
Oak	0.93241	Oak	0.74011
Beech	0.90084	Beech	0.71954
Douglas Fir	0.94585	Douglas Fir	0.76814
Bois d'Or Pellets	0.89468	Bois d'Or Pellets	0.80416
V_{thSO_2}	$\text{m}^3/\text{kg}_{\text{fuel}}$	V_{thwetFG}	$\text{m}^3/\text{kg}_{\text{fuel}}$
Oak	0.00035	Oak	5.34758
Beech	0.00021	Beech	5.05471
Douglas Fir	0.00014	Douglas Fir	5.44294
Bois d'Or Pellets	0.00005	Bois d'Or Pellets	5.25476
$V_{\text{thCO}_2+\text{SO}_2}$	$\text{m}^3/\text{kg}_{\text{fuel}}$	$V_{\text{real,dryFG}}$	$\text{m}^3/\text{kg}_{\text{fuel}}$
Oak	0.93276	Oak	5.53701
Beech	0.90105	Beech	5.20398
Douglas Fir	0.94599	Douglas Fir	5.61868
Bois d'Or Pellets	0.89473	Bois d'Or Pellets	5.35072
V_{thN_2}	$\text{m}^3/\text{kg}_{\text{fuel}}$	$V_{\text{realH}_2\text{O}}$	$\text{m}^3/\text{kg}_{\text{fuel}}$
Oak	3.67472	Oak	0.74011
Beech	3.43412	Beech	0.71954
Douglas Fir	3.72881	Douglas Fir	0.76814
Bois d'Or Pellets	3.55587	Bois d'Or Pellets	0.80675
V_{thdryFG}	$\text{m}^3/\text{kg}_{\text{fuel}}$	$V_{\text{realwetFG}}$	$\text{m}^3/\text{kg}_{\text{fuel}}$
Oak	4.60747	Oak	6.29209
Beech	4.33517	Beech	5.93750
Douglas Fir	4.67480	Douglas Fir	6.40202
Bois d'Or Pellets	4.45060	Bois d'Or Pellets	6.16937

Table A4.7 - Fuel volumes and masses

V_{fuel}	m^3	m_{fuel}	kg	$Q_{\text{in,fuel}}$	kJ
Oak	4.23813E-07	Oak	0.00031786	Oak	5.897
Beech	4.21052E-07	Beech	0.000336842	Beech	5.880
Douglas Fir	5.89437E-07	Douglas Fir	0.000312401	Douglas Fir	5.892
Bois d'Or Pellets	4.64444E-07	Bois d'Or Pellets	0.000324182	Bois d'Or Pellets	5.766

Table A4.8 - Calculated air masses and resulted heat from air

Air Masses			
$m_{\text{th,dry,air}}$	kg/kg_{fuel}	$m_{\text{real,wet,air}}$	kg/kg_{fuel}
Oak	5.98465	Oak	7.25339
Beech	5.59269	Beech	6.77834
Douglas Fir	6.07659	Douglas Fir	7.36482
Bois d'Or Pellets	5.79519	Bois d'Or Pellets	7.02377
$m_{\text{real,dry,air}}$	kg/kg_{fuel}	m_{air}	kg
Oak	7.18158	Oak	0.00231
Beech	6.71123	Beech	0.00228
Douglas Fir	7.29190	Douglas Fir	0.00230
Bois d'Or Pellets	6.95423	Bois d'Or Pellets	0.00228
$m_{\text{th,wet,air}}$	kg/kg_{fuel}	$Q_{\text{in,air}}$	kJ
Oak	6.04449	Oak	0.01160
Beech	5.64862	Beech	0.01148
Douglas Fir	6.13735	Douglas Fir	0.01157
Bois d'Or Pellets	5.85314	Bois d'Or Pellets	0.01145

Table A4.9 - Air and flue gas volumes results

Air Volumes		Flue Gas Volumes	
V_{thO_2}	m³N/kg_{fuel}	$V_{\text{thCO}_2 \text{ FG}}$	m³N/kg_{fuel}
Oak	0.97602	Oak	0.93241
Beech	0.91225	Beech	0.90084
Douglas Fir	0.99107	Douglas Fir	0.94585
Bois d'Or Pellets	0.94512	Bois d'Or Pellets	0.89468
$V_{\text{thdry,air}}$	m³N/kg_{fuel}	$V_{\text{thSO}_2 \text{ FG}}$	m³N/kg_{fuel}
Oak	4.64769	Oak	0.00035
Beech	4.34405	Beech	0.00021
Douglas Fir	4.71940	Douglas Fir	0.00014
Bois d'Or Pellets	4.50060	Bois d'Or Pellets	0.00005
$V_{\text{thH}_2\text{O air}}$	m³N/kg_{fuel}	$V_{\text{thN}_2 \text{ FG}}$	m³N/kg_{fuel}
Oak	0.07483	Oak	3.67472
Beech	0.06994	Beech	3.43412
Douglas Fir	0.07598	Douglas Fir	3.72881
Bois d'Or Pellets	0.07246	Bois d'Or Pellets	3.55587
		$V_{\text{thH}_2\text{O FG}}$	m³N/kg_{fuel}
		Oak	0.74011
		Beech	0.71954
		Douglas Fir	0.76814
		Bois d'Or Pellets	0.80416

Table A4.10 - Specific volume heat coefficients of air and flue gas components

°C	K	kJ/(m ³ _N ·K)	kJ/(m ³ _N ·K)	kJ/(m ³ _N ·K)	kJ/(m ³ _N ·K)	kJ/(m ³ _N ·K)	kJ/(m ³ _N ·K)	kJ/(m ³ _N ·K)
t	T	cpCO ₂	cpN ₂	cpO ₂	cpH ₂ O	cpair	cpSO ₂	cpwet air
0	273.15	1.5998	1.2946	1.3059	1.4943	1.2971	1.7330	1.3200
100	373.15	1.7003	1.2958	1.3176	1.5052	1.3004	1.8130	1.3250
200	473.15	1.7874	1.2996	1.3352	1.5223	1.3071	1.8880	1.3300
300	573.15	1.8627	1.3067	1.3561	1.5424	1.3172	1.9550	1.3430
400	673.15	1.9297	1.3163	1.3775	1.5655	1.3289	2.0180	1.3500
500	773.15	1.9887	1.3276	1.3980	1.5897	1.3427	2.0680	1.3700
600	873.15	2.0411	1.3402	1.4168	1.6149	1.3565	2.1140	1.3800
700	973.15	2.0884	1.3536	1.4344	1.6412	1.3708	2.1520	1.3950
800	1073.15	2.1311	1.3670	1.4499	1.6680	1.3842	2.1810	1.4100
900	1173.15	2.1692	1.3796	1.4645	1.6957	1.3976	2.2150	1.4250
1000	1273.15	2.2035	1.3917	1.4775	1.7229	1.4097	2.2360	1.4350
1100	1373.15	2.2349	1.4034	1.4893	1.7501	1.4214	2.2610	1.4580
1200	1473.15	2.2638	1.4143	1.5006	1.7769	1.4327	2.2780	1.4650
1300	1573.15	2.2898	1.4252	1.5106	1.8028	1.4432	2.3070	1.4730
1400	1673.15	2.3136	1.4348	1.5202	1.8283	1.4528	2.3570	1.4800
1500	1773.15	2.3354	1.4440	1.5294	1.8527	1.4620	2.3990	1.4940
1600	1873.15	2.3555	1.4528	1.5378	1.8761	1.4708	2.4280	1.5030
1700	1973.15	2.3743	1.4612	1.5462	1.8996	1.4788	2.4533	1.5100
1800	2073.15	2.3915	1.4687	1.5541	1.9213	1.4867	2.4740	1.5200
1900	2173.15	2.4074	1.4759	1.5617	1.9423	1.4939	2.4870	1.5240
2000	2273.15	2.4221	1.4826	1.5692	1.9628	1.5010	2.5000	1.5300
2100	2373.15	2.4359	1.4893	1.5759	1.9825	1.5073	2.5110	1.5400
2200	2473.15	2.4484	1.4951	1.5830	2.0009	1.5135	2.5220	1.5460
2300	2573.15	2.4602	1.5010	1.5897	2.0189	1.5194	2.5330	1.5520
2400	2673.15	2.4711	1.5064	1.5964	2.0365	1.5253	2.5370	1.5580
2500	2773.15	2.4811	1.5114	1.6027	2.0528	1.5303	2.5410	1.5630

Table A4.11 - Obtained results for the 5th degree regression for the specific volume heat coefficients

	cpCO ₂	cpN ₂	cpO ₂	cpH ₂ O	cpair	cpSO ₂	cpwet air
C5(T⁵)	7,78764E-18	-8,8145E-18	-9,16E-18	-2,2672E-18	-8,89722E-18	5,62884E-17	-1,08E-17
C4(T⁴)	-8,2717E-14	8,30671E-14	7,45559E-14	3,027E-14	8,12991E-14	-5,1036E-13	1,00994E-13
C3(T³)	3,68905E-10	-2,99998E-10	-2,14336E-10	-1,513E-10	-2,81853E-10	1,73445E-09	-3,55508E-10
c2(T²)	-9,22771E-07	4,90563E-07	2,21012E-07	3,18496E-07	4,33344E-07	-2,81011E-06	5,56358E-07
c1(T¹)	0,001463914	-0,000238355	0,000112717	-2,33889E-05	-0,000163897	0,002499182	-0,000247382
c0(T⁰)	1,265507041	1,330343561	1,253064629	1,4767932	1,313923344	1,181542702	1,35639762

Table A4.12 - Results of the theoretical and real heat entering the combustion

Q_{in_th}	kJ	Q_{in_real}	kJ
Oak	18591	Oak	17662
Beech	17497	Beech	16622
Douglas Fir	18898	Douglas Fir	17953
Bois d'Or Pellets	17842	Bois d'Or Pellets	16950

Table A4.13 - Combustion air components specific heat coefficients

$c_{p_{air}}(T_{atm})$	$\text{kJ}/(\text{m}^3\text{N}\cdot\text{K})$	$c_{p_{air}}(T_{ref})$	$\text{kJ}/(\text{m}^3\text{N}\cdot\text{K})$	$c_{p_{H_2O}}(T_{atm})$	$\text{kJ}/(\text{m}^3\text{N}\cdot\text{K})$	$c_{p_{H_2O}}(T_{ref})$	$\text{kJ}/(\text{m}^3\text{N}\cdot\text{K})$
Oak	1.29660	Oak	1.29648	Oak	1.49371	Oak	1.49308
Beech	1.29660	Beech	1.29648	Beech	1.49371	Beech	1.49308
Douglas Fir	1.29660	Douglas Fir	1.29648	Douglas Fir	1.49371	Douglas Fir	1.49308
Bois d'Or Pellets	1.29660	Bois d'Or Pellets	1.29648	Bois d'Or Pellets	1.49371	Bois d'Or Pellets	1.49308

Table A4.14 - Flue gas components heat transfer coefficients at reference temperature T_{ref}

T_{ref}	K	$c_{p_{CO_2}}$	$\text{kJ}/(\text{m}^3\text{N}\cdot\text{K})$	$c_{p_{SO_2}}$	$\text{kJ}/(\text{m}^3\text{N}\cdot\text{K})$
Oak	288.15	Oak	1.6190	Oak	1.7064
Beech	288.15	Beech	1.6190	Beech	1.7064
Douglas Fir	288.15	Douglas Fir	1.6190	Douglas Fir	1.7064
Bois d'Or Pellets	288.15	Bois d'Or Pellets	1.6190	Bois d'Or Pellets	1.7064
$c_{p_{N_2}}$	$\text{kJ}/(\text{m}^3\text{N}\cdot\text{K})$	$c_{p_{H_2O}}$	$\text{kJ}/(\text{m}^3\text{N}\cdot\text{K})$	$c_{p_{wet\ air}}$	$\text{kJ}/(\text{m}^3\text{N}\cdot\text{K})$
Oak	1.2958	Oak	1.4931	Oak	1.3235
Beech	1.2958	Beech	1.4931	Beech	1.3235
Douglas Fir	1.2958	Douglas Fir	1.4931	Douglas Fir	1.3235
Bois d'Or Pellets	1.2958	Bois d'Or Pellets	1.4931	Bois d'Or Pellets	1.3235

Table A4.15 - The 8 - iteration calculation performed to find the flue gas temperature T_{FG}

Iteration 1		Iteration 2		Iteration 3		Iteration 4	
T_{FG}	[K]	T_{FG}	[K]	T_{FG}	[K]	T_{FG}	[K]
Oak	1523.15	Oak	2002,91	Oak	1929,54	Oak	1939,07
Beech	1523.15	Beech	1992,75	Beech	1920,69	Beech	1930,12
Douglas Fir	1523.15	Douglas Fir	2000,81	Douglas Fir	1927,64	Douglas Fir	1937,17
Bois d'Or Pellets	1523.15	Bois d'Or Pellets	1961,83	Bois d'Or Pellets	1894,44	Bois d'Or Pellets	1903,36
$c_{p_{CO_2}}$	$\text{kJ}/(\text{m}^3\cdot\text{K})$	$c_{p_{CO_2}}$	$\text{kJ}/(\text{m}^3\cdot\text{K})$	$c_{p_{CO_2}}$	$\text{kJ}/(\text{m}^3\cdot\text{K})$	$c_{p_{CO_2}}$	$\text{kJ}/(\text{m}^3\cdot\text{K})$
Oak	2.2767	Oak	2,3797	Oak	2,3665	Oak	2,3682
Beech	2.2767	Beech	2,3779	Beech	2,3648	Beech	2,3666
Douglas Fir	2.2767	Douglas Fir	2,3794	Douglas Fir	2,3661	Douglas Fir	2,3679
Bois d'Or Pellets	2.2767	Bois d'Or Pellets	2,3724	Bois d'Or Pellets	2,3599	Bois d'Or Pellets	2,3616
$c_{p_{N_2}}$	$\text{kJ}/(\text{m}^3\cdot\text{K})$	$c_{p_{N_2}}$	$\text{kJ}/(\text{m}^3\cdot\text{K})$	$c_{p_{N_2}}$	$\text{kJ}/(\text{m}^3\cdot\text{K})$	$c_{p_{N_2}}$	$\text{kJ}/(\text{m}^3\cdot\text{K})$
Oak	1.4201	Oak	1,4631	Oak	1,4574	Oak	1,4581
Beech	1.4201	Beech	1,4624	Beech	1,4567	Beech	1,4574
Douglas Fir	1.4201	Douglas Fir	1,4630	Douglas Fir	1,4572	Douglas Fir	1,4580
Bois d'Or Pellets	1.4201	Bois d'Or Pellets	1,4599	Bois d'Or Pellets	1,4545	Bois d'Or Pellets	1,4553

Table A4.15 - The 8 - iteration calculation performed to find the flue gas temperature T_{FG} (continuation)

c_{pSO_2}	$\text{kJ}/(\text{m}^3\cdot\text{K})$	c_{pSO_2}	$\text{kJ}/(\text{m}^3\cdot\text{K})$	c_{pSO_2}	$\text{kJ}/(\text{m}^3\cdot\text{K})$	c_{pSO_2}	$\text{kJ}/(\text{m}^3\cdot\text{K})$
Oak	2.3123	Oak	2,4512	Oak	2,4326	Oak	2,4351
Beech	2.3123	Beech	2,4487	Beech	2,4303	Beech	2,4328
Douglas Fir	2.3123	Douglas Fir	2,4507	Douglas Fir	2,4321	Douglas Fir	2,4346
Bois d'Or Pellets	2.3123	Bois d'Or Pellets	2,4410	Bois d'Or Pellets	2,4232	Bois d'Or Pellets	2,4257
c_{pH_2O}	$\text{kJ}/(\text{m}^3\cdot\text{K})$	c_{pH_2O}	$\text{kJ}/(\text{m}^3\cdot\text{K})$	c_{pH_2O}	$\text{kJ}/(\text{m}^3\cdot\text{K})$	c_{pH_2O}	$\text{kJ}/(\text{m}^3\cdot\text{K})$
Oak	1.7898	Oak	1,9060	Oak	1,8895	Oak	1,8917
Beech	1.7898	Beech	1,9038	Beech	1,8875	Beech	1,8896
Douglas Fir	1.7898	Douglas Fir	1,9055	Douglas Fir	1,8891	Douglas Fir	1,8912
Bois d'Or Pellets	1.7898	Bois d'Or Pellets	1,8968	Bois d'Or Pellets	1,8814	Bois d'Or Pellets	1,8835
$c_{p\text{air}}$	$\text{kJ}/(\text{m}^3\cdot\text{K})$	$c_{p\text{air}}$	$\text{kJ}/(\text{m}^3\cdot\text{K})$	$c_{p\text{air}}$	$\text{kJ}/(\text{m}^3\cdot\text{K})$	$c_{p\text{air}}$	$\text{kJ}/(\text{m}^3\cdot\text{K})$
Oak	1.4688	Oak	1,5124	Oak	1,5067	Oak	1,5074
Beech	1.4688	Beech	1,5116	Beech	1,5060	Beech	1,5067
Douglas Fir	1.4688	Douglas Fir	1,5123	Douglas Fir	1,5065	Douglas Fir	1,5073
Bois d'Or Pellets	1.4688	Bois d'Or Pellets	1,5092	Bois d'Or Pellets	1,5038	Bois d'Or Pellets	1,5046
Iteration 5		Iteration 6		Iteration 7		Iteration 8	
T_{FG}	[K]	T_{FG}	[K]	T_{FG}	[K]	T_{FG}	[K]
Oak	1937,81	Oak	1937,97	Oak	1937,95	Oak	1937,96
Beech	1928,86	Beech	1929,02	Beech	1929,00	Beech	1929,01
Douglas Fir	1935,90	Douglas Fir	1936,07	Douglas Fir	1936,04	Douglas Fir	1936,05
Bois d'Or Pellets	1902,15	Bois d'Or Pellets	1902,31	Bois d'Or Pellets	1902,29	Bois d'Or Pellets	1902,30
c_{pCO_2}	$\text{kJ}/(\text{m}^3\cdot\text{K})$	c_{pCO_2}	$\text{kJ}/(\text{m}^3\cdot\text{K})$	c_{pCO_2}	$\text{kJ}/(\text{m}^3\cdot\text{K})$	c_{pCO_2}	$\text{kJ}/(\text{m}^3\cdot\text{K})$
Oak	2,3680	Oak	2,3680	Oak	2,3680	Oak	2,3680
Beech	2,3664	Beech	2,3664	Beech	2,3664	Beech	2,3664
Douglas Fir	2,3677	Douglas Fir	2,3677	Douglas Fir	2,3677	Douglas Fir	2,3677
Bois d'Or Pellets	2,3613	Bois d'Or Pellets	2,3614	Bois d'Or Pellets	2,3613	Bois d'Or Pellets	2,3613
c_{pN_2}	$\text{kJ}/(\text{m}^3\cdot\text{K})$	c_{pN_2}	$\text{kJ}/(\text{m}^3\cdot\text{K})$	c_{pN_2}	$\text{kJ}/(\text{m}^3\cdot\text{K})$	c_{pN_2}	$\text{kJ}/(\text{m}^3\cdot\text{K})$
Oak	1,4580	Oak	1,4581	Oak	1,4581	Oak	1,4581
Beech	1,4573	Beech	1,4573	Beech	1,4573	Beech	1,4573
Douglas Fir	1,4579	Douglas Fir	1,4579	Douglas Fir	1,4579	Douglas Fir	1,4579
Bois d'Or Pellets	1,4552	Bois d'Or Pellets	1,4552	Bois d'Or Pellets	1,4552	Bois d'Or Pellets	1,4552

Table A4.15 - The 8 - iteration calculation performed to find the flue gas temperature T_{FG} (continuation)

cp_{SO_2}	$kJ/(m^3 \cdot K)$	cp_{SO_2}	$kJ/(m^3 \cdot K)$	cp_{SO_2}	$kJ/(m^3 \cdot K)$	cp_{SO_2}	$kJ/(m^3 \cdot K)$
Oak	2,4348	Oak	2,4348	Oak	2,4348	Oak	2,4348
Beech	2,4324	Beech	2,4325	Beech	2,4325	Beech	2,4325
Douglas Fir	2,4343	Douglas Fir	2,4343	Douglas Fir	2,4343	Douglas Fir	2,4343
Bois d'Or Pellets	2,4253	Bois d'Or Pellets	2,4254	Bois d'Or Pellets	2,4254	Bois d'Or Pellets	2,4254
cp_{H_2O}	$kJ/(m^3 \cdot K)$	cp_{H_2O}	$kJ/(m^3 \cdot K)$	cp_{H_2O}	$kJ/(m^3 \cdot K)$	cp_{H_2O}	$kJ/(m^3 \cdot K)$
Oak	1,8914	Oak	1,8914	Oak	1,8914	Oak	1,8914
Beech	1,8893	Beech	1,8894	Beech	1,8894	Beech	1,8894
Douglas Fir	1,8909	Douglas Fir	1,8910	Douglas Fir	1,8910	Douglas Fir	1,8910
Bois d'Or Pellets	1,8832	Bois d'Or Pellets	1,8832	Bois d'Or Pellets	1,8832	Bois d'Or Pellets	1,8832
cp_{air}	$kJ/(m^3 \cdot K)$	cp_{air}	$kJ/(m^3 \cdot K)$	cp_{air}	$kJ/(m^3 \cdot K)$	cp_{air}	$kJ/(m^3 \cdot K)$
Oak	1,5073	Oak	1,5073	Oak	1,5073	Oak	1,5073
Beech	1,5066	Beech	1,5066	Beech	1,5066	Beech	1,5066
Douglas Fir	1,5072	Douglas Fir	1,5072	Douglas Fir	1,5072	Douglas Fir	1,5072
Bois d'Or Pellets	1,5045	Bois d'Or Pellets	1,5045	Bois d'Or Pellets	1,5045	Bois d'Or Pellets	1,5045

Table A4.16 - Molar masses of the air and flue gas components

Parameter	Symbol	Calculated data		Parameter	Symbol	Value	u.m.
		Value	u.m.				
Molar mass of C	M_C	12.01115	kg/kmol	Molar mass of CO_2	M_{CO_2}	44.00995	kg/kmol
Molar mass of H	M_H	1.00797	kg/kmol	Molar mass of H_2O	M_{H_2O}	18.01534	kg/kmol
Molar mass of O	M_O	15.9994	kg/kmol	Molar mass of HCl	M_{HCl}	36.46	kg/kmol
Molar mass of Cl	M_{Cl}	35.4527	kg/kmol	Molar mass of SO_2	M_{SO_2}	64.0628	kg/kmol
Molar mass of S	M_S	32.064	kg/kmol	Molar mass of N_2	M_{N_2}	28.01348	kg/kmol
Molar mass of N	M_N	14.00674	kg/kmol	Molar mass of O_2	M_{O_2}	31.9988	kg/kmol

Table A4.17 - Results obtained for products entering combustion (wet ash free)

$m^{waf}_{O_2 in comb}$	kg/kg_{fuel}	$m^{waf}_{N_2 in comb}$	kg/kg_{fuel}
Oak	1.70657	Oak	5.64934
Beech	1.57035	Beech	5.19841
Douglas Fir	1.69341	Douglas Fir	5.60579
Bois d'Or Pellets	1.62056	Bois d'Or Pellets	5.36461
LHV^i_{fuel}	kg/kg_{fuel}	$m^{waf}_{air in comb}$	kg/kg_{fuel}
Oak	18,553	Oak	7.35591
Beech	17,456	Beech	6.76876
Douglas Fir	18,860	Douglas Fir	7.29920
Bois d'Or Pellets	17,786	Bois d'Or Pellets	6.98517

Table A4.18 - Masses of the products resulted from combustion (wet ash free)

$m^{\text{waf}}_{\text{CO}_2\text{out}_{\text{comb}}}$	kg/kg _{fuel}	$m^{\text{waf}}_{\text{SO}_2\text{out}_{\text{comb}}}$	kg/kg _{fuel}	$m^{\text{waf}}_{\text{N}_2\text{out}_{\text{comb}}}$	kg/kg _{fuel}
Oak	1.87352	Oak	0.00102	Oak	5.65323
Beech	1.78234	Beech	0.00060	Beech	5.20134
Douglas Fir	1.85735	Douglas Fir	0.00040	Douglas Fir	5.60639
Bois d'Or Pellets	1.76291	Bois d'Or Pellets	0.00014	Bois d'Or Pellets	5.36511
$m^{\text{waf}}_{\text{H}_2\text{Oout}_{\text{comb}}}$	kg/kg _{fuel}	$m^{\text{waf}}_{\text{O}_2\text{out}_{\text{comb}}}$	kg/kg _{fuel}	$m^{\text{waf}}_{\text{FG}}$	kg/kg _{fuel}
Oak	0.54371	Oak	0.28443	Oak	8.35591
Beech	0.52276	Beech	0.26173	Beech	7.76876
Douglas Fir	0.55283	Douglas Fir	0.28224	Douglas Fir	8.29920
Bois d'Or Pellets	0.58691	Bois d'Or Pellets	0.27009	Bois d'Or Pellets	7.98517

Table A4.19 - Coefficients for the flue gases compounds (Mărculescu, 2017)

Compound i	Symbol	a_i	b_i	c_i
Carbon Dioxide	CO ₂	1.005	0.0001997	-1046.0
Nitrogen	N ₂	1.021	0.0001345	-1793.0
Oxygen	O ₂	0.936	0.0001308	-6537.5
Sulfur Dioxide	SO ₂	0.722	0.0001229	-12029.0
Water	H ₂ O	1.697	0.0005718	0.0

Table A4.20 - Sums of products between coefficients of the flue gas products

$\sum_i^n m_i \cdot a_i$		$\sum_i^n m_i \cdot \frac{b_i}{2}$		$\sum_i^n m_i \cdot c_i$	
Oak	8.96930630	Oak	0.00076239	Oak	-13967.706
Beech	8.34921381	Beech	0.00071372	Beech	-12908.627
Douglas Fir	8.91723493	Douglas Fir	0.00075989	Douglas Fir	-13844.972
Bois d'Or Pellets	8.61694341	Bois d'Or Pellets	0.00074227	Bois d'Or Pellets	-13231.074

Table A4.21 - Equation (4.88) coefficients of the combustion adiabatic temperature terms

T_{FG}^2 coefficient (C ₁)		T_{FG}^1 coefficient (C ₂)	
Oak	0.00076239	Oak	8.96930630
Beech	0.00071372	Beech	8.34921381
Douglas Fir	0.00075989	Douglas Fir	8.91723493
Bois d'Or Pellets	0.00074227	Bois d'Or Pellets	8.61694341
T_{FG}^0 coefficient (C ₃)		$T_{\text{FG}}^{(-1)}$ coefficient (C ₄)	
Oak	-19940.39364	Oak	13967.70574
Beech	-18985.69866	Beech	12908.62738
Douglas Fir	-20615.92810	Douglas Fir	13844.97225
Bois d'Or Pellets	-19447.01289	Bois d'Or Pellets	13231.07355

Table A4.22 - Extract of the wooden species tables of the equation (4.88) function containing temperatures, results and "found" function (step:10)

Oak			Beech			Douglas Fir			Bois d'Or Pellets		
T_{FG} [K]	f(T_{FG})	Found?	T_{FG} [K]	f(T_{FG})	Found?	T_{FG} [K]	f(T_{FG})	Found?	T_{FG} [K]	f(T_{FG})	Found?
1888.15	-281	no	1928.15	-233	no	1948.15	-353	no	1908.15	-314	no
1898.15	-162	no	1938.15	-122	no	1958.15	-234	no	1918.15	-199	no
1908.15	-43	1908.15	1948.15	-10	1948.15	1968.15	-115	1968.15	1928.15	-85	1928.15
1918.15	76	no	1958.15	101	no	1978.15	4	no	1938.15	30	no
1928.15	194	no	1968.15	212	no	1988.15	123	no	1948.15	145	no

Tabel A4.23 - Refined results of the function “Found?”

Step: 1 K											
Oak			Beech			Douglas Fir			Bois d'Or Pellets		
T[K]	f(T1)	Found?	T[K]	f(T1)	Found?	T[K]	f(T1)	Found?	T[K]	f(T1)	Found?
1908.15	-43	no	1948.15	-10	1948.15	1968.15	-115	no	1928.15	-85	no
1909.15	-31	no	1949.15	1	no	1969.15	-103	no	1929.15	-73	no
1910.15	-20	no	1950.15	12	no	1970.15	-91	no	1930.15	-62	no
1911.15	-8	1911.15	1951.15	23	no	1971.15	-79	no	1931.15	-50	no
1912.15	4	no	1952.15	34	no	1972.15	-67	no	1932.15	-39	no
1913.15	16	no	1953.15	45	no	1973.15	-55	no	1933.15	-27	no
1914.15	28	no	1954.15	56	no	1974.15	-43	no	1934.15	-16	no
1915.15	40	no	1955.15	67	no	1975.15	-32	no	1935.15	-4	1935.15
1916.15	52	no	1956.15	79	no	1976.15	-20	no	1936.15	7	no
1917.15	64	no	1957.15	90	no	1977.15	-8	1977.15	1937.15	19	no
1918.15	76	no	1958.15	101	no	1978.15	4	no	1938.15	30	no
Step: 0.1 K											
Oak			Beech			Douglas Fir			Bois d'Or Pellets		
T[K]	f(T1)	Found?	T[K]	f(T1)	Found?	T[K]	f(T1)	Found?	T[K]	f(T1)	Found?
1911.15	-8	no	1948.15	-10	no	1977.15	-8	no	1935.15	-4	no
1911.25	-7	no	1948.25	-9	no	1977.25	-7	no	1935.25	-3	no
1911.35	-5	no	1948.35	-8	no	1977.35	-5	no	1935.35	-2	no
1911.45	-4	no	1948.45	-7	no	1977.45	-4	no	1935.45	-1	1935.45
1911.55	-3	no	1948.55	-6	no	1977.55	-3	no	1935.55	0	no
1911.65	-2	no	1948.65	-5	no	1977.65	-2	no	1935.65	1	no
1911.75	-1	1911.75	1948.75	-4	no	1977.75	-1	1977.75	1935.75	3	no
1911.85	1	no	1948.85	-3	no	1977.85	1	no	1935.85	4	no
1911.95	2	no	1948.95	-2	no	1977.95	2	no	1935.95	5	no
1912.05	3	no	1949.05	0	1949.05	1978.05	3	no	1936.05	6	no
1912.15	4	no	1949.15	1	no	1978.15	4	no	1936.15	7	no
Step: 0.01 K											
Oak			Beech			Douglas Fir			Bois d'Or Pellets		
T[K]	f(T1)	Found?	T[K]	f(T1)	Found?	T[K]	f(T1)	Found?	T[K]	f(T1)	Found?
1911.75	-0.56	no	1949.05	-0.42	no	1977.75	-0.56	no	1935.45	-0.90	no
1911.76	-0.44	no	1949.06	-0.31	no	1977.76	-0.44	no	1935.46	-0.79	no
1911.77	-0.32	no	1949.07	-0.20	no	1977.77	-0.32	no	1935.47	-0.67	no
1911.78	-0.20	no	1949.08	-0.09	1949.08	1977.78	-0.20	no	1935.48	-0.56	no
1911.79	-0.09	1911.79	1949.09	0.03	no	1977.79	-0.08	1977.79	1935.49	-0.44	no
1911.8	0.03	no	1949.1	0.14	no	1977.8	0.04	no	1935.5	-0.33	no
1911.81	0.15	no	1949.11	0.25	no	1977.81	0.16	no	1935.51	-0.21	no
1911.82	0.27	no	1949.12	0.36	no	1977.82	0.27	no	1935.52	-0.10	1935.52
1911.83	0.39	no	1949.13	0.47	no	1977.83	0.39	no	1935.53	0.02	no
1911.84	0.51	no	1949.14	0.58	no	1977.84	0.51	no	1935.54	0.13	no
1911.85	0.63	no	1949.15	0.69	no	1977.85	0.63	no	1935.55	0.25	no

Table A4.24 – Equation (4.88) results using FOUND? and SOLVER Excel functions

Wooden Species	Combustion Adiabatic Temperature [K]	
	FOUND? [step: 0.01]	SOLVER
Oak	1911.79	1911.797
Beech	1949.08	1949.088
Douglas Fir	1977.79	1977.797
Bois d'Or Pellets	1935.52	1935.529

Table A4.25 – JANAF* Flue Gasses temperature - dependent coefficients (NIST, Chase, 1009)

$H^{\circ} - H^{\circ}_{298.15} = A \cdot t + B \cdot t^2/2 + C \cdot t^3/3 + D \cdot t^4/4 - E/t + F - H$										
Compound	Symbol	T [K]	A _i	B _i	C _i	D _i	E _i	F _i	G _i	H _i
Carbon dioxide	CO ₂	< 1200 K	25.00	55.19	-33.69	7.95	-0.14	-403.61	228.24	-393.52
		≥ 1200 K	58.17	2.72	-0.49	0.04	-6.45	-425.92	263.61	-393.52
Nitrogen	N ₂	< 500 K	28.99	1.85	-9.65	16.64	0.00	-8.67	226.42	0.00
		< 2000 K	19.51	19.89	-8.60	1.37	0.53	-4.94	212.39	0.00
Oxygen	O ₂	≥ 2000 K	35.52	1.13	-0.20	0.01	-4.55	-18.97	224.98	0.00
		< 700 K	31.32	-20.24	57.87	-36.51	-0.01	-8.90	246.79	0.00
Sulfur dioxide	SO ₂	< 2000 K	30.03	8.77	-3.99	0.79	-0.74	-11.32	236.17	0.00
		≥ 2000 K	20.91	10.72	-2.02	0.15	9.25	5.34	237.62	0.00
Water	H ₂ O	< 1200 K	21.43	74.35	-57.75	16.36	0.09	-305.77	254.89	-296.84
		≥ 1200 K	57.48	1.01	-0.08	0.01	-4.05	-324.41	302.78	-296.84
Carbon oxide	CO	< 1700 K	30.09	6.83	6.79	-2.53	0.08	-250.88	223.40	-241.83
		≥ 1700 K	41.96	8.62	-1.50	0.10	-11.16	-272.18	219.78	-241.83
Carbon oxide	CO	< 1300 K	25.57	6.10	4.05	-2.67	0.13	-118.01	227.37	-110.53
		≥ 1300 K	35.15	1.30	-0.21	0.01	-3.28	-127.84	231.71	-110.53

*JANAF - Joint Army Navy Air Force

Table A4.26 - Sums of products between coefficients of the flue gas products for T_{ref}

$\sum_i^n \frac{m_i}{M_i} \cdot \frac{D_i}{4}$	$\sum_i^n \frac{m_i}{M_i} \cdot \frac{C_i}{3}$	$\sum_i^n \frac{m_i}{M_i} \cdot \frac{B_i}{2}$
Oak 0,82109	Oak -0,87831	Oak 1,38945
Beech 0,75728	Beech -0,82010	Beech 1,31918
Douglas Fir 0,81369	Douglas Fir -0,86887	Douglas Fir 1,37971
Bois d'Or Pellets 0,77597	Bois d'Or Pellets -0,82043	Bois d'Or Pellets 1,32207
$\sum_i^n \frac{m_i}{M_i} \cdot A_i$	$\sum_i^n \frac{m_i}{M_i} \cdot F_i - \sum_i^n \frac{m_i}{M_i} \cdot H_i$	$\sum_i^n \frac{m_i}{M_i} \cdot E_i$
Oak 8,22354	Oak -2,56888	Oak -0,00304
Beech 7,63699	Beech -2,38824	Beech -0,00288
Douglas Fir 8,17781	Douglas Fir -2,55427	Douglas Fir -0,00295
Bois d'Or Pellets 7,91423	Bois d'Or Pellets -2,47008	Bois d'Or Pellets -0,00252

Table A4.27 - Equation (4.88) coefficients of the combustion adiabatic temperature terms

T _{ref} ⁴ coefficient (C _{1ref})	T _{ref} ³ coefficient (C _{2ref})	T _{ref} ² coefficient (C _{3ref})
Oak 821.09417	Oak -878.31459	Oak 1389.44668
Beech 757.28152	Beech -820.10407	Beech 1319.17615
Douglas Fir 813.69478	Douglas Fir -868.87251	Douglas Fir 1379.71476
Bois d'Or Pellets 775.96935	Bois d'Or Pellets -820.42647	Bois d'Or Pellets 1322.07366
T _{ref} ¹ coefficient (C _{4ref})	T _{ref} ⁰ coefficient (C _{5ref})	T _{ref} ⁽⁻¹⁾ coefficient (C _{6ref})
Oak 8223.53643	Oak 14675.23358	Oak -3.04289

Beech	7636.98736	Beech	14087.57629	Beech	-2.87935
Douglas Fir	8177.80516	Douglas Fir	15381.01274	Douglas Fir	-2.95427
Bois d'Or Pellets	7914.22880	Bois d'Or Pellets	14386.41177	Bois d'Or Pellets	-2.51851

Table A4.28 - Values of the free term of the equation (4.95) and (4.103) right member and (4.104) left member for T_{ref}

$-t_{ref}^4 \cdot C_{1ref} - t_{ref}^3 \cdot C_{2ref} - t_{ref}^2 \cdot C_{3ref} - t_{ref}^1 \cdot C_{4ref} - t_{ref}^0 \cdot C_{5ref} - t_{ref}^{(-1)} \cdot C_{6ref}$			
Oak	Beech	Douglas Fir	Bois d'Or Pellets
-17.155	-16.393	-17.847	-16.771

Table A4.29 - Extract of the wooden species tables of the equation function (4.95) and (4.103) right member and (4.104) left member containing temperatures, results and "found" function (step:10)

Oak			Beech			Douglas Fir			Bois d'Or Pellets		
T_{FG} [K]	f(T_{FG})	Found?	T_{FG} [K]	f(T_{FG})	Found?	T_{FG} [K]	f(T_{FG})	Found?	T_{FG} [K]	f(T_{FG})	Found?
1883.15	-300	no	1923.15	-248	no	1953.15	-257	no	1903.15	-313	no
1893.15	-182	no	1933.15	-138	no	1963.15	-138	no	1913.15	-199	no
1903.15	-63	1903.15	1943.15	-27	1943.15	1973.15	-20	1973.15	1923.15	-85	1923.15
1913.15	55	no	1953.15	84	no	1983.15	98	no	1933.15	30	no
1923.15	174	no	1963.15	195	no	1993.15	217	no	1943.15	144	no

Table A4.30 - Extract of the wooden species tables of the equation function (4.95) and (4.103) right member and (4.104) left member containing temperatures, results and "found" function (step:1)

Oak			Beech			Douglas Fir			Bois d'Or Pellets		
T_{FG} [K]	f(T_{FG})	Found?	T_{FG} [K]	f(T_{FG})	Found?	T_{FG} [K]	f(T_{FG})	Found?	T_{FG} [K]	f(T_{FG})	Found?
1905.15	-40	no	1942.15	-38	no	1971.15	-44	no	1927.15	-39	no
1906.15	-28	no	1943.15	-27	no	1972.15	-32	no	1928.15	-27	no
1907.15	-16	no	1944.15	-16	no	1973.15	-20	no	1929.15	-16	no
1908.15	-4	1908.15	1945.15	-5	1945.15	1974.15	-8	1974.15	1930.15	-5	1930.15
1909.15	8	no	1946.15	6	no	1975.15	4	no	1931.15	7	no

Table A4.31 - Equation function (4.95) and (4.103) right member and (4.104) left member results using FOUND? and SOLVER Excel functions

Wooden Species	Combustion Adiabatic Temperature [K]	
	FOUND? [step: 1]	SOLVER
Oak	1.908.15	1.908.50
Beech	1.945.15	1.945.58
Douglas Fir	1.974.15	1.974.85
Bois d'Or Pellets	1.930.15	1.930.55

Table A4.32 - Heat capacity values for water

[°C]	K	[kJ/(kg K)]	[°C]	K	[kJ/(kg K)]
0.01	273.16	4.2199	50	323.15	4.1815
10	283.15	4.1955	60	333.15	4.1851
20	293.15	4.1844	70	343.15	4.1902
25	298.15	4.1816	80	353.15	4.1969
30	303.15	4.1801	90	363.15	4.2053
40	313.15	4.1796	100	373.15	4.2157

Table A4.33 - Results for heat transfer coefficients of hot and cold water and the mass flow of water carrying heat to the consumer

THW _{out}	°C	TCW _{in}	°C	fmHW _{out}	kg/min
Oak	60	Oak	15	Oak	4.03059
Beech	60	Beech	15	Beech	3.76695
Douglas Fir	60	Douglas Fir	15	Douglas Fir	4.10420
Bois d'Or Pellets	60	Bois d'Or Pellets	15	Bois d'Or Pellets	3.84603
c _p (THW _{out})	kJ/(kg·K)	c _p (TCW _{in})	kJ/(kg·K)	fmHW _{out}	kg/h
Oak	4.18	Oak	4.19	Oak	0.06718
Beech	4.18	Beech	4.19	Beech	0.06278
Douglas Fir	4.18	Douglas Fir	4.19	Douglas Fir	0.06840
Bois d'Or Pellets	4.18	Bois d'Or Pellets	4.19	Bois d'Or Pellets	0.06410

Table A4.34 - The “Found?” function for the species, with a step of 1

Oak					Douglas Fir				
T _{int}	c _p (T _{int})	P _{thcheck}	Difference	Found?	T _{int}	c _p (T _{int})	P _{thcheck}	Difference	Found?
[°C]	kJ/(kg·K)	kW	kW	[°C]	[°C]	kJ/(kg·K)	kW	kW	[°C]
42.00	4.17925	7.295	0.80	no	42.00	4.17925	7.429	0.66	no
43.00	4.17912	7.573	0.52	no	43.00	4.17912	7.712	0.38	no
44.00	4.17901	7.852	0.24	44	44.00	4.17901	7.995	0.10	44
45.00	4.17893	8.131	-0.04	no	45.00	4.17893	8.279	-0.19	no
46.00	4.17889	8.410	-0.32	no	46.00	4.17889	8.564	-0.47	no
Beech					Bois d'Or Pellets				
T _{int}	c _p (T _{int})	P _{thcheck}	Difference	Found?	T _{int}	c _p (T _{int})	P _{thcheck}	Difference	Found?
[°C]	kJ/(kg·K)	kW	kW	[°C]	[°C]	kJ/(kg·K)	kW	kW	[°C]
44.00	4.17901	7.338	0.75	no	44.00	4.17901	7.492	0.60	no
45.00	4.17893	7.599	0.49	no	45.00	4.17893	7.758	0.33	no
46.00	4.17889	7.860	0.23	46	46.00	4.17889	8.025	0.07	46
47.00	4.17887	8.122	-0.03	no	47.00	4.17887	8.293	-0.20	no
48.00	4.17888	8.385	-0.29	no	48.00	4.17888	8.561	-0.47	no

Table A4.35 - Intermediary temperature results for steps 0.1 and 0.01

Oak, step 0.1					Oak, step 0.01				
T _{int}	c _p (T _{int})	P _{thcheck}	Difference	Found?	T _{int}	c _p (T _{int})	P _{thcheck}	Difference	Found?
[°C]	kJ/(kg·K)	kW	kW	[°C]	[°C]	kJ/(kg·K)	kW	kW	[°C]
44.00	4.17901	7.851690	-0.24	no	44.80	4.17895	8.074911	-0.0173	no
44.10	4.17900	7.879571	-0.21	no	44.81	4.17895	8.077704	-0.0145	no
44.20	4.17899	7.907458	-0.18	no	44.82	4.17895	8.080496	-0.0117	no
44.30	4.17898	7.935352	-0.16	no	44.83	4.17894	8.083289	-0.0089	no
44.40	4.17898	7.963251	-0.13	no	44.84	4.17894	8.086082	-0.0062	no
44.50	4.17897	7.991157	-0.10	no	44.85	4.17894	8.088875	-0.0034	no
44.60	4.17896	8.019069	-0.07	no	44.86	4.17894	8.091668	-0.0006	44.86
44.70	4.17895	8.046987	-0.05	no	44.87	4.17894	8.094461	0.0022	no
44.80	4.17895	8.074911	-0.02	44.8	44.88	4.17894	8.097255	0.0050	no
44.90	4.17894	8.102841	0.01	no	44.89	4.17894	8.100048	0.0078	no
45.00	4.17893	8.130778	0.04	no	44.90	4.17894	8.102841	0.0106	no

Table A4.35 - Intermediary temperature results for steps 0.1 and 0.01 (continuation)

Beech, step 0.1					Beech, step 0.01				
T _{int} [°C]	c _p (T _{int}) kJ/(kg*K)	P _{th} _{check} kW	Difference kW	Found?	T _{int} [°C]	c _p (T _{int}) kJ/(kg*K)	P _{th} _{check} kW	Difference kW	Found?
46.00	4.17889	7.860360	-0.23	no	46.80	4.17887	8.069907	-0.0223	no
46.10	4.17888	7.886533	-0.21	no	46.81	4.17887	8.072529	-0.0197	no
46.20	4.17888	7.912712	-0.18	no	46.82	4.17887	8.075150	-0.0171	no
46.30	4.17888	7.938897	-0.15	no	46.83	4.17887	8.077772	-0.0145	no
46.40	4.17888	7.965087	-0.13	no	46.84	4.17887	8.080394	-0.0118	no
46.50	4.17887	7.991283	-0.10	no	46.85	4.17887	8.083016	-0.0092	no
46.60	4.17887	8.017485	-0.07	no	46.86	4.17887	8.085638	-0.0066	no
46.70	4.17887	8.043693	-0.05	no	46.87	4.17887	8.08826	-0.0040	no
46.80	4.17887	8.069907	-0.02	46.8	46.88	4.17887	8.090882	-0.0014	46.88
46.90	4.17887	8.096127	0.00	no	46.89	4.17887	8.093504	0.0013	no
47.00	4.17887	8.122352	0.03	no	46.90	4.17887	8.096127	0.0039	no
Douglas Fir, step 0.1					Douglas Fir, step 0.1				
T _{int} [°C]	c _p (T _{int}) kJ/(kg*K)	P _{th} _{check} kW	Difference kW	Found?	T _{int} [°C]	c _p (T _{int}) kJ/(kg*K)	P _{th} _{check} kW	Difference kW	Found?
44.00	4.17901	7.995083	-0.10	no	44.30	4.17898	8.080273	-0.0120	no
44.10	4.17900	8.023474	-0.07	no	44.31	4.17898	8.083114	-0.0091	no
44.20	4.17899	8.051870	-0.04	no	44.32	4.17898	8.085954	-0.0063	no
44.30	4.17898	8.080273	-0.01	44.3	44.33	4.17898	8.088795	-0.0034	no
44.40	4.17898	8.108682	0.02	no	44.34	4.17898	8.091636	-0.0006	44.34
44.50	4.17897	8.137097	0.04	no	44.35	4.17898	8.094477	0.0022	no
44.60	4.17896	8.165519	0.07	no	44.36	4.17898	8.097318	0.0051	no
44.70	4.17895	8.193947	0.10	no	44.37	4.17898	8.100159	0.0079	no
44.80	4.17895	8.222381	0.13	no	44.38	4.17898	8.103000	0.0108	no
44.90	4.17894	8.250821	0.16	no	44.39	4.17898	8.105841	0.0136	no
45.00	4.17893	8.279268	0.19	no	44.40	4.17898	8.108682	0.0164	no
Bois d'Or Pellets, step 0.1					Bois d'Or Pellets, step 0.01				
T _{int} [°C]	c _p (T _{int}) kJ/(kg*K)	P _{th} _{check} kW	Difference kW	Found?	T _{int} [°C]	c _p (T _{int}) kJ/(kg*K)	P _{th} _{check} kW	Difference kW	Found?
46.00	4.17889	8.025368	-0.07	no	46.20	4.17888	8.078819	-0.0134	no
46.10	4.17888	8.052091	-0.04	no	46.21	4.17888	8.081492	-0.0107	no
46.20	4.17888	8.078819	-0.01	46.2	46.22	4.17888	8.084165	-0.0081	no
46.30	4.17888	8.105553	0.01	no	46.23	4.17888	8.086839	-0.0054	no
46.40	4.17888	8.132293	0.04	no	46.24	4.17888	8.089512	-0.0027	no
46.50	4.17887	8.159040	0.07	no	46.25	4.17888	8.092185	0.0000	46.25
46.60	4.17887	8.185792	0.09	no	46.26	4.17888	8.094859	0.0026	no
46.70	4.17887	8.212550	0.12	no	46.27	4.17888	8.097532	0.0053	no
46.80	4.17887	8.239314	0.15	no	46.28	4.17888	8.100206	0.0080	no
46.90	4.17887	8.266084	0.17	no	46.29	4.17888	8.102880	0.0106	no
47.00	4.17887	8.292860	0.20	no	46.30	4.17888	8.105553	0.0133	no

Table A4.36 - Combustion temperature values for different configurations

		T_{FG} [°C]					
%W _t		0	10	20	30	40	50
Iteration	Oak, $\lambda=1$	1899.14	1824.88	1737.94	1634.65	1509.75	1355.17
	Beech, $\lambda=1$	1885.56	1807.81	1717.07	1609.70	1480.40	1321.15
	Douglas Fir, $\lambda=1$	1896.29	1823.42	1738.01	1636.40	1513.33	1360.75
	Bois d'Or Pellets, $\lambda=1$	1900.58	1828.74	1744.44	1644.06	1522.32	1371.17
Gaskell	Oak, $\lambda=1$	1859.96	1797.71	1722.23	1629.52	1513.68	1365.71
	Beech, $\lambda=1$	1898.00	1825.56	1739.60	1636.10	1509.19	1349.92
	Douglas Fir, $\lambda=1$	1933.30	1862.37	1778.50	1677.76	1554.34	1399.33
	Bois d'Or Pellets, $\lambda=1$	1924.75	1856.51	1775.44	1677.59	1557.16	1405.25
Iteration	Oak, $\lambda=1.5$	1408.17	1363.86	1310.93	1246.54	1166.41	1063.71
	Beech, $\lambda=1.5$	1403.43	1356.68	1300.97	1233.40	1149.60	1042.62
	Douglas Fir, $\lambda=1.5$	1407.15	1363.60	1311.55	1248.17	1169.22	1067.89
	Bois d'Or Pellets, $\lambda=1.5$	1408.70	1365.87	1314.63	1252.20	1174.34	1074.30
Gaskell	Oak, $\lambda=1.5$	1390.82	1353.17	1306.40	1247.48	1171.77	1071.92
	Beech, $\lambda=1.5$	1425.38	1380.27	1325.73	1258.61	1174.23	1065.16
	Douglas Fir, $\lambda=1.5$	1448.32	1404.04	1350.83	1285.68	1204.05	1098.67
	Bois d'Or Pellets, $\lambda=1.5$	1440.10	1397.79	1346.65	1283.70	1204.41	1101.56
Iteration	Oak, $\lambda=2$	1125.60	1094.92	1057.83	1012.08	954.16	878.34
	Beech, $\lambda=2$	1124.18	1091.67	1052.46	1004.20	943.27	863.77
	Douglas Fir, $\lambda=2$	1125.24	1095.07	1058.59	1013.54	956.47	881.69
	Bois d'Or Pellets, $\lambda=2$	1125.76	1096.13	1060.26	1015.96	959.78	886.10
Gaskell	Oak, $\lambda=2$	1112.09	1086.13	1053.38	1011.44	956.57	882.74
	Beech, $\lambda=2$	1142.55	1110.78	1071.92	1023.46	961.60	880.14
	Douglas Fir, $\lambda=2$	1159.25	1127.95	1089.99	1042.99	983.28	904.91
	Bois d'Or Pellets, $\lambda=2$	1151.84	1122.07	1085.73	1040.47	982.67	906.38
Iteration	Oak, $\lambda=2.5$	941.18	917.96	889.68	854.48	809.44	749.67
	Beech, $\lambda=2.5$	941.25	916.58	886.60	849.35	801.80	738.87
	Douglas Fir, $\lambda=2.5$	941.12	918.27	890.45	855.79	811.41	752.47
	Bois d'Or Pellets, $\lambda=2.5$	941.18	918.75	891.42	857.37	813.73	755.73
Gaskell	Oak, $\lambda=2.5$	927.60	908.20	883.46	851.41	808.96	751.03
	Beech, $\lambda=2.5$	954.51	930.37	900.62	863.21	814.93	750.56
	Douglas Fir, $\lambda=2.5$	967.52	943.66	914.55	878.25	831.72	769.94
	Bois d'Or Pellets, $\lambda=2.5$	960.89	938.29	910.50	875.63	830.68	770.66
Iteration	Oak, $\lambda=3$	810.72	792.11	769.35	740.84	704.10	654.89
	Beech, $\lambda=3$	811.52	791.73	767.55	737.32	698.43	646.49
	Douglas Fir, $\lambda=3$	810.80	792.50	770.09	742.02	705.82	657.31
	Bois d'Or Pellets, $\lambda=3$	810.63	792.67	770.68	743.11	707.54	659.84
Gaskell	Oak, $\lambda=3$	796.50	781.22	761.55	735.85	701.51	654.14
	Beech, $\lambda=3$	820.49	801.21	777.32	747.07	707.75	654.84
	Douglas Fir, $\lambda=3$	831.10	811.99	788.56	759.20	721.33	670.63

Bois d'Or Pellets, $\lambda=3$	825.15	807.09	784.78	756.63	720.10	670.92
%W	0	10	20	30	40	50

Table A4.37 - Thermal power entered in combustion results

		$P_{\text{fuel}} [\text{kW}_{\text{th}}]$						
		$\%W_t$	0	10	20	30	40	50
$\lambda=1$	Oak, $\lambda=1$		14.43	12.79	11.15	9.51	7.88	6.24
	Beech, $\lambda=1$		13.58	12.02	10.47	8.92	7.36	5.81
	Douglas Fir, $\lambda=1$		14.67	13.01	11.34	9.68	8.02	6.36
	Bois d'Or Pellets, $\lambda=1$		14.95	13.26	11.57	9.88	8.19	6.50
$\lambda=1.5$	Oak, $\lambda=1.5$		14.43	12.79	11.15	9.51	7.88	6.24
	Beech, $\lambda=1.5$		13.58	12.02	10.47	8.92	7.36	5.81
	Douglas Fir, $\lambda=1.5$		14.67	13.01	11.34	9.68	8.02	6.36
	Bois d'Or Pellets, $\lambda=1.5$		14.95	13.26	11.57	9.88	8.19	6.50
$\lambda=2$	Oak, $\lambda=2$		14.43	12.79	11.15	9.51	7.88	6.24
	Beech, $\lambda=2$		13.58	12.02	10.47	8.92	7.36	5.81
	Douglas Fir, $\lambda=2$		14.67	13.01	11.34	9.68	8.02	6.36
	Bois d'Or Pellets, $\lambda=2$		14.95	13.26	11.57	9.88	8.19	6.50
$\lambda=2.5$	Oak, $\lambda=2.5$		14.43	12.79	11.15	9.51	7.88	6.24
	Beech, $\lambda=2.5$		13.58	12.02	10.47	8.92	7.36	5.81
	Douglas Fir, $\lambda=2.5$		14.67	13.01	11.34	9.68	8.02	6.36
	Bois d'Or Pellets, $\lambda=2.5$		14.95	13.26	11.57	9.88	8.19	6.50
$\lambda=3$	Oak, $\lambda=3$		14.43	12.79	11.15	9.51	7.88	6.24
	Beech, $\lambda=3$		13.58	12.02	10.47	8.92	7.36	5.81
	Douglas Fir, $\lambda=3$		14.67	13.01	11.34	9.68	8.02	6.36
	Bois d'Or Pellets, $\lambda=3$		14.95	13.26	11.57	9.88	8.19	6.50

Table A4.38 - Flue gas thermal power resulted after combustion

		$P_{\text{FG}} [\text{kW}]$						
		$\%W_t$	0	10	20	30	40	50
$\lambda=1$	Oak, $\lambda=1$		13.74	12.18	10.62	9.07	7.51	5.95
	Beech, $\lambda=1$		12.93	11.45	9.98	8.50	7.02	5.54
	Douglas Fir, $\lambda=1$		13.97	12.39	10.81	9.23	7.64	6.06
	Bois d'Or Pellets, $\lambda=1$		14.23	12.63	11.02	9.41	7.80	6.20
$\lambda=1.5$	Oak, $\lambda=1.5$		13.74	12.18	10.63	9.07	7.51	5.95
	Beech, $\lambda=1.5$		12.93	11.45	9.98	8.50	7.02	5.55
	Douglas Fir, $\lambda=1.5$		13.97	12.39	10.81	9.23	7.65	6.07
	Bois d'Or Pellets, $\lambda=1.5$		14.23	12.63	11.02	9.41	7.81	6.20
$\lambda=2$	Oak, $\lambda=2$		13.74	12.18	10.63	9.07	7.51	5.95
	Beech, $\lambda=2$		12.93	11.45	9.98	8.50	7.03	5.55
	Douglas Fir, $\lambda=2$		13.97	12.39	10.81	9.23	7.65	6.07
	Bois d'Or Pellets, $\lambda=2$		14.23	12.63	11.02	9.41	7.81	6.20
$\lambda=2.5$	Oak, $\lambda=2.5$		13.74	12.18	10.63	9.07	7.51	5.96
	Beech, $\lambda=2.5$		12.93	11.45	9.98	8.50	7.03	5.55
	Douglas Fir, $\lambda=2.5$		13.97	12.39	10.81	9.23	7.65	6.07
	Bois d'Or Pellets, $\lambda=2.5$		14.23	12.63	11.02	9.42	7.81	6.20

$\lambda=3$	Oak, $\lambda=3$	13.74	12.18	10.63	9.07	7.51	5.96
	Beech, $\lambda=3$	12.93	11.46	9.98	8.50	7.03	5.55
	Douglas Fir, $\lambda=3$	13.97	12.39	10.81	9.23	7.65	6.07
	Bois d'Or Pellets, $\lambda=3$	14.23	12.63	11.02	9.42	7.81	6.20

Table A4.39 - The results of power delivered to the consumer by the Stirling engine

	%W _t	Pelec _{netreal} [kW _{el}]					
		0	10	20	30	40	50
$\lambda=1$	Oak, $\lambda=1$	1.01	1.01	1.01	0.92	0.56	0.19
	Beech, $\lambda=1$	1.01	1.01	1.01	0.79	0.45	0.10
	Douglas Fir, $\lambda=1$	1.01	1.01	1.01	0.96	0.59	0.22
	Bois d'Or Pellets, $\lambda=1$	1.01	1.01	1.01	1.00	0.63	0.25
$\lambda=1.5$	Oak, $\lambda=1.5$	1.01	1.01	1.01	0.92	0.56	0.20
	Beech, $\lambda=1.5$	1.01	1.01	1.01	0.79	0.45	0.10
	Douglas Fir, $\lambda=1.5$	1.01	1.01	1.01	0.96	0.59	0.22
	Bois d'Or Pellets, $\lambda=1.5$	1.01	1.01	1.01	1.01	0.63	0.25
$\lambda=2$	Oak, $\lambda=2$	1.01	1.01	1.01	0.92	0.56	0.20
	Beech, $\lambda=2$	1.01	1.01	1.01	0.79	0.45	0.10
	Douglas Fir, $\lambda=2$	1.01	1.01	1.01	0.96	0.59	0.22
	Bois d'Or Pellets, $\lambda=2$	1.01	1.01	1.01	1.01	0.63	0.25
$\lambda=2.5$	Oak, $\lambda=2.5$	1.01	1.01	1.01	0.92	0.56	0.20
	Beech, $\lambda=2.5$	1.01	1.01	1.01	0.79	0.45	0.10
	Douglas Fir, $\lambda=2.5$	1.01	1.01	1.01	0.96	0.59	0.22
	Bois d'Or Pellets, $\lambda=2.5$	1.01	1.01	1.01	1.01	0.63	0.25
$\lambda=3$	Oak, $\lambda=3$	1.01	1.01	1.01	0.92	0.56	0.20
	Beech, $\lambda=3$	1.01	1.01	1.01	0.79	0.45	0.10
	Douglas Fir, $\lambda=3$	1.01	1.01	1.01	0.96	0.59	0.22
	Bois d'Or Pellets, $\lambda=3$	1.01	1.01	1.01	1.01	0.63	0.25

Table A4.40 - Results of the domestic hot water mass flow delivered to the user

	%W _t	fm _{H2O} [kg/min]					
		0	10	20	30	40	50
$\lambda=1$	Oak, $\lambda=1$	4.03	3.52	3.02	2.54	2.17	1.79
	Beech, $\lambda=1$	3.77	3.29	2.81	2.41	2.05	1.69
	Douglas Fir, $\lambda=1$	4.10	3.59	3.08	2.58	2.20	1.82
	Bois d'Or Pellets, $\lambda=1$	4.19	3.67	3.15	2.63	2.24	1.85
$\lambda=1.5$	Oak, $\lambda=1.5$	4.03	3.52	3.02	2.54	2.17	1.79
	Beech, $\lambda=1.5$	3.77	3.29	2.81	2.41	2.05	1.70
	Douglas Fir, $\lambda=1.5$	4.10	3.59	3.08	2.58	2.20	1.82
	Bois d'Or Pellets, $\lambda=1.5$	4.19	3.67	3.15	2.63	2.24	1.85
$\lambda=2$	Oak, $\lambda=2$	4.03	3.52	3.02	2.54	2.17	1.79
	Beech, $\lambda=2$	3.77	3.29	2.81	2.41	2.05	1.70
	Douglas Fir, $\lambda=2$	4.10	3.59	3.08	2.58	2.20	1.82
	Bois d'Or Pellets, $\lambda=2$	4.19	3.67	3.15	2.63	2.24	1.85
$\lambda=2.5$	Oak, $\lambda=2.5$	4.03	3.52	3.02	2.54	2.17	1.79
	Beech, $\lambda=2.5$	3.77	3.29	2.81	2.41	2.05	1.70
	Douglas Fir, $\lambda=2.5$	4.10	3.59	3.08	2.58	2.20	1.82
	Bois d'Or Pellets, $\lambda=2.5$	4.19	3.67	3.15	2.63	2.24	1.85

$\lambda=3$	Oak, $\lambda=3$	4.03	3.52	3.02	2.54	2.17	1.79
	Beech, $\lambda=3$	3.77	3.29	2.81	2.41	2.05	1.70
	Douglas Fir, $\lambda=3$	4.10	3.59	3.08	2.58	2.20	1.82
	Bois d'Or Pellets, $\lambda=3$	4.19	3.67	3.15	2.63	2.24	1.85

Table A4.41 - Results of thermal power delivered to the consumer

	%W _t	Pth_delivered					
		0	10	20	30	40	50
$\lambda=1$	Oak, $\lambda=1$	12.39	10.84	9.28	7.82	6.67	5.51
	Beech, $\lambda=1$	11.58	10.11	8.63	7.40	6.30	5.21
	Douglas Fir, $\lambda=1$	12.62	11.04	9.46	7.94	6.77	5.60
	Bois d'Or Pellets, $\lambda=1$	12.89	11.28	9.67	8.07	6.88	5.69
$\lambda=1.5$	Oak, $\lambda=1.5$	12.40	10.84	9.28	7.82	6.67	5.51
	Beech, $\lambda=1.5$	11.58	10.11	8.63	7.40	6.31	5.21
	Douglas Fir, $\lambda=1.5$	12.62	11.04	9.46	7.94	6.77	5.60
	Bois d'Or Pellets, $\lambda=1.5$	12.89	11.28	9.67	8.07	6.89	5.70
$\lambda=2$	Oak, $\lambda=2$	12.40	10.84	9.28	7.82	6.67	5.52
	Beech, $\lambda=2$	11.59	10.11	8.63	7.40	6.31	5.21
	Douglas Fir, $\lambda=2$	12.62	11.04	9.46	7.94	6.77	5.60
	Bois d'Or Pellets, $\lambda=2$	12.89	11.28	9.68	8.08	6.89	5.70
$\lambda=2.5$	Oak, $\lambda=2.5$	12.40	10.84	9.28	7.82	6.67	5.52
	Beech, $\lambda=2.5$	11.59	10.11	8.63	7.40	6.31	5.22
	Douglas Fir, $\lambda=2.5$	12.62	11.04	9.46	7.94	6.77	5.60
	Bois d'Or Pellets, $\lambda=2.5$	12.89	11.28	9.68	8.08	6.89	5.70
$\lambda=3$	Oak, $\lambda=3$	12.40	10.84	9.28	7.82	6.67	5.52
	Beech, $\lambda=3$	11.59	10.11	8.63	7.40	6.31	5.22
	Douglas Fir, $\lambda=3$	12.62	11.04	9.46	7.94	6.77	5.60
	Bois d'Or Pellets, $\lambda=3$	12.89	11.28	9.68	8.08	6.89	5.70

Table A4.42 - Thermal efficiency results of the MCHP system, reported to the fuel thermal power of the same configuration

	%W _t	η_{th}					
		0	10	20	30	40	50
$\lambda=1$	Oak, $\lambda=1$	85.70%	84.51%	82.97%	81.92%	84.32%	88.00%
	Beech, $\lambda=1$	85.12%	83.84%	82.19%	82.69%	85.30%	89.29%
	Douglas Fir, $\lambda=1$	85.85%	84.68%	83.17%	81.72%	84.08%	87.67%
	Bois d'Or Pellets, $\lambda=1$	86.02%	84.88%	83.40%	81.49%	83.79%	87.29%
$\lambda=1.5$	Oak, $\lambda=1.5$	85.70%	84.51%	82.97%	81.91%	84.32%	87.99%
	Beech, $\lambda=1.5$	85.12%	83.84%	82.19%	82.69%	85.29%	89.28%
	Douglas Fir, $\lambda=1.5$	85.85%	84.68%	83.18%	81.71%	84.07%	87.66%
	Bois d'Or Pellets, $\lambda=1.5$	86.02%	84.88%	83.40%	81.49%	83.79%	87.29%
$\lambda=2$	Oak, $\lambda=2$	85.70%	84.51%	82.97%	81.91%	84.32%	87.99%
	Beech, $\lambda=2$	85.12%	83.84%	82.19%	82.69%	85.29%	89.28%
	Douglas Fir, $\lambda=2$	85.85%	84.68%	83.18%	81.71%	84.07%	87.66%
	Bois d'Or Pellets, $\lambda=2$	86.02%	84.88%	83.40%	81.49%	83.79%	87.28%
$\lambda=2.5$	Oak, $\lambda=2.5$	85.70%	84.51%	82.98%	81.91%	84.32%	87.98%
	Beech, $\lambda=2.5$	85.12%	83.84%	82.19%	82.69%	85.29%	89.27%
	Douglas Fir, $\lambda=2.5$	85.85%	84.68%	83.18%	81.71%	84.07%	87.65%
	Bois d'Or Pellets, $\lambda=2.5$	86.02%	84.88%	83.41%	81.49%	83.79%	87.28%

$\lambda=3$	Oak, $\lambda=3$	85.70%	84.51%	82.98%	81.91%	84.32%	87.98%
	Beech, $\lambda=3$	85.12%	83.84%	82.19%	82.68%	85.29%	89.27%
	Douglas Fir, $\lambda=3$	85.85%	84.68%	83.18%	81.71%	84.07%	87.65%
	Bois d'Or Pellets, $\lambda=3$	86.02%	84.88%	83.41%	81.48%	83.79%	87.28%

Table A4.43 - Power efficiency reported to the fuel thermal power of the same configuration

	%W _t	η_{el}					
		0	10	20	30	40	50
$\lambda=1$	Oak, $\lambda=1$	6.99%	7.88%	9.04%	9.68%	7.08%	3.11%
	Beech, $\lambda=1$	7.43%	8.38%	9.62%	8.84%	6.03%	1.71%
	Douglas Fir, $\lambda=1$	6.88%	7.75%	8.89%	9.90%	7.35%	3.47%
	Bois d'Or Pellets, $\lambda=1$	6.75%	7.60%	8.71%	10.14%	7.65%	3.87%
$\lambda=1.5$	Oak, $\lambda=1.5$	6.99%	7.88%	9.04%	9.68%	7.08%	3.12%
	Beech, $\lambda=1.5$	7.43%	8.38%	9.62%	8.85%	6.03%	1.72%
	Douglas Fir, $\lambda=1.5$	6.87%	7.75%	8.88%	9.90%	7.35%	3.47%
	Bois d'Or Pellets, $\lambda=1.5$	6.75%	7.60%	8.71%	10.14%	7.66%	3.88%
$\lambda=2$	Oak, $\lambda=2$	6.99%	7.88%	9.03%	9.68%	7.08%	3.12%
	Beech, $\lambda=2$	7.43%	8.38%	9.62%	8.85%	6.04%	1.73%
	Douglas Fir, $\lambda=2$	6.87%	7.75%	8.88%	9.90%	7.35%	3.48%
	Bois d'Or Pellets, $\lambda=2$	6.75%	7.60%	8.71%	10.14%	7.66%	3.88%
$\lambda=2.5$	Oak, $\lambda=2.5$	6.99%	7.88%	9.03%	9.69%	7.09%	3.13%
	Beech, $\lambda=2.5$	7.43%	8.38%	9.62%	8.85%	6.04%	1.73%
	Douglas Fir, $\lambda=2.5$	6.87%	7.75%	8.88%	9.90%	7.35%	3.48%
	Bois d'Or Pellets, $\lambda=2.5$	6.75%	7.60%	8.71%	10.15%	7.66%	3.88%
$\lambda=3$	Oak, $\lambda=3$	6.99%	7.88%	9.03%	9.69%	7.09%	3.13%
	Beech, $\lambda=3$	7.43%	8.38%	9.62%	8.85%	6.04%	1.73%
	Douglas Fir, $\lambda=3$	6.87%	7.75%	8.88%	9.90%	7.36%	3.48%
	Bois d'Or Pellets, $\lambda=3$	6.75%	7.60%	8.71%	10.15%	7.66%	3.89%

Table A4.44 - Results of the added MCHP efficiencies reported to the fuel power of the same configuration

	%W _t	η_{total}					
		0	10	20	30	40	50
$\lambda=1$	Oak, $\lambda=1$	92.69%	92.39%	92.01%	91.60%	91.40%	91.11%
	Beech, $\lambda=1$	92.54%	92.22%	91.81%	91.53%	91.32%	91.00%
	Douglas Fir, $\lambda=1$	92.72%	92.43%	92.06%	91.61%	91.42%	91.13%
	Bois d'Or Pellets, $\lambda=1$	92.77%	92.48%	92.12%	91.63%	91.44%	91.16%
$\lambda=1.5$	Oak, $\lambda=1.5$	92.69%	92.39%	92.01%	91.60%	91.40%	91.11%
	Beech, $\lambda=1.5$	92.54%	92.23%	91.81%	91.53%	91.32%	91.00%
	Douglas Fir, $\lambda=1.5$	92.72%	92.43%	92.06%	91.61%	91.42%	91.13%
	Bois d'Or Pellets, $\lambda=1.5$	92.77%	92.48%	92.12%	91.63%	91.45%	91.16%
$\lambda=2$	Oak, $\lambda=2$	92.69%	92.39%	92.01%	91.60%	91.40%	91.11%
	Beech, $\lambda=2$	92.54%	92.23%	91.82%	91.53%	91.32%	91.00%
	Douglas Fir, $\lambda=2$	92.72%	92.43%	92.06%	91.61%	91.42%	91.13%
	Bois d'Or Pellets, $\lambda=2$	92.77%	92.48%	92.12%	91.63%	91.45%	91.16%
$\lambda=2.5$	Oak, $\lambda=2.5$	92.69%	92.39%	92.01%	91.60%	91.40%	91.11%
	Beech, $\lambda=2.5$	92.54%	92.23%	91.82%	91.53%	91.32%	91.00%
	Douglas Fir, $\lambda=2.5$	92.72%	92.43%	92.06%	91.61%	91.42%	91.13%
	Bois d'Or Pellets, $\lambda=2.5$	92.77%	92.48%	92.12%	91.63%	91.45%	91.16%

$\lambda=3$	Oak, $\lambda=3$	92.69%	92.39%	92.01%	91.60%	91.40%	91.11%
	Beech, $\lambda=3$	92.54%	92.23%	91.82%	91.53%	91.32%	91.00%
	Douglas Fir, $\lambda=3$	92.72%	92.43%	92.06%	91.61%	91.42%	91.13%
	Bois d'Or Pellets, $\lambda=3$	92.77%	92.48%	92.12%	91.63%	91.45%	91.16%

Table A4.45 - The thermal efficiencies reported to the fuel power of “zero” fuel moisture

	%W _t	η^{th} at daf					
		0	10	20	30	40	50
$\lambda=1$	Oak, $\lambda=1$	85.70%	74.93%	64.16%	54.06%	46.09%	38.11%
	Beech, $\lambda=1$	85.12%	74.27%	63.42%	54.36%	46.33%	38.30%
	Douglas Fir, $\lambda=1$	85.85%	75.10%	64.35%	53.98%	46.02%	38.07%
	Bois d'Or Pellets, $\lambda=1$	86.02%	75.30%	64.57%	53.89%	45.95%	38.01%
$\lambda=1.5$	Oak, $\lambda=1.5$	85.71%	74.94%	64.17%	54.07%	46.10%	38.13%
	Beech, $\lambda=1.5$	85.12%	74.28%	63.43%	54.37%	46.34%	38.31%
	Douglas Fir, $\lambda=1.5$	85.86%	75.11%	64.36%	53.99%	46.03%	38.08%
	Bois d'Or Pellets, $\lambda=1.5$	86.03%	75.31%	64.58%	53.90%	45.96%	38.02%
$\lambda=2$	Oak, $\lambda=2$	85.71%	74.95%	64.18%	54.07%	46.10%	38.13%
	Beech, $\lambda=2$	85.13%	74.28%	63.44%	54.38%	46.35%	38.32%
	Douglas Fir, $\lambda=2$	85.86%	75.12%	64.37%	53.99%	46.04%	38.09%
	Bois d'Or Pellets, $\lambda=2$	86.03%	75.31%	64.59%	53.91%	45.97%	38.03%
$\lambda=2.5$	Oak, $\lambda=2.5$	85.71%	74.95%	64.18%	54.08%	46.11%	38.14%
	Beech, $\lambda=2.5$	85.13%	74.29%	63.44%	54.38%	46.35%	38.33%
	Douglas Fir, $\lambda=2.5$	85.86%	75.12%	64.38%	54.00%	46.05%	38.09%
	Bois d'Or Pellets, $\lambda=2.5$	86.04%	75.31%	64.59%	53.91%	45.97%	38.04%
$\lambda=3$	Oak, $\lambda=3$	85.72%	74.95%	64.19%	54.08%	46.11%	38.14%
	Beech, $\lambda=3$	85.14%	74.29%	63.45%	54.38%	46.36%	38.33%
	Douglas Fir, $\lambda=3$	85.87%	75.12%	64.38%	54.00%	46.05%	38.09%
	Bois d'Or Pellets, $\lambda=3$	86.04%	75.32%	64.60%	53.91%	45.98%	38.04%

Table A4.46 - The power efficiencies reported to the fuel power with “zero” fuel moisture

	%W _t	η^{el} at daf					
		0	10	20	30	40	50
$\lambda=1$	Oak, $\lambda=1$	6.99%	6.99%	6.99%	6.39%	3.87%	1.35%
	Beech, $\lambda=1$	6.99%	6.99%	6.99%	6.39%	3.87%	1.35%
	Douglas Fir, $\lambda=1$	6.99%	6.99%	6.99%	6.39%	3.87%	1.35%
	Bois d'Or Pellets, $\lambda=1$	6.99%	6.99%	6.99%	6.39%	3.87%	1.35%
$\lambda=1.5$	Oak, $\lambda=1.5$	6.99%	6.99%	6.99%	6.39%	3.87%	1.35%
	Beech, $\lambda=1.5$	6.99%	6.99%	6.99%	6.39%	3.87%	1.35%
	Douglas Fir, $\lambda=1.5$	6.99%	6.99%	6.99%	6.39%	3.87%	1.35%
	Bois d'Or Pellets, $\lambda=1.5$	6.99%	6.99%	6.99%	6.39%	3.87%	1.35%
$\lambda=2$	Oak, $\lambda=2$	6.99%	6.99%	6.99%	6.39%	3.87%	1.35%
	Beech, $\lambda=2$	6.99%	6.99%	6.99%	6.39%	3.87%	1.35%
	Douglas Fir, $\lambda=2$	6.99%	6.99%	6.99%	6.39%	3.87%	1.35%
	Bois d'Or Pellets, $\lambda=2$	6.99%	6.99%	6.99%	6.39%	3.87%	1.35%
$\lambda=2.5$	Oak, $\lambda=2.5$	6.99%	6.99%	6.99%	6.39%	3.87%	1.35%
	Beech, $\lambda=2.5$	6.99%	6.99%	6.99%	6.39%	3.87%	1.35%
	Douglas Fir, $\lambda=2.5$	6.99%	6.99%	6.99%	6.39%	3.87%	1.35%
	Bois d'Or Pellets, $\lambda=2.5$	6.99%	6.99%	6.99%	6.39%	3.87%	1.35%

$\lambda=3$	Oak, $\lambda=3$	6.99%	6.99%	6.99%	6.40%	3.88%	1.36%
	Beech, $\lambda=3$	6.99%	6.99%	6.99%	6.40%	3.88%	1.36%
	Douglas Fir, $\lambda=3$	6.99%	6.99%	6.99%	6.40%	3.88%	1.36%
	Bois d'Or Pellets, $\lambda=3$	6.99%	6.99%	6.99%	6.40%	3.88%	1.36%

Table A4.47 - The MCHP efficiencies of the configurations reported to the fuel power of the same air excess, but “zero” fuel moisture

	%W _t	$\eta^{\text{total at daf}}$					
		0	10	20	30	40	50
$\lambda=1$	Oak, $\lambda=1$	92.69%	81.92%	71.15%	60.45%	49.95%	39.46%
	Beech, $\lambda=1$	92.10%	81.26%	70.41%	60.75%	50.20%	39.64%
	Douglas Fir, $\lambda=1$	92.84%	82.09%	71.34%	60.37%	49.89%	39.41%
	Bois d'Or Pellets, $\lambda=1$	93.01%	82.29%	71.56%	60.28%	49.82%	39.36%
$\lambda=1.5$	Oak, $\lambda=1.5$	92.70%	81.93%	71.16%	60.46%	49.97%	39.48%
	Beech, $\lambda=1.5$	92.11%	81.27%	70.42%	60.76%	50.21%	39.66%
	Douglas Fir, $\lambda=1.5$	92.85%	82.10%	71.35%	60.38%	49.91%	39.43%
	Bois d'Or Pellets, $\lambda=1.5$	93.02%	82.29%	71.57%	60.29%	49.83%	39.38%
$\lambda=2$	Oak, $\lambda=2$	92.70%	81.93%	71.17%	60.47%	49.98%	39.49%
	Beech, $\lambda=2$	92.12%	81.27%	70.43%	60.77%	50.22%	39.67%
	Douglas Fir, $\lambda=2$	92.85%	82.11%	71.36%	60.39%	49.91%	39.44%
	Bois d'Or Pellets, $\lambda=2$	93.02%	82.30%	71.58%	60.30%	49.84%	39.39%
$\lambda=2.5$	Oak, $\lambda=2.5$	92.70%	81.94%	71.17%	60.47%	49.98%	39.49%
	Beech, $\lambda=2.5$	92.12%	81.28%	70.43%	60.78%	50.23%	39.68%
	Douglas Fir, $\lambda=2.5$	92.85%	82.11%	71.36%	60.39%	49.92%	39.45%
	Bois d'Or Pellets, $\lambda=2.5$	93.02%	82.30%	71.58%	60.30%	49.85%	39.39%
$\lambda=3$	Oak, $\lambda=3$	92.70%	81.94%	71.17%	60.47%	49.99%	39.50%
	Beech, $\lambda=3$	92.12%	81.28%	70.43%	60.78%	50.23%	39.69%
	Douglas Fir, $\lambda=3$	92.86%	82.11%	71.37%	60.40%	49.92%	39.45%
	Bois d'Or Pellets, $\lambda=3$	93.03%	82.30%	71.58%	60.31%	49.85%	39.40%

Anexa 5: Mathematical model for the simulation of transient regimes

Table A5.1 - Projection of the cash – flow for the economic simulation of the Test code VN MASTER 10-1 mar 07

year	0	1	2	3	4	5	6	7	8	9	10
Earnings	-15.000	1.864	1.864	1.864	1.864	1.864	1.864	1.864	1.864	1.864	1.864
Cash - flow	-15.000	-13.136	-11.272	-9.408	-7.544	-5.680	-3.815	-1.951	-87	1.777	3.641
Discount factor	1,00	0,95	0,91	0,86	0,82	0,78	0,75	0,71	0,68	0,64	0,61
Discounted cash - flow	-15.000	-13.225	-11.534	-9.924	-8.390	-6.929	-5.538	-4.214	-2.952	-1.750	-606

year	0	11	12	13	14	15	16	17	18	19	20
Earnings	-15.000	1.864	1.864	1.864	1.864	1.864	1.864	1.864	1.864	1.864	1.864
Cash - flow	-15.000	5.505	7.369	9.233	11.097	12.961	14.826	16.690	18.554	20.418	22.282
Discount factor	1,00	0,58	0,56	0,53	0,51	0,48	0,46	0,44	0,42	0,40	0,38
Discounted cash - flow	-15.000	484	1.522	2.511	3.452	4.349	5.203	6.016	6.790	7.528	8.231

Table A5.2 - Projection of the cash – flow for the economic simulation of the Test code VN MASTER 14-3 jun 11

year	0	1	2	3	4	5	6	7	8	9	10
Earnings	-15.000	1.572	1.572	1.572	1.572	1.572	1.572	1.572	1.572	1.572	1.572
Cash - flow	-15.000	-13.428	-11.855	-10.283	-8.710	-7.138	-5.566	-3.993	-2.421	-848	724
Discount factor	1,00	0,95	0,91	0,86	0,82	0,78	0,75	0,71	0,68	0,64	0,61
Discounted cash - flow	-15.000	-13.502	-12.076	-10.718	-9.424	-8.192	-7.019	-5.901	-4.837	-3.824	-2.858

year	0	11	12	13	14	15	16	17	18	19	20
Earnings	-15.000	1.572	1.572	1.572	1.572	1.572	1.572	1.572	1.572	1.572	1.572
Cash - flow	-15.000	2.297	3.869	5.441	7.014	8.586	10.159	11.731	13.303	14.876	16.448
Discount factor	1,00	0,58	0,56	0,53	0,51	0,48	0,46	0,44	0,42	0,40	0,38
Discounted cash - flow	-15.000	-1.939	-1.063	-229	565	1.321	2.041	2.727	3.381	4.003	4.596

**Table A5.3 - Projection of the cash – flow for the economic simulation of the Test code VN
MASTER 10-1 jun 25**

year	0	1	2	3	4	5	6	7	8	9	10
Earnings	-15.000	1.421	1.421	1.421	1.421	1.421	1.421	1.421	1.421	1.421	1.421
Cash - flow	-15.000	-13.579	-12.159	-10.738	-9.317	-7.897	-6.476	-5.056	-3.635	-2.214	-794
Discount factor	1,00	0,95	0,91	0,86	0,82	0,78	0,75	0,71	0,68	0,64	0,61
Discounted cash - flow	-15.000	-13.647	-12.358	-11.131	-9.962	-8.849	-7.789	-6.780	-5.818	-4.902	-4.030

year	0	11	12	13	14	15	16	17	18	19	20
Earnings	-15.000	1.421	1.421	1.421	1.421	1.421	1.421	1.421	1.421	1.421	1.421
Cash - flow	-15.000	627	2.048	3.468	4.889	6.310	7.730	9.151	10.571	11.992	13.413
Discount factor	1,00	0,58	0,56	0,53	0,51	0,48	0,46	0,44	0,42	0,40	0,38
Discounted cash - flow	-15.000	-3.200	-2.409	-1.655	-938	-254	397	1.016	1.607	2.169	2.704

**Table A5.4 - Projection of the cash – flow for the economic simulation of the Test code VN
MASTER 10-1 jun 18**

year	0	1	2	3	4	5	6	7	8	9	10
Earnings	-15.000	2.060	2.060	2.060	2.060	2.060	2.060	2.060	2.060	2.060	2.060
Cash - flow	-15.000	-12.940	-10.881	-8.821	-6.762	-4.702	-2.643	-583	1.476	3.536	5.595
Discount factor	1,00	0,95	0,91	0,86	0,82	0,78	0,75	0,71	0,68	0,64	0,61
Discounted cash - flow	-15.000	-13.039	-11.171	-9.391	-7.697	-6.083	-4.547	-3.083	-1.689	-361	903

year	0	11	12	13	14	15	16	17	18	19	20
Earnings	-15.000	2.060	2.060	2.060	2.060	2.060	2.060	2.060	2.060	2.060	2.060
Cash - flow	-15.000	7.655	9.714	11.774	13.833	15.893	17.952	20.012	22.071	24.131	26.190
Discount factor	1,00	0,58	0,56	0,53	0,51	0,48	0,46	0,44	0,42	0,40	0,38
Discounted cash - flow	-15.000	2.107	3.254	4.346	5.386	6.377	7.320	8.219	9.075	9.890	10.666